VOLUME 7 ISSUE 2 JUNE 2022

IJEG

International Journal of Engineering and Geosciences

e-ISSN 2548-0960

Assist. Prof. Dr. Yelda TURKAN
Oregon State University,
USA

Dr. G. Sanka N. PERERA
Sabaragamuwa University Faculty of Geomatics
Sri Lanka

Dr. Hsiu-Wen CHANG
National Cheng Kung University, Department of Geomatics
Taiwan

The International Journal of Engineering and Geosciences (IJEG)

The International Journal of Engineering and Geosciences (IJEG) is a tri-annually published journal. The journal includes a wide scope of information on scientific and technical advances in the geomatics sciences. The International Journal of Engineering and Geosciences aims to publish pure and applied research in geomatics engineering and technologies. IJEG is a double peer-reviewed (blind) OPEN ACCESS JOURNAL that publishes professional level research articles and subject reviews exclusively in English. It allows authors to submit articles online and track his or her progress via its web interface. All manuscripts will undergo a refereeing process; acceptance for publication is based on at least two positive reviews. The journal publishes research and review papers, professional communication, and technical notes. IJEG does not charge for any article submissions or for processing.

CORRESPONDENCE ADDRESS
Journal Contact: engineeringandgeoscience@gmail.com

CONTENTS

Volume 7 - Issue 2

RESEARCH ARTICLES

International Journal of Engineering and Geosciences
https://dergipark.org.tr/en/pub/ijeg
e-ISSN 2548-0960

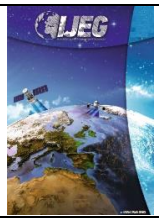

Automatic extraction of the polygon obtained by the intersection of parcels with the geometric algorithms

Emirhan Ozdemir [1], Faruk Yıldırım [2], Fatih Kadi *[2]

[1]*Iğdır University, Vocational School of Higher Education for Technical Sciences, Iğdır, Turkey*
[2]*Karadeniz Technical University, Engineering Faculty, Department of Geomatics Engineering, Trabzon, Turkey*

Keywords
Mapping techniques
Point – parcel relations
GIS software

ABSTRACT

Today, many mapping techniques (development plan implementation, expropriation, urban and rural arrangement, etc.) are applied geometrically. One of the situations that will be encountered in these applications is the relative status of the parcels. Firstly, point-plot relationships for arbitrary points were examined in this study. It was investigated whether these points were inside or outside the parcel. The aim is to determine the positions of the points relative to the parcels and to observe whether there is an intersection. If there is an intersection between the main parcel and the test parcel as a result of the point-parcel examination, the intersection points of these two parcels are found. Parcel corner points and intersection points are ordered according to the specified criteria and the intersection parcel is obtained. The area of the intersection parcel obtained is calculated. All possible special cases of the two parcels are examined relative to each other. With the proposed method, the results for each of the special cases are obtained and presented. The accuracy of the results was compared with CAD and GIS software and their advantages and disadvantages were examined. The proposed method is designed to be two or more parcels in many surveying techniques and gives high accuracy results. In addition, it is foreseen that the proposed method will provide great convenience in calculations functionally and temporally.

1. INTRODUCTION

The intersection of two or more parcels is an important situation in surveying and mapping applications (expropriation, urban area design, land consolidation, GIS applications). Today, there are many algorithms that determine the relationships between the parcel and the point. The important thing is to examine the intersection situations of two or more parcels by using these algorithms. These algorithms differ in terms of processing times and applicability of special cases. The proposed method aims to automatically select the corners and intersection points of the parcels, and to create the intersection parcel and obtain its area without error.

There are many mathematical and geometric methods that examine whether any point whose coordinate is known is inside or outside of another parcel whose coordinates are known to all vertices. These methods are classified according to the shape of the plots (convex and concave) (Kitay 1985; Yomralıoğlu 2000; Yanalak and İpbüker 2003). The Proposed method first recognizes the corner points of at least two plots. The location of any selected corner point is examined relative to the other parcel. This is repeated for all vertices. The aim is to determine whether the selected corner point is inside or outside the other plot. Thus, this situation will be taken into account in the order to be made while finding the intersection plot. Then, the intersection situations of the parcels are examined. If there is an intersection, the coordinates of the intersection points are determined (Figure 1). All obtained points are ranked according to the criteria determined by the proposed method (Figure 4). Finally, as a result of the sorting, the intersection plot is obtained and its area is calculated correctly.

* **Corresponding Author**
(emirhan.ozdmr@hotmail.com) ORCID ID 0000-0001-8306-834X
(yfaruk@ktu.edu.tr) ORCID ID 0000-0003-3898-7341
*(fatihkadi@ktu.edu.tr) ORCID ID 0000-0002-6152-6351

Cite this article
Ozdemir E, Yıldırım F & Kadi F (2022). Automatic extraction of the polygon obtained by the intersection of parcels with the geometric algorithms. International Journal of Engineering and Geosciences, 7(2), 91-100

Research Article / DOI: 10.26833/ijeg.886819
Received: 25/02/2021; Accepted: 14/06/2021

There are different methods to obtain the intersection plot obtained by the intersection of multiple plots. However, these methods may fail to give good results in all situations. Therefore, each special condition encountered while developing the method was examined separately and the most suitable algorithm was determined by considering the processing time. As a result, the accuracy evaluation of the proposed method was compared with CAD and GIS software. Thus, it has been determined that the proposed method obtains correct results in all special cases.

2. Material and METHODS

2.1. Point in Polygon Test for Concave and Convex Parcels

There are 3 methods for point in polygon test in both types of parcels. These are Ray Intersection, Sum of Angles and Swath methods. Among these methods, ray intersection and swath methods do not provide solutions for some special cases (passing through the corner point, being on the edge). The sum of angles method is more disadvantageous than the other two methods, due to both the processing time and the rounding errors caused by the sum of angles. Instead of these three methods, an algorithm that takes special cases into account has been developed.

There is more than one type of representation of a line in the plane. The vector equality of a line segment defined by the coordinates of the starting (x_0, y_0) and ending (x_1, y_1) point is expressed by the following equation.

$$L = \{(x_0, y_0) + (r[x_1 - x_0], r[y_1 - y_0] | \, 0 < r < 1\} \quad (1)$$

In the plane, the line segments L and L′ are defined by the points P_0, P_1 and P_0', P_1' respectively (Figure 1). In order for both line segments to intersect with each other, Equation 2 must be provided.

$$P_0 + r(P_1 - P_0) = P_0' + r'(P_1' - P_0') \quad (2)$$

Using the coordinate values of the points, r and r' values are calculated with the help of equations 3, 4, 5, 6, 7, 8 and 9.

$$x_0 + r(x_1 - x_0) = x_0' + r'(x_1' - x_0') \quad (3)$$

$$y_0 + r(y_1 - y_0) = y_0' + r'(y_1' - y_0') \quad (4)$$

$$D = \begin{vmatrix} (y_1 - y_0) & -(y_1' - y_0') \\ (x_1 - x_0) & -(x_1' - x_0') \end{vmatrix} \quad (5)$$

$$D_1 = \begin{vmatrix} (y_0' - y_0) & -(y_1' - y_0') \\ (x_0' - x_0) & -(x_1' - x_0') \end{vmatrix} \quad (6)$$

$$D_2 = \begin{vmatrix} (y_1 - y_0) & (y_0' - y_0) \\ (x_1 - x_0) & (x_0' - x_0) \end{vmatrix} \quad (7)$$

$$r = D_1/D, \; r' = D_2/D \quad (8)$$

If r and r′ values are between 0 and 1, the segments L and L′ intersect at a single point. But if the D determinant is equal to zero, these line segments are parallel. If the determinants D, D_1, and D_2 are equal to zero, these line segments overlap.

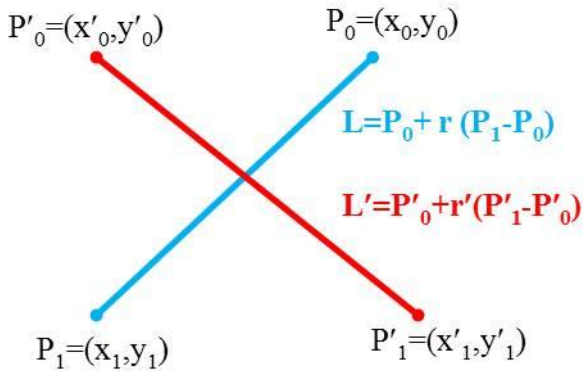

Figure 1. Line segments L and L′

The coordinates of the Q point (x_0, y_0) given for the inquiry are the first point of the beam. The ray is defined as vectorial in equation 9.

$$R = \{(x_0, y_0) + r(m_x, 2M_y) | r > 0\} \quad (9)$$

In Equation 9, when the coordinates of the end point of the ray are defined as r = 1, equation number 10 is obtained.

$$(x', y') = (x_0 + m_x, y_0 + 2M_y) \quad (10)$$

In Eq. 10, m_x and M_y are used to draw a direction to the beam. Thus, the beam will not be like the special cases in figure 1 and figure 2. For the M_y value, $|y_0 - y_i|$ the largest value of the absolute value difference is taken. $|x_0 - x_i|$ The smallest value of the absolute value difference other than zero is taken for m_x (Figure 2).

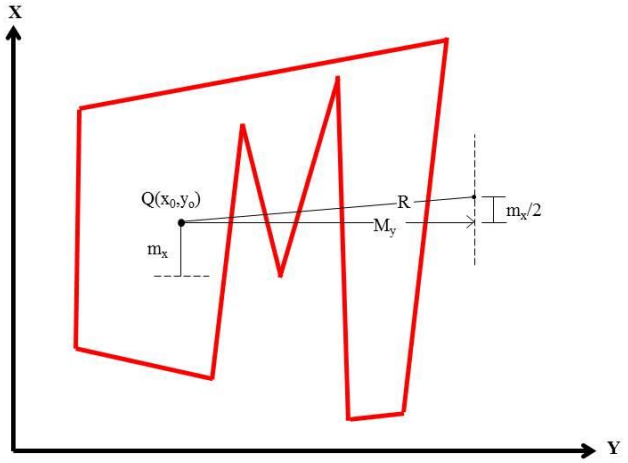

Figure 2. M_y and m_x rays

A number of determinant calculations are required for the calculation of the number of points where the R ray whose starting point is Q (x_0, y_0) intersects the parcel (Equations 11, 12 and 13). The total number of intersections is calculated from the product of the determinants $D_i'(D_i - D_i')$ and $D_i'' D_i$.

D_i, D_i' and D_i'' parameters are calculated using the following equations.

$$D_i = \begin{vmatrix} 2M_y & -(y_{i+1} - y_i) \\ m_x & -(x_{i+1} - x_i) \end{vmatrix} \quad (11)$$

$$D_i' = \begin{vmatrix} 2M_y & (y_i - y_0) \\ m_x & (x_i - x_0) \end{vmatrix} \quad (12)$$

$$D_i'' = \begin{vmatrix} (y_i - y_0) & -(y_{i+1} - y_i) \\ (x_i - x_0) & -(x_{i+1} - x_i) \end{vmatrix} \quad (13)$$

If the determinant products are positive, the R ray cuts the S_i edge of the parcel. In other cases, it doesn't. Thus, the number of intersections is calculated. If this number is odd, point Q is inside the parcel, if it is even, the point is outside the parcel (Taylor 1994; Huang and Shih 1997; Jianqiang et al. 2018).

2.2. The Intersection of Parcels and the Production of the Parcel using the Corner Points of the Common Area

The corner points of the area obtained from the intersection of the two parcels are complex and these points are not numbered clockwise. First of all, these complex points should be given point numbers in the clockwise direction for calculation of the parcel area. Nowadays there are a lot of methods that have different geometric algorithms for this process. The main goal of these methods is to be applicable to both concave and convex parcels (Sutherland and Hodgman 1974; Weiler and Atherton, 1977). In addition, the algorithm of intersection of convex polygons has been developed (Cyrus and Beck 1978). Today, there are algorithms that have different special cases for the area calculation of the polygon obtained by the intersection of two parcels (Barsky and Liang 1984; Nicholl et al. 1987; Maillot 1992; Day 1992; Möller 1997; Greiner and Hormann 1998; Huang and Liu 2002).

Special cases are the numbering of the corner points of the parcels in clockwise direction, being applicable for concave and convex parcels, and processing time. First of all, corner points of the polygon obtained by the intersection of many parcels should be numbered clockwise. Then, by selecting any of the polygons, the correct equations of each side are generated with the help of consecutive vertices. The same process step is applied to all polygons to obtain the correct equations of all sides. It is checked whether each line intersect. If there are lines that intersect, a new name is given to the point where they intersect (Figure 3a.). And this point is added between those two vertices in the table where the vertices are written sequentially (Figure 4). This is done for all sides until the sequence is complete. This sequence starts from the left and continues until the first intersection point. This point is defined as the first point of the common region and all points in between up to the other intersection point are written as the edges of the common region. When the second intersection is reached, it stops. If the second intersection point exists in the initial ranking, it is accepted at that time and the same process is continued based on that order. This process continues until it reaches the point defined as the first point of the polygon formed as a result of the intersection. Thus, the coordinates of all corner points of the common area have been determined (Figure 3a, 3b). All sides of the 1st polygon (A → B → C) and the 2nd polygon (D → E → F → G → H) are defined in the clockwise direction. Check whether the first edge (AB) of the 1st polygon intersects all sides of the second polygon. Edge AB and sides EF and HD of the second parcel intersect. Those intersecting points are given the names a and b, respectively. The same process steps are then applied for the BC edge. This edge intersects the FG edge and the GH edge. These points are given the names c and d, respectively. Finally, the same process steps are applied for the CA edge. Thus, the final names of polygons after intersection are obtained by the 1st polygon [A → b → a → B → c → d → C] and the 2nd polygon [D → E → a → F → c → G → d → H → b] (Figure 3b).

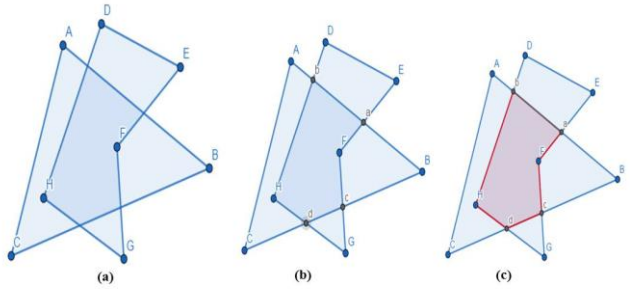

Figure 3. Two intersecting polygons and intersection points

It has been started from point b, which is the first intersection point of the 1st polygon, and continued until the second intersection point a. Point a is in the order in the 2nd polygon and has been continued from there to c. If point c was not in the order in the 1st polygon, the process would stop at that point. But point c is present in the order in the 1st polygon. Then it is continued from point c in the 1st polygon to point d, which is the next intersection point. Likewise, point d is present in the order in the 2nd polygon. Finally, considering the order in the 2nd polygon, the intersection point after point d is point b. This point is the point originally defined. Thus, the corner coordinates of the polygon formed have been determined (Figure 4).

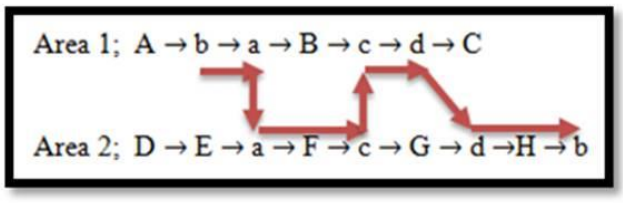

Figure 4. Two intersecting polygons and intersection points

When these points are joined, an intersection polygon has been formed (Figure 3c).

2.2. Proposed Method

The aim of this study is to calculate the corner coordinates and area calculation of the generated common area as a result of the coincidence of any two

convex or concave parcels (polygons) in Geomatics Engineering applications with the help of MATLAB software. While calculating this common area, it will be sufficient to give the coordinates of only two parcels with the help of developed algorithms. In addition, unlike GIS and CAD software, it is aimed to develop algorithm faster and eliminating user errors without the need for the user to determine intersection points and intersection zones. In the developed algorithm, the vertex coordinates of the polygon obtained from the intersection of two parcels are determined automatically by the algorithm without the need for the user. Because, while the intersection point of two lines is determined, any of these two direct lines can intersect with the other edges of the parcel whose coordinates are known. Another advantage of the proposed algorithm is that when determining the corner coordinates of the Polygon formed after the intersection step, it automatically queries whether other points of the intersection parcel other than the intersection points are the corner points of the parcel (Figure 5).

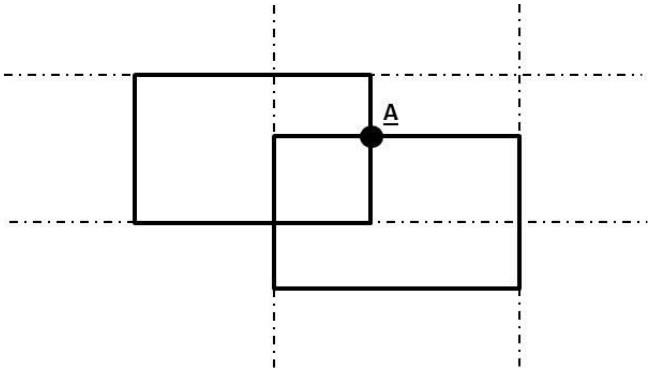

Figure 5. Determining the intersection point

2.3. Application

A large number of application parcels have been selected in order to examine special cases. These special cases are discussed in detail below. The calculated areas and corner coordinates are controlled by GIS software and the advantages and disadvantages are examined. A main parcel (P) has been identified, covering all special cases that may occur for cartography activities.

Table 1. Coordinates of the corner points of the main parcel

Corner Points	Y(m)	X(m)	Corner Points	Y(m)	X(m)
1	20	140	12	270	100
2	70	200	13	230	90
3	90	160	14	280	60
4	140	190	15	220	30
5	140	230	16	160	50
6	180	220	17	130	20
7	200	180	18	120	80
8	240	210	19	60	40
9	310	180	20	70	110
10	250	140	21	40	80
11	290	120			

10 parcels with different special conditions to intersect with this main parcel have been determined. The coordinate information of these parcels, which were determined to examine special cases, is presented in Table 2.

Table 2. Coordinates of the corner points of the parcels to be intersected

Type of Parcel	Corner Points	Y(m)	X(m)	Type of Parcel	Corner Points	Y(m)	X(m)
A	A1	220	50	F	F1	280	170
	A2	250	20		F2	270	100
	A3	230	10		F3	170	100
	A4	200	20	G	G1	280	170
B	B1	220	220		G2	250	95
	B2	250	230		G3	170	100
	B3	280	210	H	H1	150	70
	B4	260	180		H2	200	50
C	C1	300	80		H3	175	25
	C2	300	50		H4	110	20
	C3	240	50	I	I1	290	70
D	D1	120	200		I2	280	60
	D2	160	200		I3	220	30
	D3	160	160	J	J1	40	220
	D4	120	160		J2	200	220
E	E1	280	170		J3	110	30
	E2	270	100		J4	20	100
	E3	170	100				

2.3.1. Case number 1

A parcel that intersects with the main plot at two different points has been used. In the figure 6, the positions of the two parcels with respect to each other and the common area has been generated as a result of the intersection of these parcels have been shown in detail with the corner coordinates (Figure 6).

2.3.2. Case number 2

Another parcel that intersects the main plot at two different points has been taken and the area where both

of them have been intersected is shown in detail (Figure 7).

2.3.3. Case number 3

A parcel intersecting at two different points to the right of the main plot has been selected. These parcels, which intersect at two different points, have been selected in different parts of the main parcel (Figure 8).

2.3.4. Case number 4

An edge of the main plot and an edge of the selected parcel intersect vertically. This situation has been examined as a special case (Figure 9).

2.3.5. Case number 5

The difference of this case from other cases is that the main parcel and the selected parcel have more than 2 intersections. In the light of the obtained results, it has been seen that the algorithm developed in MATLAB software has been worked in this case as well (Figure 10).

2.3.6. Case number 6

One of the special cases is that a corner point of the main parcel and the selected parcel is the same. It is seen that this situation works flawlessly even when the corner points of the main parcel and selected parcel are the same (Figure 11).

2.3.7. Case number 7

The intersection points of the main parcel and the selected parcel and the corner point of the selected parcel is as follows (Figure 12.).

2.3.8. Case number 8

The case that at least one side of the main parcel and the selected parcel are parallel to each other has been shown in the figure (Figure 13.).

2.3.9. Case number 9

The common side of the main parcel and the selected parcel has been shown below (Figure 14.).

2.3.10. Case number 10

In this case, many special cases coexist. These special cases are that the corner points of the two parcels are the same, one is that the edges of these parcels are perpendicular to each other and the number of intersections of the sides is more than two on the same side. This option sets an example for most situations in the field. It works flawlessly according to the mentioned algorithm (Figure 15).

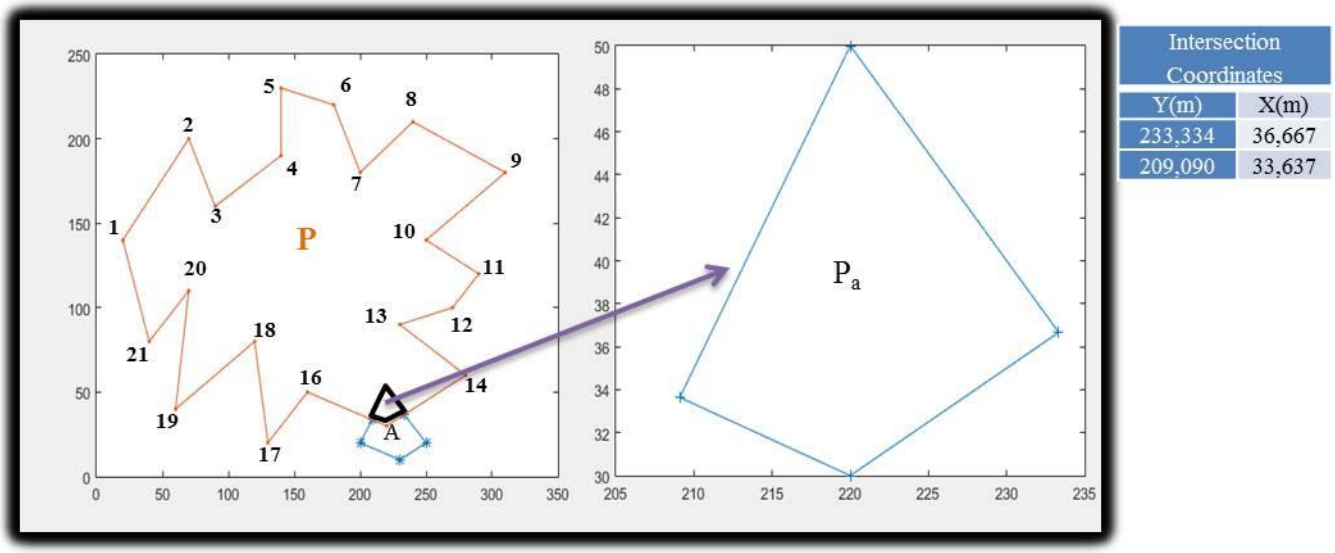

Intersection Coordinates	
Y(m)	X(m)
233,334	36,667
209,090	33,637

Figure 6. New P_a parcel produced after intersection with P and A parcels

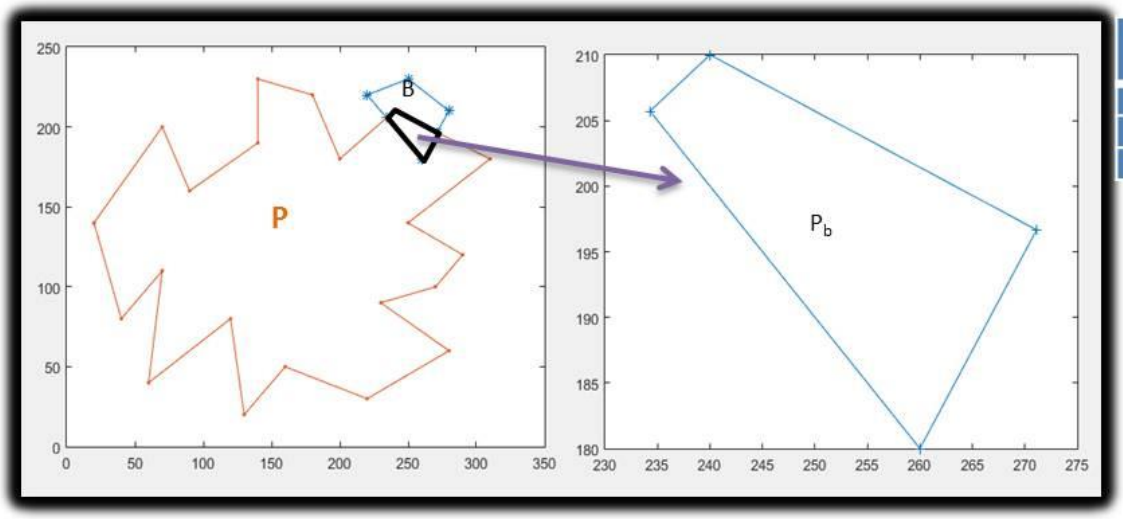

Intersection Coordinates	
Y(m)	X(m)
270,910	65,455
260,000	50,000

Figure 7. New P_b parcel produced after intersection with P and B parcels

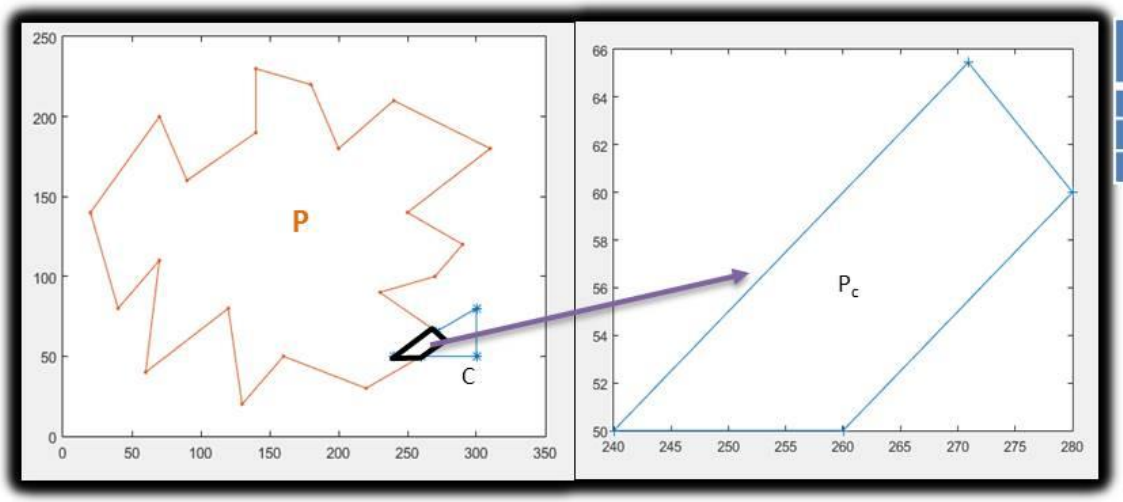

Intersection Coordinates	
Y(m)	X(m)
270,910	65,455
260,000	50,000

Figure 8. New P_c parcel produced after intersection with P and C parcels

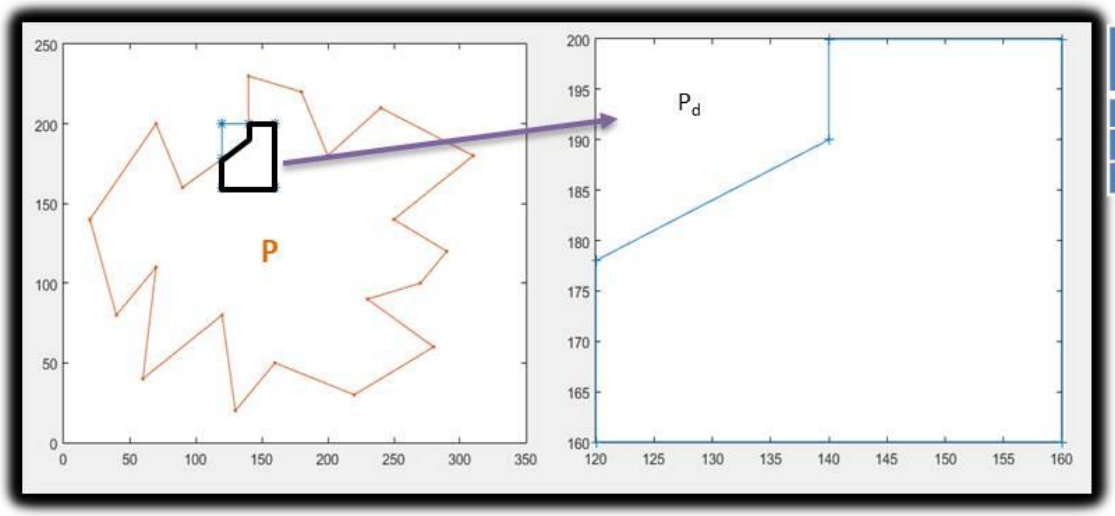

Intersection Coordinates	
Y(m)	X(m)
120,000	178,000
140,000	200,000

Figure 9. New P_d parcel produced after intersection with P and D parcels

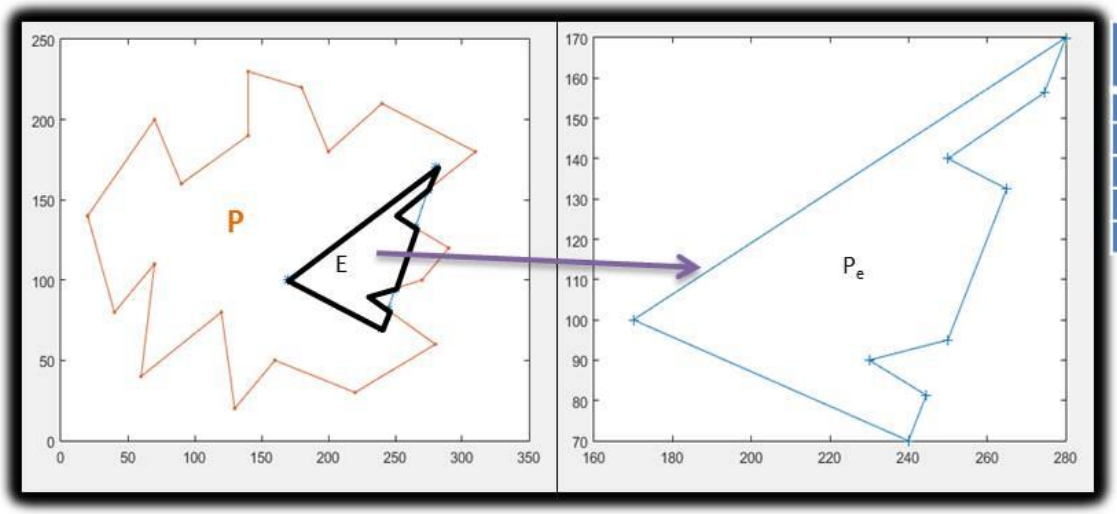

Intersection Coordinates	
Y(m)	X(m)
274,545	156,364
265,000	132,500
250,000	95,000
244,516	81,290

Figure 10. New P_e parcel produced after intersection with P and E parcels

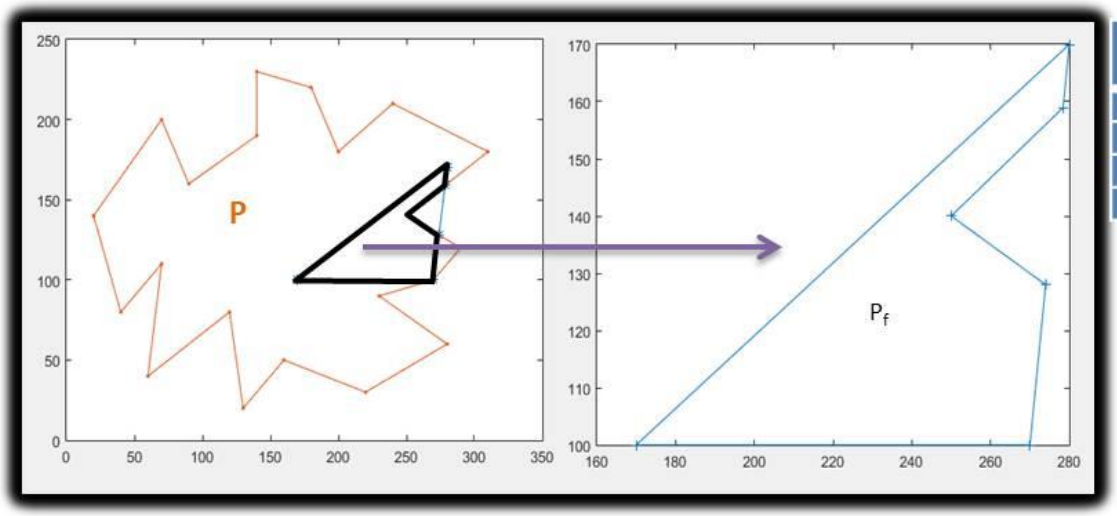

Intersection Coordinates	
Y(m)	X(m)
158,947	278,421
128,000	274,000
100,000	270,000

Figure 11. New P_f parcel produced after intersection with P and F parcels

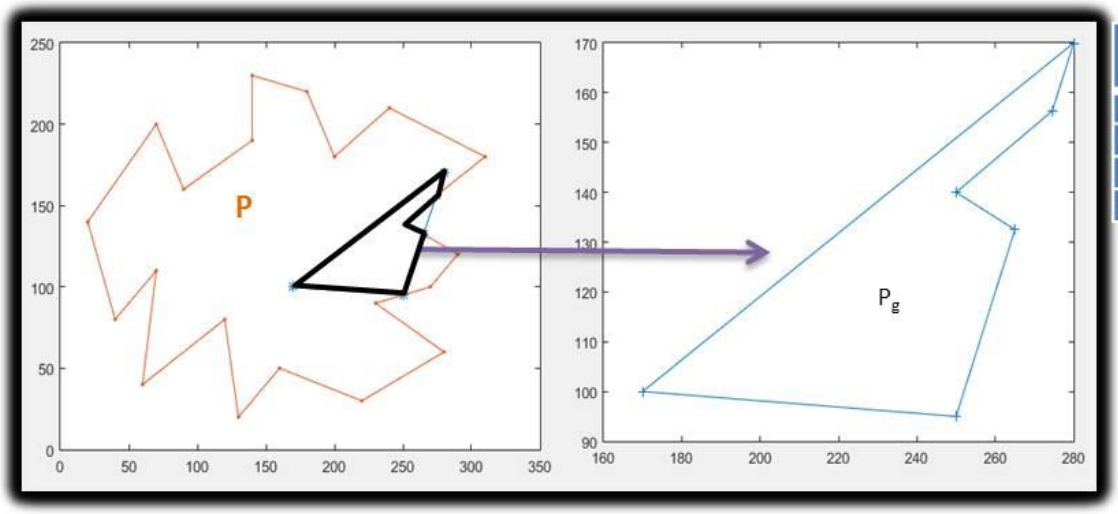

Intersection Coordinates	
Y(m)	X(m)
274,545	156,364
265,000	132,500
250,000	95,000

Figure 12. New P_g parcel produced after intersection with P and G parcels

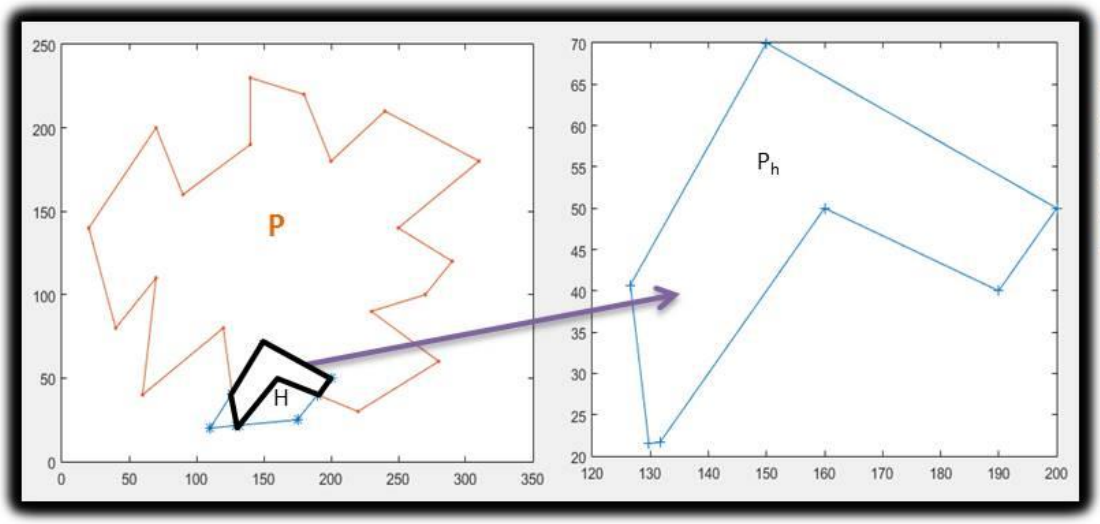

Intersection Coordinates	
Y(m)	X(m)
40,000	190,000
21,667	131,667
21,519	129,747
40,689	126,552

Figure 13. New P_h parcel produced after intersection with P and H parcels

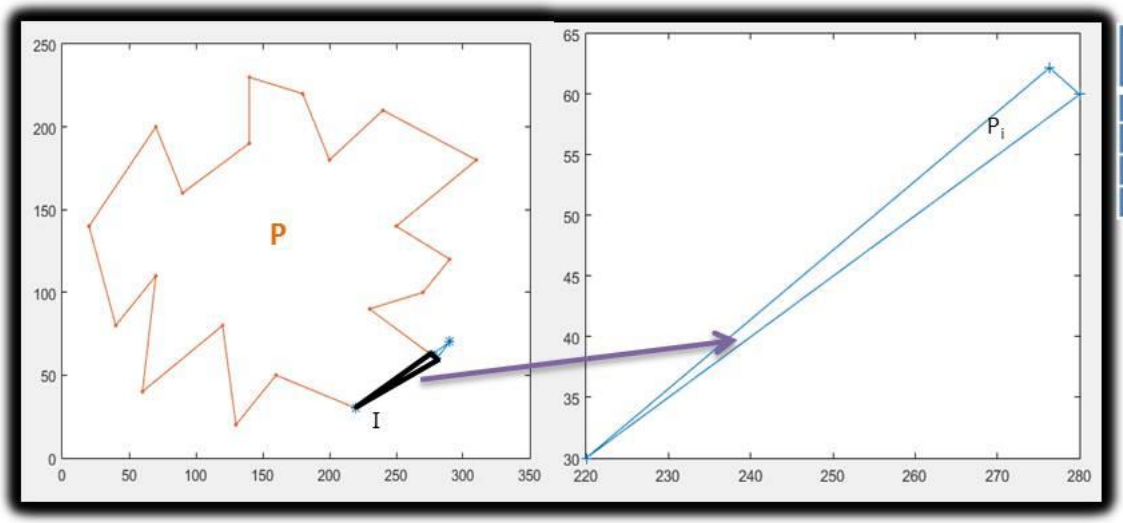

Intersection Coordinates	
Y(m)	X(m)
276,341	62,195
280,000	60,000
220,000	30,000

Figure 14. New P_h parcel produced after intersection with P and H parcels

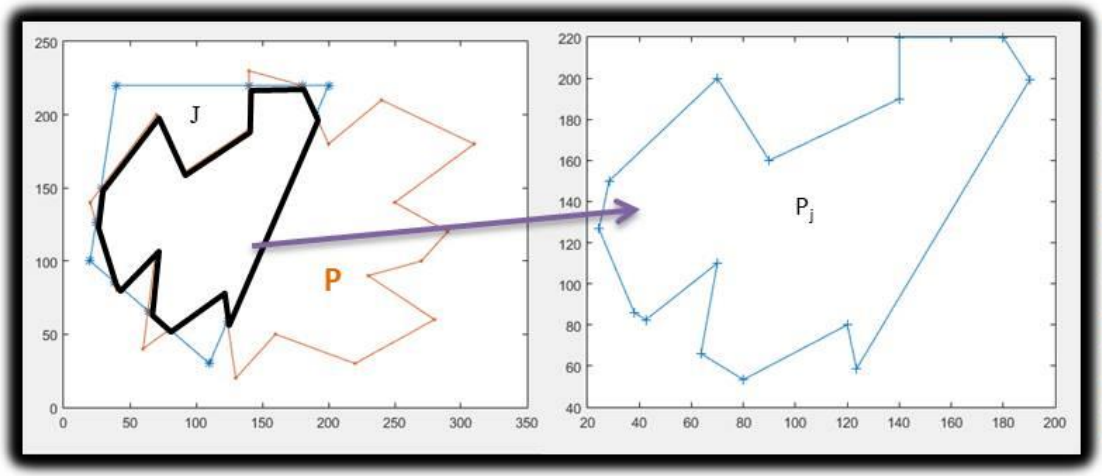

Intersection Coordinates	
Y(m)	X(m)
28,334	150,000
140,000	220,000
180,000	220,000
190,270	199,460
123,562	58,630
80,000	53,334
63,714	66,000
42,500	82,500
38,000	86,000
24,445	126,667

Figure 15. New P_j parcel produced after intersection with P and J parcels

2.4. Comparison with GIS Software

In this study, the operation steps for the area calculation of the polygon formed as a result of the intersection of two parcels have been also applied in the ArcGIS software. Applications on all selected parcels in the special cases described above have been made using ArcGIS (clip command) software. The results have been compared (Figure 16).

In this study, the operation steps for the area calculation of the common polygon formed as a result of the intersection of two parcels were also performed in

ArcGIS software (Table 3). Both methods give error-free results for the special cases. While area and intersection coordinates are calculated in ArcGIS software, the corner coordinates of the parcel consisting of intersection are not automatically presented to the user in an ordered manner. However, with the effort of the user, the ordered corner coordinates of the parcel can be obtained. This causes time loss and user errors. It is sufficient to give the corner coordinates of only two parcels as input data to the algorithm developed in this study. With the help of the developed algorithm, the intersection points of the main parcel and the selected parcel are automatically obtained and presented to the user.

Table 3. Coordinates of the corner points of the parcels to be intersected

Parcels	Area (m²)
A	242,424
B	461,905
C	254.546
D	1280,000
E	3761,841
F	3102,107
G	2860,229
H	1341,628
I	120,730
J	14726,000

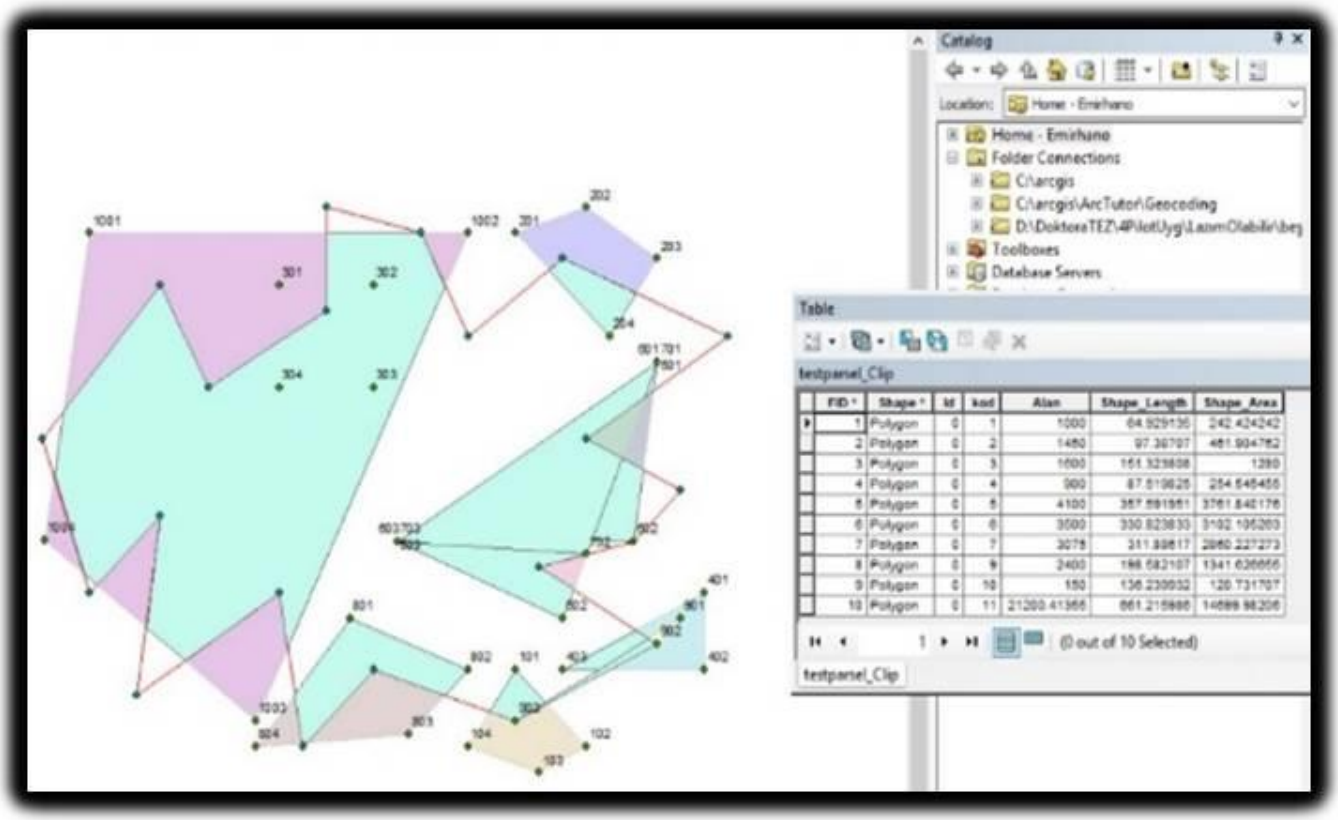

Figure 16. Representation and analysis of the application made in ArcGIS software

3. RESULTS and DISCUSSIONS

It is aimed to determine the common polygon formed by two overlapping convex or concave parcels and to calculate the corner coordinates and area of this polygon in this study. In this context, an algorithm has been developed considering special variables. With the help of the developed algorithm, the intersection of a main parcel selected with different parcels with ten different special conditions was examined. The corner points and area of the common parcel formed as a result of the intersection were found. The results obtained were compared with the results obtained from the ArcGIS software by applying the same process steps. Areas and intersection coordinates gave consistent results with millimeter precision. Corner points should be numbered consecutively for the area calculation of the parcel formed as a result of the intersection. This process step is determined by the user in CAD software. A method that can produce results by sequentially ordering the corner points of concave and convex parcels without the need for the user is presented to the users.

The dynamic nature of CAD and GIS software used in surveying and mapping applications allows users to make a patch program to fix a defect detected in these programs or a later error. It provides great contributions to the users in determining the corner point coordinates and area values without the need for the user, especially during the expropriation and zoning applications, which are among the survey and map applications, during the determination of the current status of the parcels before and after the implementation and the calculation of the area values. Using the algorithm developed in this context will minimize both time loss and user errors caused by point and parcel selection.

Author contributions

Emirhan Özdemir: Conceptualization, Methodology, Software**; Faruk Yıldırım:** Data curation, Writing-Original draft preparation, Software, Validation; **Fatih Kadı:** Visualization, Investigation, Writing-Reviewing and Editing.

Conflicts of interest

The authors declare no conflicts of interest.

REFERENCES

Barsky B A & Liang Y D (1984). A New Concept and Method for Line Clipping, ACM Transactions on Graphics, 3(1), 1–22.

Cyrus M & Beck J (1978). Generalized Two- and Three-Dimensional Clipping, Computers &Graphics, 3(1), 23–28.

Day J D (1992). A New Two-Dimensional Line Clipping Algorithm for Small Windows, Computer Graphics Forum, 11(4), 241–245.

Greiner G & Hormann K (1998). Efficient Clipping of Arbitrary Polygons, ACM Transactions on Graphics, 17(2), 71–83.

Huang C W & Shih T Y (1997). On The Complexity of Point-in-Polygon Algorithms, Computers & Geosciences, 23(1), 109-118.

Huang Y Q & Liu Y K (2002). An Algorithm for Line Clipping against a Polygon Based on Shearing Transformation, Computer Graphics Forum, 21(4), 683–688.

Jianqiang H, Jianzhi S, Yi C, Qiang C & Li T (2018). Tan Optimal Reliable Point-in-Polygon Test and Differential Coding Boolean Operations on Polygons Symmetry, 10, 477-503.

Kitay M G (1985). Land Acquisitionin Developing Countries, Lincolh İnstitue, Boston, Usa.

Maillot P G (1992). A New, Fast Method for 2D Polygon Clipping: Analysis and Software Implementation, ACM Transactions on Graphics, 11(3), 276–290.

Möller T (1997). A Fast Triangle-Triangle Intersection Test, Journal of Graphics Tools, 2(2), 25–30.

Nicholl T M, Lee D T & Nicholl R A (1987). An Efficient New Algorithm for 2-D Line Clipping: Its Development and Analysis, ACM SIGGRAPH Computer Graphics, 21(4), 253–262.

Taylor G (1994). Point in Poligon Test, Survey Review, 32(254), 479-484.

Sutherland I E & Hodgman G W (1974). Reentrant Polygon Clipping, Communications of the ACM, 17(1), 32–42.

Weiler K & Atherton P (1977). Hidden surface removal using polygon area sorting, ACM SIGGRAPH Computer Graphics, 11(2), 214–222.

Yanalak M & İpbüker C (2003). Hesaplamalı Geometri, Harita Dergisi, 129, 50-62.

Yomralıoğlu T (2000). Coğrafi Bilgi Sistemleri: Temel Kavramlar ve Uygulamaları, 5.Baskı (2009), s.480, ISBN 975-97369-0-X, İstanbul.

International Journal of Engineering and Geosciences
https://dergipark.org.tr/en/pub/ijeg
e-ISSN 2548-0960

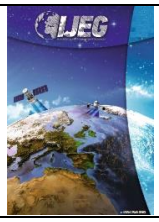

Assessment of shoreline change and its relation with Mangrove vegetation: A case study over North Konkan region of Raigad, Maharashtra, India

Barnali Das [1], Anargha Dhorde [*1]

[1]*Nowrosjee Wadia College, Department of Geography, Pune, India*

Keywords
Shoreline Change
DSAS
Mangroves
Remote sensing

ABSTRACT

Vulnerability of SLR varies from place to place with 20th century observing greatest threat to it. Mangroves along the shore are the one to first sustain this impact of SLR. In the present study, an attempt has been made to understand the relation between shoreline changes with mangrove habitat through remote sensing data and geospatial technique. Shoreline change rate has been calculated for the years 2000, 2012 and 2019, in Digital Shoreline Analysis System by End Point Rate. Change analysis indicates that in last 20 years erosion dominated the study area with an average rate of -0.02m/yr. During 2000 to 2012, relatively higher erosional rates (-0.35m/yr) were observed. While from 2012 to 2019 accretion process dominated this area with a rate of 0.43m/yr. Sonakothakar, Mothe Bhal and Dadar with denudation, have observed landward progradation of mangroves whereas, at Aware, a zone of accretion exhibited a seaward progradation of mangroves. A direct relation with the shoreline change has been observed with mangrove habitat. Mangroves are consider as salt feeder and so spatial changes in their colony is ought to be frequent in the present context of climate change and SLR. This type of integrated study will help to understand active process over the shore and help to conserve mangrove habitat. Such regional scale studies should be carried out before implementing any coastal conservation projects.

1. INTRODUCTION

Shorelines are dynamic in nature and often respond to the changes in sea level. Global mean sea level (GMSL) was envisaged to be accelerating at considerable rate during 19th century with a further leap in its rate in 20th century (Church and White 2006). The speed of GMSL rise during 1900 to 2009 was estimated about 1.7 ± 0.2 mm/year which raise up to 3.2 ± 0.4mm/year at the end of 20th century (Mimura 2013). Vulnerability of Sea Level Rise (SLR) varies from place to place, with developing countries being much more susceptible to it (Dasgupta et al. 2009). In the Indian scenario east coast are much more vulnerable to erosion as compared to west coast, however, 36% of Maharashtra coast is under the process of erosion (Mohanty et al. 2017).

Mangroves thrive on mudflats along the shore intervene by numerous small inlets and creeks. Mangrove habitat is considered as a boon to mankind. However, mangrove habitat is under continuous threat of shoreline change. It was observed that during early Holocene period there was high SLR to which mangroves were able to withstand the effect however, this characteristic of withstanding varies time to time and from place to place (Woodroffe 1990). At places resilient nature of mangroves was noted that was attributed to the anthropogenic pressure and physiographic settings (Nitto et al. 2014). However, certain studies have shown that mangrove ecosystem is very dynamic in nature and they can even migrate landward in order to balance with SLR (McLeod and Salm 2006). Mangrove forest structure exhibits an interesting pattern of transition from

* **Corresponding Author**
(barnali25das@gmail.com) ORCID ID 0000-0002-6103-4656
*(anarghawakhare@gmail.com) ORCID ID 0000-0002-5678-7397

Cite this article
Das Barnali & Dhorde A (2022). Assessment of shoreline change and its relation with Mangrove vegetation: A case study over North Konkan region of Raigad, Maharashtra, India. International Journal of Engineering and Geosciences, 7(2), 101-111

Research Article / DOI: 10.26833/ijeg.912657
Received: 10/04/2021; Accepted: 12/05/2021

seaward fringe to land ward, with healthy strong tree near the sea to dwarf forest far inland (Feller et al. 2015).

SLR has eroded considerable parts of coast, wetlands and mudflats in India (Dwivedi and Sharma 2005). However, mangroves act as a stabilizer and protector to SLR, deforestation to which may boost up erosion rate like Alibag coast in Maharashtra (Vidya et al. 2015). Over last two decades it has been observed that mangroves in the study area have increased profusely. There is spatial expansion of mangrove habitat, along within patch increase in density (Das and Dhorde 2021). Over the time span mangrove colony expanded and became dense over the area. This change in the physiography of mangrove habitat do correspond to SLR. Impact of changing shoreline on mangrove vegetation needs to be addressed in order to understand the relation between the two. Thus, present study aims at understanding the relation of mangrove growth with shoreline change. The specific objectives set are i) Detecting the changes in Shoreline and ascertaining the zones of denudation and accretion and ii) assessing the growth/decline in mangroves within the selected patches.

2. STUDY AREA

Raigad district is located on the west coast of Maharashtra, India. This coast is intertwined by rocky and sandy coast. A number of creeks are also observed to have developed marsh ecosystem at places. Within these belts of mudflats and marshes, lining the creeks, clusters of Mangrove patches are observed. In the present study, mangrove patches are located around three main creeks namely, Karanja creek, Dharamtar creek and Rewas creek along with numerous minute creeks intervening the mangrove habitat. Various local newspaper articles cited that in the last two decades these mangrove clusters, especially along the northern Raigad, has shown exponential growth. A few patches of mangroves from the North Raigad region are selected for the present study (fig 1). The study area extends between 18° 53' 12.28"N and 18° 45' 16.2"N latitudes, and 72° 52' 14"E and 73° 1' 42.2"E longitudes. In Raigad there are 11 true mangrove species and 15 mangrove associates (Mhatre et al. 2013).

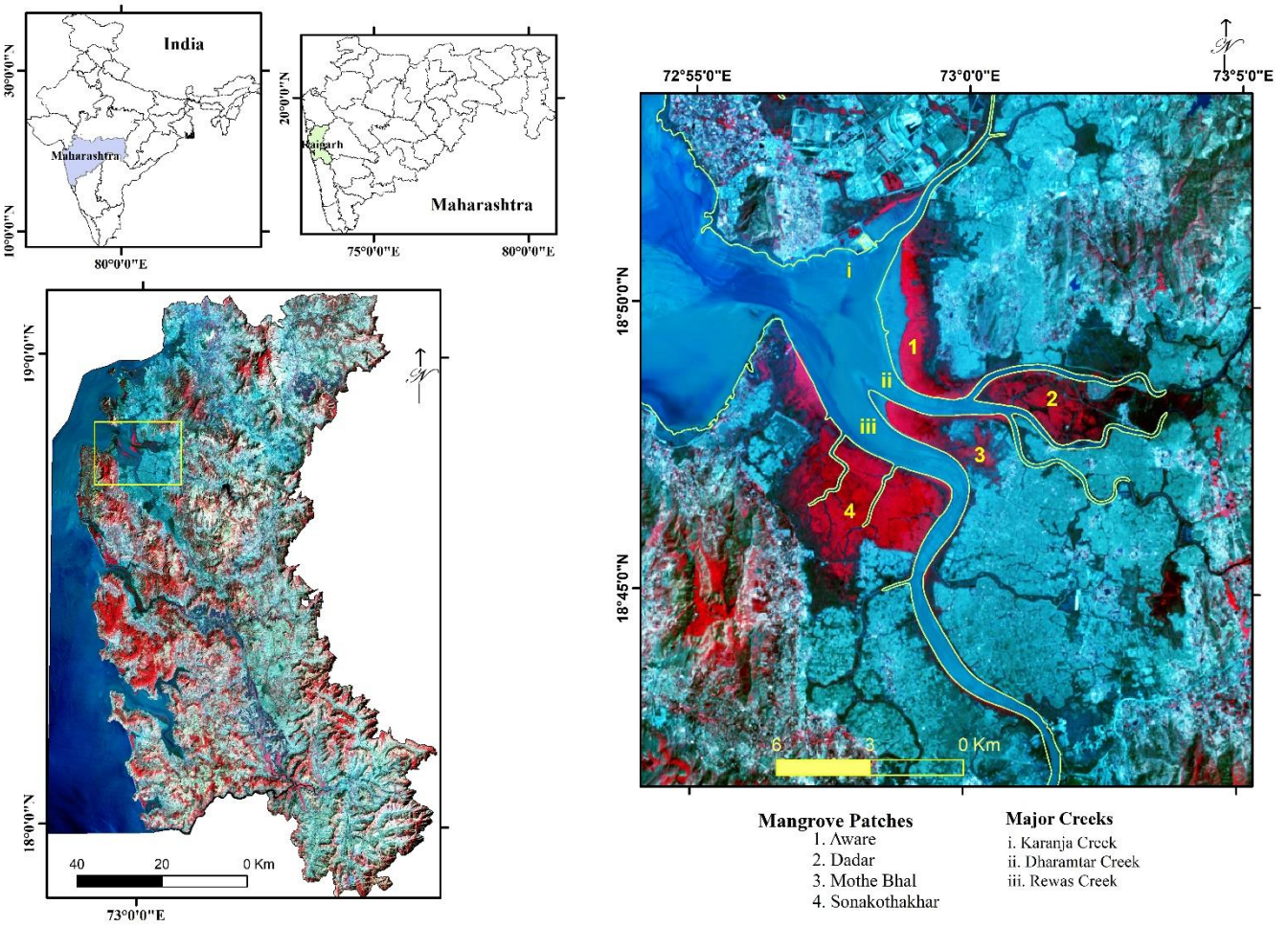

Figure 1. Location map

3. DATA & METHOD

3.1. Data Base

Since shorelines are highly dynamic and exposure of mangroves depends upon the tidal conditions, the level and condition of tides during satellite pass has to be taken into consideration. Table 1 presents the dates and tidal condition selected for retrieving the satellite images. All the images taken into consideration depicts ebbing condition which might give maximum exposure of the land. Moreover, delineation of the land-water

boundary would yield better results. Landsat 7 ETM+ and Landsat 8 OLI data have been downloaded from USGS Earth Explorer site. For the study, pre-monsoon season of the year 2000, 2012 and 2019 have been taken into consideration. All the data are cloud free.

Table 1: Detail of Dates selected and Tide condition for each scene

Date & Year	Satellite & Sensor	Approx. Satellite Pass time	Time	Tide Level	Tide Stage
13/04/2000	Landsat 7 TM (Level II)	10:37am	12:29pm	0.72	Ebbing
14/04/2012	Landsat 7 TM (Level I)	10:37am	11:13am	1.40	Ebbing
25/03/2019	Landsat 8 OLI (Level II)	10:37am	10:58am	0.96	Ebbing

3.2. Image processing

Image pre-processing was carried out for all the images wherein the images were subjected to geometric and radiometric corrections. The image of 2012 was processed for image correction as it had problem of scan line error. This problem was fixed with the help of Landsat toolbox plugin in ArcGIS. Sacn line error has been fixed separately for all the bands. Post processing was carried out over the images for layer stacking and obtaining certain indices which were essential for further analysis. Green (G), Red (R), Near Infra-Red (NIR) and Shortwave Infra-Red (SWIR) bands were layer stacked to derive False Color Composite (FCC) image for respective years (fig 2a,2b and 2c). Various band combiation and ratios were deployed to derive indices like

Normalized Difference Vegetation Index (NDVI),

$$NDVI = \frac{NIR - R}{NIR + R} \quad (1)$$

Normalized Difference Moisture Index (NDMI),

$$NDMI = \frac{NIR - SWIR}{NIR + SWIR} \quad (2)$$

Normalized Difference Water Index (NDWI)

$$NDWI = \frac{G - NIR}{G + NIR} \quad (3)$$

Table 2. Tasseled cap coefficients for Landsat 7 ETM+ (Huang et al. 2002)

Index	Band 1	Band 2	Band 3	Band 4	Band 5	Band 7
Brightness	0.3561	0.3972	0.3904	0.6966	0.2286	0.1596
Greenness	-0.3344	-0.3544	-0.4556	0.6966	-0.0242	-0.2630
Wetness	0.2626	0.2141	0.0926	0.0656	-0.7629	-0.5388

Table 3. Tasseled cap coefficients for Landsat 8 OLI (Baig et al. 2014)

Index	Band 2	Band 3	Band 4	Band 5	Band 6	Band 7
Brightness	0.3029	0.2786	0.4733	0.5599	0.5080	0.1872
Greenness	-0.2941	-0.2430	-0.5424	0.7276	0.0713	-0.1608
Wetness	0.1511	0.1973	0.3283	0.3407	-0.7117	-0.4559

All the indices were computed in ArcGIS 10.3.1. Separation of land pixel to that of water pixel yield shoreline. Shoreline delineation from satellite image is difficult task as the pixel represents mixed spectra of features. Remote sensing based indices like NDVI, NDMI, TC and NDWI yields better result as far as discrimination of various features are concern. NDVI index quantify the pixel based on the presence of greenness. Its range varies from +1 to -1 with negative value indicating absence of vegetation and positive range indicating presence of vegetation. NDMI quantify the pixel based on the moisture content and many times yield better result as conmpared to NDVI (Wilson and Sader 2002). TC with the help of the coeeficient given in Table 2 and 3, calculate Brightness, Greenness and Wetness of a scene for Landsat 7 and Landsat 8 respectively. Brightness is associated with bare land surface, Greenness is associated with vegetation cover and Wetness indicates soil moisture content (Huang et al. 2002). NDWI index enhance water features by subduing soil and other terrestrial features (Mcfeeters 1996). Images derived from these indices enhance different features and thus objects can be segregated and classified.

In order to delineate the shoreline and obtain the erosional and depositional rates along the shoreline, Digital Shoreline Analysis System (DSAS) was employed.

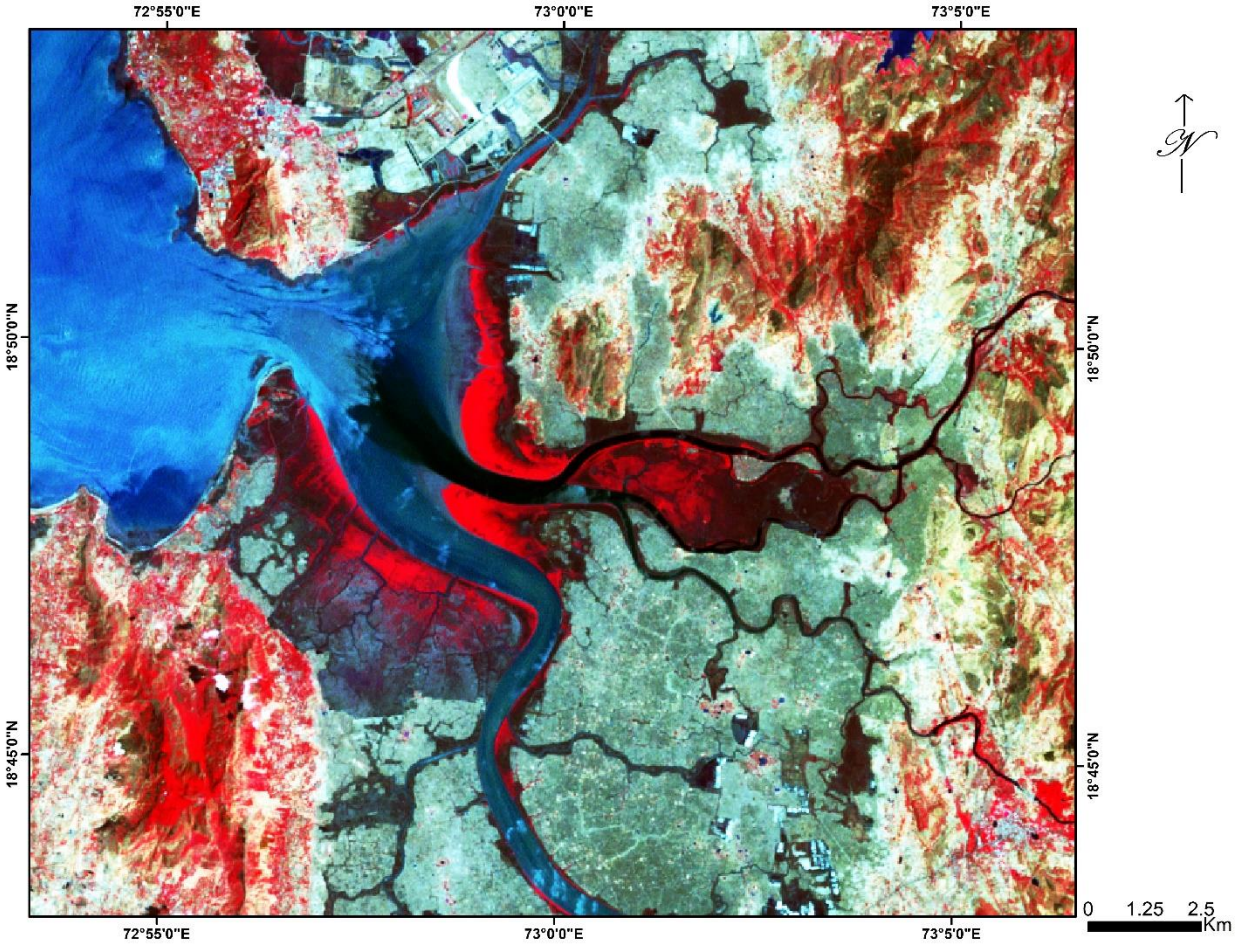
72°55'0"E
73°0'0"E
73°5'0"E
18°50'0"N
18°45'0"N
N
0 1.25 2.5
Km

(a)

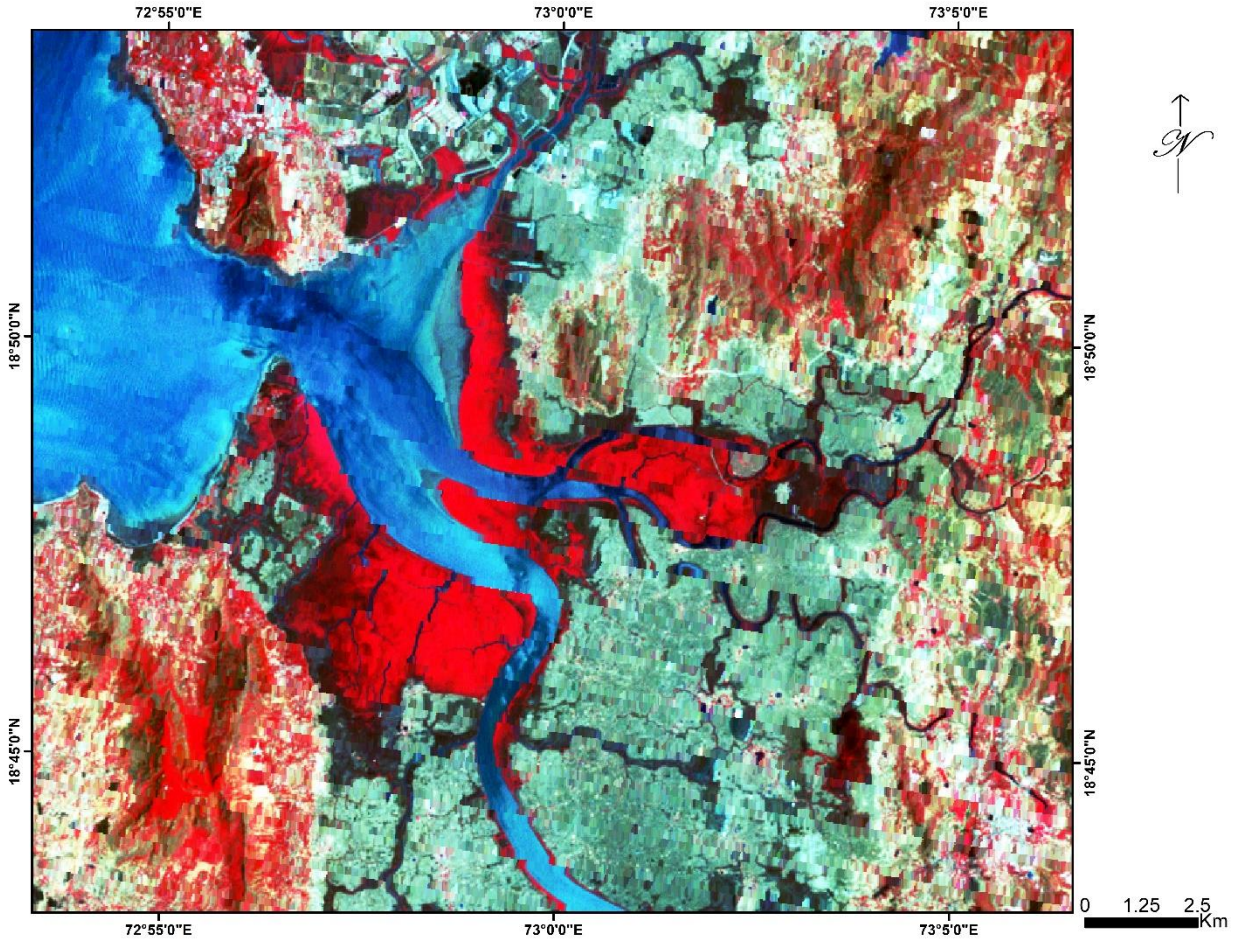
72°55'0"E
73°0'0"E
73°5'0"E
18°50'0"N
18°45'0"N
N
0 1.25 2.5
Km

(b)

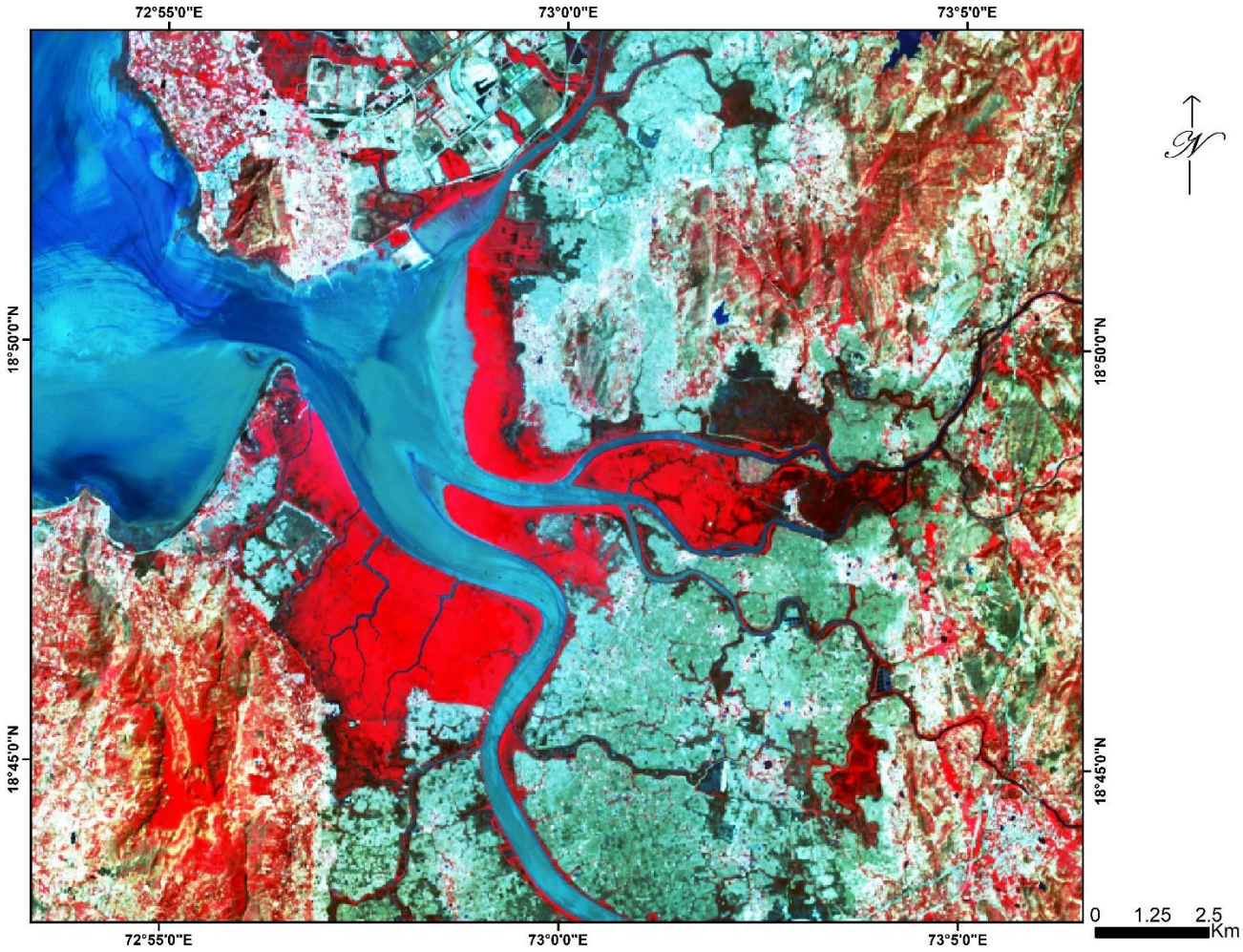

(c)

Figure 2. False Color Composite image of **(a)** 2000, **(b)** 2012 and **(c)** 2019

3.3. Shoreline Extraction and Rates calculation

The general methodology adopted for the present study is outlined in figure 3. Manual digitization was performed on FCC image to obtain shoreline. For automated shorelines DSAS plugin which is an extension of Arc GIS has been employed. The unsupervised Iterative Self Organized Data Analysis (ISODATA) clustering algorithm is consider as highly accepted and successful method to classify complex areas (Braud and Feng 1998). In the present study, an attempt has been made to classify the combined image i.e. NDVI_TC, NDMI _TC and NDWI image with help of ISODATA approach. This classifies raster images are then converted to binary image of only two class i.e., land and sea. Vector to raster conversion then applied on binary image to generate line that abut land and water.

For each raster image i.e., NDVI_TC, NDMI _TC and NDWI a separate shoreline has been derived. These shorelines were then compared with the manually digitized shorelines to obtain the deviation statistics (Table 4). Shoreline with minimum deviation in respective year was taken into consideration for further work of change detection analysis (fig 4). It has been observed that shoreline generated on NDVI-TC combined image has minimum deviation of 0.23 m and 0 m for the year 2000 and 2012 respectively. Whereas, for the year 2019 NDMI-TC combined image generates shoreline with the minimum deviation of 0.03 m. Rate of changes along the selected stretches of shoreline were obtained in the DSAS software. Keeping the time section into consideration, automated shoreline for two years has been merged for further rate calculation i.e. 2000-2019, 2000-2012 and 2012-2019. Baseline plays an important role in rate calculation. Baseline has been generated with 150m buffer from the merged automated shoreline. DSAS employ several perpendicular transect from a baseline (in this study 150m away from the merged automated shoreline) and records point of intersection between transect and shorelines for different years. The transect is of 1000 m in length with 100 m spacing. As an example, to transect and baseline year 2000-2019 has been shown (fig 5). DSAS automatically calculate several statistical methods for shoreline change viz. End Point Rate (ERP), Jackknife Rate (JKR), Linear Regression Rate (LRR), Shoreline Change Envelope (SCE), Net Shoreline Movement (NSM), Least Median of Square (LMS) and Weighted Linear Regression (WLR). All these methods have some advantages and disadvantages. In the present study shoreline change by ERP rate is taken into consideration as for relatively small data it gives good results (Esmail et al., 2019). Moreover, it shows normal distribution and is simple and universally prevalent method (Nassar et al. 2018).

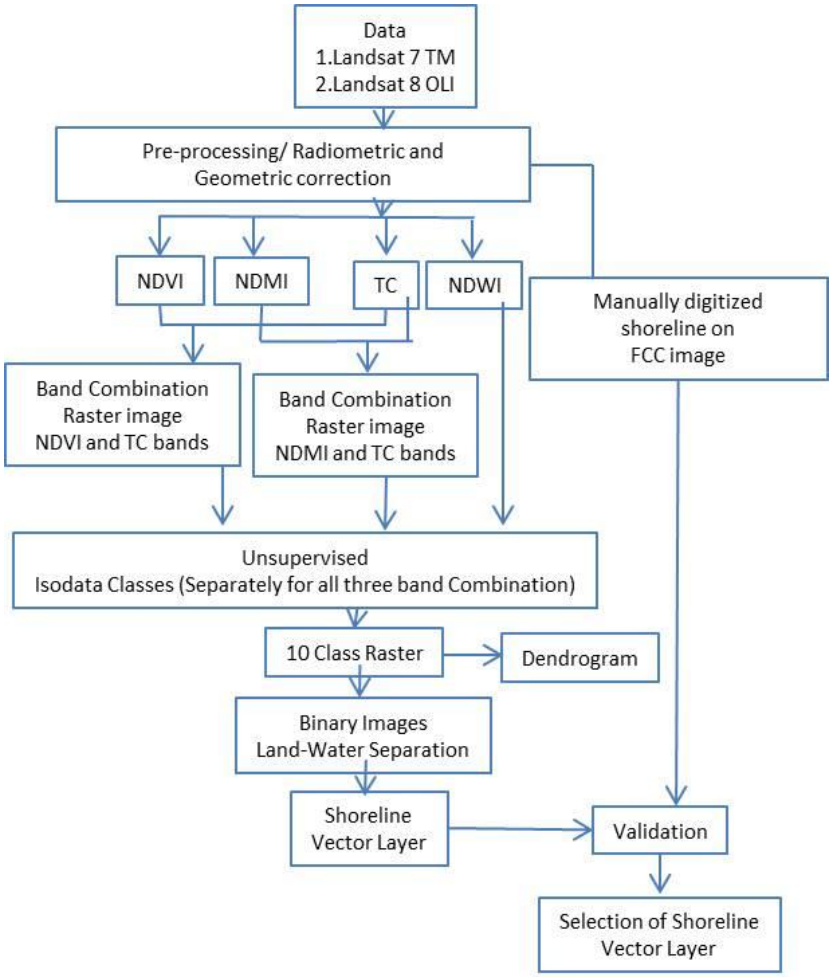

Figure 3. Methodology for Shoreline Extraction

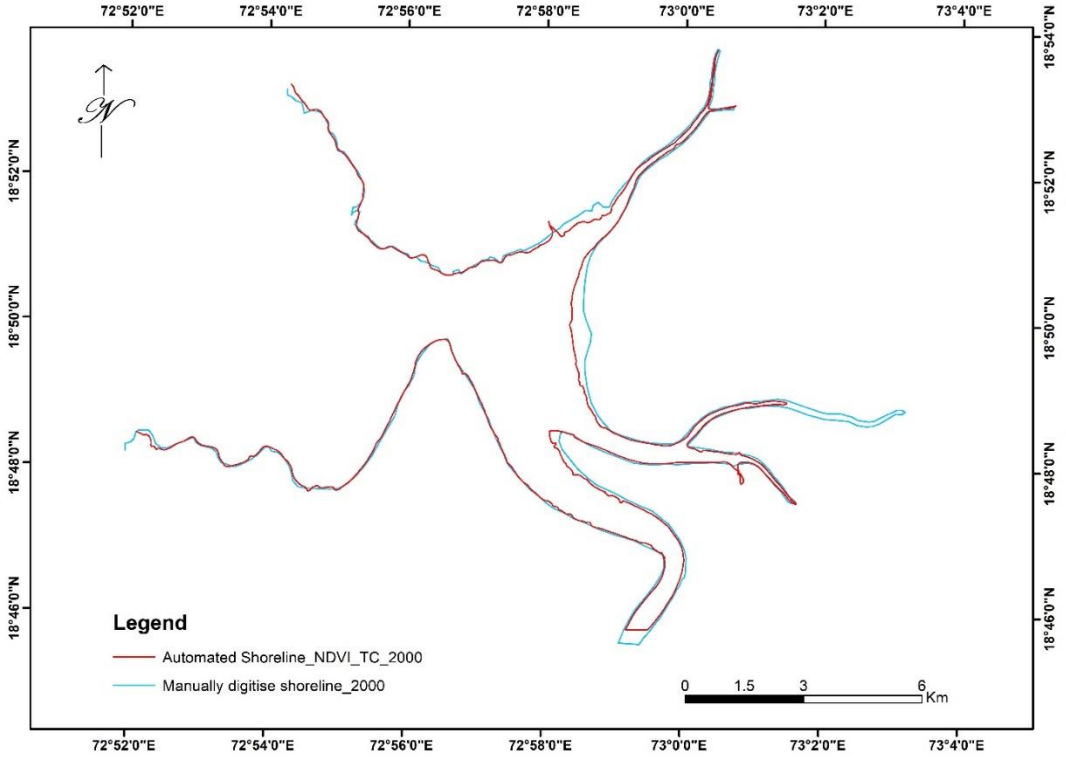

(a)

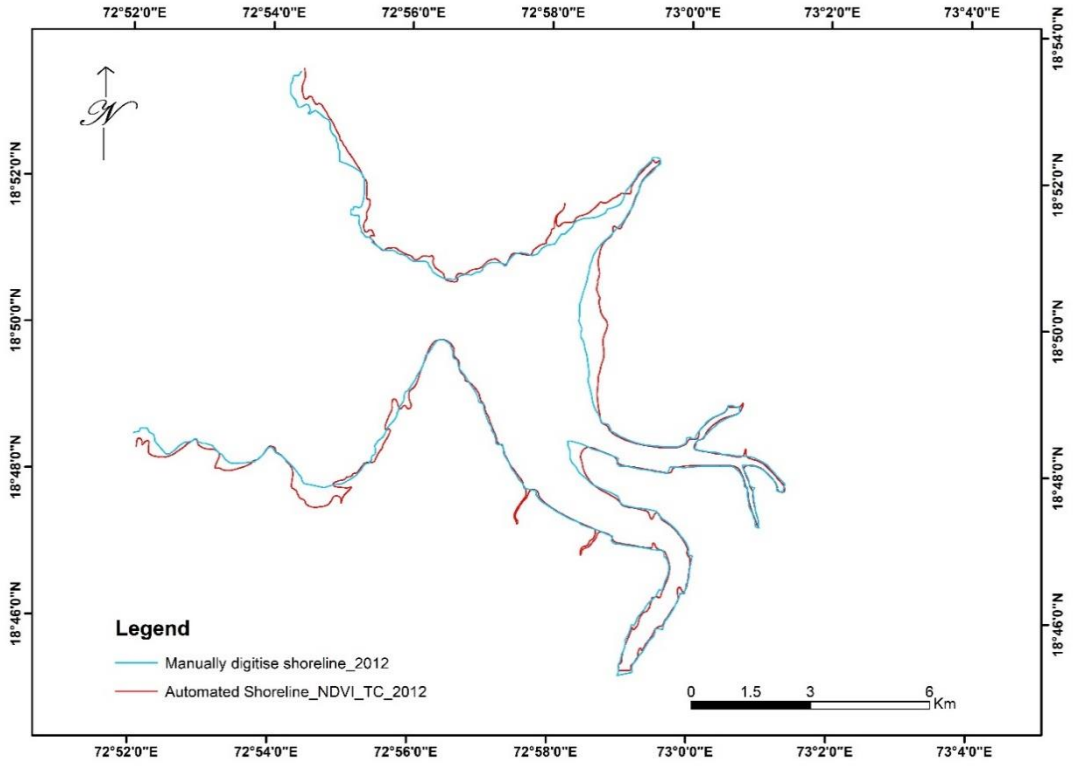

(b)

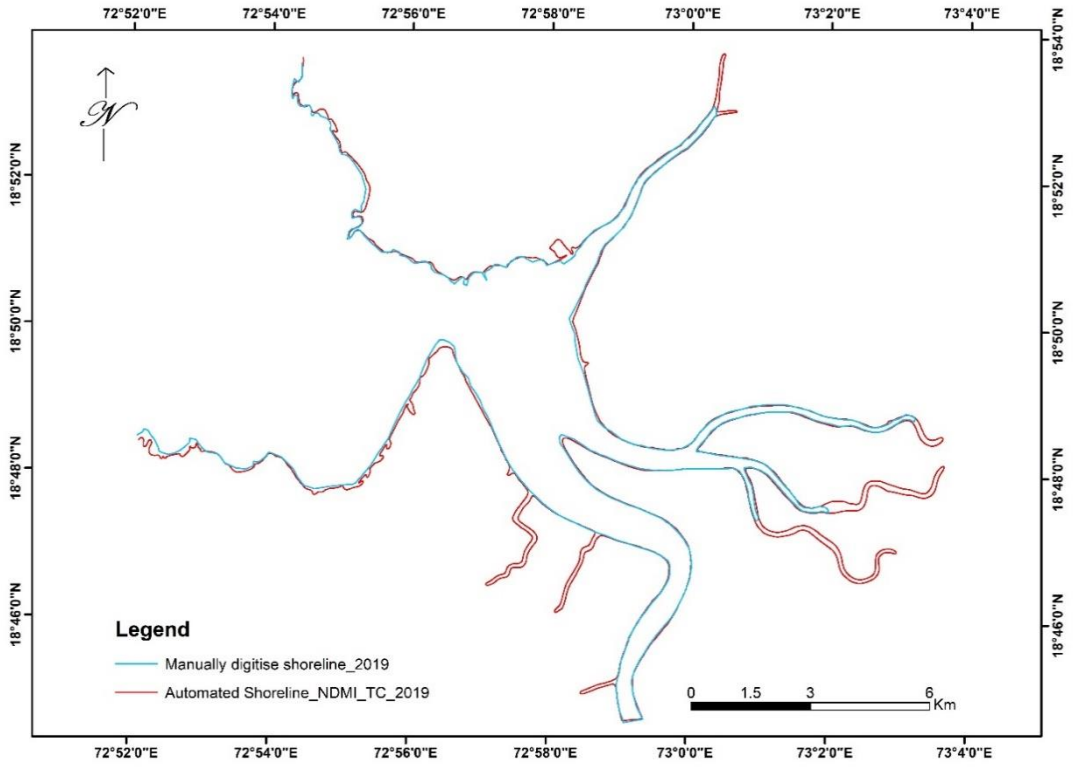

(c)

Figure 4. Shoreline with minimum deviation from manually digitize Shoreline (a) NDVI TC 2000, (b) NDVI_TC 2012 and (c) NDMI_TC 2019

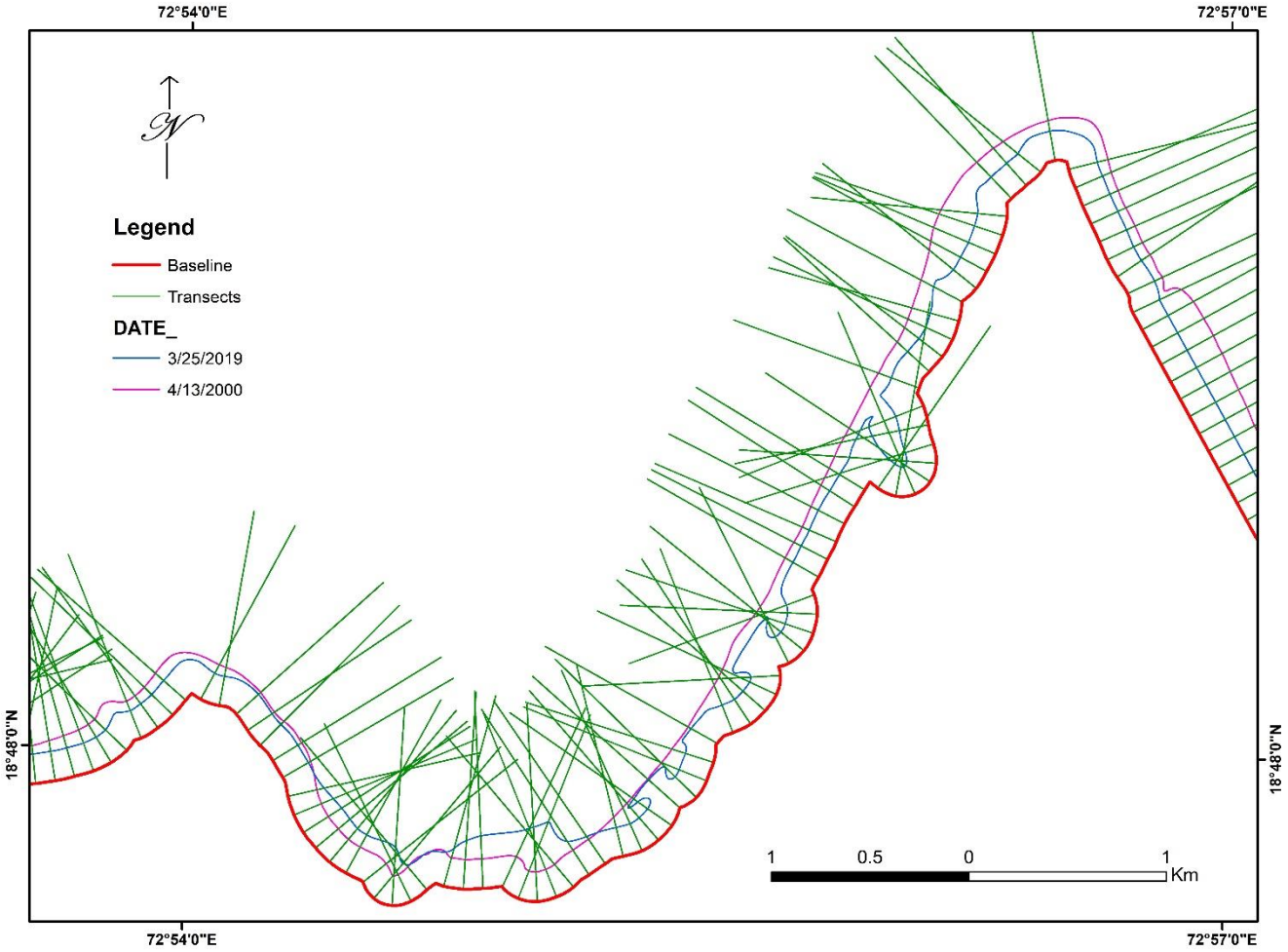

Figure 5. Transect along the baseline for the year 2000-2019

Table 4. Within pair difference between manually created shoreline and other methods.

Method	Deviation from Manually Digitized Shoreline		
	2000	2012	2019
NDWI	Min = 0.62 Mean=210.85 Max=999.18	Min = 0.17 Mean=256.38 Max=998.28	Min = 0.06 Mean=324.86 Max=999.73
NDVI_TC	Min = 0.23 Mean=243.3 Max=998.47	Min = 0.00 Mean=236.50 Max=999.83	Min = 0.14 Mean=151.20 Max=997.78
NDMI_TC	Min = 0.54 Mean=339.77 Max=999.64	Min = 0.32 Mean=386.98 Max=999.73	Min = 0.03 Mean=143.40 Max=998.91

4. RESULTS & DISCUSSION

Shoreline change analysis for the present study has been carried over a span of 20 years ranging from 2000 to 2019. A time sectional analysis was also attempted between 2000 to 2012 and 2012 to 2019. Change detection analysis of the study area indicated that the shoreline has undergone both accretion and denudation process in last 20 years. Transects demarcated for accretion and denudation rates, indicates that almost 70.99% of the area has undergone erosion during the entire study period (2000 to 2019). While, almost 71.41% (2000 to 2012) and 67.79% (2012 to 2019) of the transects were subjected to erosion. However, during 2012 to 2019 it was observed that although 67.79% area was under erosion but the rate of erosion was relatively less than the rate of accretion.

Change analysis indicated that in the last 20 years erosion process dominated over the study area with an average rate of -0.02m/yr. During 2000 to 2012, erosion rate was high with -0.35m/yr whereas, from 2012 to 2019 accretion process dominated over denudation with a rate of 0.43m/yr (fig 6). Overlay of NDVI for mangrove patches clearly depicts that mangrove colony have undergone changes. During 2000 to 2019 it has been observed that overall NDVI value leap up spatially. İn the year 2000 NDVI value about < 0.4 dominate spatially over the patches whereas in the year 2019 NDVI value about <0.8 dominate the mangrove patches. Year 2012 shows a slow transition in NDVI value indicating healthy mangrove habitat.

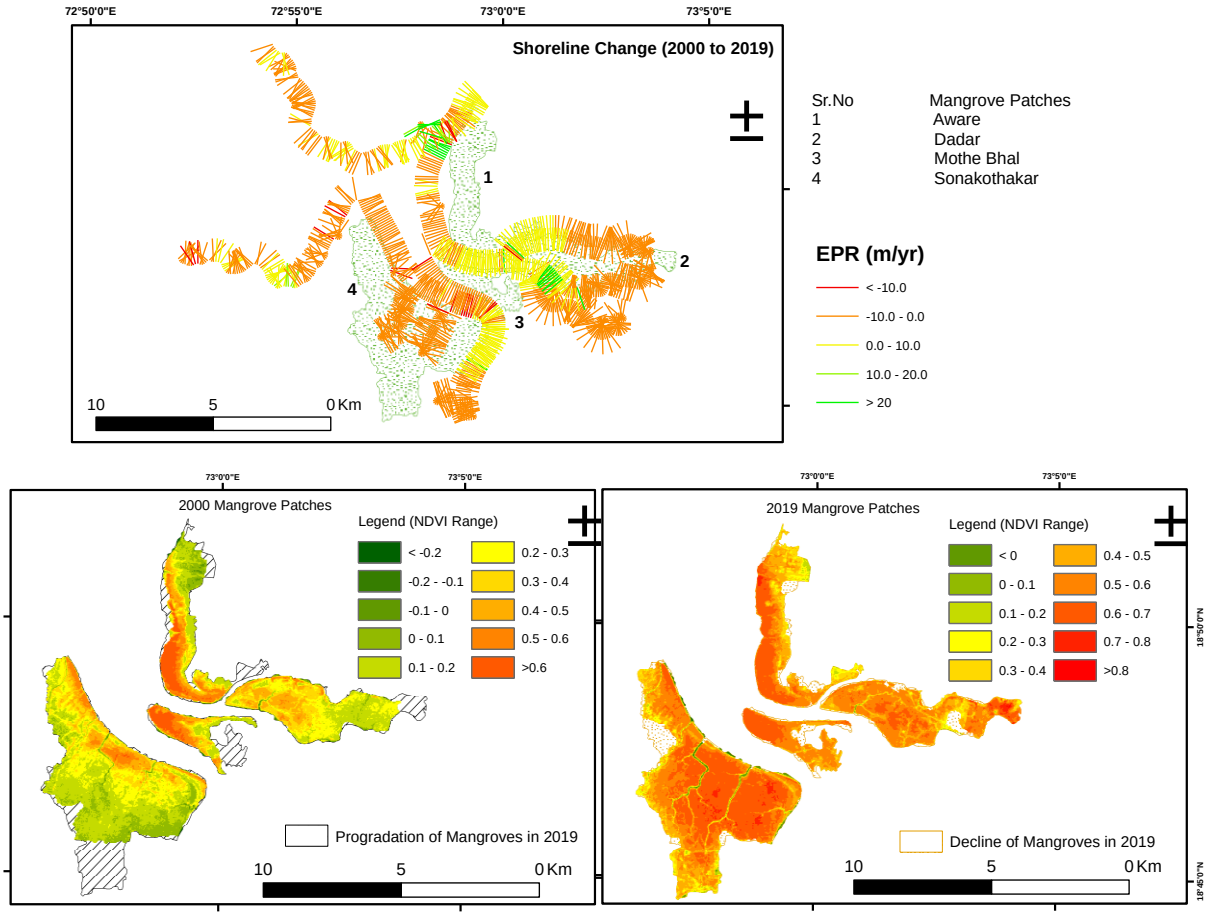
72°50'0"E
72°55'0"E
73°0'0"E
73°5'0"E
Shoreline Change (2000 to 2019)
Sr.No Mangrove Patches
1 Aware
2 Dadar
3 Mothe Bhal
4 Sonakothakar
EPR (m/yr)
< -10.0
-10.0 - 0.0
0.0 - 10.0
10.0 - 20.0
> 20
10 5 0 Km
2000 Mangrove Patches
Legend (NDVI Range)
< -0.2
-0.2 - -0.1
-0.1 - 0
0 - 0.1
0.1 - 0.2
0.2 - 0.3
0.3 - 0.4
0.4 - 0.5
0.5 - 0.6
>0.6
Progradation of Mangroves in 2019
2019 Mangrove Patches
Legend (NDVI Range)
< 0
0 - 0.1
0.1 - 0.2
0.2 - 0.3
0.3 - 0.4
0.4 - 0.5
0.5 - 0.6
0.6 - 0.7
0.7 - 0.8
>0.8
Decline of Mangroves in 2019

(a)

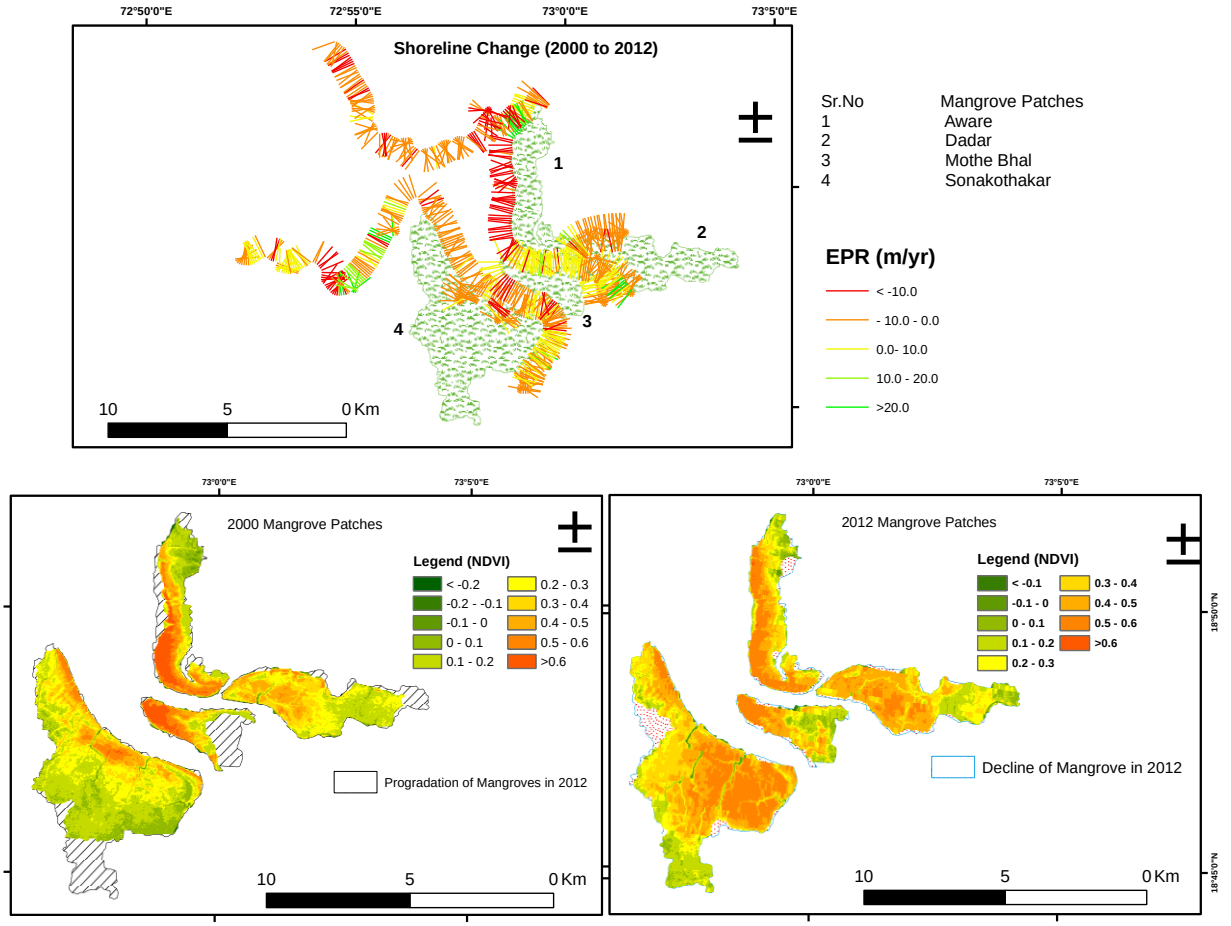
72°50'0"E
72°55'0"E
73°0'0"E
73°5'0"E
Shoreline Change (2000 to 2012)
Sr.No Mangrove Patches
1 Aware
2 Dadar
3 Mothe Bhal
4 Sonakothakar
EPR (m/yr)
< -10.0
- 10.0 - 0.0
0.0- 10.0
10.0 - 20.0
>20.0
10 5 0 Km
2000 Mangrove Patches
Legend (NDVI)
< -0.2
-0.2 - -0.1
-0.1 - 0
0 - 0.1
0.1 - 0.2
0.2 - 0.3
0.3 - 0.4
0.4 - 0.5
0.5 - 0.6
>0.6
Progradation of Mangroves in 2012
2012 Mangrove Patches
Legend (NDVI)
< -0.1
-0.1 - 0
0 - 0.1
0.1 - 0.2
0.2 - 0.3
0.3 - 0.4
0.4 - 0.5
0.5 - 0.6
>0.6
Decline of Mangrove in 2012

(b)

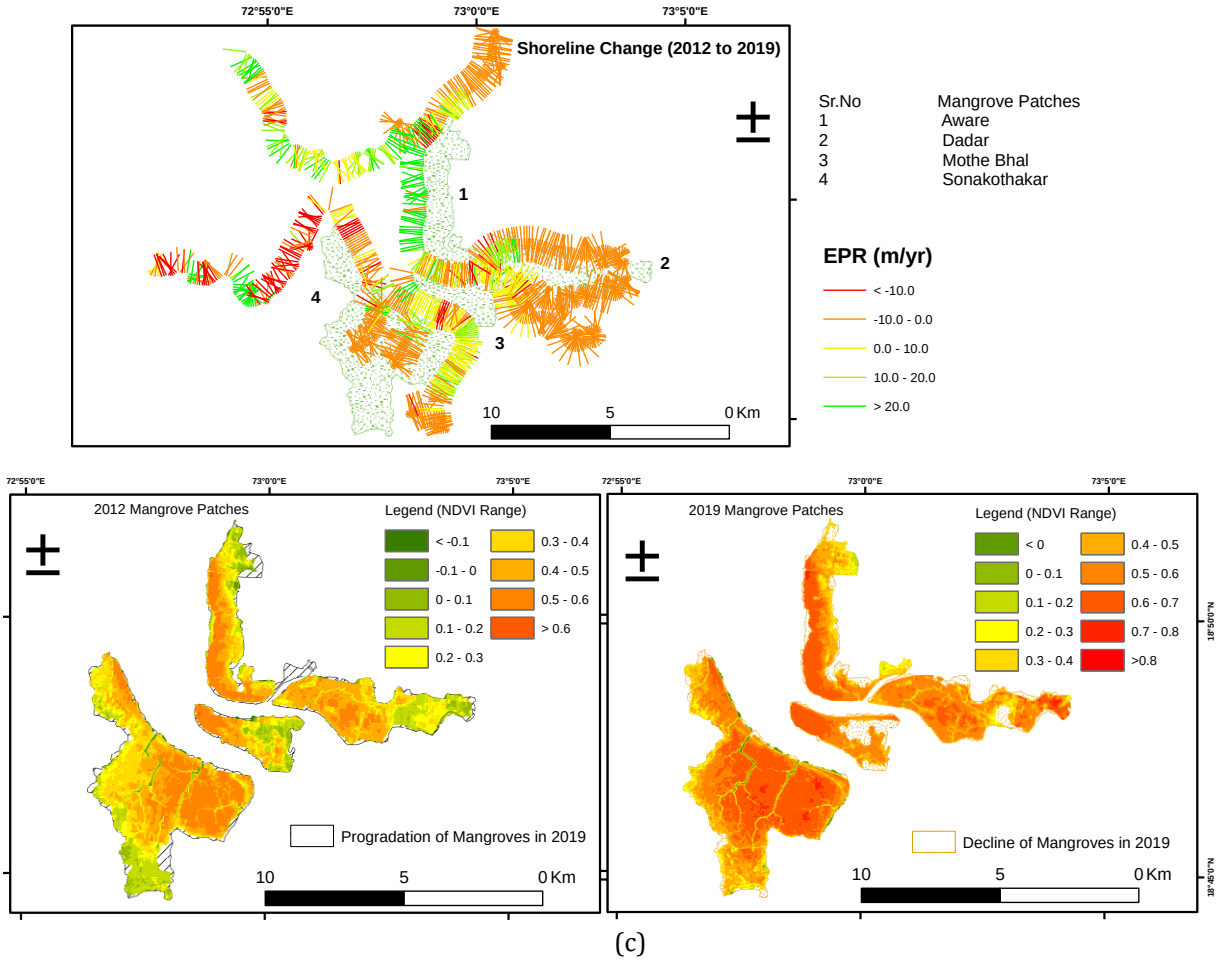

Figure 6. Shoreline change and Mangrove spatial extent transformation during **(a)** 2000-2019, **(b)** 2000-2012 and **(c)** 2012-2019

In the regions of denudation like Sonakothakar, Mothe Bhal and Dadar, it was observed that there is landward progradation of mangrove habitat whereas accretion dominated over Aware region with no major landward progradation but a seaward progradation was observed. This is mainly due to the stable shoreline as a result of accretion. NDVI values overall have risen from 0.6 to 0.8 during 2000 to 2019. However, steady inter patch transformation was observed during the time with major part of the patch reaching towards higher NDVI values. This leap in NDVI values during the time span indicates the healthy status of mangrove vegetation. Mangroves are salt tolerant species. Inland shift of shoreline often leads to saltwater penetration through soil and creeks, in such cases, mangroves then act as a feeder to salinity (Prerna et al. 2015; Lambs et al. 2015) which is reflected in their overall health status. Minor decline of the mangroves was also observed in the study area it is only because of anthropogenic pressure over the region.

5. CONCLUSION

The present study concludes that shoreline over north Konkan region is under immense impact of shoreline change with processes of accretion and denudation varying from time to time. Process of erosion increased over Sonakothakar, Mothe Bhal and Dadar whereas Aware observed accretion. This change has direct relation with mangrove habitat. Areas with denudation clearly witnessed an inland encroachment of mangrove vegetation over time whereas seaward progradation of mangroves was observed in the areas dominated by accretion processes. Over the time span, whether erosion or deposition zone, mangrove NDVI values exhibited an increasing trend indicating overall good health of the species. With intensified effect of climate change, sea level ought to increase, leading to landward migration of mangroves (Gilman et al. 2008). This type of integrated study not only will help to understand active process over the shore but also will help to conserve mangrove habitat. Such regional scale studies should be carried out before implementing any coastal conservation projects.

ACKNOWLEDMENT

This study is partly presented in "Intercontinental Geoinformation days (IGD) 2020.

Author contributions

Barnali Das: Conceptualization, Methodology, Analysis, Mapping, Compilation, Writing-Original draft and its preparation. **Anargha Dhorde:** Visualization, Checking draft and Editing.

Conflicts of interest

The work is original and authors declare no conflicts of interest.

REFERENCES

Baig MHA, Zhang L, Shuai T & Tong Q (2014). Derivation of a tasselled cap transformation based on Landsat 8 at-satellite reflectance. Remote Sensing Letters Vol 5, Pg 423-43.

Braud Jr, DH and Feng W, (1998). Semiautomated Construction of the Louisiana Coastline Digital Land/Water Boundary Using Landsat Thematic Mapper Satellite Imagery, Louisiana Applied Oil Spill Research and Development Program, OSRAPD Technical Report Series, 97-002.

Church J & White N (2006). A 20th century acceleration in global sea-level rise. Geophysical Research Letters, 33, L01602, doi:10.1029/2005GL024826

Das B & Dhorde A (2021). Geostatistical approach to assess mangrove spatial variability: a bi-decadal scenario over Raigarh coast of Maharashtra. Journal of Coastal Conservation, 25:23, https://doi.org/10.1007/s11852-021-00813-8

Dasgupta S, Laplante B, Meisner C, Wheeler D & Yan J (2009). The impact of sea level rise on developing countries: a comparative analysis. Climatic Change, 93, 379–388, DOI 10.1007/s10584-008-9499-5

Dwivedi D N & Sharma VK (2005). Analysis of Sea Level Rise and its Impact on Coastal Wetlands of IndiaProceedings of the 14th Biennial Coastal Zone Conference, New Orleans, Louisiana.

Gilman E L, Ellison J, Duke N C & Field C (2008). Threats to mangroves from climate change and adaptation options: a review. *Aquatic botany*, *89*(2), 237-250.

Esmaila M, Mahmoda W E & Fatha H (2019). Assessment and prediction of shoreline change using multi-temporal satellite images and statistics: Case study of Damietta coast, Egypt. Applied Ocean Research, 82, 274–282

Feller I C, Lovelock C E, McKee K L & Thompson R (2005) Variation in Mangrove Forest Structure and Sediment Characteristics in Bocas del Toro Panama. Caribbean Journal of Science. 41(3), 456-464.

Huang C, Wylie B, Yang L, Homer C & Zylstra G (2002). Derivation of a tasselled cap transformation based on Landsat 7 at-satellite reflectance. International Journal of Remote Sensing, Vol 23, Pg 1741-1748

Lambs L, Bompy F, Imbert D, Corenblit D & Dulormne M (2015). Seawater and Freshwater Circulations through Coastal Forested Wetlands on a Caribbean Island. Water. 7, 4108-4128, doi:10.3390/w7084108

Mcfeeters S K (1996). The use of the Normalized Difference Water Index (NDWI) in the delineation of open water features. International Journal of Remote Sensing, 17, 1425-1432

McLeod E & Salm R V (2006) Managing Mangroves for Resilience to Climate Change Gland, Switzerland, IUCN

Mhatre K, Singh R, Cerejo S & Shinde R (2013). Diversity of Mangroves in Raigad District, Maharashtra and need for their conservation. International Journal of Environmental Sciences, 2(4), 205-209. ISSN 2249-2127.

Mimura N (2013). Review Sea-level rise caused by climate change and its implications for society. Proceedings of Japan Academy, doi: 10.2183/pjab.89.281

Mohanty P C, Mahendra R S, Nayak R K & Kumar T S (2017). Impact of sea level rise and coastal slope on shoreline change along the Indian coast Natural Hazards, 89:1227–1238. DOI: 10.1007/s11069-017-3018-9

Nassar K, Mahmod W E, Fath H, Masria A, Nadaoka K & Negm N (2018). Shoreline change detection using DSAS technique: Case of North Sinai coast, Egypt. Marine Georesources & Geotechnology, DOI: 10.1080/1064119X.2018.1448912

Nitto D D, Neukermans G, Koedam N, Defever H, Pattyn F, Kairo J G & Dahdouh-Guebas F (2014) Mangroves facing climate change: landward migration potential in response to projected scenarios of sea level rise. Biogeosciences, 11, 857–871. doi:10.5194/bg-11-857-2014

Prerna R, Naidu V S, Sukumaran S & Gajbhiye S N (2015). "Observed decadal changes in extent of mangroves and coral reefs in southern Gulf of Kachchh using principal component analysis and geo-spatial techniques: a case study ". J Coast Conservation, 19, 257–267. DOI 10.1007/s11852-015-0385-9

Vidya, Biradar R S, Inamdar A B, Srivastava S & Pikle M (2015). Assessment of shoreline changes of Alibag coast (Maharashtra, India) using remote sensing and GIS. Journal of Marine Biology, 57 (2)

Wilson E H & Sader S A (2002). Detection of forest harvest type using multiple dates of Landsat TM imagery. Remote Sensing of Environment. 80, 385 – 396.

Woodroffe C D (1990). The impact of sea-level rise on mangrove shorelines. Progress in Physical Geography, 14, 483–520, 1990.

International Journal of Engineering and Geosciences
https://dergipark.org.tr/en/pub/ijeg
e-ISSN 2548-0960

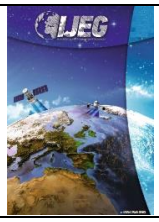

An analysis on the corrosion of a cultural heritage

Ömer Bozdoğan[1], Aydan Yaman*[2], Hacı Murat Yılmaz[2]

[1]*Map and Trade Limited Company of Bozdoğan, Aksaray, Turkey*
[2]*Aksaray University, Engineering Faculty, Department of Geomatics Engineering, Aksaray, Turkey*

Keywords
Corrosion
Cultural Heritage
Çanlı Church
Deformation
Photogrammetry

ABSTRACT

Many historical landmarks and cultural heritage are being constantly destroyed through natural events and human actions. It is important to conduct corrosion analysis and two and three-dimension documentation studies to restore and transfer these landmarks to the new generations. It is particularly important to record, keep these historical heritages digitally and take precautions against the potential corrosion due to the wars, natural disasters and climatic factors that continue to the present. In this study, the corrosion in Çanlı Church (ÇanlıKilise) located in Akhisar village of the province of Aksaray in Turkey was determined and the reasons were examined. By using close-range photogrammetry method, three-dimension models and facade charts of three facades (North, West, South) of Çanlı Church have been acquired, as a result of measurements performed in four different times (2006, 2010, 2016, 2019). Overlapping all these charts in the same scale, the corrosions occurred on the facades of Çanlı Church have been examined. The meteorological data within the period when the measurements were performed were reviewed. As a result, corrosion on the North, West and South facades of Çanlı Church have been found at the level of 8%, 3%, 13% respectively. It was concluded that the storm has greater effect on the corrosion.

1. INTRODUCTION

Cultural Heritage is a treasury that consists of individuals' histories and sustains the common spirit of comradeship and support among them. It documents the experiences the human beings have had throughout the history and ensures the proper building of the future as well as the continuity of the customs called tradition. Cultural heritage is the wealth of a country, for all these reasons (Korumaz et al. 2011). We should protect and take care of it not only for future generations but also for all humanity. It is still very hard even in the 21st century to protect and keep the cultural heritages as they are. The air pollution and seasonal changes, human activities and natural disasters pose a great potential threat for cultural heritages. Protection of cultural heritage is increasingly attracting attention worldwide (Ratnayake et al. 2018).

It is important to perform the maintenance and repairs of these still standing historical landmarks and explore the causes of corrosion, to pass them to the next generations (Bozdoğan and Yılmaz 2019).

Since the corrosion and degradation of the artifacts happen in a short time these landmarks should be examined for a long period and the potential changes should be examined (Demirkesen and Demir 2006).

Photogrammetry is frequently used to document cultural heritages (Yakar et al. 2015). As the digital technology progresses, close range photogrammetry has become more efficient and a cost-effective method (Yılmaz et al. 2000). 3D models and texture mapping help us in detecting the complex structures. (Atkinson 1996).

Ensuring the measure of unattainable or dangerous structures and too high or too low buildings is another major advantage of close-range photogrammetry. Regarding the documentation, this data can be used in the future, shared with other users and easily stored in the computer environment (Arias et al. 2005; Berndt and Carlos 2000; Desmond et al. 2003; Guidi et al. 2004; Pieraccini et al. 2001; Yakar and Yılmaz 2008). Protection of cultural heritage and the factors creating this heritage is one of the primary duties of modern societies. However, this effort is very important not only for transferring it to the next generation but also for

*Corresponding Author

(omer@bozdogan.co) ORCID ID 0000-0002-3559-2136
*(aydan.ketenci@hotmail.com) ORCID ID 0000-0001-8739-066X
(hmuraty@gmail.com) ORCID ID 0000-0002-9725-5792

Cite this article

Bozdogan O, Yaman A & Yılmaz H M (2022). An analysis on the corrosion of a cultural heritage. International Journal of Engineering and Geosciences, 7(2), 112-127

Research Article / DOI: 10.26833/ijeg.891616

Received: 03/08/2021; Accepted: 06/25/2021

enlightening and educating people and for a better understanding of cultural heritage. The societies that know their cultural heritage well and understanding it, discovered the inner peace and have always been showing respect to public security understanding. For instance, according to the studies of European Council and UNESCO, the cities with low tendencies to commit crime and engaging in violence are the places where the cultural and historical architectural texture is very well preserved.

There are so many historical, cultural artefacts such as mosques and churches in the city of Aksaray, which was under Roman Empire, Seljuq Empire, several beylics and finally Ottoman rule throughout history. This study aims to determine the corrosion and degradation, deformation amount in other words, occurred in Çanlı Church in time, and considering the meteorological data, the causes of the corrosion was studied within the scope of this study.

1.1. Corrosion in Historical and Cultural Heritage

The word 'corrosion' that is used for structures means that any building wears out and loses material and mass over time, due to weather conditions and other factors affecting the structure. The change that happens in historical artifacts is considered as 'corrosion' Historical structures may change, due to the several reasons such as ground subsidence, floods, storms, by losing their authentic structural balance (Örmecioğlu 2010).

These changes are usually as follows:

- Chemical and physical decays and cracks occurred in structure's material in or out of building, that are called 'deformation'
- vertical and horizontal changes and that are called 'position change'

To determine the exact corrosion, the objects should be constantly monitored depending on the time. By monitoring just for once the amount of corrosion cannot be found. The measurement should be done periodically or in cases where special conditions occur in different times.

The regions and buildings in the world, are being affected by different factors that are temporary or permanent. These factors are as follows:

- Physical attributes of the ground,
- The current weight of the building,
- Kind of material used in the building,
- earth movements in the region,
- The factors such as traffic load, weather, and wind force etc. that affect the building,
- Dynamic pressure of the water.

1.2. *Aksaray Çanlı Church*

There are many historical and cultural heritage in Turkey as in the world. The city of Aksaray hosted several civilizations in its history.

There are plenty of historical and cultural heritage in Aksaray. One of the most significant of those is Çanlı Church. It is in the village of Akhisar about 3 miles northeast of the village center and around 10 miles from Aksaray city (Figure 1).

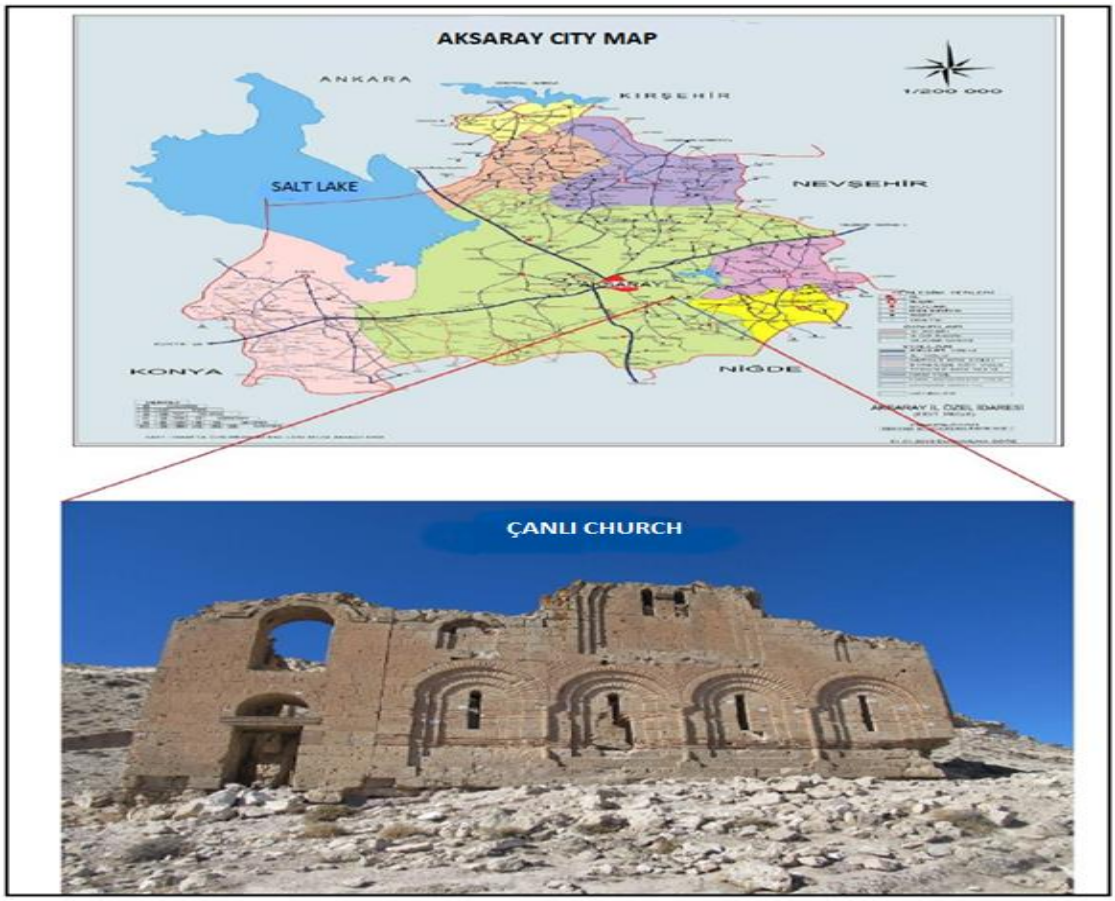

Figure 1. Çanlı Church and its location (Bozdoğan&Yılmaz 2019)

While Çanlı Church is famous for the mummies pulled from its ground, its environment is also known as a significant religious center. Çanlı Church is one of the perfect examples of Byzantine art. It is one of the places that remained intact in the region and reflect the Byzantine art in a best way. Çanlı Church and its environment are one of the most important areas that should be introduced into the tourism. However, it is still like a ruin. The area with various sized houses dating back to 10th-14th centuries and carved into the rocks in the church and its environment, look like a Byzantine town. However, since it has not been put under protection yet and it is far away from the centers and the church still gets the attention of the treasure hunters and thus the destruction is growing. The biggest lack in protection plan may be ignoring the buildings that are located at a far distance. Figure 2 represents a photograph of North-west facade of the church from a study conducted in 1981 (Yılmaz et al. 2007). According to this study, the state of the North-west facade for 2006 can be seen in Figure 3, for 2010 in Figure 4, for 2016 in Figure 5 and for 2019 in Figure 6. The east facade of the church was completely destroyed.

The bell, that the church was named after, could not be seen in the photograph, since it was stolen in ancient times. As seen in the picture, this historical building is about to be destroyed due to the neglect. In addition to the local people looking for treasure, it is also thought that weather conditions have destroyed the structure.

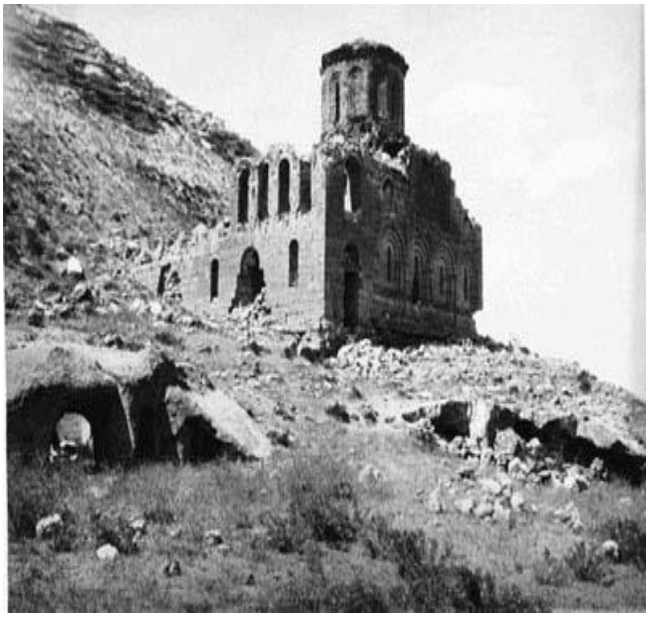

Figure 2. The situation of Çanlı Church in 1981

Figure 3. The situation of Çanlı Church in 2006 (Bozdoğan & Yılmaz 2019)

Figure 4. The situation of Çanlı Church in 2010 (Bozdoğan & Yılmaz 2019)

Figure 5. The situation of Çanlı Church in 2016 (Bozdoğan & Yılmaz 2019)

Figure 6. The situation of Çanlı Church in 2019

2. MATERIAL AND METHOD

A local network has been established in the site. The checkpoints have been marked on church and the coordinates of these points have measured by electronic telemeter and the coordinate was transformed in the system ITRF-96. Then the overlapping photographs of the church have been taken by using a calibrated digital camera.

The date obtained as a result of the measurements in the site, have been transferred to the PhotoModeler Scan Program. By performing photogrammetric evaluation, the facade drawings were made. This procedure has been repeated in 2006, 2010, 2016 and 2019.

The drawing of the north facade of Çanlı Church for 2006 is shown in Figure 7, the drawing for 2010 is shown in Figure 8, the drawing for 2016 is shown in Figure 9, and the drawing for 2019 is shown in Figure 10.

The drawing of the west facade of Çanlı Church for 2006 is shown in Figure 11, the drawing for 2010 is shown in Figure 12, the drawing for 2016 is shown in Figure 13, and the drawing for 2019 is shown in Figure 14. The drawing of the south facade of Çanlı Church for 2006 is shown in Figure 15, the drawing for 2010 is shown in Figure 16, the drawing for 2016 is shown in Figure 17, and the drawing for 2019 is shown in Figure 18.

On the north facade some corrosions indicated by N3, N4, N5, N6, N7 and N8 were found (Figure 10). On West facade the stones in the areas indicated by arrow marks W1, W2, W3, W4, W5 and W6 fell (Figure 12).

A serious deformation is seen in the parts indicated by S4 on the south facade and stone aggregates fell in the part numbered S5. In comparison with the 2006 measurement indicated by S1, S2 and S3, it was found that the stones fell (Figure 15).

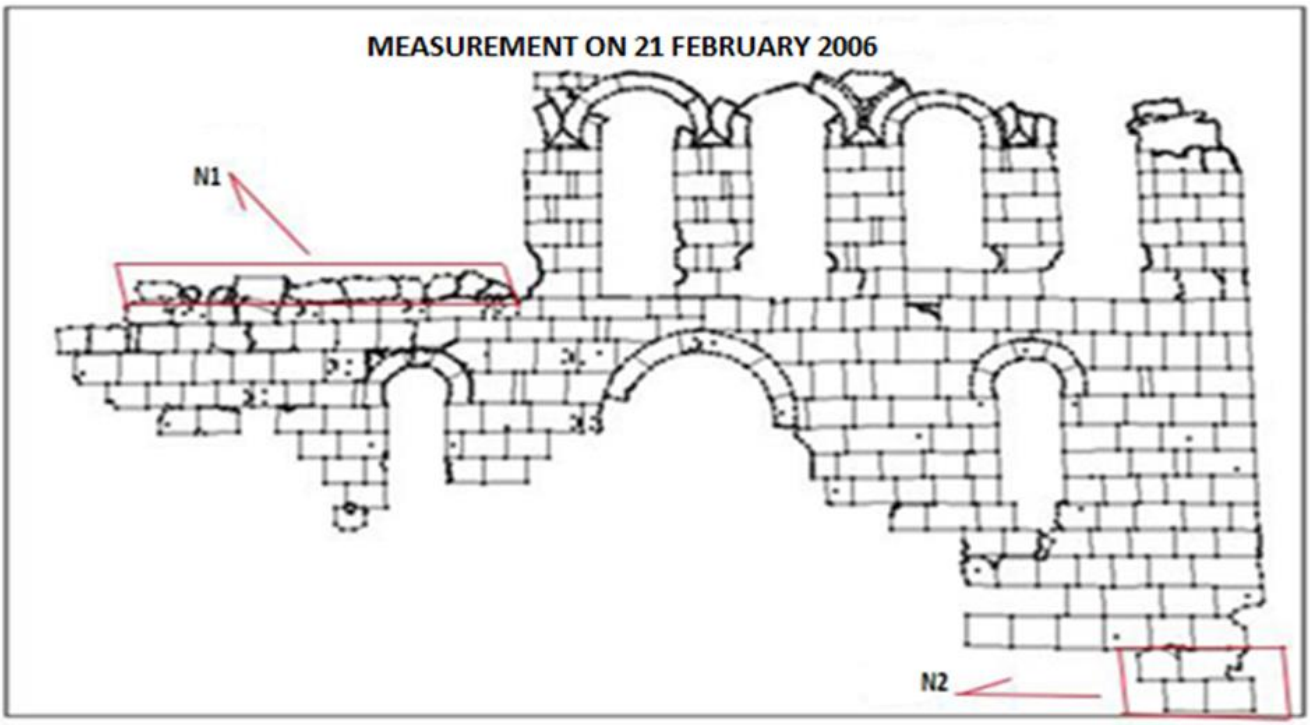

Figure 7. Measurement of Çanlı Church's north facade for 2006 (Bozdoğan & Yılmaz 2019)

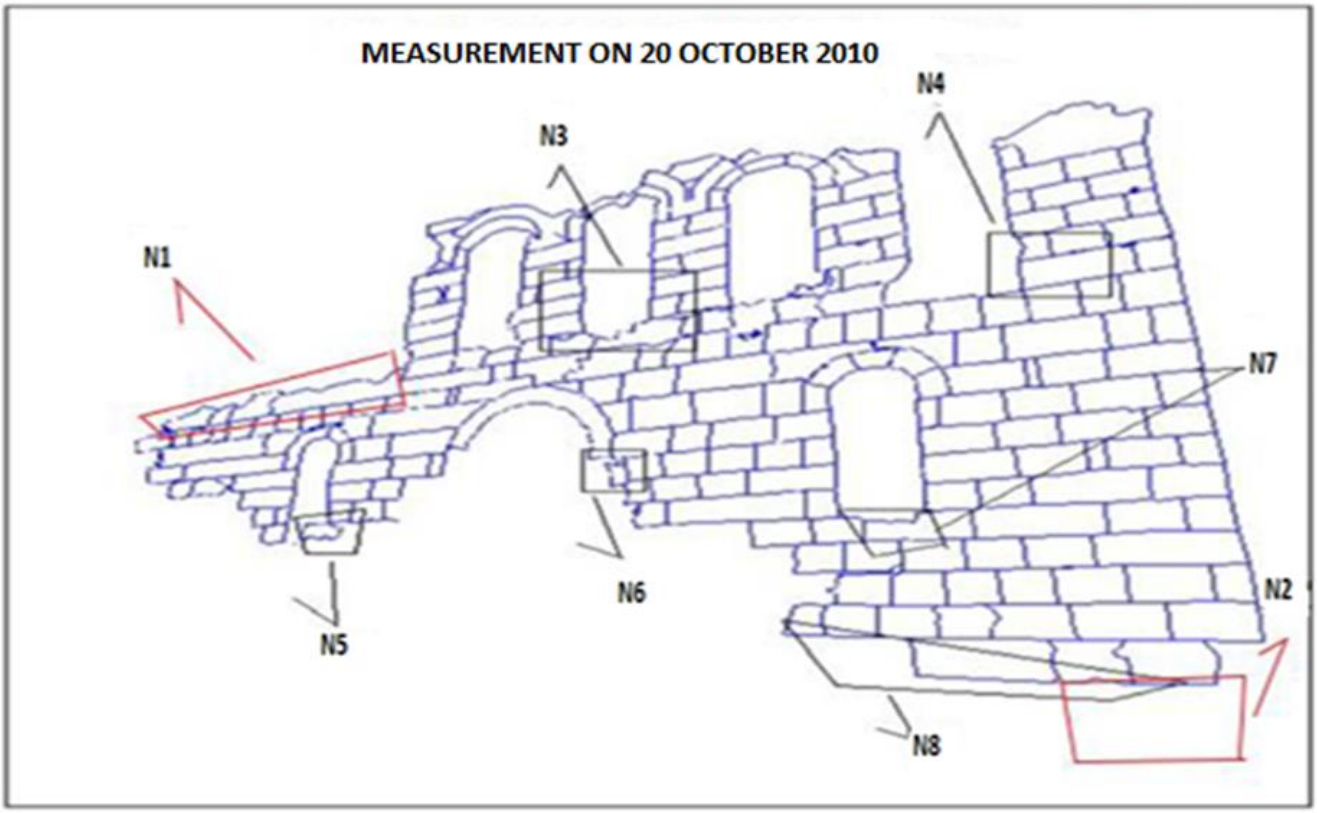

Figure 8. Measurement of Çanlı Church's north facade for 2010 (Bozdoğan & Yılmaz 2019)

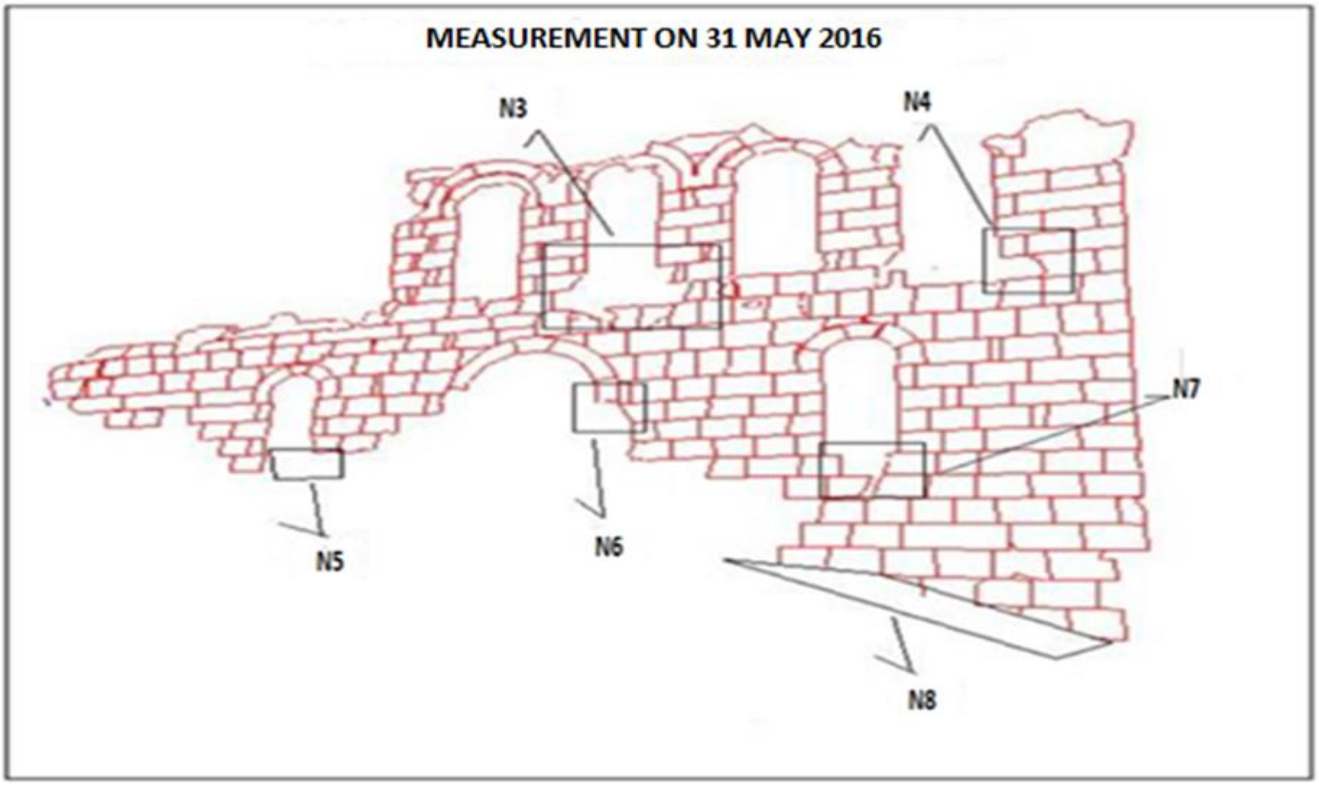

Figure 9. Measurement of Çanlı Church's north facade for 2016 (Bozdoğan & Yılmaz 2019)

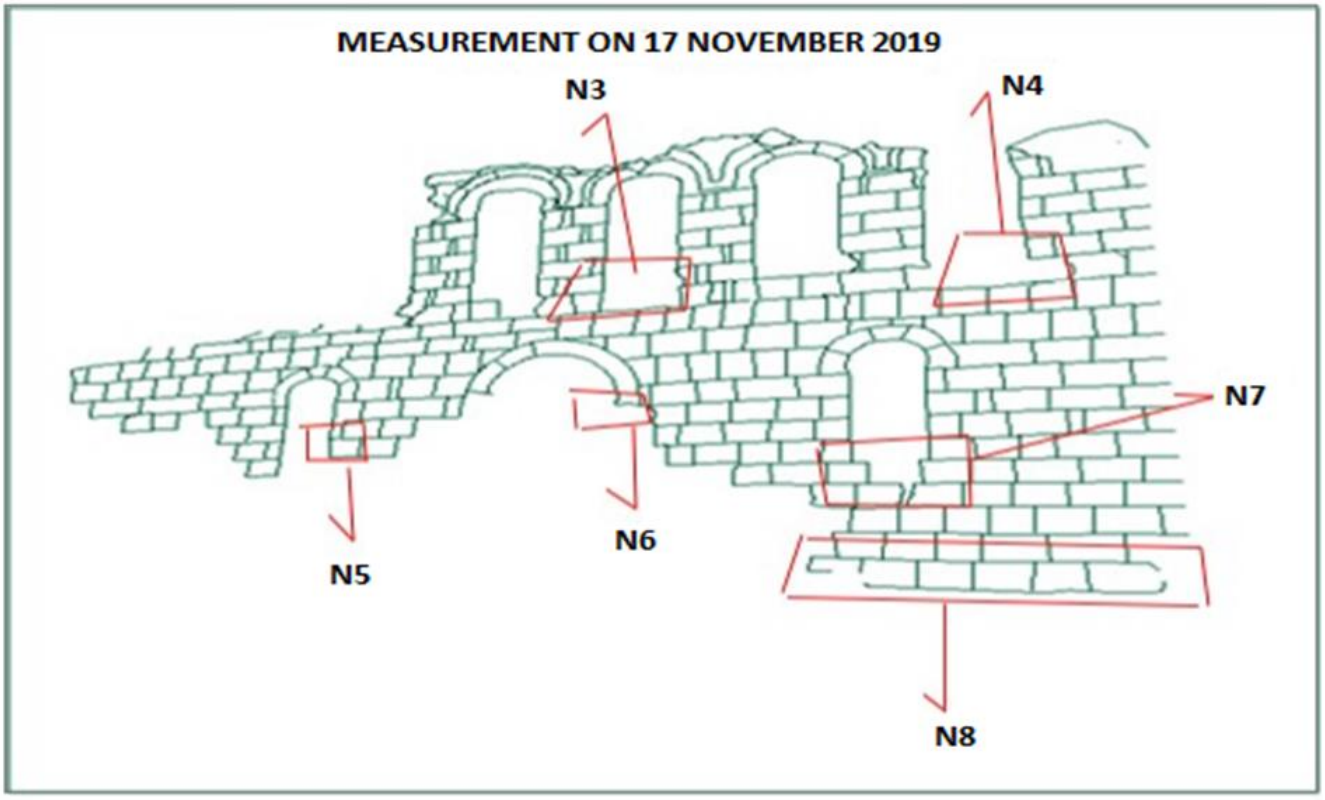

Figure 10. Measurement of Çanlı Church's north facade for 2019

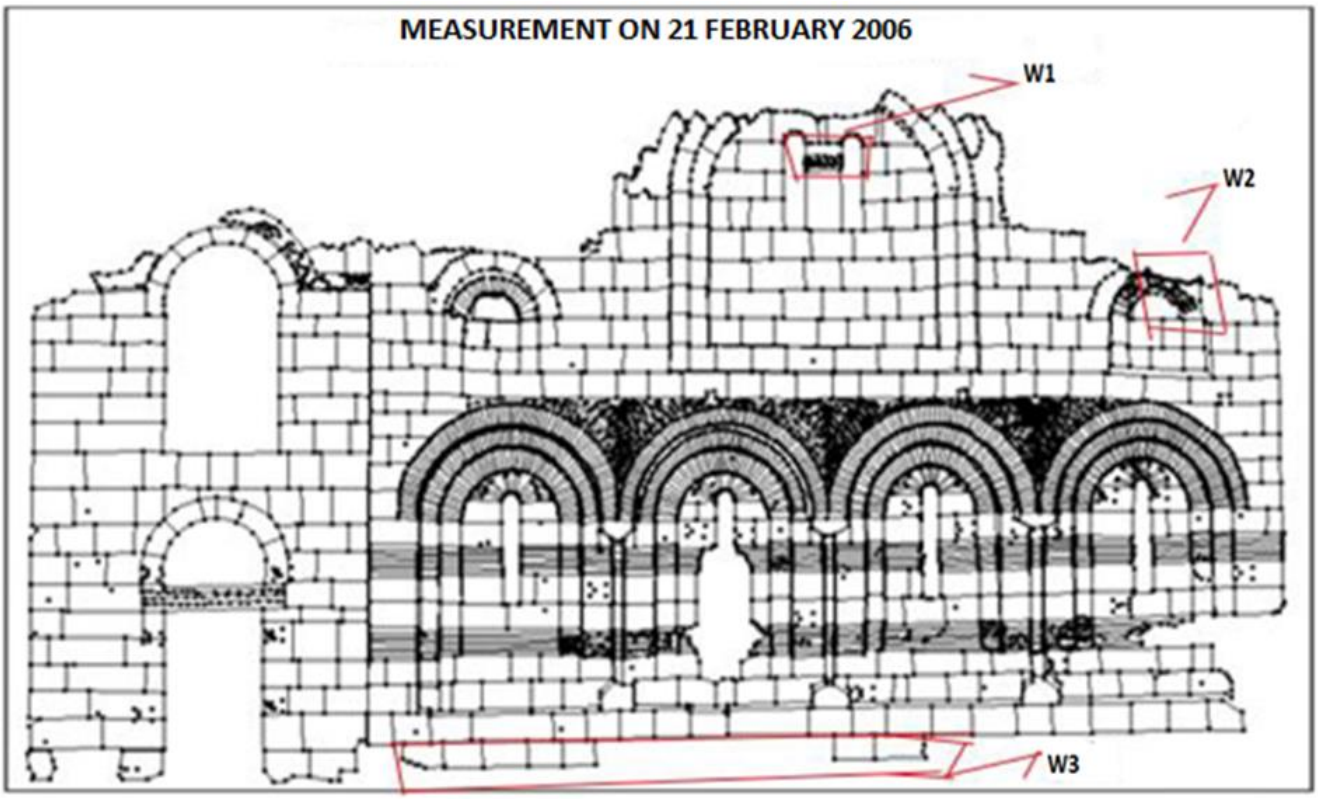

Figure 11. Measurement of Çanlı Church's west facade for 2006 (Bozdoğan & Yılmaz 2019)

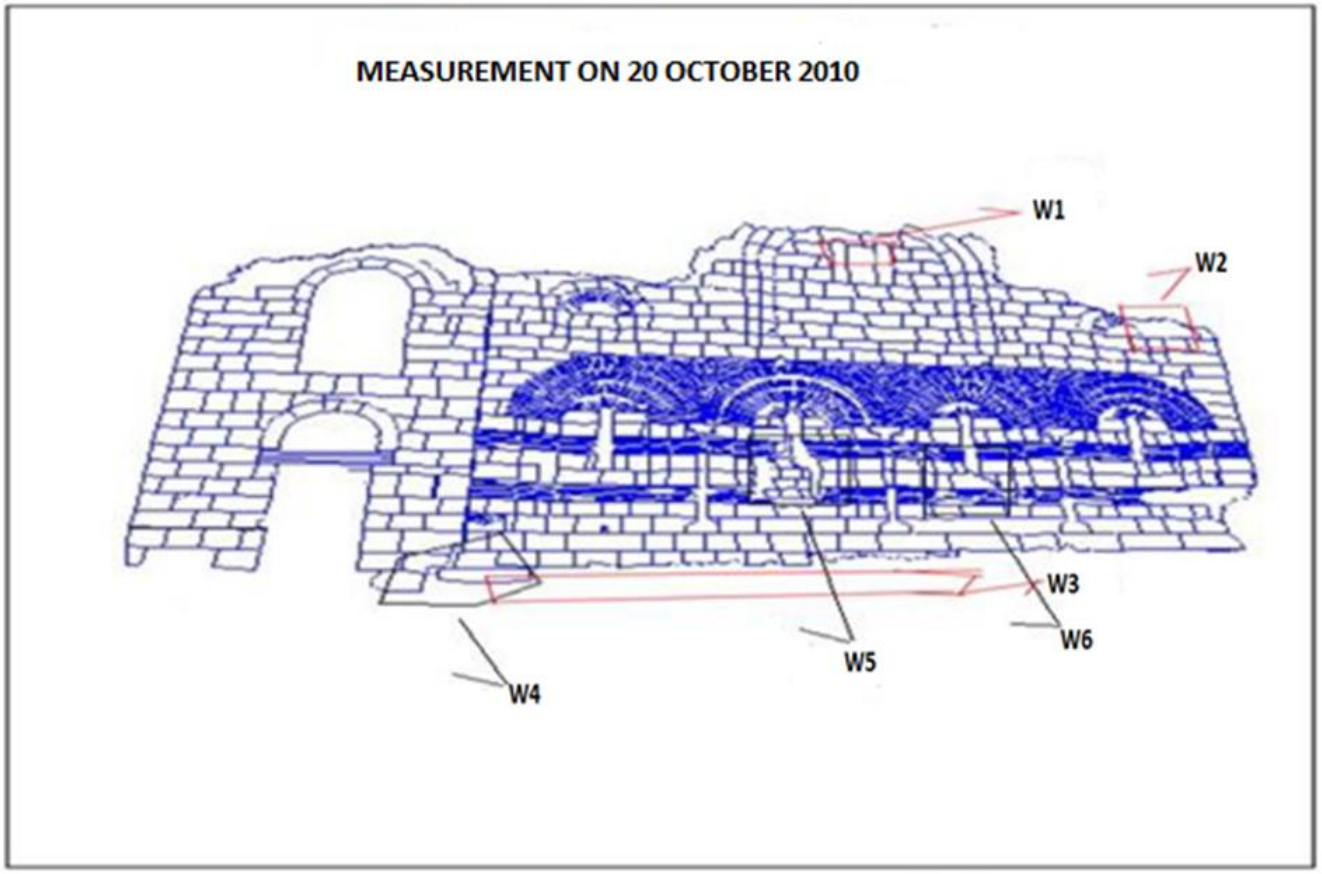

Figure 12. Measurement of Çanlı Church's west facade for 2010 (Bozdoğan & Yılmaz 2019)

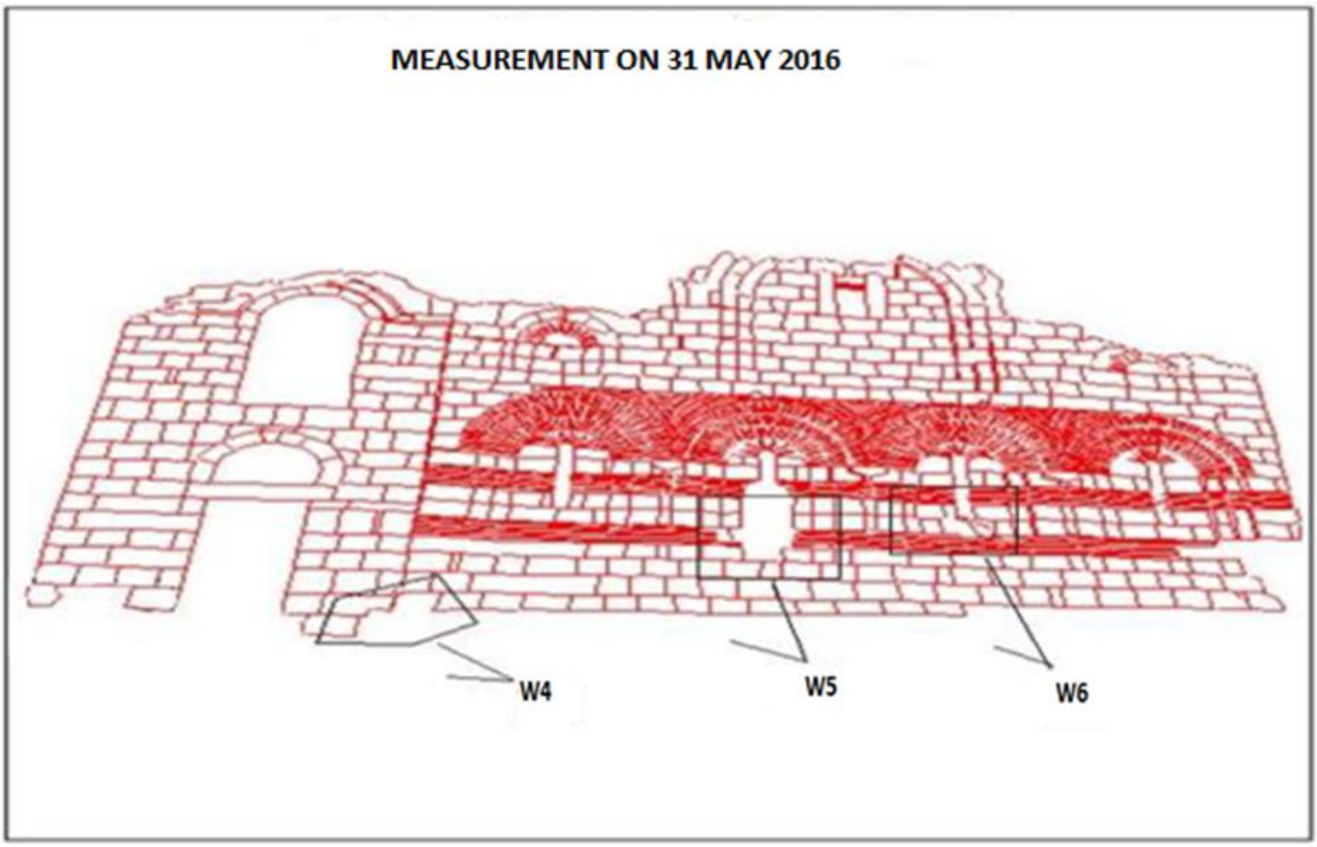

Figure 13. Measurement of Çanlı Church's west facade for 2016 (Bozdoğan & Yılmaz 2019)

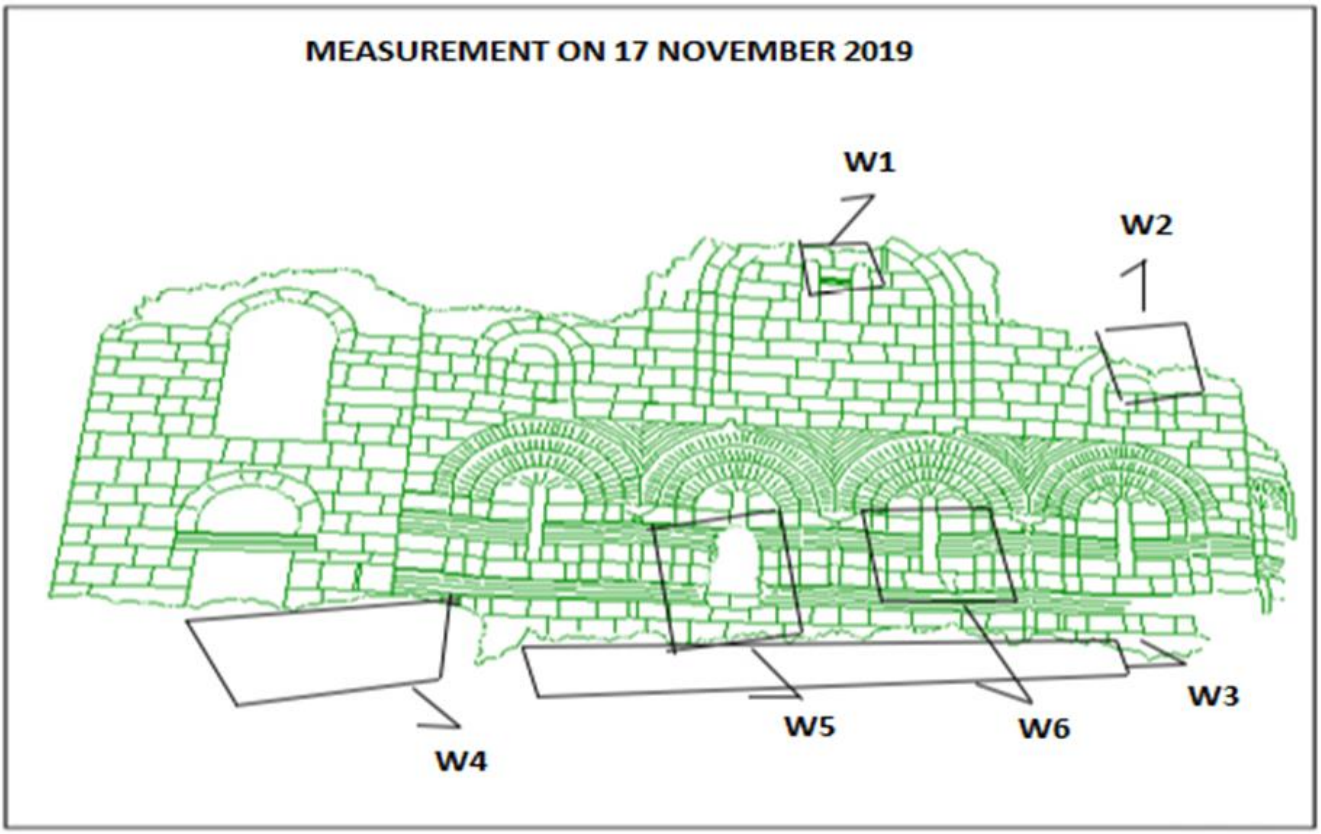

Figure 14. Measurement of Çanlı Church's west facade for 2019

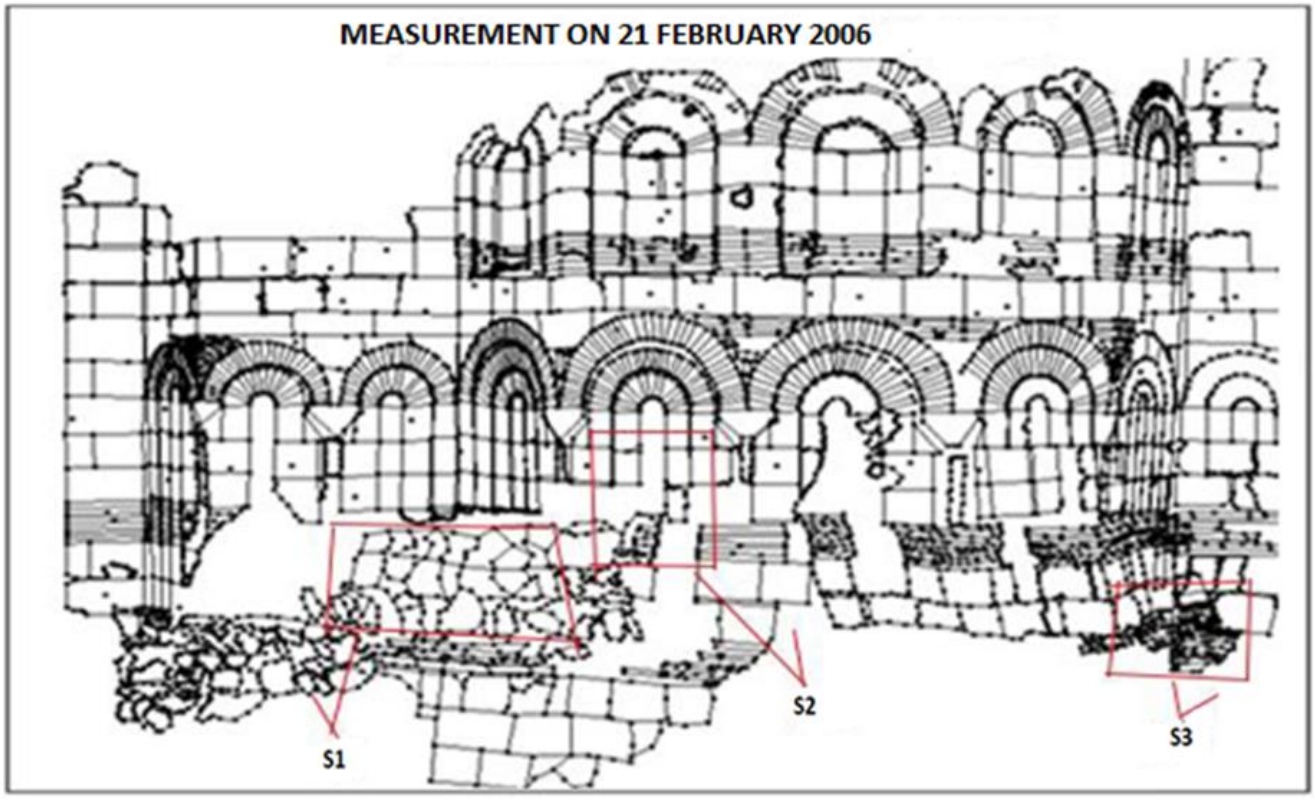

Figure 15. Measurement of Çanlı Church's south facade for 2006 (Bozdoğan & Yılmaz 2019)

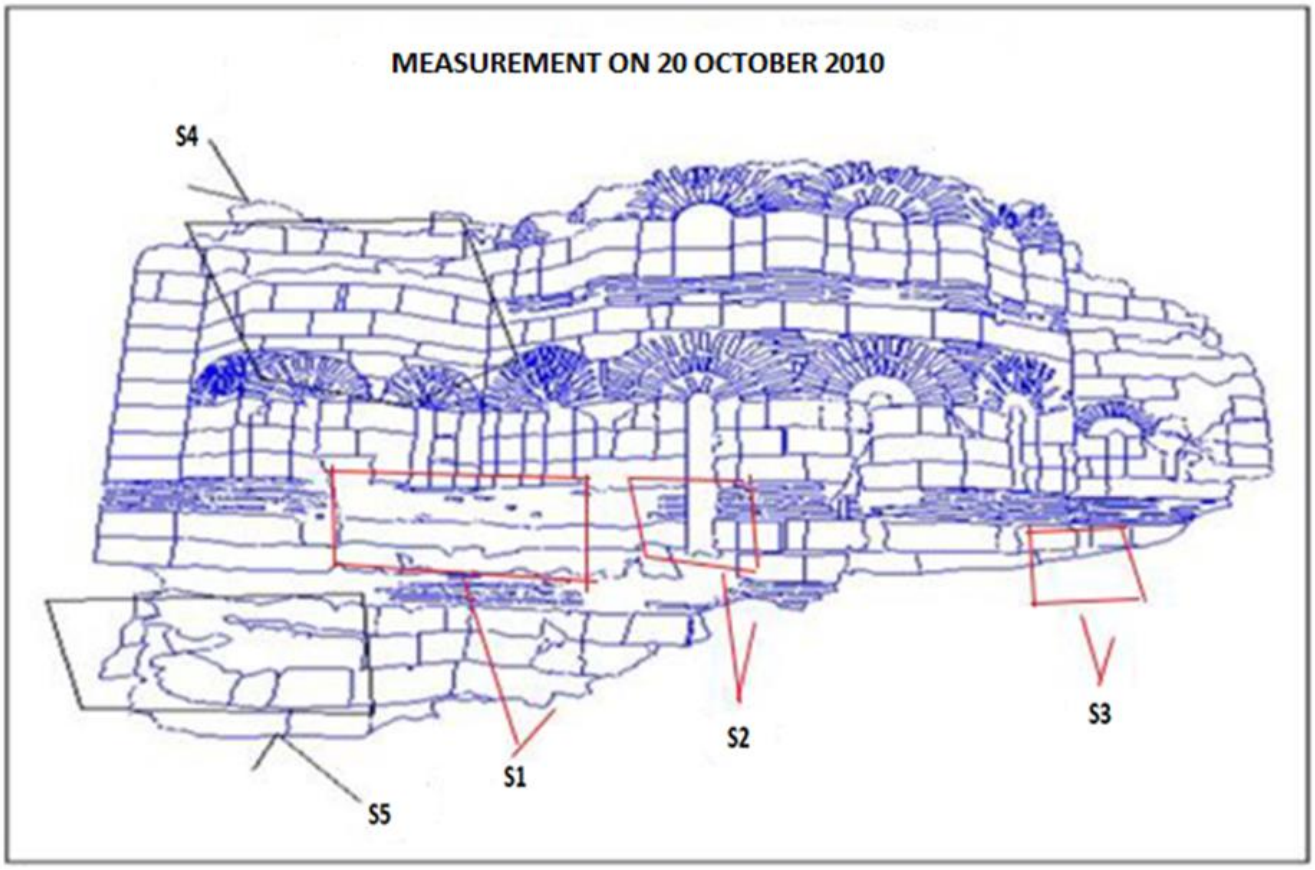

Figure 16. Measurement of Çanlı Church's south facade for 2010 (Bozdoğan & Yılmaz 2019)

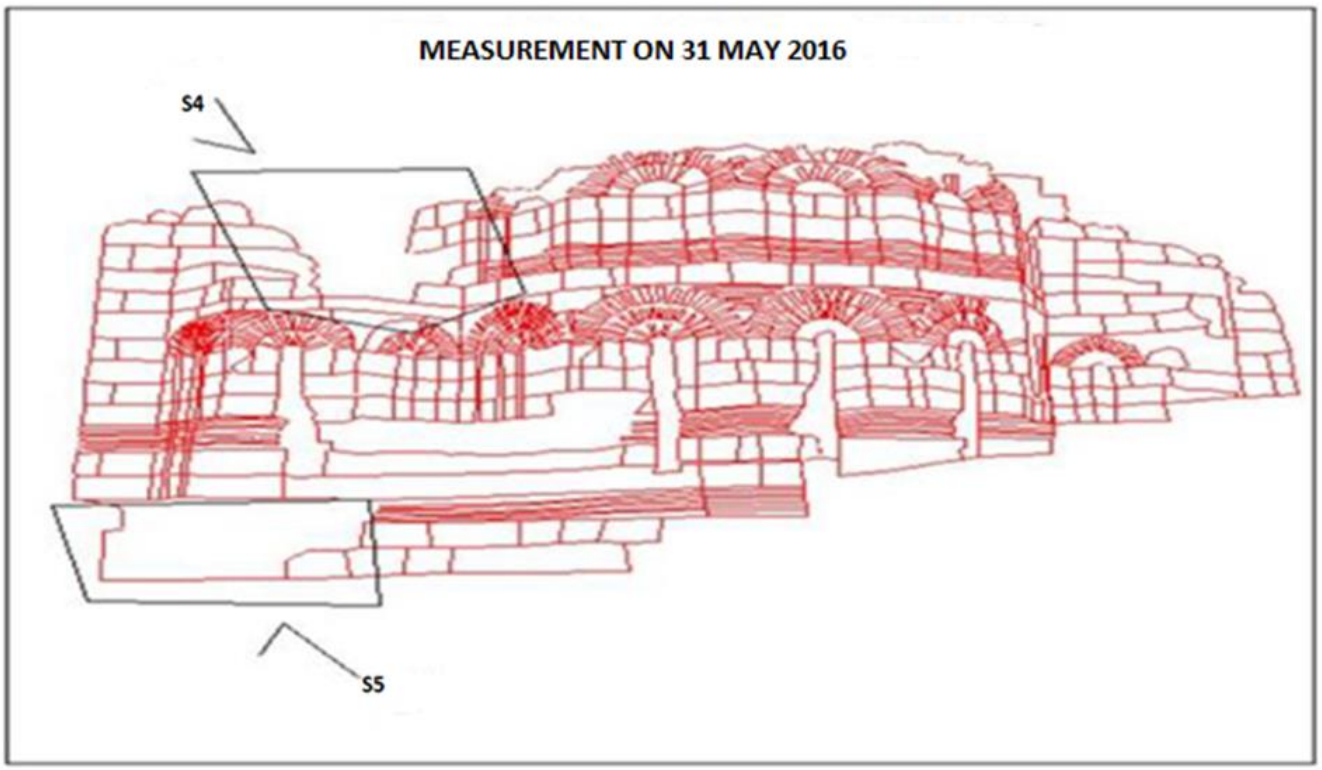

Figure 17. Measurement of Çanlı Church's south facade for 2016 (Bozdoğan & Yılmaz 2019)

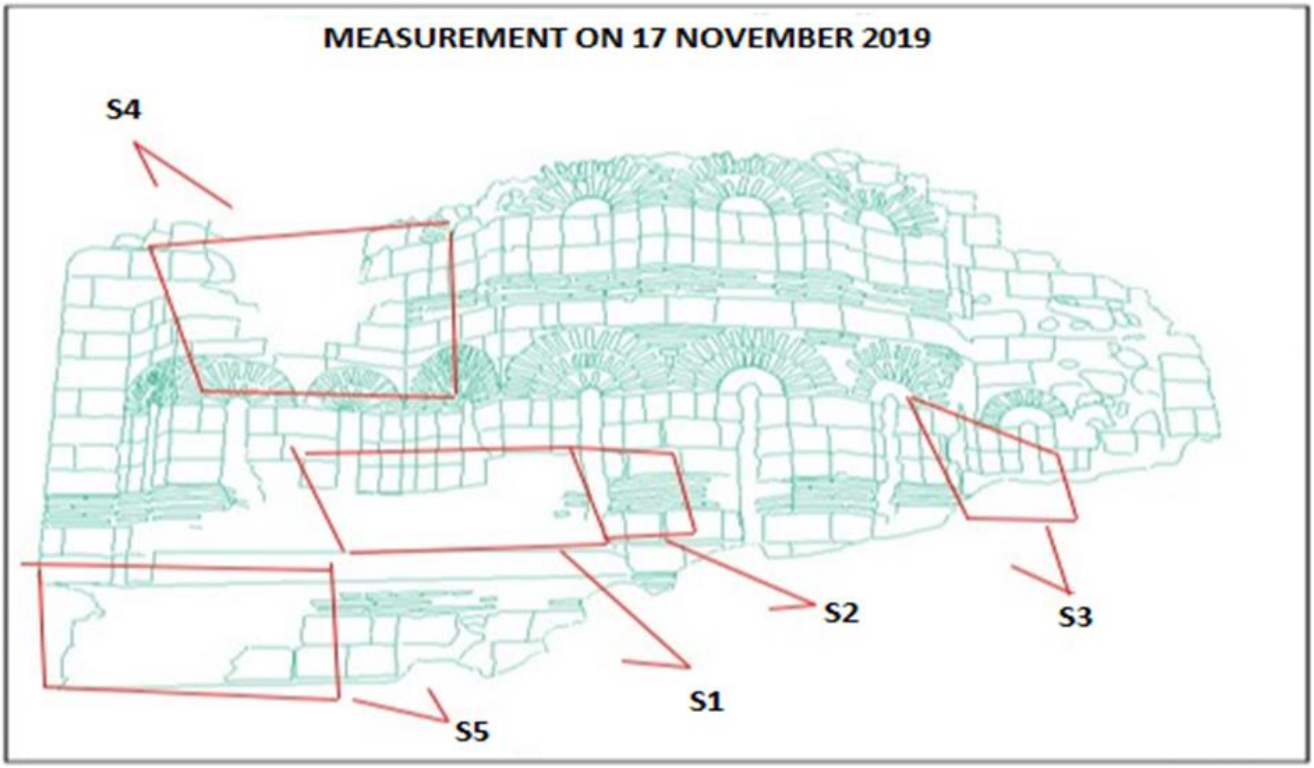

Figure 18. Measurement of Çanlı Church's south facade for 2019

2.1. Meteorological Data

In accordance with the data received from the General Directorate of Meteorology, it was researched what causes the changes occurred in the measurements at different times.

When the meteorological data examined, it was found that the monthly minimum pressure value (hPa) was at highest level (904.9 hPa) in October 2014 and at lowest level (880.1 hPa) in December 2010 (Figure 19).

It was observed that the monthly average temperature (°C) value was highest at 27.3 °C in August 2010 and lowest at -3.7 ° C in January 2008 (Figure 20).

It was seen that the monthly average relative humidity value was highest at 80.1 % in January 2012 and lowest at 27.2% in September 2017 (Figure 21).

When the monthly number of stormy days examined, it was seen that the storm was at highest level in March 2009 and in March 2013 and that it lasted 3 days. After the 7th month of 2018 no storm has been seen (Figure 22).

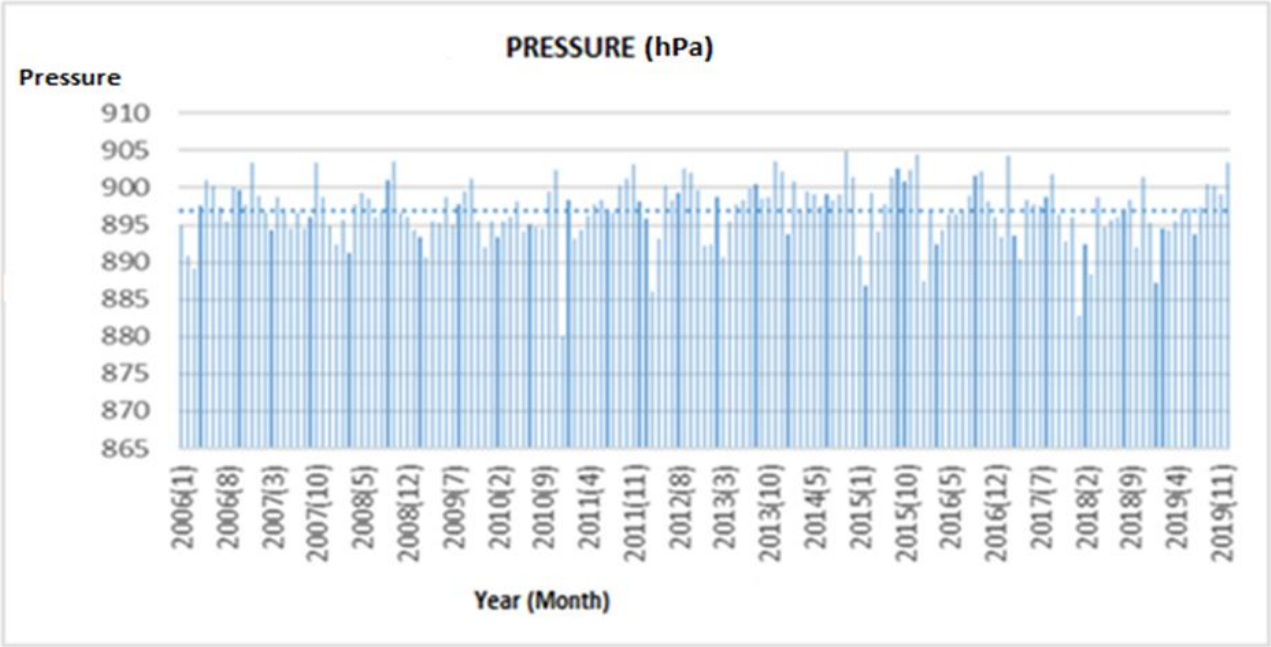

Figure 19. Monthly minimum pressure values

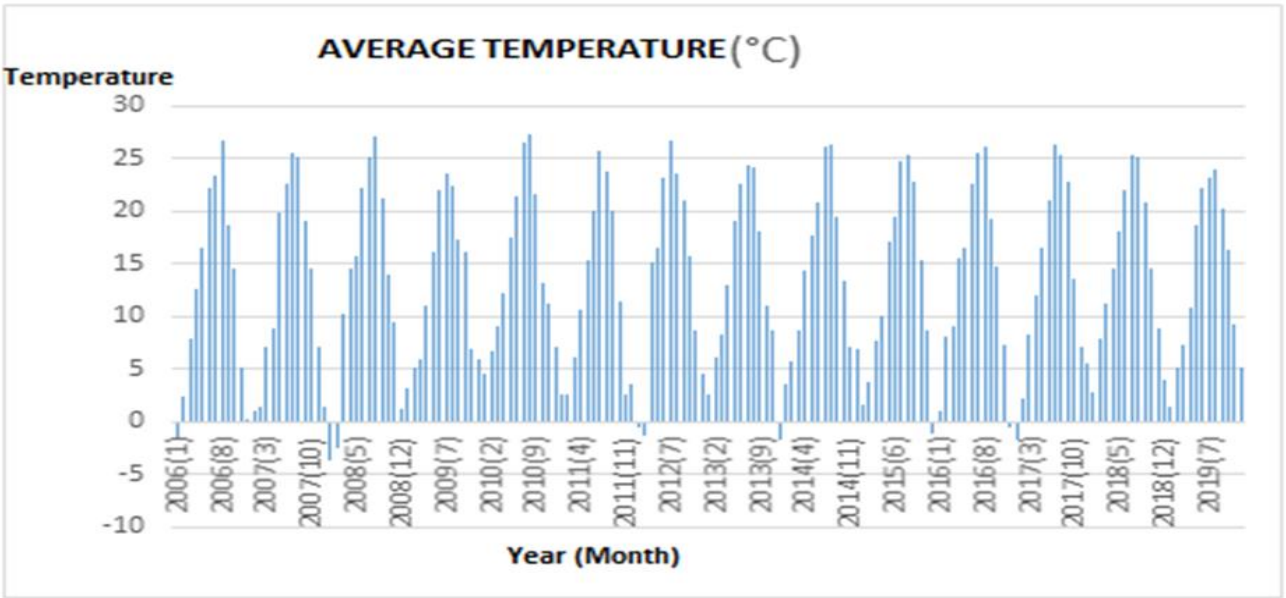

Figure 20. Monthly average temperature values

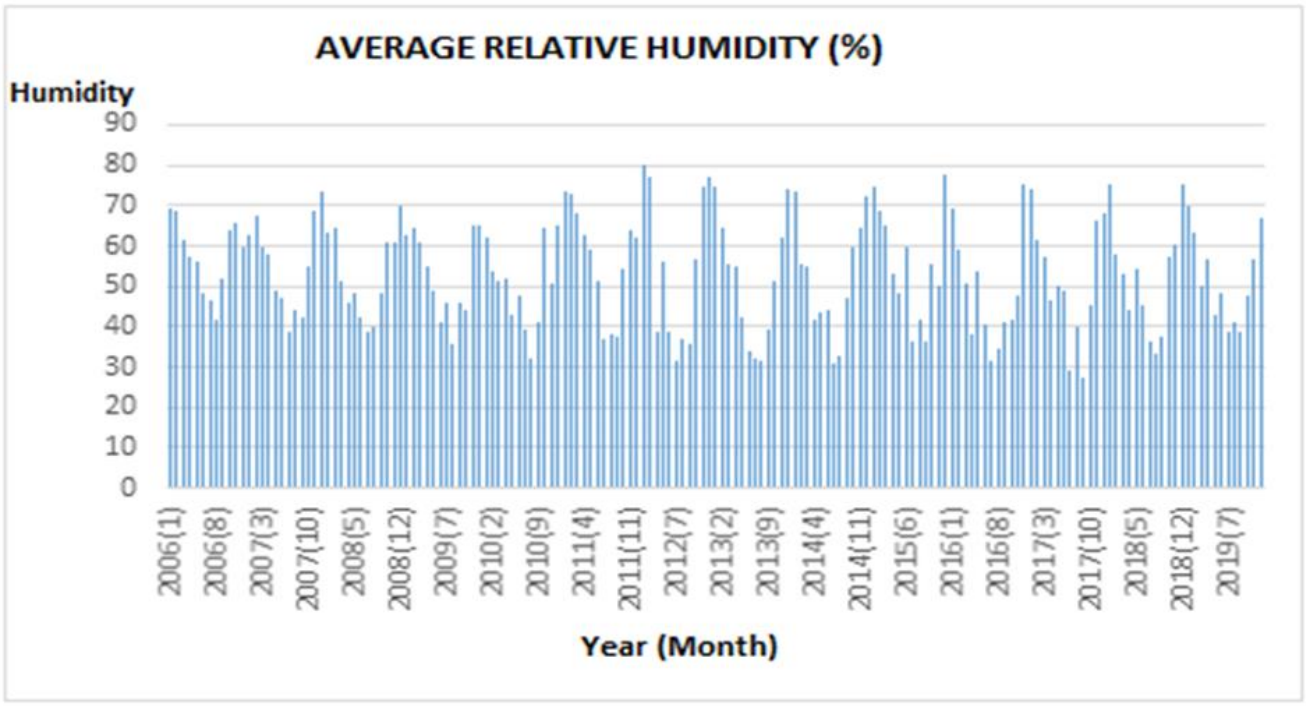

Figure 21. Monthly average relative humidity values

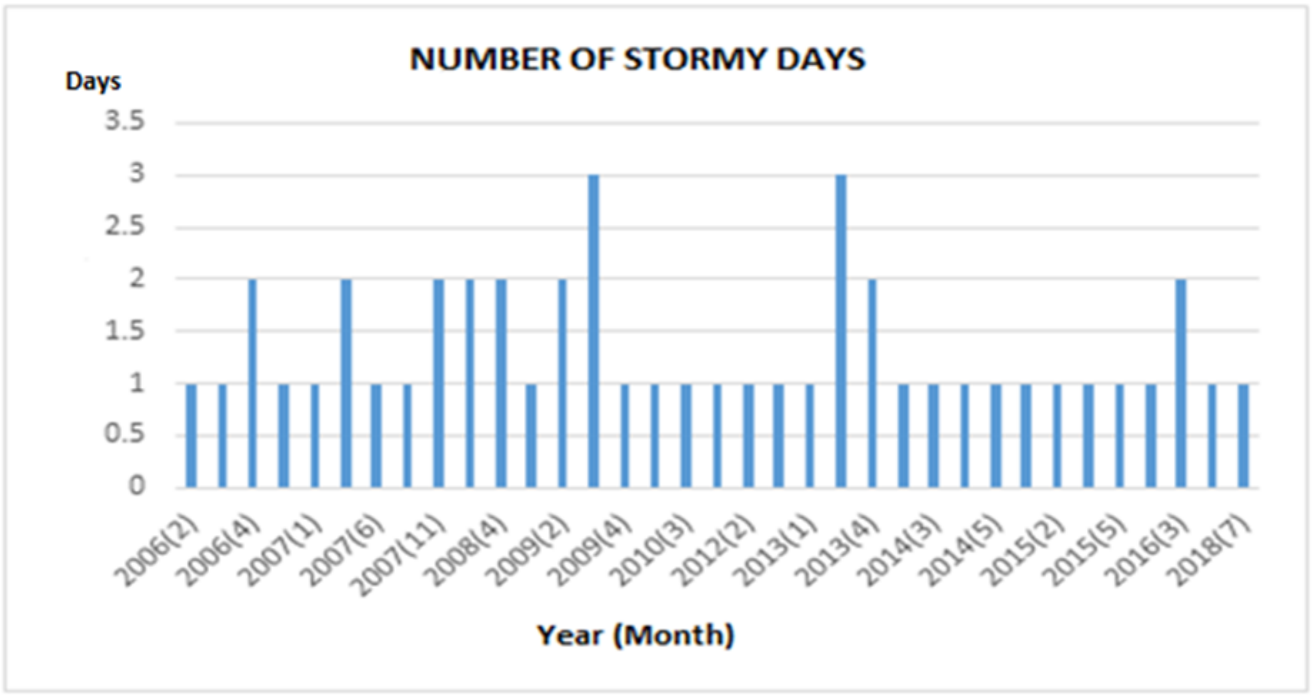

Figure 22. Monthly number of stormy days

When the monthly average snow-covered days examined, it was seen that it was at highest level in January 2017 with 25 days (Figure 23). When the snowy days are examined, it has been seen that the number of snowy days was at highest level in December 2016 and that it was at lowest level in March 2007, in March and April, 2008, in December 2009, in April 2011, in January and December, 2014, in May 2015, in February 2016 and in November 2018 were observed as the lowest number of days (Figure 24).

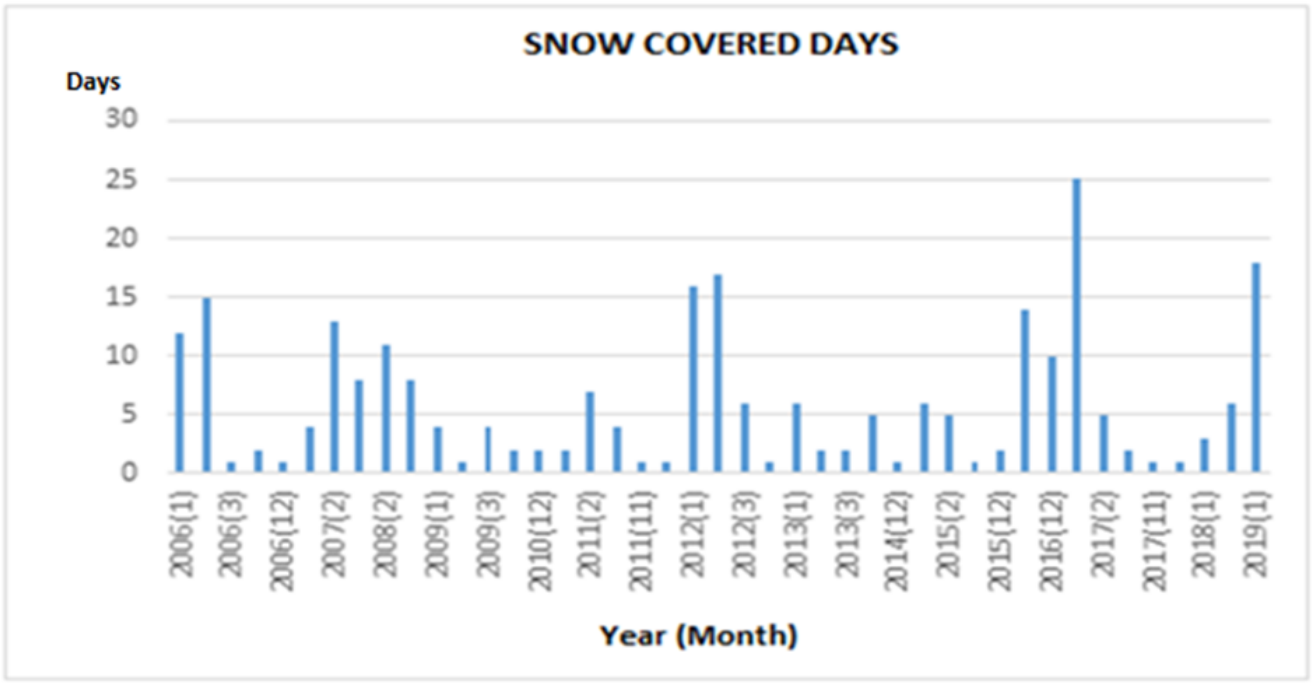

Figure 23. Monthly snow-covered days

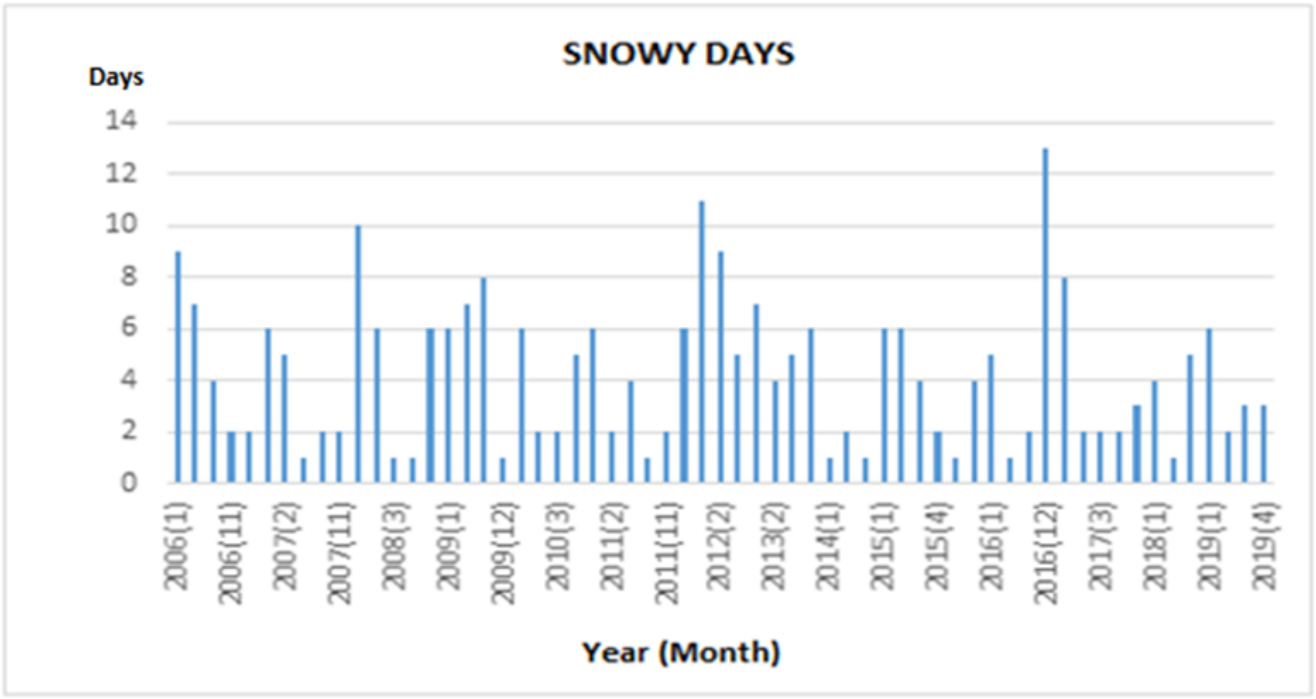

Figure 24. Monthly snowy day

When the monthly average wind speed (m Sec) is examined, it has been seen that it was at the highest level in July 2006 with 3.7 m/Sec and at lowest level in November and December 2019 with 1.2 m/Sec. (Figure 25). When monthly total precipitation (mm) was examined that it was at the highest level in June 2015 with 119 mm and at lowest level in July 2008, in August 2009, in July 2014, in July 2016 and in June and September 2017 with 0.0 mm (Figure 26).

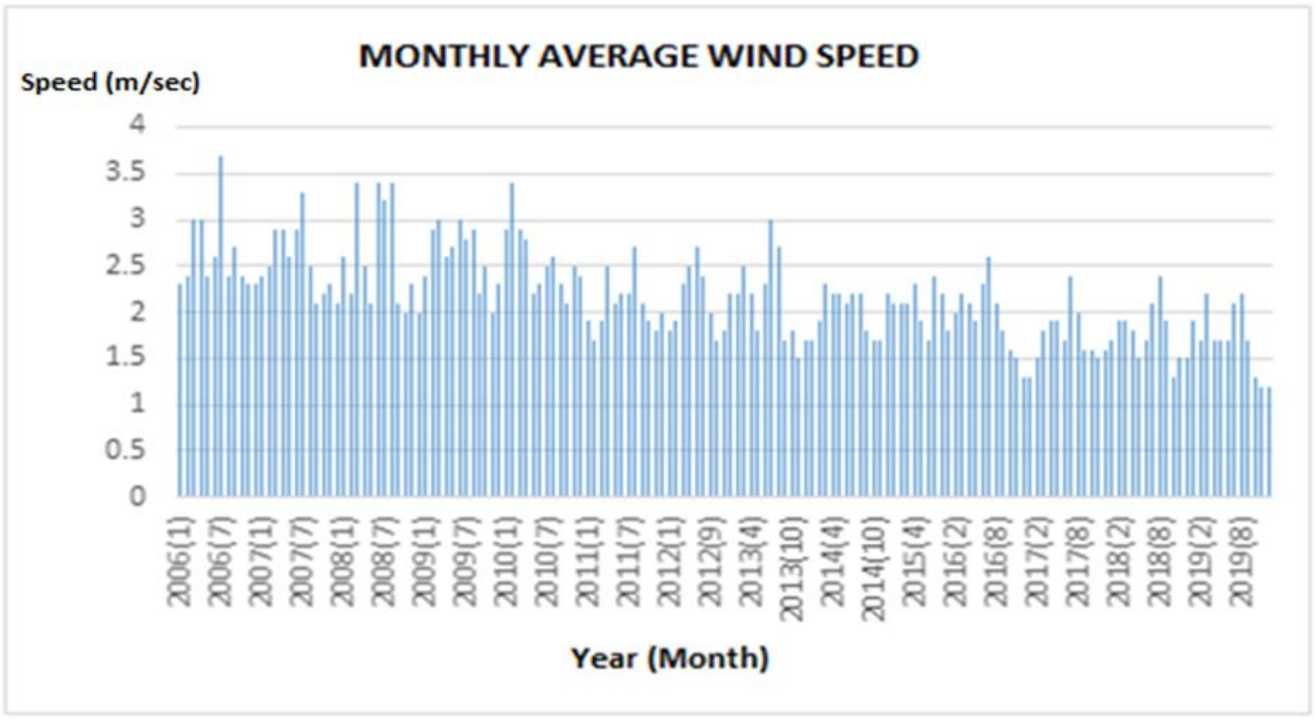

Figure 25. Monthly average wind speed (m/sec)

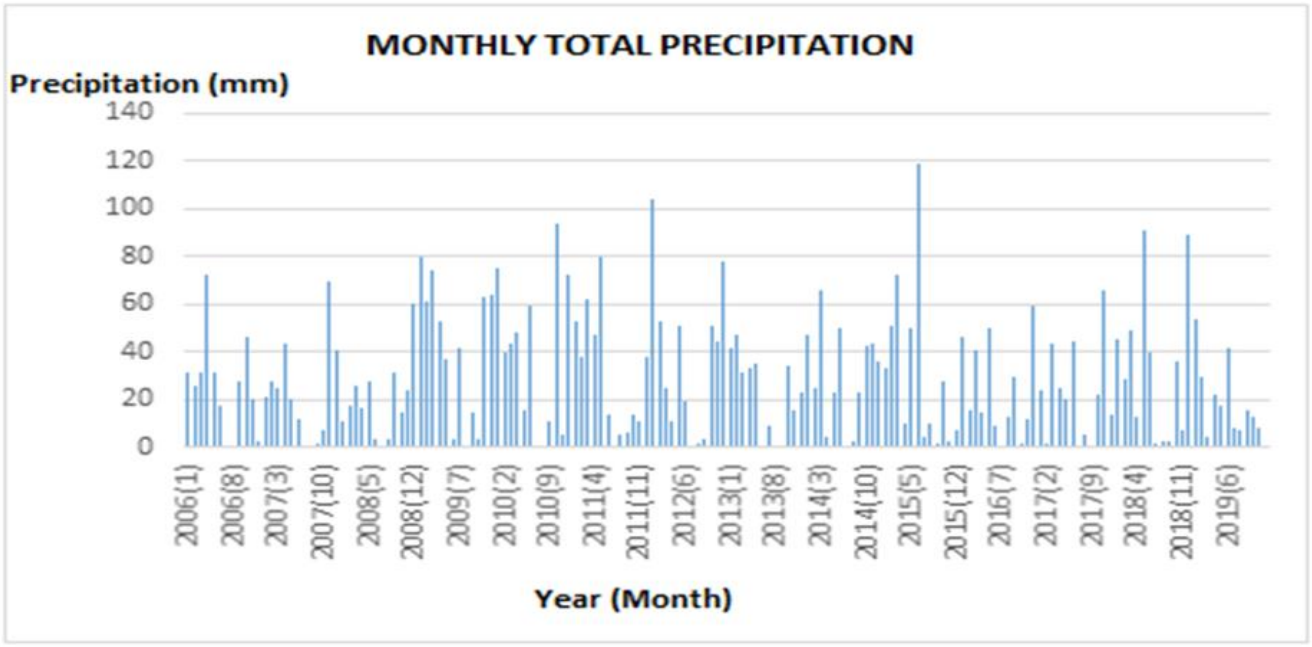

Figure 26. Monthly total precipitation (mm).

3. FINDINGS AND DISCUSSION

In this study, the corrosion occurred in Çanlı Church in Merkez district of the province Aksaray for 13 years, have been reviewed. In this context, the facade drawings obtained from the measurements made on February 21, 2006, October 20, 2010, May 31, 2016 and November 17, 2019 were compared to each other and the corrosion in the church was associated with the data of meteorological events occurred between the dates. On the North facade of the church 6 serious corrosion have been found. It has been seen that the stones fell in three areas on the west facade. On the south facade one serious corrosion has been seen and stone aggregates fell in one place. The corrosion values are seen on Table 1.

Table 1. The corrosion occurred in facades of Çanlı Church

	North	West	South
Area (m^2)	4.251.891	3.860.913	7.629.097
Eroded Area (m^2)	3.911.740	3.745.086	6.637.314
Eroded Rate (%)	8	3	13

When Table 1 was examined, the north facade area was calculated as 4.251.891,00 m^2, the west facade area was 3.860.913,00 m^2 and the south facade area was 7.629.097,00 m^2, in the studies conducted in 2006 and in comparison, with the areas in 2019, it is seen that the highest corrosion is on the South facade with 13%.

When the meteorological data is examined, it is seen that the year 2009 is the stormiest time in the last ten years. It is thought that the corrosion occurred in the church was mostly caused by storm. The storm generally occurred in the north-south direction. That is the why the most eroded facade in the church is the south facade. The falling parts have been toppled towards the inside.

Rainfall, that normally ranged from 2.5 to 72.8 mm in 2006, reached 119 mm by mid-2015. It is believed that this soakage will cause dissolution in the structure. When combined with the heavy storm in 2009, corrosion occurred in the church.

It was found that the snow was not much above average and it has been noted that it did not have any effect on corrosion.

The monthly average wind speed rose to the highest value between 2006-2019 and it is believed that the heavy winds occurred after rain was effective in corrosion.

In addition, when the number of stones for each facade is examined, it has been observed that there has been a serious decrease in the number of stones over the years. The number of stones present in the facades during the years of the study is also given in Table 2.

Table 2. The number of stones on the facades for different years

	North	South	West
2006	331	438	522
2010	320	425	511
2016	305	390	497
2019	295	382	492

4.RESULTS

In this study, the corrosion in the Çanlı Church located in Akhisar village of the province Aksaray and the reasons of corrosion were examined. By using close range photogrammetry method, three-dimension models and facade charts of three facades of Çanlı Church have been acquired, as a result of measurements done in four different times.

Overlapping all these charts in the same scale, the corrosions occurred on the facades of Çanlı Church have been determined.

While the north facade area was 4.251.891,00 m^2, it decreased to 3.911.740,00 m2 and that indicates 8 % corrosion. The West facade area was 3.860.913,00 m^2, it decreased to 3.745.086,00 m^2 and that indicates a 3 % corrosion. The south facade area was 7.629.097,00 m2, it decreased to 6.637.314,00 m2 and that indicates a 13 % corrosion.

In addition, it has been determined that there has been much stone loss and deformation on the facades over the years.

The meteorological data within the period when the measurements were performed were reviewed and it has been concluded that the storm was more effective on corrosion and deformation.

It is crucial to emphasize one more time; as long as the cultural heritages, the common value of humanity, are ignored, they are destined to perish over time.

Author contribution

Ömer Bozdoğan: Field work, Software, Investigation, Data acquisition, writing; **Aydan Yaman**: Field work, Software, Analysis, Writing-Orginal draft preparation; **Hacı Murat Yılmaz**: Metodology, Reviewing and Editing

Conflicts of interest

The authors declare no conflicts of interest.

REFERENCES

Arias P J, Herraez H, Lorenzo C & Ordonez (2005) Control of structural problems in cultural heritage monuments using close-range photogrammetry and computer methods, Computers and Structures, 83, 1754-1766.

Atkinson K B (1996). Close-range Photogrammetry and Machine Vision, Whittles Publishing, Scotland.

Berndt E & Carlos J, (2000) Cultural heritage in the mature era of computer graphics, IEEE Computer Graphics and Applications 20 (1) 36-37.

Bozdoğan Ö & Yılmaz H M (2019). Tarihive Kültürel Miraslarda Aşınma: Aksaray Çanlı Kilise, Tufuab X. Teknik Sempozyumu, Bildiri özetleri kitabı, 17.

Demirkesen A C &Demir H (2006). Tarihi Kültür Varlıklarının Korunmasında Harita Mühendisliği Disiplininin Rolü, Mimarlık Dergisi, 331.

Desmond L G, Collins P, Negron T G & Callaghan J (2003) Gateway into the past: Photogrammetric documentation of the Arch, Labna, Yucatan, Mexico, in: L.P. Barba (Ed.), AntropologiayTe´cnica 7 (IIA) 55-66.

Guidi G, Beraldin A &Atzeni C (2004), High-accuracy 3-D modeling of cultural heritage: the digitizing of Donatello's ''Maddalena'' image, Proc. IEEE Trans. On 13 (3) 370-380.

Korumaz A G, Dülgerler O N & Yakar M (2011). Kültürel mirasın belgelenmesinde dijital yaklaşımlar. *Selçuk Üniversitesi Mühendislik, Bilim ve Teknoloji Dergisi*, *26*(3), 67-83.

Örmecioğlu H T (2010). Main Principles and Aproaches in Structural Strenghtening of Historical Buildings, Journal of Polytechnic Vol: 13 No: 3 pp. 233-237.

Pieraccini M, Guidi G &Atzeni C (2001), 3D digitizing of cultural heritage, Journal of Cultural Heritage 2, 63-70.

Ratnayake A, Rahrigine M & Drewello R (2018). Preservation of Archeological Sites Using 3DScanning Documentation Case Study: Sri Dalada Maligawa, Kandy, Sri Lanka. National Information Technology Conference.

Yakar M & Yılmaz H M (2008). Kültürel Miraslardan Tarihi Horozluhan 'ın Fotogrametrik Rölöve Çalışması ve 3 Boyutlu Modellenmesi. Selçuk Üniversitesi Mühendislik, Bilim ve Teknoloji Dergisi, 23(2), 25-33.

Yakar M, Orhan O, Ulvi A, Yiğit A Y & Yüzer M M (2015). Sahip Ata Külliyesi Rölöve Örneği. *TMMOB Harita ve Kadastro Mühendisleri Odası*, *10*.

Yılmaz H M, Karabörk H & Yakar M (2000). Yersel fotogrametrinin kullanım alanları. *Niğde Üniversitesi Mühendislik Bilimleri Dergisi*, *4*(1), 1.

Yılmaz H M, Yakar M & Yıldız F (2007), Aksaray Çanlı Kilisesi Fotogrametrik Çalışmaları, Türkiye Bilimsel Fotogrametri ve Uzaktan Algılama Birliği IV. Sempozyumu, TUFUAB

International Journal of Engineering and Geosciences
https://dergipark.org.tr/en/pub/ijeg
e-ISSN 2548-0960

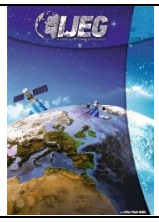

Agricultural land consolidation vs. land fragmentation in Russia

Alexander Sagaydak [*1], **Anna Sagaydak** [1]

[1]*State University of Land Use Planning, Department of Agricultural Economics and Farm Management, Moscow, Russia*

Keywords
Agricultural Land Consolidation
Agricultural Land Market
Project Analysis Principles Approach
Russia
Republic of Kalmykia

ABSTRACT

The development of Agricultural Land Consolidation in Russia has always been unique, compared to other countries due to the state land policy, the vastness of the territory, and the variety of natural and soil conditions. Because of it, the internationally recognized and generally accepted approaches and models of it cannot always be accepted and applied. The consolidation of agricultural land in the country is developing sometimes spontaneously and is chaotic. At the federal level, there is an extended trend of the absorption of private land by parastatals. There is also an extended trend of decreasing the land use of coops and increasing the land use of joint-stock companies and partnerships. The development of Agricultural Land Consolidation in Russia is primarily dependent on regional land policies. In Kalmykia, the unique trend continues to increase the number of private farms with an increase in their average size. In this regard, the super goal of the paper is to research how to apply Project Analysis Principles Approach to strengthen the development of Agricultural Land Consolidation in Russia. The specific objective of the paper is to research the role and importance of Agricultural Land Market tools to support the consolidation of agricultural lands.

1. INTRODUCTION

1.1. Scope of work

The development of land tenure in Russia has always been contradictory, spiral. It has always found its implementation in the struggle of two main trends: consolidation and fragmentation of agricultural land.

The consolidation and fragmentation of agricultural land at first glance act as opposite phenomena. Nevertheless, they are closely interrelated. Fragmentation of agricultural land objectively determines the need for further consolidation and vice versa.

Currently, the trend of consolidation of agricultural land is dominant. Agricultural Land Consolidation looks like complex phenomena, including technical, institutional, financial, economic, environmental, and social aspects, characterized by increasing scale and efficiency of agricultural production.

In this regard, the super goal of Agricultural Land Consolidation is to increase the efficiency of agricultural production to eliminate hunger, food shortages, poverty, and the gap in living conditions and incomes between urban and rural areas due to the rapidly growing world population and coronavirus pandemic.

The specific objectives of Agricultural Land Consolidation are an integration of small agricultural land parcels into large tracts of agricultural land; optimization of the size of agricultural land parcels, elimination of mosaic land ownership; increase the efficiency of use of agricultural machinery; the development production and social infrastructure in the countryside.

The main principles of Agricultural Land Consolidation are the following: voluntariness; openness; transparency; technical, institutional, financial, economic, environmental, and social feasibility; consideration of women, youth, and indigenous people as the main stakeholders; step by step implementation; taking into account local conditions; government and non-government organization support.

The other reason for the development of land consolidation in agriculture is that large agricultural

* **Corresponding Author**

*(asagaydak@yahoo.com) ORCID ID 0000 – 0002 – 6316 –6134
(ann1806@mail.ru) ORCID ID 0000 –0003 – 4389 – 8570

Cite this article

Sagaydak A & Sagaydak A (2022). Agricultural land consolidation vs. land fragmentation in Russia. International Journal of Engineering and Geosciences, 7(2), 128-141

Research Article / DOI: 10.26833/ijeg.919939

Received: 18/04/2021; Accepted: 14/09/2021

producers are less sensitive to macroeconomic instability and the disparity of prices for agricultural and industrial commodities.

There are two primary forms of Agricultural Land Consolidation: compulsory and voluntary. One of the effective tools of voluntary Agricultural Land Consolidation is Agricultural Land Market.

The Agricultural Land Market is an Imperfect Competition Market because the number of sellers and buyers of agricultural land parcels doesn't fit each other.

Agricultural Land Market Transaction Information isn't clear and transparent. Agricultural Land Market Transactions are localized very much. The supply and demand for agricultural land allotments are 100% inelastic.

In Agricultural Land Market available externalities: the state registration of the Agricultural Land Market Transactions; restrictions on the sale and purchase of agricultural land parcels; inappropriate agricultural land use: agricultural land and water pollution; illegal redistribution of agricultural land for non-agricultural and commercial purposes.

Transactions in the Agricultural Land Market are mainly carried out between neighbors who know each other well.

They look like the third party in the Agricultural Land Market and prevent the formation of equilibrium prices of agricultural land allotments.

1.2. Empirical Literature

The problem of land consolidation in agriculture and its geodetic support is reflected in numerous scientific studies, publications such as Backman (2010), Backman (2016), Becker and Halimi (2019), Biarel et al. (1992), Krigsholm et al. (2016), Konttinen (2016), Meijer and Emmens (2016), Satana et al. (2017), Sky (2015), Sulonen and Kotilainen (2016), Thomas (2006), Van den Noort (1987) and others, as well as, manuals, recommendations, and guidelines of international organizations (Voluntary Guidelines on the Responsible Governance of Tenure of Land, Fisheries and Forests in the Context of National Food Security (2012) FAO, Rome), Legal guide released by FAO in 2020 (Legal guide on land consolidation: Based on regulatory practices in Europe. FAO Legal Guide, No. 3. Rome, FAO (2020).

Backman (2010) and Backman (2016) studied and assessed the development and performance of Agricultural Land Consolidation based on cost-benefit analysis. He found and shaped out advantages of Agricultural Land Consolidation for landlords and society as a whole based on the Swedish experience. Backman found the main costs for a Land Consolidation project are an investigation of the composition and size of every owner's farm; individual talks with the landowners at "days of wishes"; elaboration of the design of the new consolidated properties; valuation of all properties; mediation and negotiation with all participating landowners; surveying of the new boundaries. The costs for a Land Consolidation project are influenced by: degree of fragmentation; the number of real properties/parcels; the number of landowners and their attitude; the size of the consolidation area; the length of all boundaries. Besides the measurable costs and disadvantages of Land Fragmentation for the proprietors, some factors cannot be measured e.g.: inefficient management in forestry; insecure ownership of many properties; inaccurate property registers and cadastral index maps; uncertain boundaries; ignorance among the proprietors regarding rights and location of boundaries causing disputes and conflicts; decision problems in co-owned properties.

Becker and Halimi (2019) treated Agricultural Land Consolidation as a multi-purpose instrument for the development of rural areas.

Biarel et al. (1992) studied the negative economic effect of farm fragmentation in African countries. They found that the existence of fragmented landholdings is an important feature in less developed agricultural systems. The costs of fragmentation include increased traveling time between fields (hence lower labor productivity and higher transport costs for inputs and outputs), negative externalities (such as reduced scope for irrigation and soil conserving investments as well as the loss of land for boundaries and access routes), and greater potential for disputes between neighbors. In light of these costs, numerous land reform policies have been aimed at enforcing, or at least subsidizing, the consolidation of holdings. These policies are premised on the assumption that fragmentation is necessarily inefficient and that agricultural production and social welfare can be increased through land consolidation.

Krigsholm et al. (2016), Konttinen (2016), Sulonen and Kotilainen (2016) analyzed the status, the efficiency of Land Consolidation on regional and agricultural development in Finland. They studied two land consolidation cases from Finland and evaluated their regional economic effects by using an input-output (IO) model. They found regional IO models provide multipliers that can be used to estimate the economy-wide effects that an initial change in economic activity, in this case, a land consolidation project, has on a regional economy. This study aimed to assess the regional economic impacts associated with the implementation of land consolidations. Particularly, they were focused on modeling: 1) total regional effects, 2) direct multiplier effects, and 3) indirect multiplier effects. They found and estimated the total regional impacts and direct and indirect multiplier effects. In short, direct multiplier effects were formed by increased consumption in households and sub-contractors that receive a salary that originates from the land consolidation project. Indirect multiplier effects were rippling down effects from subcontracts (i.e., subcontractor's subcontracts.

Konttinen (2016) evaluated the efficiency of Agricultural Land Consolidation in Finland. The author concluded that in the last two decades land consolidations in Finland were concentrated in agricultural areas. The main goal of the projects was a reduction of agricultural costs. Key figures when assessing the impact of a land consolidation project were parcel size and distance to the farmhouse.

Sulonen and Kotilainen (2016) investigated the determinants of Agricultural Land Consolidation for lessors in Finland. They discovered the lessors' concern that land consolidation causes additional and

unnecessary costs for them. Experiences of costs, such as cost distribution and how well the rents of arable lands cover the costs of land consolidation are most negative among lessors. Nevertheless, the status of lessor may be improved in the future by focusing on informing and cost-sharing.

Meijer and Emmens (2016) studied, analyzed, and shaped out the financial arrangements for land consolidation. They examined the Agricultural Land Consolidation costs. They found two types of costs. The first is financial settlements. These are costs that are the result of the exchanges. For example, costs for increasing property area or improving soil quality. When a landowner gets more or less property due to land consolidation he will have to pay or has to be compensated. The second types of cost are procedure and implementation costs. These are the costs that will contribute to the landowners in the progress. The amount of these costs will depend on the project costs in total. The landowners who benefit more from the land consolidation pay more than those who do less. The benefits of allotment have to be evaluated. In the Netherlands, this is done by an independent commission.

Thomas (2006) tried to systematize Land Consolidation Approaches applied in Europe.

Satana et al. (2017) evaluated the Turkish Experience in Consolidation of Irrigated Land and assessed implications of Agricultural Land Consolidation Projects for Productivity and Efficiency for the agrarian sector of the national economy.

Sky (2015) examined the Agricultural Land experience in Norway based on the international experience of land consolidation. The author concluded although the organization and objectives of land consolidation vary from country to country, the actual process is surprisingly similar between countries. This means that a comparison between different nations is relevant. Norway is the only state where all land consolidation is dealt with by a special court. Land consolidation can have economic, social, legal, spatial, and environmental impacts, but a fundamental principle, not just in Norway, is that no party shall suffer loss as a result of land consolidation. This, therefore, constitutes an important prerequisite for the final solution. Almost all national land consolidation legislation admits the possibility of compelling unwilling parties to take part in the process.

Although there has been ample literature on Agricultural Land Consolidation available, we have focused on those studies that mostly evaluate the various Agricultural Land Consolidation Patterns' performance in the different countries of the world. From the above discussed empirical work, we can say that studies primarily related to Agricultural Land Consolidation Patterns are done in different countries of the world, for example, in Netherlands, Norway, Turkey, Sweden, and Finland. Nevertheless, the authors of the present study attempt to evaluate the performance of Agricultural Land Consolidation in Russia and Kalmykia, a federal subject of the Russian Federation.

However, because the development of land relations in Russia has always been unique in comparison with other countries in Europe and the world, due to the state policy, national and religious differences, the vastness of the territory, and the variety of climate, natural and soil conditions generally accepted approaches and models of Agricultural Land Consolidation cannot always be accepted and applied in the Russian Federation.

Due to the absence of theoretical studies in Russia on the matter, the consolidation of agricultural land in the country is developing sometimes spontaneously and chaotic.

In Russia, the problem of land consolidation in agriculture is also a subject of nationwide political discussion and closely related to developing the agricultural sector of the national economy: based on small private farms or large agricultural enterprises.

Some economists suppose that only the development of small private farms is necessary. In this regard, other economists think that only further development of agricultural holdings is necessary. Nevertheless, there is concern that the development of the agricultural holdings leads to the emergence of the so-called "latifundium", which should be treated as a system of land tenure based on sizeable private land ownership.

Also, satellite imagery and UAVs for implementing the Agricultural Land Consolidation Projects and the demarcation of the boundaries of the agricultural land allotments on the ground in rural areas remain controversial and poorly studied.

2. METHOD

2.1. Methodology

The methodology includes the study of theoretical foundations and practical recommendations for improving the consolidation of agricultural land in Russia based on the Project Analysis Principles Approach developed by the World Bank.

At the same time, using statistical methods and monographic surveys, trends in the development of Agricultural Land Consolidation at both the federal and regional levels were identified, which are: the concentration of land ownership by agricultural holdings and an increase in the average size of private farms while reducing their number.

In Kalmykia, a federal subject of Russia, the unique trend continues to increase the number of private farms with an increase in their average size.

In concept, this methodology is very close to the view expressed in the 2020 FAO Legal guide, according to which the consolidation of agricultural land is carried out by agricultural holdings and private farms (Legal guide on land consolidation: Based on regulatory practices in Europe. FAO Legal Guide, No. 3. Rome, FAO (2020).

Authors have declared that no competing interests exist related to this paper. The information used for this research paper is commonly and predominantly use statistical products in Russia and Kalmykia, a federal subject of the Russian Federation.

2.2. Legal Framework

The state cadastral valuation of agricultural land is carried out based on Federal Law No. 237-FZ of July 3, 2016 “On State Cadastral Valuation" and by the Order of

the Ministry of Economic Development of Russia of May 12, 2017, No. 226 “On Approval of Methodological Guidelines on State Cadastral Valuation", which approved the main methodological approaches for conducting state cadastral valuation of real estate, including agricultural land.

2.3. Institutional Framework

In Kalmykia, there is a local office of the Rosreestr, which is responsible for the organization of a unified system of state cadastral registration of real estate, state registration of rights to immovable property, and real estate transactions and spatial data infrastructure.

The main task of the local branch of the Rosreestr is to maintain and provide information from the state real estate cadaster in Kalmykia.

Figure 1 displays Kalmyk cadastral region and cadastral districts of Kalmykia.

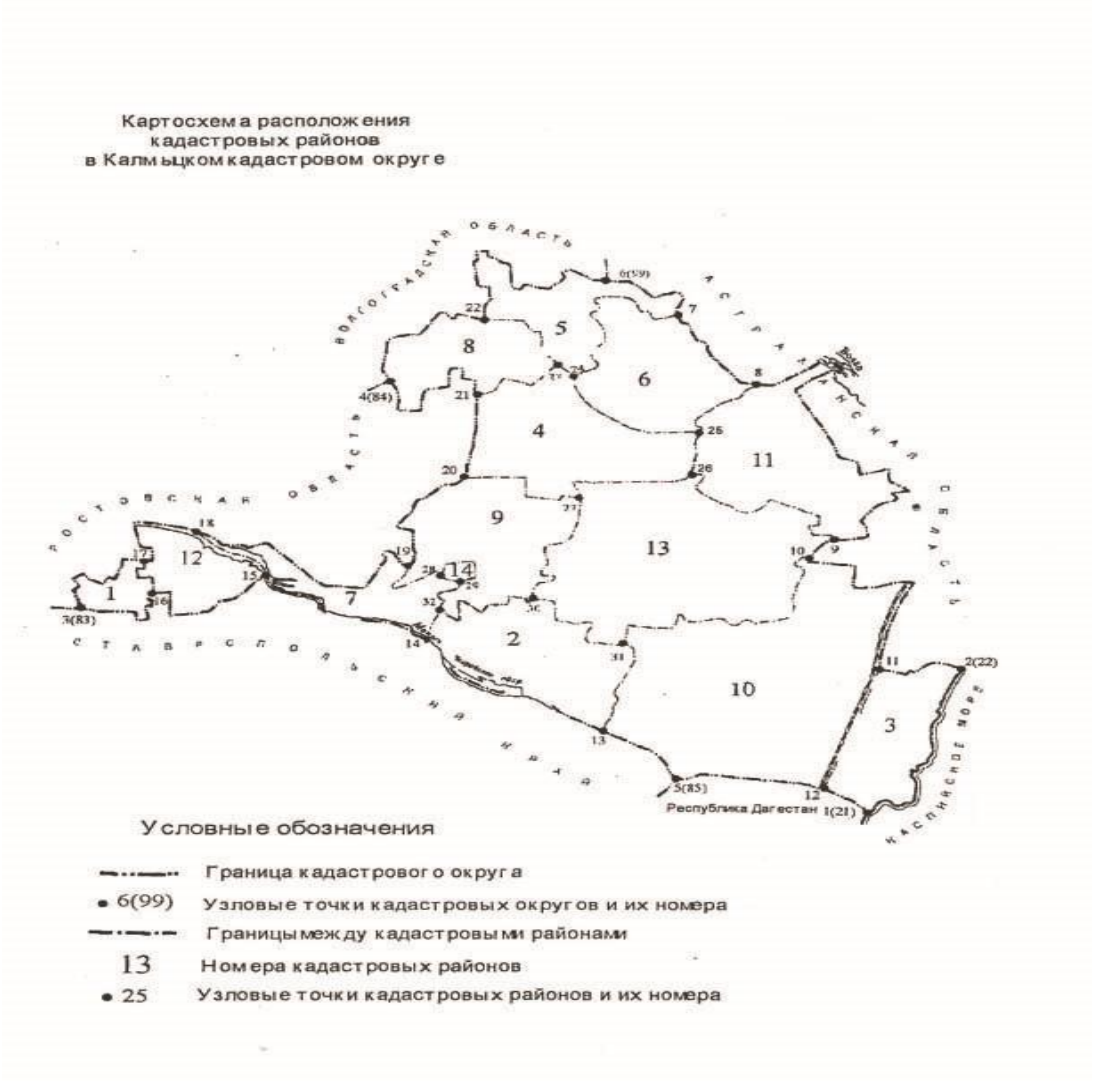

Figure 1. Kalmyk cadastral region and cadastral districts of Kalmykia (Source: The State (National) Report on the Status and Use of Lands in Russia in 2019, Rosreestr (2020))

3. RESULTS

3.1. The development of Agricultural Land Consolidation in Russia

In 2019, the total agricultural land area reduced in Russia by .4 M ha from 222.4 M ha to 222.0 M ha, or by .2%, compared to 1990 (see Table 1).

In 2019, the cropland area decreased by 9.6 M ha from 132.3 M ha to 122.7 M ha, or by 7.3%, compared to 1990(The State (National) Report on the Status and Use of Lands in Russia in 2019, Rosreestr (2020).

In 2019, the area of pasture land increased by 5.1 %, and idle lands by 16.3 times, compared to 1990(The State (National) Report on the Status and Use of Lands in Russia in 2019, Rosreestr (2020) (see Table 1).

Table 1. Agricultural Land, Russia, 1990-2019, M ha

Item	2019	1990	2019/1990, %
Agricultural land - total, including:	222.0	222.4	99.8
Cropland	122.7	132.3	92.7
Pasture	92.4	87.9	105.1
Idle land	4.9	.3	16.3 times

Source: The State (National) Report on the Status and Use of Lands in Russia in 2019, Rosreestr (2020)

In 2019, the state and municipal-owned land amounted to 1,579.5 M ha, or 92.2 %, private land -111.1 M ha, or 6.5 %, and land owned by legal entities – 21.9 M ha, or 1.3 %, of total Russia's territory.

The state and municipal-owned land in Russia increased by .1 M ha from 1,579.4 M ha to 1,579.5 M ha in 2019, compared to 2018, or by less than .1 %.

The share of the state and municipal-owned land in the total land of Russia was not changed in 2019, compared to 2018.

The private land area decreased by 1.0 M ha in 2019, compared to 2018 from 112.1 M ha to 111.1 M ha or by .9 %.

In 2019, the share of private land in the total land of Russia decreased by .1 pp. from 6.6% to 6.5%, compared to 2018.

At the same time, the area of land owned by legal entities increased by .9 M ha in 2019 compared to 2018 from 21.0 M ha to 21.9 M ha, or by 4.3 %.

The share of land owned by legal entities in the total land of Russia increased in 2019, compared to 2018 by .1 pp. from 1.2% to 1.3 %.

The state and municipal-owned agricultural land amounted to 254.1 M, ha, or 66.6 %, private land - 106.6 M ha, or 27.9 %, and land owned by legal entities – 20.9 M ha, or 5.5 %, of total Russia's agricultural land in 2019.

Thus, in 2019, the private agricultural land area decreased by 1.0 M ha from 107.6 M ha to 106.6 M ha, or by 1.0 %, compared to 2018.

In 2019, the area of agricultural land owned by legal entities increased by .9 M ha from 20.0 M ha to 20.9 M ha, or by 4.5 %, compared to 2018.

Moreover, in 2019, the state and municipal-owned agricultural land area decreased by .7 M ha from 254.8 M ha to 254.1 M ha, or by .3 %, compared to 2018.

In 2019, the share of the state and municipal-owned agricultural land was not changed in the total agricultural land of Russia, compared to 2018.

In 2019, the share of agricultural land owned by legal entities increased by .3 pp from 5.2% to 5.5% in the total agricultural land of Russia, compared to 2018.

In 2019, the share of the privately-owned agricultural land decreased by .3 pp from 28.2 % to 27.9 % in the total agricultural land of Russia, compared to 2018.

Thus, there is an extended trend of the absorption of private land by legal entities at the federal level.

In particular, this is also evident in the fact that a dominant role in agricultural land use in Russia has played joint-stock companies and production coops.

In 2019, the share of joint-stock companies and partnerships in the total area of agricultural land use of parastatals increased by .6 pp. from 54.0% to 54.6% in Russia, compared to 2018 (The State (National) Report on the Status and Use of Lands in Russia in 2019, Rosreestr (2020) (see Table 2).

In 2019, the share of joint-stock companies and partnerships in cropland of parastatals increased by .7 pp. from 59.4% to 60.1% in Russia, compared to 2018.

At the same time, in 2019, the share of production coops in the total area of agricultural land use of parastatals decreased by .6 pp. from 35.1% to 34.5% in Russia, compared to 2018.

Table 2. Parastatal's Land Use, Russia, 2019, K ha

Item	Total	Cropland
Joint-Stock Companies and Partnerships	62,503	44,430.2
Production Coops	34,428.8	22,395.2
State and Municipal Enterprises	5,448	2,413.5
Research Institutions	1,627.9	1,242.7
Subsidiary Farms	868.2	527.0
Other	4,367.4	2,800.2
Tribal Land	15.9	.4
Cossack Society Land	95.2	66.1
Total	114,354.4	73,875.3

Source: The State (National) Report on the Status and Use of Lands in Russia in 2019, Rosreestr (2020)

In 2019, the share of production coops in cropland of parastatals decreased by .7 pp. from 31.0% to 30.3% in Russia, compared to 2018(The State (National) Report on the Status and Use of Lands in Russia in 2019, Rosreestr (2020).

Thus, there is an extended trend of decreasing land use of production coops and increasing land use of joint-stock companies and partnerships, indicating further development of the Agricultural Land Consolidation by large and medium agricultural enterprises.

The average size of the ten most extensive agricultural holdings amounted to 608.2 K ha in 2020. In 2020, it increased by 18.6 %, compared to 2018. In 2020, it increased by 5.8 %, compared to 2019. It varied from 380 K ha to 1,047 K ha in 2020 (see Table 3) (Rating of the largest owners of agricultural land in Russia in May 2020, 2020).

Table 3. Agricultural Holdings Land Ownership, Russia, 2020, K ha

Item	Agricultural land	%
Miratorg	1,047	17.2
Prodimex&Agrokultura	865	14.2
Agrokomplex	653	10.8
Rusagro	643	10.6
EcoNiva-APK	599	9.9
Step+RZ Agro	542	8.9
BIO-TON	452	7.4
Volga –Don Agroinvest	451	7.4
Avangard-Agro	450	7.4
Vasilina	380	6.2
Total	6,082	100.0

Source: Rating of the largest owners of agricultural land in Russia in May 2020(2020)

Private farms play an important role in Russian agricultural private land use (see Table 4).

In 2019, the share of private farms in the total area of the private agricultural land use increased by .2 pp from 32.0% to 32.2%, compared to 2018 due to land consolidation (The State (National) Report on the Status and Use of Lands in Russia in 2019, Rosreestr (2020).

In 2019, the share of private farms in the total private area of the cropland use increased by .1 pp from 40.2% to 40.3%, compared to 2018 due to land consolidation

(The State (National) Report on the Status and Use of Lands in Russia in 2019, Rosreestr (2020).

Table 4. Private Land Use, Russia, 2019, K ha

Item	Total	Cropland
Private Farms	25,807.1	17,472.3
Individual Entrepreneurs	3,403.4	2,499.6
Personal Subsidiary Farms of Citizens	7,467.4	5,129.3
Service Land	53.5	10.6
Horticulture Farms	1,116.9	53.1
Vegetable Growing Farms	272.7	270.1
Outreach Dacha Farms	100.4	76.7
Housing Parcels	595.5	495.6
Livestock Farms	388.0	57.9
Grazing Farms	15,197.8	1,168.3
Land Parcels Owners	12,655.7	9,283.8
Land Shares Owners	12,211.6	6,594.8
Total	79,270.0	43,112.1

Source: The State (National) Report on the Status and Use of Lands in Russia in 2019, Rosreestr (2020)

In 2019, the number of private farms decreased by 7.5 %, compared to 1995 in Russia due to the severe macroeconomic environment, the disparity of prices for agricultural and industrial commodities, lack of developed infrastructure.

However, the average size of agricultural land occupied by the private farm has been increased due to land consolidation.

It was estimated at 76.6 ha in 2019. Thus, in 2019, it increased by 78.6 %, compared to 1995(The State (National) Report on the Status and Use of Lands in Russia in 2019, Rosreestr (2020) (see Table 5).

Table 5. Russia's Private Farming, 1995-2019

Item	2019	1995	2019/ 1995, %
Number of farms, K	258.3	279.1	92.5
Total land area, K ha	19,795.5	11,982.1	165.2
Average land size, ha	76.6	42.9	178.6

Source: The State (National) Report on the Status and Use of Lands in Russia in 2019, Rosreestr (2020)

The development of Agricultural Land Consolidation in Russia is mostly dependent on regional land policies.

Kalmykia is located in the South-East of the European part of Russia. Kalmykia agricultural land amounted to 6,937.3K ha, or 92.8%, of the total regional land in 2019(see Table 6).

Here we can observe a unique trend of increasing area of agricultural land in 2010-2019.

In 2019, the total area of agricultural land increased by 52.1 K ha, or .8 %, from 6,885.2 K ha to 6,937.3 K ha, compared to 2010(Regional Report on the Status and Use of Lands in Kalmykia in 2019, Kalmykiareestr (2020).

The main role in Kalmykia agricultural land use plays joint-stock companies and partnerships and production coops (see Table 7). In general, parastatals occupied 1,755.8 K ha or 25.3% of the total agricultural land area of the region in 2019.

Table 6. Kalmykia's Land, 2010-2019, K ha

Land	2019	2010	2019/2010, %
Agricultural	6,937.3	6,885.2	100.8
Urban	62.4	62.4	100.0
Industrial	15.7	15.0	104.7
Special	121.6	121.6	100.0
Forest	60.2	60.2	100.0
Water	60.1	59.1	101.4
Reserve	215.8	269.6	80.0
Total	7,473.1	7,473.1	100.0

Source: Regional Report on the Status and Use of Lands in Kalmykia in 2019, Kalmykiareestr (2020)

In 2019, the area of land use of parastatals decreased by 279.3 K ha, or 13.7%, from 2,035.1 to 1,755.8 K ha, compared to 2015.

In 2019, the share of the above-mentioned land use in the total agricultural land area of the region decreased by 4.1 pp from 29.4% to 25.3 %, compared to 2015(Regional Report on the Status and Use of Lands in Kalmykia in 2019, Kalmykiareestr (2020).

Table 7. Parastatal's Land Use, Kalmykia, 2019, K ha

Item	Area	Land leasing
Joint-Stock Companies and Partnerships	690.5	22.7
Production Coops	767.3	15.7
State and Municipal Enterprises	134.0	-
Research Institutions	30.5	-
Others	133.3	-
Total	1,755.8	38.4

Source: Regional Report on the Status and Use of Lands in Kalmykia in 2019, Kalmykiareestr (2020)

Joint-stock companies and partnerships occupied 690.5 K ha or 9.9% of the total agricultural land used in the region in 2019.

In 2019, the area of agricultural land used decreased by 43.3 K ha, or 5.9%, from 733.8 to 690.5 K ha, compared to 2015.

In 2019, the land use of joint-stock companies and partnerships increased from 647.1 K ha to 690.5 K ha, or by 43.4 K ha, or by 6.7%, compared to 2018.

The share of land use of joint-stock companies and partnerships in the total area of agricultural land in the region increased by .6 pp from 9.3% to 9.9% over this period.

In2019, the share of the above-mentioned land use in the total agricultural land area of the region decreased by .7 pp from 10.6% to 9.9% compared to 2015.

They have also used most of the agricultural land shares (94.1%) rented by parastatals in Kalmykia.

In 2019, the percentage of land shares rented by joint-stock companies and partnerships increased by 44.0 pp from 49.7 % to 94.1%, compared to 2018 due to a sharp decrease in the share of production coops.

The share of these businesses in the state and municipal-owned lands amounted to 90.0% of their total area in 2019.

In 2019, the share of the above-mentioned land use in the total land use of joint-stock companies and partnerships decreased by 6.0 pp from 96.0% to 90.0%, compared to 2015.

In 2019, compared to 2018, the share of state and municipal land used by joint-stock companies and partnerships decreased by 3.1 pp from 93.1% to 90.0%.

In general, joint-stock companies and partnerships occupied 39.3 % of the total land area owned by parastatals in 2019.

Thus, in 2019, their share in the land use of parastatals in Kalmykia increased by 3.3 pp from 36.0% to 39.3%, compared to 2018.

Production coops occupied 767.3 K ha, or 11.1%, of the total agricultural land area of the region in 2019.

In 2019, the production coops area decreased by 212.2 K ha, or 27.6 %, from 979.5 to 767.3 K ha, compared to 2015.

In 2019, the land use of production coops decreased from 834.8 K ha to 767.3 K ha by 67.5 K ha, or 8.1%, compared to 2018.

In 2019, the share of the above-mentioned land use in the total agricultural land area of the region decreased by 1.0 pp from 12.1% to 11.1%, compared to 2015.

In 2019, the share of the above-mentioned land use in the total agricultural land area of the region decreased by .9 pp from 11.1% to 10.2 %, compared to 2018.

The share of the state and municipal-owned lands used by production coops amounted to 97.0 % of their total area in 2019.

In 2019, the share of land use of production coops in the total land use of production coops decreased by 2.3 pp from 99.3% to 97.0 % compared to 2015.

In 2019, the share of production coops in the land use structure in the region increased by 1.6 pp from 95.4% to 97.0% compared to 2018.

In general, production coops occupied 43.5 % of the total land area owned by parastatals in 2019.

In 2019, the share of production coops in the land used structure of parastatals decreased from 48.1% to 43.5%, or by 4.6 pp, compared to 2015.

In 2019, the share of coops in the structure of land used of parastatals decreased by 3.0 pp from 46.5% to 43.5%, compared to 2018.

An important role in Kalmykia private agricultural land tenure plays land shares.

The total land share area amounted to 881.0 K ha, or 59.8 %, of the private land area.

In 2019, the area of land shares decreased by 221.8 K ha, or 20.1%, from 1,102.8 to 881.0 K ha, compared to 2015. In 2019, the share of the above-mentioned land in the total private land area of the region decreased by 7.3 pp from 26.3% to 19.5 19.0 %, compared to 2015. In 2019, land shares in the region decreased by 9.1 K ha from 890.1 K ha to 881.0 K ha, or by 1.0%, compared to 2018.

In 2019, the share of the above-mentioned land in the total private land area of the region decreased by .5 pp from 19.5% to 19.0 %, compared to 2018(Regional Report on the Status and Use of Lands in Kalmykia in 2019, Kalmykiareestr (2020) (see Table 8).

In Kalmykia, we can observe a unique and extended trend: the increase in the number of private farms and the increase in their average size (see Table 9).

Table 8. Private Land Use, Kalmykia, 2019, K ha

Item	Total land area	Private ownership
Private Farms	3,212.9	61.5
Individual Entrepreneurs	4.6	1.7
Personal Subsidiary Farms of Citizens	7.2	2.1
Horticulture Farms	1.3	.9
Vegetable Growing Farms	-	-
Housing Parcels	5.5	3.9
Livestock Farms	1.3	.7
Land Parcels Owners	521.7	521.7
Land Share Owners	881.0	881.0
Total	4,635.5	1,473.5

Source: Regional Report on the Status and Use of Lands in Kalmykia in 2019, Kalmykiareestr (2020)

Table 9. Kalmykia's Private Farming, 1992-2019

Item	2019	1992	2019/1992, times
Number of farms	3,042	292	10.4
Total land area, K ha	3,212.9	168	19.1
Average land size, ha	1,056	575	1.8

Source: Regional Report on the Status and Use of Lands in Kalmykia in 2019, Kalmykiareestr(2020)

In 2019, the number of private farms in Kalmykia increased, compared to 1992 by 10.4 times. In 2019, the land area occupied by private farms in the region increased, compared to 1992 by 19.1 times. The average size of the private farm amounted to 1,056 ha in Kalmykia in 2019. It increased in 2019, compared to 1992 by 1.8 times, due to land consolidation based on renting and buying of agricultural land shares. It is significantly different from the average for Russia, where a reduction in their number accompanies an increase in the area above-mentioned farms.

3.2. Agricultural Land Market Tools

The Agricultural Land Market in Kalmykia has been steadily developed despite the increase in the cadastral value of the land.

To encourage land consolidation, it is necessary to develop the Agricultural Land Market based on land auctions. In turn, the market price of land is the basis for Agricultural Land Taxation and Agricultural Land Mortgage transactions.

The Starting Agricultural Land Market Auction Price Model (SALAPM) was developed (Sagaydak and Sagaydak, 2016) and Agricultural Land Values and Taxation Rates were determined for 2021 (see Table 10) based on that concept.

Land tax is calculated as .3 % of the starting auction price of agricultural land. In theory, the contract land rent rate can't be less than land tax rates. Otherwise, the landowner will not be interested to give land on lease.

Therefore, it is necessary to provide at least the average level of profitability for the landowner that can be taken as 40 % compared to the rate of land tax. You can see the above mentioned-market prices of agricultural land calculated for the local municipalities on the map of Kalmykia designed by Yandex (see Figure 2).

Table 10. Agricultural Land Values and Taxation, Kalmykia, Rub/ha (draft)

Municipalities	Cadastral Value	Starting Auction Price	Mortgage Value	Land Tax
Gorodovikovskoe	84,580	14,912	10,438	44.74
Iki-Burulskoe	10,760	1,904	1,332	5.71
Ketchenerovskoe	11,800	2,080	1,456	6.24
Laganskoe	2,800	494	345	1.48
Maloderbetovskoe	12,430	2,186	1,530	6.56
Oktyabr'skoe	4,200	740	518	2.22
Priyoutnenskoe	19,800	3,490	2,443	10.47
Sarpinskoe	13,570	2,397	1,678	7.19
Tselinnoe	10,980	1,939	1,357	5.82
Chernozemelskoe	2,900	511	358	1.53
Youstinskoe	3,150	546	382	1.64
Yashaltinskoe	39,050	6,874	4,812	20.62
Yashkul'skoe	2,440	2,115	1,481	6.34
Average	15,760	2,961	2,073	8.88

However, when determining the starting auction price of agricultural land, such important price-forming factors as demand and supply for specific land parcels in the agricultural sector of the national economy in Russia are not taken into account.

At the same time, the starting auction price of land in agriculture acts as a basic, relatively certain component of the market price of agricultural land, while the influence of supply and demand on the price of land parcels introduces uncertainty in the pricing process for land.

Accounting for the above price-forming factors can be carried out based on determining the market values of "put" and "call" options for agricultural land parcels.

The put option acts as a contract between the seller and the buyer of the derivative. The owner has the opportunity to sell an agricultural land parcel at a pre-agreed strike price during the term of the contract.

Figure 2. Map of Market Prices in Kalmykia, Rub/ha, designed by Yandex(draft)

The value of this option determines by the premium that the buyer of the derivative pays to its seller and determine by the yield of this financial instrument, depending on changes in the market price of the land parcel under the influence of supply and demand factors for agricultural land.

If the market price of the agricultural land parcel exceeds the fixed price of the derivative, the option holder will not sell it.

If the agricultural land parcel market price is lower than the exercise price of the option, then the owner of the derivative sells it.

In this case, the profit of the option holder will be equal to the spread between the fixed strike price of the derivative and the market price of the land, minus the premium paid to them when purchasing the option.

Therefore, the market price of an agricultural land parcel will be equal to:

$$R_m' = P_s + C_{put} \quad (1)$$

where

$R_{m'}$– market price of an agricultural land parcel, Rub; P_s-starting auction price of the agricultural land parcel, Rub;C_{put} – value (premium) of the "put" option, Rub.

The call option also acts as a contract between the buyer and the seller of the derivative, which allows the buyer of the option to buy land in the future at a fixed strike price for a period specified in the contract.

The seller of the option obliges to sell his land parcel if the buyer-owner of the derivative wants to purchase land since he was already paid a premium after the contract.

At the same time, the buyer-owner of the "call" option makes a profit if the land price tends to increase. As a result, the market price of an agricultural land parcel will be equal to:

$$R_m'' = P_s + C_{call} \quad (2)$$

where

R_m'' – market price of an agricultural land parcel, Rub; P_s-starting auction price of the agricultural land parcel, Rub;C_{Call}– the cost (premium) of the "call" option, Rub.

However, the ratio of the option value of "put" and "call" the land in agriculture reflects their parity, equivalence, as prices of option "put" in the short term and call option in the long term equal to contract value "forward" for sale agricultural land with the same fixed strike price.

Ensuring the principle of equivalence of the values of the above-mentioned derivatives is implemented based on fulfilling the condition of the need for the absence of arbitration transactions with them in spatial and temporal aspects. This means that if the value of a land parcel of agricultural land is higher than the fixed exercise price of the option, then a contract for the land is concluded based on the "call" option, and if it is lower-the "put" option.

In each particular case, the actual price of an agricultural land parcel may deviate from the fixed prices of their execution established in the contracts of "put" and "call" options.

The development of the process of consolidation of agricultural land leads to a quantitative increase in the amount of land rent and, accordingly, to an increase in the market value of land parcels in the agricultural sector of the national economy in Russia.

Experience shows that the market value (premium) of "call" options in terms of growth of their value is on average about 3% of the offer price at land auctions.

Therefore, the market price of agricultural land can be represented as the sum of the starting auction price of it and the value (premium) of the «call" option for land parcels. This approach to determining the market value of agricultural land was tested on the materials of Kalmykia (see Table 11).

Table 11. Agricultural Land Market Prices, Kalmykia, Rub/ha (draft)

Municipalities	Starting Auction Price	Call Premium	Land Market Price
Gorodovikovskoe	14,912	447	15,359
Iki-Burulskoe	1,904	57	1,961
Ketchenerovskoe	2,080	62	2,142
Laganskoe	494	15	509
Maloderbetovskoe	2,186	66	2,252
Oktyabr'skoe	740	22	762
Priyoutnenskoe	3,490	105	3,595
Sarpinskoe	2,397	72	2,469
Tselinnoe	1,939	58	1,997
Chernozemelskoe	511	15	526
Youstinskoe	546	16	562
Yashaltinskoe	6,874	206	7,080
Yashkul'skoe	2,115	63	2,178
Average	2,961	89	3,050

According to Table 11, the market price of agricultural land parcels can be interpreted as the auction price of land, adjusted for the interaction of supply and demand factors due to the situation on the land market.

This methodology implies further development of the Agricultural Land Market, auction trade in agricultural land parcels, and financial and credit relations, both in the agricultural sector and in the national economy of Russia as a whole.

It's also important to implement a Logical Framework Methodology for designing Agricultural Land Consolidation Projects.

As we mentioned before, the super goal of Agricultural Land Consolidation Projects is to implement and develop Agricultural Land Consolidation to increase the efficiency of agricultural production to eliminate hunger and food shortages as well as poverty due to the rapidly growing world population and coronavirus pandemic.

Thus, Agricultural Land Consolidation looks like a complex social and economic process, including technical, institutional, financial, economic, environmental, and social aspects, highlighting advanced and internationally recognized the World Bank's Agricultural Project Analysis Methodology.

The aim of Technical Analysis of Agricultural Land Consolidation is the implementation of land use planning activities focused on the removal of mosaic agricultural land ownership, optimization of the configuration and size of agricultural land parcels and the development of the highway network, social and production facilities in the countryside to increase agricultural production and reduce of its costs.

The goal of Institutional Analysis of Agricultural Land Consolidation Projects describes the selection of institutions or beneficiaries interested in implementing

them based on indicators of financial and economic efficiency. The stakeholder may be any legal entity, for instance, private farms, agricultural holdings.

The purpose of the Financial Analysis of Agricultural Land Consolidation Projects is to determine their financial efficiency for any organization directly involved and responsible in their implementation based on cost-benefit analysis.

It should be noted that with increasing the size of agricultural land parcels the financial efficiency of agricultural production is increasing due to the relative reduction of transaction costs per unit of agricultural land area used.

The maximum efficiency of farming is reached when the level of transaction costs per unit of agricultural land used is reduced to a minimum level.

However, following increasing the size of agricultural land allotments used leads to decreasing financial efficiency of farming due to the increase in transaction costs per unit of agricultural land area used (Figure 3).

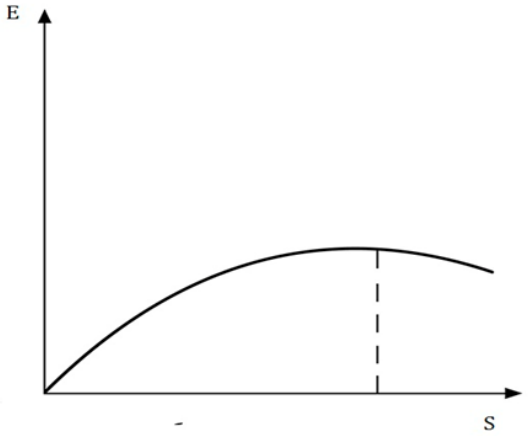

Figure 3. Dependence of the efficiency of the Agricultural Land Consolidation Project (E) on its scale(S)

In this regard, the main problem is analyzing and evaluating the financial efficiency of Agricultural Land Consolidation Projects based on cost-benefit analysis (Backman, 2010), (Backman, 2016).

The most important condition for applying cost-benefit analysis for the evaluation of financial efficiency of Agricultural Land Consolidation Projects is to ensure adequate assessment and comparability of financial indicators of costs, benefits, and efficiency criteria based on an international financial reporting system, for example, US GAAP. It could create additional incentives to attract outside investors to come and input their capital in agriculture.

In that sense, the allocation of capital as investments in agriculture is based on Agricultural Land Consolidation.

The Economic Analysis of Agricultural Land Consolidation Projects aims to determine their economic efficiency for society as a whole and regions based on analysis of economic assessment costs and benefits via "shadow" price.

The Environment Analysis of Agricultural Land Consolidation Projects focuses on assessing their impact on the environment based on direct and indirect marketing valuation methods, for example, "shadow" projects.

The Social Analysis of Agricultural Land Consolidation Projects aims to assess their impact on the social, cultural, and demographic characteristics, the social organization, cultural acceptability, and different groups of population such as women, indigenous people, and youth.

The Agricultural Land Consolidation Project's Life Circle consists of Creative Design Phase and the Implementation Phase (Figure 4).

In turn, the Creative Design Phase consists of Identification, Feasibility Study, Preparation, Detailed Design, and Appraisal Stages. The Implementation Phase consists of Negotiation, Loan Approval, Implementation, Supervision, and Completion Stages.

The goals and objectives of the Agricultural Land Consolidation Project are determined at the Identification Stage.

Technical Analysis, Institutional Analysis, Financial Analysis, Economic Analysis, Environmental Analysis, and Social Analysis of the Agricultural Land Consolidation Projects are carried out at the Prefeasibility Study Stage and Feasibility Study Stage.

A business plan for the Agricultural Land Consolidation Project is developed at the Preparation Stage.

Clarification of the business plan for the Agricultural Land Consolidation Project due to changes in the macroeconomic situation is carried out at the Detailed Design Stage.

The external expertise of the Agricultural Land Consolidation Project is carried out at the Appraisal Stage.

Further, the business plan of the Agricultural Land Consolidation Project is submitted to the bank to resolve the issue of allocation of loans for its financing.

To this end, the owners and beneficiaries of the Agricultural Land Consolidation Project and the bank negotiate a loan to finance it.

The signing of the loan agreement is carried out at the Negotiation and Loan Approval Stages to finance the Agricultural Land Consolidation Project.

The Agricultural Land Consolidation Project starts at the Direct Implementation Stage. Geodetic and land use planning works focused on the consolidation of small parcels into larger agricultural land allotments are carried out here.

Monitoring of the progress of the Agricultural Land Consolidation Project in terms of cost and implementation time is carried out at the Supervision Stage using the PERT (Project Evaluation and Report Technique) and GERT (Graphical Evaluation and Report Technique) Methodologies.

As a result of the Agricultural Land Consolidation Project, agricultural land allotments should be formed, allowing for farming and the use of modern agricultural machinery and technologies effectively.

At the Completion Stage of the Agricultural Land Consolidation Project, a retrospective analysis of its implementation is also carried out, which allows identifying all the pros and cons of its implementation.

Training capabilities and public information programs should be included in the Agricultural Land Consolidation Projects framework to support the implementation and development of Agricultural Land Consolidation.

The main take-offs of the Agricultural Land Consolidation Projects should assist national and local officials as well as decision-makers involved in Agricultural Land Consolidation to analyze policy and procedural constraints and opportunities to ensure the above-mentioned process as a viable option and to strengthen movement towards eliminating hunger and food shortages and poverty due to the rapidly growing the world's population and coronavirus pandemic.

Currently, to accelerate the progress of Agricultural Land Consolidation and improve the efficiency of farming, it is very important to develop a working digital model of the Agricultural Land Consolidation Projects.

Due to it, the modified Agricultural Land Consolidation Project Logical Framework Matrix (ALCPLFM) has been designed (see Table 12).

The implementation of the Agricultural Land Consolidation Projects begins with an analysis of the relations of land ownership and land use developed in the region taking into account geographical, economic, national, religious, and other conditions.

Thus, it is necessary to determine the owners and beneficiaries of the Agricultural Land Consolidation Project.

It should be emphasized that at present the relations of land ownership in Russian agriculture are largely complex and confusing because, during the reorganization of former state and collective farms, the land shares granted to former collective farmers and workers of state farms were not allocated in kind and demarcated on the ground. In this regard, it is necessary to find the owners of land shares, many of whom have already left the countryside and live-in large cities, to obtain their consent to sell or lease their virtual land shares, which is very difficult, and sometimes impossible.

The final shaping of consolidated agricultural land massive should be carried out gradually, step by step, annually combining similar agricultural land plots in terms of geodetic and land use planning characteristics, location, and property rights.

Next, it is necessary to form optimal agricultural land allotments, determine their geographical coordinates, and demarcate their boundaries.

Implementing this task is often complicated and requires considerable time, ultimately determining the duration of the Agricultural Land Consolidation Project's Life Cycle (Figure 4).

In turn, the duration of the Agricultural Land Consolidation Project's Life Cycle determines the discount rate, which is used in the calculation of cost, benefits, and determination of indicators of financial and economic efficiency of the Agricultural Land Consolidation Projects.

The costs of a land consolidation project in agriculture are determined much more easily than the benefits of its implementation and include the following components:

- costs associated with the definition and clarification of land ownership and land use rights in the implementation of agricultural land consolidation;
- costs of carrying out geodetic works;
- costs of land use planning works; costs of state registration of land ownership rights.

Table 12. Agricultural Land Consolidation Project Logical Framework Matrix

Content	Verified Indicators	Narrative Summary	Assumptions
Super goal	Increase the efficiency of agricultural production, eliminate hunger and poverty, mitigate the negative impact of the coronavirus pandemic	Increasing financial and economic efficiency of agricultural production	Growth of land rent and price of agricultural land
Specific Objectives	Increase, optimization of the size and configuration of land parcels, elimination of mosaic land ownership	Improving the efficiency of the use of agricultural machinery	Growth of agricultural production
Activities	List of geodetic and land use planning work in physical terms, application Sattelite Imagery, and UAV	The volume of geodetic and land use planning work in physical terms	Owners and beneficiaries of the project
Investment	Financing of land use planning work	The investment required for the implement ation of land use planning work	Attracting outside investors to finance the project
Investment sources	Ensuring targeted investment financing	Lending is required to provide targeted financing for the Agricultura l Land Consolidati on Project. Commercia l bank's interest rate policy. Issuing corporate bonds, MBS, CMO	The Central Bank's policy and refinishing rate. Market interest rate Inflation rate

At the same time, in the cost structure, the largest share is occupied by the costs of conducting geodetic and land use planning works.

To reduce and optimize the financial and time costs of the Agricultural Land Consolidation Projects, Gantt charts, and network graphs to monitor the progress of its implementation should be developed.

A significant reduction in the cost of implementing Agricultural Land Consolidation Projects is also provided by the use of satellite imagery and UAVs during geodetic and land use planning works.

The benefits of the Agricultural Land Consolidation project are characterized by an increase in the value of agricultural products produced and sold and a reduction in transaction costs resulting from the consolidation of agricultural land.

At the same time, financial benefits are calculated in current or accounting prices, and economic benefits - in "shadow" or replacement prices.

Based on the financial and economic assessment of the costs and benefits of the Agricultural Land Consolidation Projects the following indicators of its financial and economic efficiency are determined: NPV (Net Present Value); PI (Profitability Index); IRR (Internal Rate of Return); PP (Payback Period); DPP (Discounted Payback Period); ROI (Return on Investment); AAR (Average Accounting Return); ROA (Return on Assets); ROE (Return on Equity); Other financial coefficients.

Agricultural Land Consolidation Projects Risk Analysis focuses on the application of the Scenario Analysis, Sensitivity Analysis, and the Monte Carlo or simulation methodology to the consolidation of agricultural land.

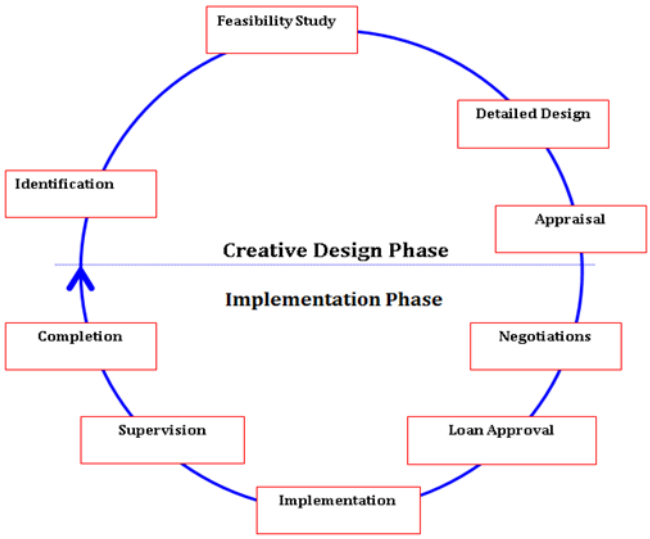

Figure 4. Agricultural Land Consolidation Project's Life Cycle

4. DISCUSSION

In the above-mentioned land cadaster valuation guidelines, there are several controversial points concerning the implementation of the state cadastral assessment of agricultural land.

In the methodology, it is practically proposed to evaluate the natural fertility of soils, i.e., the fertility of the land given from "nature".

At the same time, however, it does not take into account the fact that the economic, i.e. the actual fertility of agricultural land allotments currently available is an inseparable synthesis of natural and artificial, i.e. human-made, fertility.

The artificial fertility of the soil acts as an added value concerning the natural soil's fertility, which has no value, and changes in connection with the development of the productive forces of society.

In this regard, in our opinion, there are problems with the use of the so-called "standard yield" indicator for cadastral assessment, since it characterizes not only the quality of the soil but also the influence of factors of intensification of agricultural production on land productivity.

This problem was faced by Vasily Dokuchaev and Nikolay Annensky when assessing land in the Nizhny Novgorod province in 1882-1886.

They are forced to refine the soil's natural history survey significantly and introduced an indicator of the so-called "normal yield of grains" for land assessment.

To eliminate the influence of the intensification factors, Vasily Dokuchaev and Nikolay Annensky used the method of statistical combinational groupings. However, they failed to completely solve this problem (even with a relatively low level of intensification at that time) when assessing land in the Nizhny Novgorod province.

The above-mentioned problem was also not solved in the methodology of economic land valuation prepared by Sergey Cheremushkin in the early 60s of the last century and the temporary All-Union Land Valuation Methodology developed by the former State Institute of Land Resources (GIZR) in 1976. However, it was proposed to use two methods: selecting typical farms and correlation and regression analysis.

As a result, the fertility of the land was evaluated together with the economic factors associated with the intensification of agricultural production.

Besides, the guidelines mentioned earlier still contain problems related to the validity of the calculation of cadastral valuation indicators, such as the standard yield of crops, gross income, and land rent.

The disadvantage of the method is that it does not give any algorithm for determining the standard yield of crops.

Also: "Gross income is calculated for a unit of land area as the product of the standard yield of an agricultural crop on its market price".

However, this indicator should not be considered as gross income, but as the value of gross output for a particular crop when evaluated at market prices, which is also not sufficiently justified, since not all agricultural products can be sold on the market.

Moreover, "The determination of the cadastral value of agricultural land suitable for arable land is carried out by the method of capitalization of land rent, which is calculated as the difference between gross income and the cost of cultivating and harvesting agricultural products".

However, this does not consider the fact that gross income itself represents the difference between the value of gross agricultural output and material costs. In the interpretation of the methodology, it is not the land rent that is capitalized, but the profit, which acts as the difference between the revenue and the cost of products sold.

Due to it, a new, innovative agricultural land valuation methodology based on market economy principles should be developed and introduced in this connection.

5. CONCLUSION

The main takeaway of the paper is that necessary to implement the legal, organizational, technical, institutional, financial, economic, environmental, and social measures to support the development of Agricultural Land Consolidation based on the Agricultural Land Market in Russia.

In that sense, it's very important to revise and improve Agricultural Land Consolidation and Agricultural Land Market legislation.

The other takeaway of the paper is to implement the institutional framework for the development of Agricultural Land Consolidation and Agricultural Land Market.

It's also necessary to introduce the Agricultural Land Auctions, "call", "put", and "forward" contracts for agricultural land to stimulate the development of the Agricultural Land Market and Agricultural Land Consolidation in Russia.

There is a need to design and introduce education programs related to Agricultural Land Consolidation and Agricultural Land Market Development.

It's also imperative to start a PR campaign to strengthen people's ability to understand the role and importance of Agricultural Land Consolidation Agricultural Land Market Development.

A new, innovative agricultural land cadastral valuation methodology based on market economy principles should be developed and introduced.

One more takeaway of the paper is the necessity to launch pilot projects focused on Agricultural Land Consolidation and Agricultural Land Market Development to make a demonstration effect.

It is also crucial to apply the Project Analysis Principles Approach to design and implement Agricultural Land Consolidation Projects.

Furthermore, last but not least, a need to collect, scrutinize, disseminate, and replicate positive Agricultural Land Consolidation and Agricultural Land Market Development experience (Sagaydak and Sagaydak 2021).

ACKNOWLEDGMENT

The authors express their deep appreciation and gratitude to the editorial board for the opportunity to submit their scientific article on the problems of agricultural land consolidation for publication in this journal.

Author contributions

Alexander Sagaydak: Conceptualization, Methodology, Writing-Original draft preparation, Writing-Reviewing and Editing. **Anna Sagaydak**: Data curation, Visualization, Investigation.

Conflicts of interest

The authors declare no conflicts of interest.

REFERENCES

Backman, Mats (2010) Cost-Benefit Analysis of Land Consolidation in Sweden from View Point of Society and Landowner. XXIV Congress FIG "Facing Challenges-Building the Capacity", Sydney, Australia, 11-16 April 2010

Backman, Mats (2016) Cost-Benefit Analysis of Land Consolidation in Sweden from View Point of Society and Landowner. Proceedings of Symposium on Land Consolidation and Land Readjustment for Sustainable Development, 9-11 November 2016, Apeldoorn, Netherlands

Backman, Mats (2016). Basic Requirements for Successful Land Consolidation. Proceedings of Symposium on Land Consolidation and Land Readjustment for Sustainable Development, 9-11 November 2016, Apeldoorn, Netherlands

Becker, Michael, Halimi Kaplan (2019) Land Consolidation as a multi-purpose Instrument exploring Opportunities and addressing Challenges in Kosovo. Annual World Bank Conference on Land and Poverty, Washington DC, March 25-29, 2019

Biarel B, Hazell P, Place F & Quiggin J (1992). The economics of Farm fragmentation: evidence from Ghana and Rwanda, World Bank Economic Review, 6, 233-254

Konttinen K (2016). The effectivity of Land Consolidation in Finland. Proceedings of Symposium on Land Consolidation and Land Readjustment for Sustainable Development, 9-11 November 2016, Apeldoorn, Netherlands

Krigsholm P, Keskitalo J, Riekkinen K, Niironen J & Kolis Karin (2016). Evaluating Regional Impact of Land Consolidation Projects. Proceedings of Symposium on Land Consolidation and Land Readjustment for Sustainable Development, 9-11 November 2016, Apeldoorn, Netherlands

Legal guide on land consolidation: Based on regulatory practices in Europe. FAO Legal Guide, No. 3. Rome, FAO (2020)

Meijer G & Emmens N (2016). Financial arrangements in Land Consolidation. Proceedings of Symposium on Land Consolidation and Land Readjustment for Sustainable Development, 9-11 November 2016, Apeldoorn, Netherlands

Rating of the largest owners of agricultural land in Russia in May 2020 (2020);

Regional Report on the Status and Use of Lands in Kalmykia in 2019, Kalmykiareestr (2020).

Sagaydak A, Sagaydak A (2016). Problems of forming the auction price of land in agriculture. Zemleustroistvo, kadastr i monitoring zemel, 7, 38-47

Sagaydak A, Sagaydak A (2021). Economics and organization of agricultural production, KnoRus Publishing House. ISBN 978-5-406-07159-5.

Satana S, Ceylan A R, Sert A (2017). The Turkish Experience in Consolidation of Irrigated Land: Productivity and Efficiency Implications. Annual World Bank Conference on Land and Poverty, Washington DC, March 20-24, 2017

Sky P K (2015) Land consolidation in Norway in an international perspective. Spanish Journal of Rural Development, Vol. VI (1-2), 81-90

Sulonen K & Kotilainen, S (2016). Lessor's Status in Land Consolidation in Finland. Nordic Journal of Surveying and Real Estate Research,1-11,18-36

The State (National) Report on the Status and Use of Lands in Russia in 2019, Rosreestr (2020)

Thomas J (2006) Attempt on Systematization of Land Consolidation Approaches in Europe. Zeitschrift für Geodäsie, Geoinformation und Land management, 3, 156-161

Van den Noort P C (1987). Land consolidation in the Netherlands. Land Use Policy, 4 (1), January 1987, 11-13. Elsevier Ltd.

Voluntary Guidelines on the Responsible Governance of Tenure of Land, Fisheries and Forests in the Context of National Food Security (2012), Rome, FAO

International Journal of Engineering and Geosciences
https://dergipark.org.tr/en/pub/ijeg
e-ISSN 2548-0960

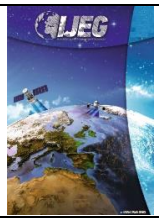

The effect of tourism and legalization policies on summer pasture in Turkey

Fatih Döner *[1]

[1]*Gumushane University, Faculty of Engineering and Natural Sciences, Department of Geomatics Engineering, Gumushane, Turkey*

Keywords
Summer pasture
Land management
Cadastre
Legalization
Tourism

ABSTRACT

In Turkey, according to Pasture Law, land allocated for farmers to spend the summer with their animals, graze their animals and benefit from grass is defined as "summer pasture (yaylak in Turkish)." Summer pasture is of national importance for its biodiversity, landscape, cultural heritage and transhumance. However, especially after 1990s, the summer pasture areas have been extensively used in tourism activities in Turkey. By changing land use, the increasing tourism activities combined with legal uncertainties and the legalization policies have caused summer pasture areas transferred into built-up areas. The effect of the tourism and legalization policies on the land use changes in summer pasture areas was evaluated in this study. It was determined that Turkey's tourism and legalization policies have adverse effect on sustainable use of summer pasture areas. These policies aimed at economic development and solving property problems of rural areas caused new legal problems and expansion of built-up areas. A better land use policy and an effective control mechanism are necessary for the sustainable use of summer pasture areas.

1. INTRODUCTION

Land policy is comprised of all socio-economic and legal regulations that determine how the benefits obtained from the land are allocated; it is related to the subjects of sustainable management of natural resources and environment and of resolution of land disputes. Land policy is an important part of national policies to realize the targets of economic development, social justice, equity, and political stability (UNECE 1996). Reasons such as the insufficient registry of rights related to land resources, weak legal regulations, and the absence of customary/traditional land use rights in land administration systems lead to the disputes over land use by making land management difficult (UN-FIG 1999; Steudler and Kaufman 2014). The land is the basis of all vital and economic activities. Land is used for activities such as agriculture, forestry, transportation and shelter, and land use changes over time depending on these activities. These changes in land use cause many environmental problems such as climate change, biodiversity reduction, air, water and soil pollution (EEA 2010).

Summer pasture (yaylak in Turkish), one of the significant resources of Turkey, has been defined in the Pasture Law as land for farmers to occupy in summers with their animals, to graze animals, and to benefit from the grassland. To define similar land, the European Union (EU) uses the term "Less Favored Area" (LFA) (EEC 1999). LFA refers to areas where farming has become less profitable due to harsh climate, high altitude, short growing season and poor soil fertility. In addition, in some studies carried out in the UK, the areas where farming has become marginal because of productivity limiting factors such as steep slopes, high altitudes, harsh climate and distance from markets have been named as 'uplands' (Reed et al. 2009; Acs et al. 2010; Hardaker 2018). Since the EU and UK definitions covers more broad land which also include summer pasture areas, the term of 'summer pasture' hereafter will be used in this study because of its suitability for Turkish laws and habitat. Summer pasture areas exist in many parts of the world are of great importance in terms of biodiversity (Koch et al. 2013; Jerrentrup et al. 2016), landscape and cultural heritage (Herzog et al. 2009), nutrition and livelihood (Danachair 1983; Zendri et al. 2013). Moreover, summer pasture areas provide climate regulation through carbon storage and renewable energy supplies (Nettier et al. 2017), clean water supplies and recreation opportunities (Hubacek et al. 2009).

Summer pasture areas are present in nearly all regions of Turkey, and they contribute greatly to the country's livestock production by providing forage. However, the summer pasture areas used for livestock

* **Corresponding Author**
*(fatihdoner@gumushane.edu.tr) ORCID ID 0000– 0002– 3620– 5687

Cite this article
Doner F (2022). The effect of tourism and legalization policies on summer pasture in Turkey. International Journal of Engineering and Geosciences, 7(2), 142-153

Research Article / DOI: 10.26833/ijeg.927503
Received: 25/04/2021; Accepted: 03/07/2021

grazing in the past have begun to be used frequently in tourism, vacation and leisure activities due to the decrease in the population of farmers and migration. As a result, there have been important changes in land use in the summer pasture areas in Turkey.

Studies aimed at examining the land use / land cover changes of pasture areas have been carried out in various countries (Merry et al. 2002; Schulz 2015; Kosmas et al 2015; Cohn et al. 2016; Akale et al. 2017; Minotti et al. 2018; Guo et al. 2019; Iversen et al. in press; Schaak and Musshoff in press; James and Lovelock in press; Upadhaya and Dwivedi 2019). Nevertheless, research to determine the impact of tourism and legalization policies on land use changes on summer pasture areas is needed considering the registration of land use rights of summer pasture areas in land registration system in Turkey.

After the introduction, in the second section, current situation of registering the legal status of land use in summer pasture areas in Turkey was examined. In the third section, the impact of tourism policies on the summer pasture areas is evaluated by examining the "Green Road Tourism Project" aims for connecting summer pasture areas of Eastern Black Sea Region in Turkey. By examining the legalization process of informal settlements in Turkey, effect of this process on summer pasture areas is evaluated in the fourth section. Finally, the study ends with conclusions in section 5.

2. REGISTRATION OF THE LEGAL SITUATION IN SUMMER PASTURE AREAS

2.1. Ottoman Empire Period

Summer pasture was always great importance to sustain livestock activities and provide tax revenue from these activities during the time of Ottoman. The roots of the current legislation regarding management of summer pasture go back to the Ottoman Empire era. For a better management, the land was divided into five classes in the Ottoman time with respect to their use by the Land Law (Arazi Kanunnamesi) declared in 1858. These classes were as follows (the Turkish terms are added in italic, in brackets) (Biyik et al 2018; Bıyık and Yavuz 2006):

- State land (Miri)
- Private land (Mülk)
- Waqf land (Vakıf)
- Tribal and collective land (Metruk)
- Waste land (Mevat)

State land comprised the portion of land with agricultural potential. Administration of these land, also called fief (dirlik), was left to Ottoman statesmen and officials in return of certain services. Private land was the land that held by individual ownership. Waqf land was land that their income was allocated to the expenses of institutions serving the community such as mosques, madrasahs, hospitals, inns and bathhouses. Tribal and collective land included non-agricultural land such as pasture, grasslands, summer pasture, winter quarters, roads, bridges, squares, bazaar and fair places. Entire community or the village/town community to which it was allocated could benefit from this land. Waste land was the land that cannot be used in effective way. Such land is rocky and clay areas (Biyik and Yomralioglu 1994; Bıyık and Yavuz 2006).

According to this classification, summer pasture was considered in the collective land class during the Ottoman period. In the 104th article of the Land Law, the summer pasture was defined as the land used in summer season and abandoned at the end of the season. The same article stated that the property of summer pasture belongs to the State Treasury and it cannot be bought or sold and cannot be registered to someone; however, their use could be assigned to a group of people or to a village/town (Cin 1980). The article defined the use of summer pasture as follows: “Only the village/town to which the summer pasture is allocated can benefit from there for grazing. Livestock husbandry activities of other villages or towns in the pasture are not allowed. Summer pasture cannot be sold or pledged. Even a certain village/town community uses the summer pasture without permission for a long time this cannot result in losing the rights of the first user. The beneficiaries of the summer pasture cannot change its borders and cannot assign all or some part of the summer pasture to others.” As a result, from legal point of view, there could be no individual property on summer pasture. Only the village and town community, to whom the summer pasture was allocated, had a usufruct right (Ekinci, 2019).

2.2. Republic of Turkey Period

After the Declaration of Republic (1923), the summer pasture was firstly defined in the Village Law (Köy Kanunu), which was put into practice 1924. The second article of the law stated that settlements consisting of collective public real estate such as mosque, school, grassland and summer pasture form a village with the people living in these settlements. In those times, it was possible to border and allocate a summer pasture in case of prolonged use of it could be proven by documents, information, and witnesses. In Turkey, documents indicating the rights and boundaries related to the summer pasture areas are kept in the archive of the General Directorate of Land Registry and Cadastre (GDLRC). These documents are the counterparts of records defined from 1925 to 1967, in situ, in relation with borders and the counterparts of allocation orders pertaining to the areas which were determined by the commissions as meadow/pasture, summer pasture and winter quarters and allocated to the entities of village for common use and utilization by villagers. There are village border certificates and pasture allocation orders for 31695 villages at the archive of GDLRC. Figure 1 illustrates examples of these documents. These documents have been used in solving disputes related with village borders and areas such as meadow/pasture, summer pasture and winter quarters, etc. Furthermore, in villages, each one of which constitutes an area of cadastral survey, in surveys carried out for determination of borders, these documents have been used.

Table 1 lists the laws, which includes articles related to summer pasture, enacted during the Republic of Turkey period.

Table 1. Laws and their provisions on summer pasture

Year	Law Name	Scope of law provisions
1924	Village Law (Köy Kanunu)	Classification, boundary surveying, status changes over summer pasture
1930	Municipality Law (Belediye Kanunu)	Definition of summer pasture, rights of use on summer pasture areas and registration of summer pasture
1956	Forest Law (Orman Kanunu)	Status loss of summer pasture, assigning authorized institution for summer pasture, planning, restrictions on summer pasture areas and penalties
1973	Soil and Agricultural Reform Law (Toprak ve Tarım Reformu Kanunu)	Surveying, registration and allocation of summer pasture, establishment right of usufruct, restrictions on summer pasture areas
1982	Tourism Promotion Law (Turizmi Teşvik Kanunu)	Allocation of summer pasture for tourism activities, summer pasture tourism
1983	Law Regarding Support of Development of Forest Villagers (Orman Köylülerinin Kalkınmalarının Desteklenmesi Hakkında Kanun)	Planning of summer pasture areas
1984	Agricultural Reform Law Regarding Land Regulation in Irrigation Regions (Sulama Alanlarında Arazi Düzenlenmesine Dair Tarım Reformu Kanunu)	Definition of summer pasture
1985	Law Regarding Services Oriented for Villages (Köye Yönelik Hizmetler Hakkında Kanun)	Surveying, registration and allocation of summer pasture, assigning authorized institution for summer pasture
1985	Law Regarding Establishment and Missions of General Directorate of Agriculture Reform (Tarım Reformu Genel Müdürlüğünün Kuruluş ve Görevleri Hakkında Kanun)	Preparation of improvement projects and assigning authorized institution for summer pasture
1987	Cadastre Law (Kadastro Kanunu)	Surveying, registration and allocation of summer pasture
1998	Pasture Law (Mera Kanunu)	Definition of summer pasture, surveying, registration and allocation of summer pasture, rights, restrictions and responsibilities on summer pasture areas
2000	Law Regarding Transmitting of Petroleum with Pipelines (Petrolün Boru Hatları İle Transit Geçişine Dair Kanun)	Status change of summer pasture, assigning authorized institution, expropriation of summer pasture
2005	Law Regarding Use of Renewable Energy Resources for Electricity Production (Yenilenebilir Enerji Kaynaklarının Elektrik Enerjisi Üretimi Amaçlı Kullanımına İlişkin Kanun)	Status change of summer pasture, establishment of easement rights on summer pasture areas
2013	Electricity Market Law (Elektrik Piyasası Kanunu)	Status change of summer pasture, establishment of easement rights on summer pasture area

The third article of the Pasture Law defines the summer pasture as a place where allocated or used for the farmers to reside in the summer with their livestock, to graze their livestock and to benefit from the grass. The next article of the law describes of the beneficiaries of the summer pasture. Accordingly, right for using/benefiting of summer pasture belongs to one or more than one village community. The same article also provides the provision that summer pasture must not be subject to private property. In addition, according to the 22nd article of the law, it is obligated that in order for farmers to be benefited from a summer pasture they have to reside in the village, in where summer pasture situated, for six months. On the other hands, the types of building permitted and not permitted in the summer pasture areas are defined in the 20th article the Pasture Law. According to this article, the buildings/constructions permitted in the summer pasture areas are listed as follows: (1) constructions permitted in the Village Law numbered 442, (2) constructions built with the permission from governorship complying with the zoning legislation such as dairy, porch, shelter, and pen (fit for purpose and non-permanent) and (3) wooden constructions in summer pasture areas that are opened to tourism activities upon the request of the Ministry of Tourism. Except from those listed above, it is forbidden to build houses, barns and similar constructions on the summer pasture areas.

A workflow diagram regarding the registration of legal status of summer pasture (also called pasture cadastre) is shown in Figure 2. It begins with the determination and approval of the study areas by the Ministry of Agriculture and Forestry (MAF). Then, a commission is established with the approval of the Governorship in the province where the study will be conducted. This commission (pasture commission) consists of the following members: a deputy governor (head of the commission), provincial director of agriculture, an agricultural engineer, representatives from the General Directorate of State Hydraulic Works, General Directorate of Forestry and General Directorate of National Real Estate, a lawyer, a surveyor from the Provincial Directorate of Cadastre, a representative in the general law enforcement unit and reeve of the related village (in Turkey, reeve is an elected chief executive in villages and district municipalities). After the establishment of the commission, the field study area and field study date are announced to the public thirty days before the initiation of the field study. At the same time, the commission initiates preparatory works, sends letters to relevant institutions, and requests information and documents from the institutions about the summer

pasture. After the preparatory work is completed, a technical team is formed to carry out the determination and surveying studies in the field. The technical team consists of an agricultural engineer, a surveyor, a forest engineer, relevant village reeve, representatives from relevant institutions, and local experts. The technical team determines and surveys the boundaries of summer pasture and draws the boundaries on a map at a scale of 1/5000. The results of the technical team's field studies are declared for thirty days together with the maps, and, if no objection against the declaration is made, maps and related documents are submitted to the GDLRC and to the Provincial Directorate of MAF for registration. If there is an objection, the commission evaluates the objection within sixty days and announces its decision at the end of that period. The decision of the commission is then declared for thirty days. A lawsuit can be filed against this commission decision within thirty days. In this case, the registration takes place after the decision of court.

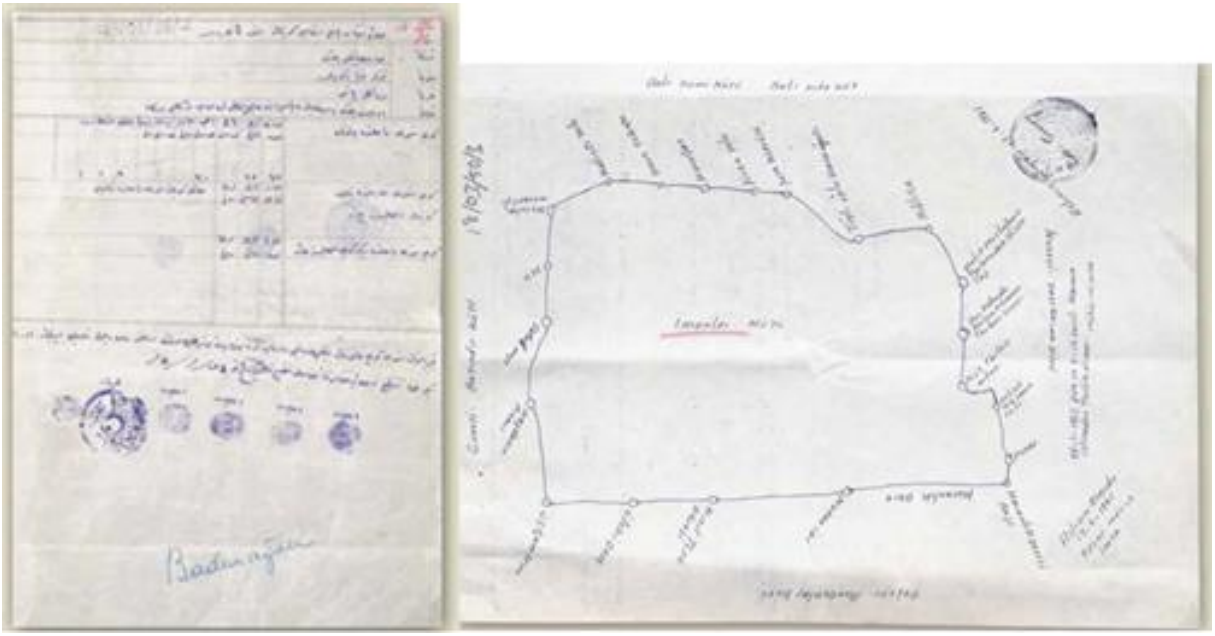

Figure 1. Certificate of summer pasture allocation decision written with old letters (left), plan certificate of the allocation decision (right) (Torun et al. 2010).

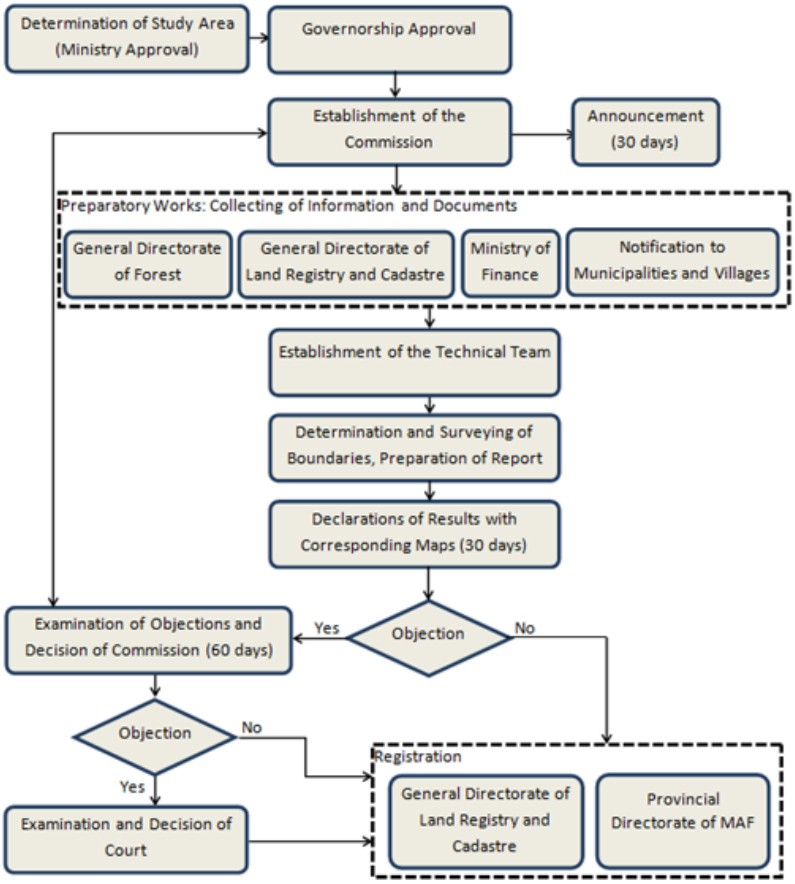

Figure 2. Flow chart of registration the legal status of summer pasture

3. EVALUATION OF THE EFFECT OF TOURISM POLICY ON SUMMER PASTURE

Summer pasture areas are temporary settlements where farmers began to send their flocks and herds to feed in spring, bringing them down again when winter closed in. The seasonal practice of moving livestock from and to summer pasture is called as transhumance. The transhumance tradition continues in Turkey for centuries. The livestock movement from villages to summer pasture typically begins in April and this movement reverses in end of September/October in Turkey. In addition to traditional transhumance activities, there are also increasing tourism and recreation activities in the summer pasture areas in recent years. The summer pasture areas are frequently used for these activities which occur as staying of city people for a certain period of time (Somuncu 2003).

Tourism activities carried out on summer pasture areas in Turkey began to be seen for the first time in the early 1990s. Based on the Tourism Promotion Law, the Ministry of Tourism (MOT) declared 12 summer pasture areas in the Black Sea Region as a tourism center in 1990 and environment plans were prepared for these areas (Bay 2014; OG 1990). As of 2019, the number of the centers has reached 21, of which 18 are located in the provinces in the Black Sea Region (Figure 3, MOT, 2020). However, utilization of summer pasture areas for tourism activities was first taken place in the long-term tourism policy of Turkey early 2000s. With the amendment made in the Tourism Promotion Law in 2004, the statement "The allocation purpose of pasture, summer pasture areas and winter quarters in the cultural and tourism protection and development zones can be changed according to the provisions of the Pasture Law No. 4342 dated 25.2.1998" was added to the law. The "Turkey 2023 Tourism Strategy Action Plan was prepared by MOT in 2007 and the region between Samsun and Artvin provinces in Black Sea Region declared as 'summer pasture tourism zone' in this plan (Figure 3). In this action plan, it was stated that until end of 2013, studies will be started to establish the infrastructure for the development of summer pasture tourism. In order to ensure this infrastructure, targets such as building new roads, improvement of the current transportation network and preparation of route maps with the theme of "summer pasture tourism" have been determined (OG 2007).

Figure 3. Summer pasture tourism center and the "summer pasture zone" declared by MOT

In 2013, the Ministry of Development launched the 'Green Road Project' to be carried out by the Eastern Black Sea Region Development Administration (DOKAP) in order to realize the targets, set out in the action plan published in 2007. This project has been described as a nature-integrated tourism project aiming to connect important summer pasture and tourism centers of eight provinces (Artvin, Bayburt, Giresun, Gümüşhane, Ordu, Rize, Samsun, Trabzon) in the Eastern Black Sea Region. The Green Road Project, which is planned to be completed by 2023 within the scope of the DOKAP action plan, consists of a 4000 km road network in total. As of 2019, 1300 km road improvement works have been completed by DOKAP. Within the scope of the road improvement works, 285 km of roads were covered with asphalt, 177 km of roads were made with stabilized coating, 99 km of roads were covered with concrete, 18 km of roads were covered with parquet, and the rest were maintained and repaired. The remaining 2700 km section is planned to be completed by the General Directorate of Highways and DOKAP until 2023 (DOKAP 2020). One of the main objectives of the Green Road Project is to increase the demand for tourism activities carried out on summer pasture areas, which is currently limited to certain months of the year, by improving the standard of the road network. In addition, the summer pasture areas to be connected to each other by a road network in the east-west direction are expected to offer more alternatives to the tourists coming to the region. Facilitating the transportation of the transhumance framers and improving the income level of local people are some other goals of the projects. In Figure 4, the planned road network for Gümüşhane province, which is one of the eight provinces within the scope of the Green Road Project, are shown on the tourism master plan. With the Green Road Project, roads that are planned to be built/improved with the first, second and third priority are shown on the master plan in green, pink and blue colors, respectively.

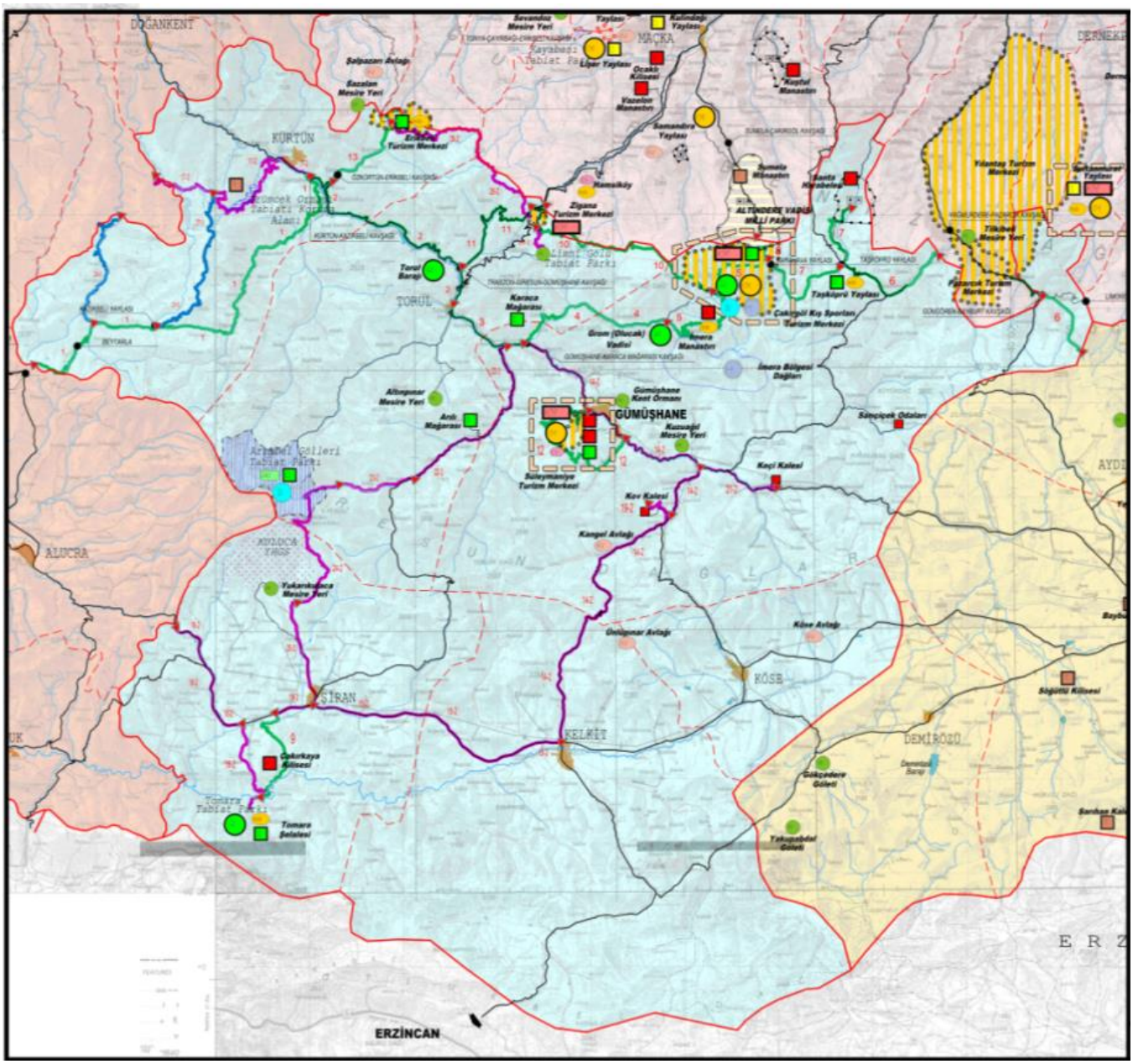

Figure 4. Green road network of Gümüşhane Province on tourism master plan (roads planned to be built/improvement with the first, second and third priority are shown on the master plan in green, pink and blue colors, respectively)

In order to evaluate the effect of tourism policy on summer pasture areas, the land use / land cover (LULC) changes of the provinces in the Eastern Black Sea region were examined. For this examination, CORINE (Coordination of Information on the Environment) 2006 and 2018 LULC data was used. CORINE is a program launched in 1985, aiming to collect information for the EU on priority issues related to the environment. Since 1994, the European Environment Agency (EEA) has included CORINE in its program. CORINE data refers to LULC data produced by computer-aided visual interpretation method over satellite images according to the LULC Classification determined by EEA (Heymann et al. 1994; Bossard et al. 2000). In Turkey, LULC data for 1990, 2000, 2006, 2012, 2018 and data sets for showing LULC changes between these years has been created so far. The CORINE LULC classification system is a three-level classification, consisting of 5, 15, 44 sub-LULC classes, respectively. Pastures areas are in the sub-LULC class expressed as 2.3. CORINE LULC maps and statistics can be accessed via the web portal of the MAF in Turkey. (MAF 2020).

In Table 2, based on the CORINE 2006, 2012 and 2018 LULC data, changes in pasture areas of Eastern Black Sea provinces and whole country are given. When Table 2 is examined, it is seen that the total pasture areas of the 7 provinces in the Eastern Black Sea region decreased by 3183,79 ha in 2018 compared to 2006. This area reduction corresponds to a 5.3% decrease in total pasture areas. In the same period, on the other hand, total pasture areas of the country was 2009092,5 ha by increased 1.7%. It should be note that summer pasture areas are not included as an independent class in the CORINE LULC subclasses. Therefore, the rate of temporal changes of pasture areas in the Eastern Black Sea Region may not be the same for summer pasture areas. Still, the decrease in pasture areas in Eastern Black Sea Region can be seen as a negative effect of the tourism policy on summer pasture.

Table 2. Temporal changes of pasture areas for Eastern Black Sea provinces and Turkey

	2006		2012		2018		2006–2018	
	Area (ha)	% of province's total area	Area (ha)	% of province's total area	Area (ha)	% of province's total area	Area (ha)	% changes
Artvin	358.89	0.05	205.2	0.03	205.2	0.03	-153.69	-42.8
Giresun	2,569.43	0.37	1350.06	0.20	1,350.06	0.20	-1,219.37	-47.4
Gümüşhane	17,469.64	2.63	16226.3	2.45	16,226.3	2.45	-1,243.34	-7.1
Ordu	441.34	0.08	1293.87	0.22	1,261.39	0.22	820.05	185.8
Rize	2,303.05	0.61	2518.92	0.67	2,518.92	0.67	215.87	9.3
Samsun	8,740.7	0.95	8987.05	0.97	8,839.13	0.96	98.43	1.1
Trabzon	27,779.7	6.07	26077.96	5.71	26,077.96	5.71	-1,701.74	-6.1
Total (7 provinces)	59,662.75	10.76	56659.36	10.25	56,478.96	10.24	-3,183.79	-5.3
Total (Turkey)	1,975,568.09	2.63	2,041,781.25	2.73	2,009,092.50	2.69	33,524.41	1,70

4. EVALUATION OF THE EFFECT OF LEGALIZATION POLICY ON SUMMER PASTURE

As a developing country, settlements in Turkey are expanding due to increasing population. As in many other countries in the world, Turkey developed various policies to address problems of informal settlements in both urban and rural areas paralleling to programs [UN 1999; Mukhija 2001, World Bank 2003; EU 2004) and policies (World Bank 1993; de Soto 2000; van Gelder 2010) of international organizations such as World Bank, United Nations, and European Union which consider tenure legalization in informal settlements as one of the fundamental conditions for economic development. The number of informal structures (former slum houses) in Turkey started to increase from the early 1950s and reached to 2.2 million in total in early 2000s (Table 3). The numbers of informal structure given in Table-4 only refer to the structures which are built by occupying a land that do not belong to the structure owner. By condensing on the development regions of urban areas, these structures prevent the development of cities and eliminate the agricultural and forest areas (Uzun and Colak 2007). On the other hand, according to data published by Ministry of Environment and Urbanization (MEU), approximately half of the 26.4 million condominiums (individual building unit) in Turkey are considered as informal structure (MEU 2018). This means that these structures do not conform to zoning/building regulations or owners of these structures do not abide by the formal administrative processes.

When Turkey's development plans are examined, it is observed that reason for increase in the number of informal structures/settlements in the country is frequently explained by late completion of cadastral studies, content/quality problems of the cadastral data and late preparation of the Pasture Law. For example, in the 7th development plan covering the period between 1996 and 2000, it was stated that a legal improvement could not be performed in order to regulate the proper use of pasture and summer pasture areas, and it was aimed to enact a Pasture Law in the plan period to fill this legal gap. In the same development plan, it was also stated that the exclusion of the treasury land out of cadastre studies has resulted in the occupation of these land over time and being subject to private property so the cadastral maps should be updated and the boundaries of the treasury land should be represented on the cadastral maps (OG 1995). In addition, in the 6th development plan covering the period between 1990 and 1994, it was expressed that the cadastre studies must be completed as soon as possible in order to determine the boundaries and solve disputes in the forest areas, which often include summer pasture areas (OG 1989). The Pasture Law enacted in 1998 and projects by GDLRC such as completion of cadastre and establishment of land information system initiated at the early-2000s were results of the development plan targets into practice (Döner 2015; Aksu and Iban 2017; Yildiz and Erden in press; Aydinoglu and Bovkir 2017). Still, an ongoing need for registration of summer pasture areas was specified under the heading of policy and measures in the last (11th) development plan, which covers the period between 2019 and 2023 (OG 2019).

In Turkey, adoption of the legalization policies has been preferred to address the informal structure/settlement problem frequently mentioned in development plans so far. (Gürbüztürk 2017; Cengiz et al. 2019; Arslanoğlu 2019). The laws, which were put into practice to legalize the informal structures/settlements in Turkey, are given in Table 4. When Table-5 is analyzed, it is understood that a total of 16 laws enacted between 1948 and 2018 include provisions to register the informal structures on the areas in cities and rural areas. Apart from these laws aiming to legalize informal structures directly, there are 7 other laws that provide infrastructure including electricity, water, and roads to the informal structures. It is broadly accepted that the policy of legalization of informal settlements has not provided a solution to the social, legal, economic and environmental problems arising from the informality in Turkey, but further increased the number of informal structures by creating new legalization anticipation for future (Dilbaz 2010; Kasparoğlu 2019; Çantalı 2019; Polat 2019). The last law given in the Table-5 is of great importance both for being more comprehensive than the previous laws and for having a great impact on summer pasture areas that are the subject of this article.

The law numbered 7143, which came into force on 08.05.2018, was announced as 'Development Peace'. This law was oriented for informal structures in urban and rural areas built before 31.12.2017. The law made it possible to register the informal structures into land registry by providing a Structure Registration Certificate (SRC) as a result of the application of the informal structure owner. Moreover, owners of informal structures built on the state land have the right to apply for SRC. The main benefits of SRC to informal structure owners were as follows: (1) canceling of previous demolition decisions for informal structures, (2) providing infrastructure including electricity, water, and roads and (3) providing security of property by registration. The deadline for SRC application was initially determined as 31.10.2018, but with an extension was 15.06.2019. The deadline of payment for SRC was 31.12.2019. SRC applications were collected on the basis of the declarations of informal structure owners by e-Government application via the internet. After confirmation of payment, SRC was prepared and delivered to the owners. One of the main purposes of the law was declared as legalizing informal structures. Another purpose of the law was to provide the economic resource needed for urban transformation projects.

Although the law was announced as a 'peace' law, it is clear that it provides an 'amnesty' for informal structures in practice. The weak control mechanism of the law has been severely criticized so far (Uşak and Yalçin 2019; Boz and Çay 2020). That is, in order to obtain a SRC it was sufficient for the owner of the informal structure to declare that the structure was built before 31.12.2017. Checking this declaration in the field is only possible when an official complaint was made. According to the law, as a result of the field inspection based on the complaint, if it is understood that the declaration of the informal structure owner is not correct, a criminal complaint is filed against the owner. After the law came into force, there has been a rapid increase in the number of informal structures especially in the pasture and summer pasture areas in the Eastern Black Sea Region. Some have started to build new structures on summer pasture areas and applied for SRC by declaring the structures were built before 31.12.2017. When this was understood, an order was sent to the governorships by MAF and it was stated that these structures must be considered as illegal according to the Pasture Law. Following this order, SRC cancellation and demolition process was initiated for the illegal structures.

For example, number of the structures demolished in summer pasture areas in Trabzon and Gümüşhane was 160 and 91, respectively, because of illegal application for SRC. In the statement made by MEU, it was announced that approximately 7.4 million applications were made to receive SRC, and that 20158 of these applications were canceled due to violation of the law numbered 7143 (Döner in press). MEU further announced that checking of SRC applications is continuing and criminal complaints will be filed for illegal applications (AA 2020). As a result, the law, which aims to provide a peace between the owners and the state by legalizing informal structures, caused an increase in the number of informal structures and new legal problems in summer pasture areas due to its weak control mechanism.

5. CONCLUSION

LULC in summer pasture areas of Turkey has changed over time by transforming to built-up areas. In this study, tourism and legalization policy of Turkey are evaluated to have an effect on this LULC change. One of the main reasons for this effect is that the Pasture Law could not be put into practice until 1998. Until this date, the existence of different institutions given responsibility with various laws for summer pasture areas caused the land use rights and boundaries of these areas not to be registered. Although the Pasture Law defines certain rights and restrictions in the use of summer pasture areas, human activities on the summer pasture areas do not comply with the definitions in the law. Actually, summer pasture areas have been allocated to the use of a certain village for transhumance since the Ottoman Empire period. However, especially after the 1990s, the villagers interpreted this use right as a property right inherited from their ancestors and started to build structures not related to transhumance on the summer pasture areas. In fact, it is not possible to establish private property rights on the summer pasture areas according to current legislation. For example, the Civil Code states that the validity period of use right (usufruct) is limited to the lifetime of beneficiary and this right cannot be transferred to heirs of the beneficiary. Accordingly, there is no legal basis for structures on summer pasture areas, except those permitted by the Pasture Law.

Table 3. Change in slums houses and population in Turkey (DPT 2007; TUIK 2020)

Year	Number of slum houses	Urban Population	Urban Population (%)	Rural Population	Rural Population (%)
1955	50,000	6,927,343	25.0	15,702,851	75.0
1960	240,000	8,859,731	31.9	18,895,089	68.1
1965	430,000	10,805,817	34.4	20,585,604	65.6
1970	600,000	13,691,101	38.5	21,914,075	61.6
1980	1,150,000	19,645,007	43.9	25,091,950	56.1
1990	1,750,000	33,326,351	59.0	23,149,684	41.0
2002	2,200,000	44,006,274	64.9	23,797,653	35.1

Table 4. Laws aiming at legalization of informal structures in Turkey

Year	Law Number	Description
1948	5218	Provide provisions to register the informal buildings in the capital Ankara for a fee to be paid to the municipality
1948	5228	With this law, scope of the previous law, was extended to cover the whole country
1949	5431	Provide provisions to register informal structures that conform to zoning regulation and to destroy others
1953	6188	It repealed three previous laws. With this law, the informal structures of people residing within the municipal areas for 2 years have been registered
1959	7367	Provide provisions to allocate the state land to the municipality to prevent informal settlements
1963	327	With this law, it was possible to provide infrastructure including electricity, water and roads to informal structures built before 1962
1966	775	The definition of 'slum houses' was given for the first time in this law. These structures were divided into 3 groups (will be demolished, rehabilitated and protected)
1983	2805	Name of the law was Zoning Amnesty Law. It covered structures built before 1981. An allocation deed was provided to owners of the informal structures
1984	2981	With this law, in areas where cadastral maps and zoning plans are available, instead of allocation deed, a title deed was provided for informal structures by approving of the municipality or the governorship
1986	3290	Some articles of the law numbered 2981 were modified. In this way, it was also provided amnesty to the informal commercial structures
1987	3366	This law extended the scope of laws numbered 2981 and 3290. It provided provisions to document a title deed instead of a deed allocation deed for informal structures
1988	3414	With this law, the article of the law numbered 775 prohibiting the sale or transfer of informal structures for 20 years was repealed
2001	4706	This law aimed to transfer the state land to the municipalities provided that the state land was sold to owners of informal structures
2012	6306	This law provided a provision that the law numbered 2981 be repealed in 2015.
2015	6639	The validity period of the law numbered 2981 was extended until 2018.
2018	7143	With this law, it was aimed to provide a registration certificate to the informal structures built before 31.12.2017 in urban and rural areas with a temporary article added to the Zoning Law.

In Turkey, the use of summer pasture areas in tourism activities started in 1990 by declaring summer pasture tourism centers based on the Tourism Promotion Law. The number of these centers, which was 12 in the Black Sea Region at the beginning, has now increased to 21, 18 of which are in the Black Sea Region. With the '2023 Tourism Strategy Action Plan' prepared in 2007 it was targeted to establish 'a summer pasture zone' in the Black Sea region and provide necessary infrastructure for the zone by the end of the 2013. To achieve this target, the Ministry of Development launched the 'Green Road Tourism Project' in 2013. With this project, it was aimed to connect the summer pasture areas of the provinces each other in the Black Sea Region by road. As of 2019, 1300 kilometers of road construction and improvement work has been carried out for the project, which consists of a total of 4000 kilometers of road network. The remaining 2700 kilometers road network is planned to be completed by 2023. CORINE 2006 and 2018 land cover statistics were used to assess land LULC changes across Turkey and provinces of 'summer pasture zone'. Accordingly, pasture area increased by 1.7% in area in the country, but it decreased by 5.3% in area in the summer pasture corridor provinces. Main aims of Turkey's summer pasture tourism policy are highlighting alternative tourism activities, expanding the normally short summer pasture tourism season to whole year, facilitating the transportation of the local people for transhumance and improving the income level of the rural areas. However, income-oriented tourism policy of Turkey combining with inadequate supervision had negative effect on summer pasture areas. A policy to ensure sustainable use of summer pasture areas by considering the protection-use balance is needed in Turkey.

Illegal settlements are expanding in the summer pasture areas where transhumance activities were carried out traditionally in the past, mainly due to the increasing transportation facilities and tourism activities. Another important reason for inappropriate land use in the summer pasture areas is the legalization policy of Turkey. Paralleling this policy, 16 legalization laws have been put into practice between 1948 and 2018. The long-term effect of the economic oriented policy and legal regulations on urban and rural areas is the increasing number of informal structures. The last legalization law that came into force in 2018 was prepared to cover more informal structures compared to previous laws. 7.4 million applications were made to MEU to take advantage of the law granting the right to apply to all informal structures (excluding exceptions defined in the law) built before 2018 in urban and rural areas. There was a rapid increase in the number of informal structures on the summer pasture areas in the Eastern Black Sea Region after the date the law came into force due to the absence of an effective control mechanism. With the intervention of MAF, the new informal structures built on the summer pasture areas in violation of the Pasture Law have started to be determined and demolished. Later, it was declared by MEU that a commission was established to detect the illegal applications and the demolition of the structures will be completed as soon as possible. As a result, the legalization policy led to the formation of new informal structures and change of LULC in the summer pasture areas.

Studies to register the legal status of the summer pasture areas should be completed firstly to ensure sustainable use summer pasture areas in Turkey. From both an economic and a social point of view, it doesn't seem to be possible to be demolished all the informal structures in the summer pasture areas immediately. Instead of the legalization policy, an effective management policy, for example permitting certain structures in accordance with traditional architecture, should be adopted with an amendment to the Pasture Law. Finally, advanced GIS techniques, spatial modeling and utilization of satellite images should be employed in the ensuring effective control of the LULC changes in the summer pasture areas.

Conflicts of interest

The authors declare no conflicts of interest.

REFERENCES

AA. Anadolu Agency - the official news agency of the Republic of Turkey, (2020). İmar Barışı'nda 30 bini aşkın yapı kayıt belgesi iptal edildi (More than 30 thousand building registration documents were canceled in the Development Peace, in Turkish). Available online: https://www.aa.com.tr/tr/turkiye/imar- barisinda-30-bini-askin-yapi-kayit-belgesi-iptal-edildi/1735457 (accessed on 15 May 2020).

Acs S, Hanley N, Dallimer M, Gaston G J, Robertson P, Wilson P & Armsworth P R (2010). The effect of decoupling on marginal agricultural systems: Implications for farm incomes, land use and upland ecology. Land Use Policy, 550–563.

Akale A T, Dagnew D C, Belete M A, Tilahun S A, Mekuria W & Steenhuis T S (2017). Impact of soil depth and topography on the effectiveness of conservation practices on discharge and soil loss in the Ethiopian highlands. Land, 6(4), 78.

Aksu C & Iban M C (2017). Considerations on the land management system approach in Turkey by the experiences of a case study. Survey Review, 51 (364), 87-96.

Arslanoğlu U (2019). The role of spatial designer in the prestigious housing projects: the case of Ankara. Master's Thesis, Middle East Technical University, Ankara.

Aydinoglu A C & Bovkir R (2017). Generic land registry and cadastre data model supporting interoperability based on international standards for Turkey. Land Use Policy, 68, 59-71.

Bay A (2014). Uludağ yöresinde (Bursa) alternatif turizm türü olarak yayla turizmi. Master's Thesis, Çanakkale Universtiy (In Turkish).

Biyik C, Doner F & Berk F (2018). Turkish Land Management at Historical Process, In Proceeding of FIG Congress 2018, 6–11 May, Istanbul, Turkey.

Bıyık C & Yavuz A (2006). Land registration and cadastre in Turkey from the Ottomans to date. Journal of Applied Sciences, 6(6), 1415-1425.

Biyik C & Yomralioglu T (1994). Land Information Systems in 1500's. In Proceeding of FIG.XX International Congress, 2-12 May, Melbourne, Australia.

Bossard M, Feranec J & Otahel J (2020). CORINE land cover technical guide–Addendum 2000. Technical report, 40. Copenhagen (European Environment Agency), 2000. Available online: http://terrestrial.eionet.eea.int (accessed on 15 May 2020).

Boz Y & Çay T (2020). New regulation to register the anomalous constructions and finance urban regeneration projects in Turkey: Development Peace. Turkish Journal of Engineering (TUJE), 4(1), 1-8.

Çantalı T E (2019). Türkiye imar affı uygulamaları, imar barışı ve gayrimenkul piyasasına etkisi. Master's Thesis, Marmara University, Istanbul (in Turkish).

Cengiz S, Atmiş E & Görmüş S (2019). The impact of economic growth-oriented development policies on landscape changes in Istanbul province in Turkey. Land Use Policy, 87.

Cin H (1980). Türk hukukunda mera yaylak ve kışlaklar. Turhan Kitapevi, Ankara, Turkey.

Cohn A S, Gil J, Berger T, Pellegrina H & Toledo C. (2016). Patterns and processes of pasture to crop conversion in Brazil: Evidence from Mato Grosso State. Land Use Policy, 55, 108-120.

Danachair C (1983). Summer pasture in Ireland. Folk Life, 22(1), 36-41.

de Soto H (2000). The mystery of capital: why capital triumphs in the west and fails everywhere else. Basic Books, New York.

Dilbaz A Y (2010). Türkiye'de 1923'ten Günümüze imar tüzesi ve değişim süreci. Master's Thesis, Yildiz Technical University, Istanbul (in Turkish).

DOKAP (2020). Doğu Karadeniz Projesi Bölge Kalkınma İdaresi Başkanlığı (Eastern Black Sea Project Regional Development Administration, In Turkish). Available online: https://www.dokap.gov.tr/projeler/ yesil-yol-projesi/1/Detay (accessed on 15 May 2020).

Döner F (2015). Evaluation of cadastre renovation studies in Turkey. Survey Review, 47(341) 141-152.

Döner F (in press). Yayla alanlarındaki yapılaşma değişiminin incelenmesi: Gümüşhane örneği. Gümüşhane Üniversitesi Fen Bilimleri Enstitüsü Dergisi. In press, doi: https://dx.doi.org/10.17714/gumusfenbil.748435

DPT (2007). Devlet Planlama Teşkilatı, Dokuzuncu Beş Yıllık Kalkınma Planı (2007–2013) Yerleşme–Şehirleşme Özel İhtisas Komisyonu Raporu (State Planning Organization Ninth Five-Year Development Plan (2007-2013) Settlement-Urbanization Specialization Commission Report, in Turkish). Ankara.

EEA (2010). The European environment - state and outlook 2010; European Environment Agency, ISBN: 978-92-9213-160-9, Copenhagen.

EEC (1999). Council Regulation (EC); No 1257/99 of 17 May 1999 on support for rural development from the European Agricultural Guidance and Guarantee Fund (EAGGF) and amending and repealing certain regulations, Official Journal L 160, 80–102.

Ekinci İ (2019). On dokuzuncu yüzyılda doğu karadeniz'de (Gümüşhane-Trabzon) yayla

anlaşmazlıkları ve düşündürdükleri. Karadeniz İncelemeleri Dergisi, (26), 311-346.

EU (2004). EU Land Policy Guidelines; European Commission, Available online: https://landportal.org/resour ce/policies-and-guidelines/eu-land-policy-guidelines (accessed on 15 May 2020).

Guo S, Jiang,ü L & Shen G Q P (2019). Embodied pasture land use change in China 2000-2015: From the perspective of globalization. Land Use Policy, 82, 476-485.

Gürbüztürk A (2017). Social housing policy and the welfare regime in Turkey: a comparative Perspective. Master's Thesis, Boğaziçi University, Istanbul.

Hardaker A (2018). Is forestry really more profitable than upland farming? A historic and present-day farm level economic comparison of upland sheep farming and forestry in the UK. Land Use Policy, 71, 98–120.

Herzog F, Böni R, Lauber S, Schneider M & Seidl I (2009). AlpFUTUR – an inter-and transdisciplinary research program on the future of summer pastures in Switzerland. In Proceeding of the 15th Meeting of the FAO CIHEAM Mountain Pastures Network, Les Diablerets, 7-9 October, Switzerland.

Heymann Y, Steenmans C, Croissille G & Bossard, M (1994). CORINE land cover; technical guide. Office for Official Publications of the European Communities, Luxembourg, p. 137.

Hubacek K, Beharry N, Bonn A, Burt T P, Holden J, Ravera F, Reed M S, Stringer L C & Tarrasón D (2009). Ecosystem services in dynamic and contested landscapes: the case of UK uplands. In: Winter, M., Lobley, M. (Eds.), Land Use and Management: The New Debate. Earthscan, London, 167–188.

Iversen E K, Lindhjem H, Jacobsen J B & Grimsrud K (in press). Moving (back) to greener pastures? Social benefits and costs of climate forest planting in Norway. Land Use Policy. In press, doi: https://doi.org/ 10.1016/j.landusepol.2019.104390

James J B & Lovelock C E (in press). Legal barriers and enablers for reintroducing tides: An Australian case study in reconverting ponded pasture for climate change mitigation. Land Use Policy. In press, doi: https://doi.org/10.1016/j.landusepol.2019.104192

Jerrentrup, J S, Klimek S, Marchiori E, Bittante G, Ramanzin M & Sturaro E (2016). Marini, L. Impact of dairy farming on butterfly diversity in Alpine summer pastures. Agriculture, Ecosystems and Environment, 232, 38–45.

Kasparoğlu M (2019). Zoning amnesty laws in Turkey and zoning peace. Master's Thesis, Istanbul Commerce University, Istanbul.

Koch B, Edwards, P J, Blanckenhorn W U, Buholzer S, Walter T, Wuest R O & Hofer G (2013). Vascular plants as surrogates of butterfly and grasshopper diversity on two Swiss subalpine summer pastures. Biodivers Conserv, 22, 1451–1465.

Kosmas C, Detsis V, Karamesouti M, Kounalaki K, Vassiliou P & Salvati L (2015). Exploring long-term impact of grazing management on land degradation in the socio-ecological system of Asteroussia Mountains, Greece. Land, 4(3), 541-559.

MAF (2020). Ministry of Agriculture and Forestry, CORINE Projesi, (CORINE Project). Available online: https:// corine.tarimorman.gov.tr/corineportal/nedir.html (accessed on 15 May 2020).

Merry F D, Hildebrand P E., Pattie P & Carter D R (2002). An analysis of land conversion from sustainable forestry to pasture: a case study in the Bolivian Lowlands. Land Use Policy, 19, 207-215.

MEU (2018). Çevre ve Şehircilik Bakanlığı İmar Barışı Broşürü (Ministry of Environment and Urbanization, Development Peace Booklet, in Turkish). Available online: https://webdosya.csb.gov.tr/db/ imarbarisi/icerikler/brosur-20180603111057.pdf (accessed on 15 May 2020).

Minotti M, Giancola C, Marzio P D & Martino P D (2018). Land use dynamics of drove roads: the case of Tratturo Castel di Sangro-Lucera (Molise, Italy). Land, 7(1), 3.

Mukhija V (2001). Upgrading housing settlements in developing countries: the impact of existing physical condition, Cities, 18 (4), 213–222.

Nettier B, Dobremez L, Lavorel S & Brunschwig G (2017). Resilience as a framework for analyzing the adaptation of mountain summer pasture systems to climate change. Ecology and Society, 22 (4), 25.

OG (2007). Official Gazette, Turkey 2023 Tourism Strategy Action Plan, (in Turkish). Published in the Official Gazette dated 02.03.2007 and numbered 26450. Available online: https://www. resmigazete.gov.tr/eskiler/2007/03/20070302-17.htm (accessed on 15 May 2020).

OG (1990). Official Gazette, Tourism Promotion Law (in Turkish). Available online: (https://www. resmigazete.gov.tr/arsiv/20452.pdf (accessed on 15 May 2020).

OG (1995). Official Gazette, Presidency of the Republic of Turkey, Strategy and Budget Directorate, Seventh Development Plan. Available online: https://www.resmigazete.gov.tr/arsiv/22354_1.pdf (accessed on 15 May 2020).

OG (1989). Official Gazette. Presidency of the Republic of Turkey, Strategy and Budget Directorate, Sixth Development Plan. Available online: https://www.resmigazete.gov.tr/arsiv/20217_1.pdf (accessed on 15 May 2020).

OG (2019). Official Gazette, Presidency of the Republic of Turkey, Strategy and Budget Directorate, Eleventh Development Plan, 2019. Available online: https://www.resmigazete.gov.tr/eskiler/2019/07/20190723M1. pdf (accessed on 15 May 2020).

Polat Z A (2019). Analysis of the regulation of "zoning reconciliation" in local governments. Planlama, 29(3), 202–209.

Reed M S, Bonn A, Slee W, Beharry-Borg N, Birch J, Brown I, Burt T P, Chapman D, Chapman P J, Clay G D, Cornell S J, Fraser E D G, Glass J H, Holden J, Hodgson J A, Hubacek K, Irvine B, Jin N, Kirkby M J, Kunin W E, Moore O, Moseley D, Prell C, Price M F, Quinn C H, Redpath S, Reid C, Stagl S, Stringer L C, Termansen M, Thorp S, Towers W & Worrall F (2009). The future of the uplands. Land Use Policy, 26, 204–S216.

Schaak H & Musshoff O (in press). Public preferences for pasture landscapes in Germany—A latent class analysis of a nationwide discrete choice experiment. Land Use Policy, doi: https://doi.org/10.1016/j.landusepol.2019.104371

Schulz T (2015). An uphill struggle against scrub encroachment: Implementation of the alpine pasturing subsidy scheme in Switzerland. Land Use Policy, 42, 318-328.

Somuncu M (2003). Türkiye'nin koruma altındaki dağlık alanlarda turizm/rekreasyon ve çevre etkileşimi: Aladağlar ve Kaçkar Dağları Milli Parkı örnekleri. In Proceeding of Coğrafi Çevre Koruma ve Turizm Sempozyumu, 16-18 Nisan, Izmir, Turkey.

Steudler D, Kaufman S (2014). Cadastre 2014 and Beyond; FIG Publication; FIG: Copenhagen, Denmark, 2014; Volume 61.

Torun A, Gültekin H, Alabuğa E, Ünal B & Toprak, Ü. (2010). Land registry archive since the Ottoman Empire. Directorate General of Land Registry and Cadastre, Publication No:1, Semih, Ofset, Ankara, Turkey, 152.

TUIK (2020). Turkish Statistical Institute. Basic statistics, address based population registration system. Available online: http://tuik.gov.tr/PreTablo.do?alt_id=1059 (accessed on 15 May 2020).

UN (1999). Global campaign for secure tenure. Available online: https://mirror.unhabitat.org/content.asp?cid=2068&catid=24&typeid=24&subMenuId=0 (accessed on 15 May 2020).

UNECE (1996). Land administration guidelines; United Nations Economic Commission for Europe, ISBN: 92-1-116644-6, New York.

UN-FIG (1999). The Bathurst declaration on land administration for sustainable development. FIG Publication; The International Federation of Surveyors (FIG): Copenhagen, Denmark.

Upadhaya S & Dwivedi P (2019). Conversion of forestlands to blueberries: Assessing implications for habitat quality in Alabaha river watershed in Southeastern Georgia, United States. Land Use Policy. In press, doi: https://doi.org/10.1016/j.landusepol.2019.104229.

Uşak B, Yalçin G A (2019). Content analysis on zoning peace regulation. Turkey Land Management Journal, 1(1), 01-10.

Uzun B, Colak H E (2007). Providing formal property rights to slum owners through tenure legalization process in Turkey. In Proceeding of FIG Working Week 2007, 13-17 May, Hon Kong SAR, China.

van Gelder J (2010). What tenure security? the case for a tripartite view. Land Use Policy, 27, 449-456.

World Bank (1993). Housing: enabling markets to work; World Bank policy paper, World Bank, Washington, DC.

World Bank (2003). Land policies for growth and poverty reduction. A World Bank Policy Research Report, 239p.

Yildiz O & Erden Ç (in press). Cadastral updating: the case of Turkey. Survey Review. In press, doi: https://doi.org/10.1080/00396265.2020.1759982

Zendri F, Sturaro E & Ramanzin M. (2013). Highland summer pastures play a fundamental role for dairy systems in an Italian Alpine Region. Agriculturae Conspectus Scientificus, 78 (3), 295-299.

International Journal of Engineering and Geosciences
https://dergipark.org.tr/en/pub/ijeg
e-ISSN 2548-0960

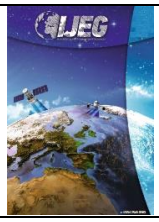

Divide and conquer object detection (DACOD) method for runway detection in remote sensing images

Atakan Körez[*1]

[1]*Gazi University, Technology Faculty, Computer Engineering, Ankara, Turkey*

Keywords
Remote sensing
Runway detection
Convolutional neural networks (CNN)
Oriented object detection

ABSTRACT

In recent years, parallel to the developments in satellite technology, obtaining and processing remote sensing images has become quite common. While airports are the first points to be targeted by enemy forces in times of war, they are very critical points in times of peace due to their significance for transportation, trade, and economy networks. The runways are the most distinctive feature of airports. There are many studies on detecting the runways in remote sensing images (RSIs). However, existing methods for detecting the runway objects that have an excessive width in high-resolution (4137 x 4552 pixels and above) RSIs may be insufficient. In this study, a Divide and Conquer Object Detection (DACOD) method is proposed for the runway objects that have an excessive width in high-resolution RSIs. In the proposed method, images are divided into images of 1024 x 1024 pixels, and the runway objects in these images are detected as oriented. Then, the detection results are merged by using the angles and the final runway detection results are obtained. The experimental results demonstrate that the proposed model yields good results (%81.5 mAP). This is an 11% mAP increase when compared to the best results in The State of The Art (SOTA) object detection models using the same dataset.

1. INTRODUCTION

Obtaining and using optical remote sensing images (RSIs) has become quite common as a result of the increase in the number of satellites sent to space with the development of technology and the development of the remote viewing equipment used in satellites. Today, RSIs are used in many areas from agricultural activities to urban planning, and from disaster management to military applications (Cheng and Han, 2016).

Airports have both strategic and economic importance. Besides being the first target of the enemy forces in times of war and peace, they are critical places in terms of their locations as crossroads of transportation, trade, and economic networks. Runways are the most distinctive feature of airports. Each airport has at least one runway. Based on this fact, the most salient elements used in airport detection in RSIs are runways.

There are many studies on detecting the runways in RSIs. We can divide these studies into 2 groups according to the methods they use. The first group consists of studies based on the determination of long and wide lines parallel to each other, which are the determining geometric features of the runways (Wu et aI., 2014; Zhang et al., 2020; Li et al., 2014; Lv et al., 2018; Akbar et al., 2019). The other group consists of the object detection studies based on the classification process made according to the textural differences of the objects that make up RSIs (Tao et al., 2010; Aytekin et al., 2013; Zongur et al., 2009; Tang et al., 2015). For this reason, in the aforementioned studies, the images are divided into small pieces of varying sizes from 32 x 32 pixels to 512 x 512 pixels and runway detection is made within these pieces.

Deep learning, a sub-branch of machine learning, has gained popularity in recent years with the development of parallel programming capabilities of graphics cards and the emergence of datasets containing large amounts of data (Bengio et aI., 2016). Convolutional neural networks (CNN), which are the best known of the deep learning techniques, have been favored especially after

* **Corresponding Author**
*(atakan.korez@gazi.edu.tr) ORCID ID 0000-0003-3704-267X

Cite this article
Korez A (2022). Divide and conquer object detection (DACOD) method for runway detection in remote sensing images. International Journal of Engineering and Geosciences, 7(2), 154-160

Research Article / DOI: 10.26833/ijeg.937061
Received: 13/05/2021; Accepted: 10/06/2021

the great success of the AlexNet (Krizhevsky et al., 2012) model in the International Large Scale Visual Recognition Challenge (ILSVRC) competition held in 2012. So, there emerged many studies that detect objects in optical RSIs using CNN (Yu et al., 2020; Wu et aI., 2020; Song et al., 2021; Ju et al., 2019; Wang et al., 2019). The RSIs used in these studies usually have a high resolution such as 4000 x 4000 pixels. Because the convolution process is an expensive operation and there are many convolution processes in the early layers of CNNs, large images are divided into small pieces (usually 1024 x 1024) to avoid the computational burden. For this reason, the data sets used in these studies (such as DOTA (Xia et aI., 2018) and HRSC2016 (Liu et aI., 2017) were created to contain small object classes such as aircraft, ships, cars, buses, etc. that can remain in 1024 x 1024 parts.

Today, there is not any data set and object detection model within the scope of detecting runway objects in high-resolution and large-size (80 MB and above) RSIs using CNN in the object detection area. In this study; the data set, containing high-resolution RSIs of various airports, is created by using Google Earth and Bing Maps, and then a model that detects the runway objects that have excessive width in this data set is presented. The specific features of the data set used are given in Table 1.

When Table 1 is examined; while the average image size of the data set used is 4137 x 4552 pixels, the average size of the runway objects contained in the images is 3221 x 87 pixels. Such large images create memory insufficiency and computational burden. Accordingly, the largest image sizes that current graphics cards can process at once are calculated using State of The Art (SOTA) object detection models and are detailed in Table 2. The graphics cards used in the tests are respectively 8 GB Nvidia GTX1080 and 16 GB Nvidia Tesla V100, and the backbone of SOTA object detection models is ResNet50 (He et al., 2016).

As can be seen in Table 2, the maximum image size that the GTX 1080 graphics card with 8 GB memory can process at one time is 2300 x 2300 pixels, while the maximum image size that the V100 graphics card with 16 GB memory can process at one time is 3600 x 3600 pixels. An Out of Memory error is obtained when an operation is attempted with a larger image for both graphics cards. The data set used in the study includes 376 images larger than 2300 x 2300 pixels and 318 images larger than 3600 x 3600 pixels. For this reason, it is inevitable to obtain an Out of Memory error in any train operation to be performed without any image pre-processing.

Table 1. Data set specific features

Specific Features	
Total Image Count	398 images
Minimum Image Size (width x height)	448 x 576 pixels
Maximum Image Size (width x height)	15904 x 11328 pixels
Average Image Size (width x height)	4137 x 4552 pixels
Maximum Runway Object Width	8216 pixels
Minimum Runway Object Height	64 pixels
Grater Runway Width Count*	60 images
Average Runway Object Size (width x height)	3221 x 87 pixels

* Number of runway objects with a width greater than the width of the image it contains

So, in this study, in order to avoid memory insufficiency (Out of Memory error) and computational burden, the images are first divided into 1024 x 1024 pixels pieces. Then, runway detection is made in these images with a method that detects objects as oriented. In the last stage; the runway detections in more than one 1024 x 1024 image piece are determined as a single runway by using the rotation angles according to the origin (Figure 1). Contributions and main objectives of proposed model are as follows;

- An object detection model is introduced that merges multiple object detection results based on rotation angles,
- Using proposed model to avoid the computational burden and overcome memory problems, it is possible to detect runway objects that have excessive width by dividing them into small pieces in high-resolution remote sensing images,
- It is the first study in this field that detects the runway objects that an excessive width in high-resolution RSIs using CNN.

In the second section of this study, the proposed model is explained in detail. The third section contains the results of the experiments performed according to the different threshold and angle combinations of the proposed model. Also in this section, to demonstrate the effectiveness of the proposed model, there is a comparison of the proposed model with SOTA object detection models. The fourth and last part is the conclusion of this study.

Table 2. Relationship between input image size and graphic cards

SOTA Model	Maximum Input Size		Flops (GFlops)		Params (Millions)	
	GTX1080	Tesla V100	GTX1080	Tesla V100	GTX1080	Tesla V100
Faster RCNN	2250 x 2250	3600 x 3600	971.35	2455.3	41.12	41.12
Mask RCNN	2200 x 2200	3600 x 3600	973.08	2501.61	43.75	43.75
Cascade RCNN	2200 x 2200	3500 x 3500	954.58	2351.96	68.93	68.93
RetinaNet	2300 x 2300	3600 x 3600	1058.36	2588.09	36.1	36.1
SSD512	2000 x 2000	3100 x 3100	1435.6	3219.51	36.04	36.04

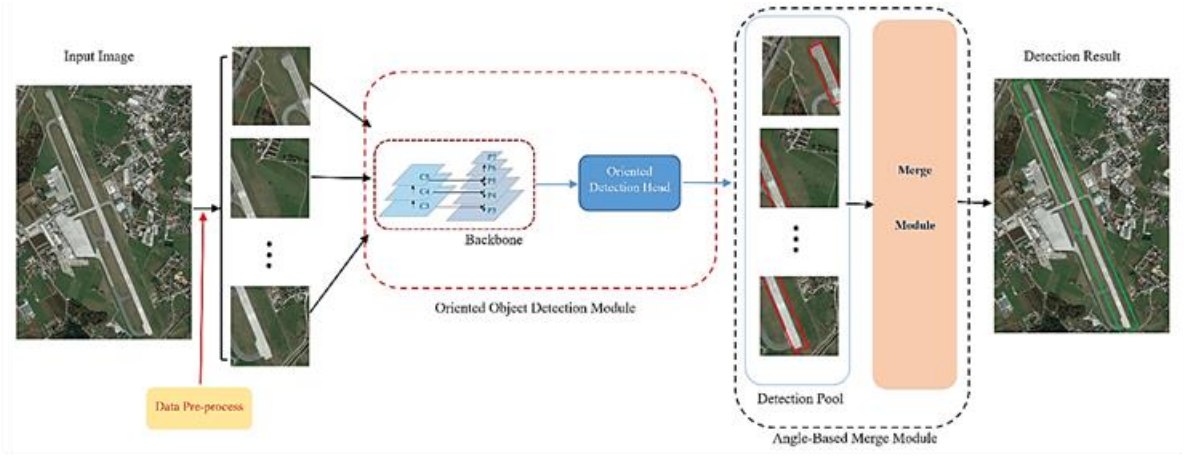

Figure 1. Overall architecture of proposed model

2. METHOD

The proposed model consists of two main components. These are; the Oriented Object Detection module using the RoI Transformer structure proposed in the study Ding (Ding et al., 2019), and the Angular-based Merge module, which angular merges the runway object detections predicted by the oriented object detection module. In this section, the mentioned modules are explained in detail.

2.1. Oriented Object Detection Module

In the detection of objects in RSI, making use of the structural properties of the objects directly affects the success. So, this module includes a backbone consisting of a Feature Pyramid Network (Tsung-Yi et al., 2017) and a ResNet50, also includes a RoI Transformer-based Oriented Detection Head. This module is designed according to training with labels suitable for oriented bounding box structure instead of standard horizontal bounding box structure. As a result of this training process, generating oriented bounding box predictions. Thus, detection results suitable for angular calculation can be transferred to the next module, Angular-based Merge.

2.2. Angular-based Merge Module

It is the module where the object detections coming from the detection module are merged according to the rotation angles and a single and complete runway detection is obtained. This module consists of 2 parts. These are the detection pool and merge module.

The detection results produced by the oriented object detection module are first collected in the detection pool. Object detections in the detection pool are delivered to the Merge module sequentially. The pool is not emptied until all of the images to be used while detecting the runway object are processed by the merge module. At the end of the final runway detection result generated by the merge module, the pool is automatically emptied. In order not to occupy more space in the GPU memory, only oriented detection results are kept in the Detection Pool.

The Merge module processes the detection results in the detection pool sequentially. The algorithm of this module is given in Algorithm 1. This algorithm consists of 3 stages.

1) Detection results in the detection pool may contain more than one bounding box. With the help of the non-maximum suppression technique, these bounding boxes are reduced to a single bounding box. The threshold value (N_t) in this process is set as 0.9, as will be mentioned in the experiments section. Obtained detection results are put into a new list (***DL***),

2) In this stage, oriented angle values of all detection results in DL are calculated at first. Then these detection results are grouped according to the angle values. In the second stage, all operations are performed over bounding boxes containing object detection. In the angle calculation process specified by (1) in Algorithm 1, the binary coordinate values (x, y) that form the bounding box are numbered starting from 0 clockwise (Figure 2),

Then, in accordance with equation 1, the angle value is calculated using the binary coordinate values of the corner points 0 and 3 of the bounding box. If the bounding box whose angle is calculated is the first, the binary coordinate value of the bounding box and the oriented angle value are added into a new group list (***GL***) and then the next bounding box is processed. The angle value of the next bounding box is calculated and compared with the angle value of the first elements of the existing group lists. The process referred to as comparison is to take the absolute value of the difference between the angles of both bounding boxes. If the result of the operation is less than 10º (in the experiments section, why this value is selected is explained), these two bounding boxes are assumed to belong to the same runway object, and the processed bounding box is added

as a new element to the relevant group list. If the angle value of the bounding box subjected to the calculation is not related to any ***GL*** (the difference is greater than 10º), this bounding box is considered to belong to a new runway object. Therefore, a new ***GL*** is created and the binary coordinate values and the oriented angle value of this bounding box are added as the first element to this new list. The comparison is done until all elements of the ***DL*** are finished.

$$\emptyset = tan^{-1}\left(\frac{y_4 - y_1}{x_4 - x_1}\right) \quad (1)$$

In Equation 1, while (*x1, y1*) binary coordinate value refers to the corner numbered 0, (*x4, y4*) binary coordinate values represent the corner numbered 3 clockwise.

3) At this stage, a single runway object is obtained by combining the bounding box values in each ***GL***. Additionally, since the dimensions of the runway objects in the images that make up the data set used within the scope of the study are larger than 1024, the number of elements of the ***GL*** to be merged should be at least 2. In the merge process specified with (2) in Algorithm 1; the binary coordinate values of the corner points 0 and 3 of the first bounding box of ***GL*** are added to a list. Then, the binary coordinate value of corner points 1 and 2 of the last element of the ***GL*** list is also added to this list, resulting in a complete bounding box. The process is completed by assigning 0.9 value selected as the threshold to the score value field of this bounding box. Bounding boxes obtained as a result of the merge process no (2) are added to the final result list (***R***). ***R*** is considered as the prediction result of proposed model

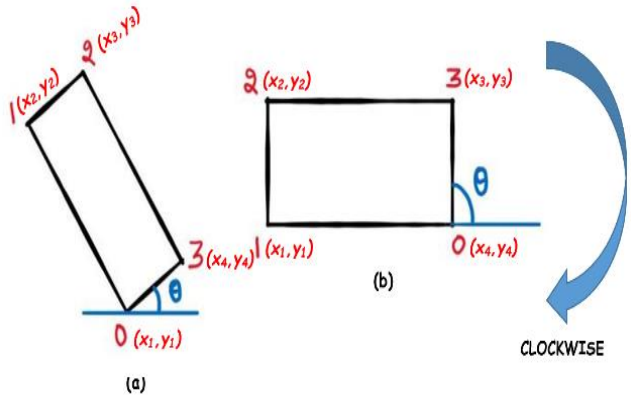

Figure 2. Bounding box numbering process. (a) Angle value less than 90º. (b) Angle value equal to 90º.

Algorithm 1 Merge Module

Input : $S=\{s_1,..,s_N\}$, $D=\{d_1,..,d_N\}$, N_t
S is list of inital detection boxes,
D is the list of detection boxes,
N_t *is the NMS threshold, where* $0 \leq N_t \leq 1$
Output : $R=\{r_1,..,r_N\}$
R is the full image runway detection results
Step1 : Reducing multiple object detections using NMS and adding them to the detection list(*DL*).
while $D \neq$ empty **do**
  if iou(d_i, s_i) $\geq N_t$ **then**
    $DL \leftarrow d_i$
end
Step2 : Grouping object detections according to oriented angles (*GL*).
j = 1, k = 1
for i in len(*DL*) **do**
  calculate angle (*DL[i]*) **(1)**
  if i = 1 **then**
    $GL_j[1] \leftarrow DL[i]$
    continue
  else
    while k ≤ j **do**
      if $|\text{angle}(GL_k[1]) - angle(DL[i])| \leq 5$ **then**
        $GL_k \leftarrow DL[i]$
        break
      else k++
    end
    if k > j **then**
      j ++
      $GL_j[1] \leftarrow DL[i]$
    end
  end
end
Step 3: Merge grouped object detections.
while j > 0 **do**
  if len(GL_j)> *1* **then**
    merge GL_j *elements* **(2)**
    $R \leftarrow GL_j$
  end
  j --
end

3. EXPERIMENTS, RESULTS AND DISCUSSION

3.1. Data Set and Evaluation Metric

Today, there are many datasets consist of remote sensing images such as DOTA and HRSC2016. However, none of these datasets contain a runway object. In this study, the data set we used is created by the Presidency of Defense Industries of The Republic of Turkey. This dataset includes high-resolution RSIs of various airports obtained from Google Earth and Bing Maps. We divide these images into small blocks with a size of 1024 × 1024 pixels, and there is a 200-pixels overlap between the adjacent small blocks. Of the 6012 images obtained after dividing, 4208 of them are used as trains and the remaining 1804 images are used for the test. Stochastic gradient descent (SGD) is chosen as the optimizer of the proposed model. The training of proposed model is completed after 24 epochs. The learning rate is initially chosen as 0.0025, it is reduced by 10% on the 16th and 22nd epochs. To evaluate the performance of proposed model, we used mean average precision (mAP) as a

benchmark that reflects the overall performance of object detection algorithms. The mAP is defined as,

$$\text{mAP} = \int_0^1 P(R)dR \quad (2)$$

where P indicates the precision rate; R suggests the recall rate.

3.2. Experiments with Different Configurations

Experiments with different configurations are carried out to measure the performance of the proposed model. The configurations we use are the nms threshold value, which has an important place in the success of the model we propose, and the angular difference value we use when comparing bounding boxes. Experimental results are given in Table 3.

Table 3. Performance comparison on threshold value and angular difference value

NMS Threshold Value	Angle Difference Value ≤ 5º	≤ 10º	≤ 15º	≤ 20º	≤ 25º
0.5	0.722*	0.728	0.743	0.732	0.717
0.6	0.743	0.750	0.754	0.738	0.730
0.7	0.771	0.768	0.773	0.746	0.739
0.8	0.787	0.801	0.798	0.761	0.752
0.9	0.794	**0.815**	0.803	0.802	0.782

* All values are *m*AP

When Table 1 is examined; it is seen that the best result is obtained with the 0.9 threshold value and configuration where the angular difference is less than 10º (0.815 mAP). The reason for this can be explained as follows,

- The long side of the runway objects in the images is often long enough to correspond to more than one 1024x1024 image piece. Moreover, their width is not as small as those of objects such as planes, cars, and ships that are frequently found in RSIs. So, they are very easy to detect. For this reason, keeping the threshold value high directly increases the success as it eliminates false detections.

- In addition to the main runways, there are smaller auxiliary runways at the airports. Since the auxiliary runways and main runways are very close to each other, when the angular difference value increases, the proposed model identifies the auxiliary runways as the main runway. According to the results of the experiments, the highest success is obtained when the angular difference is less than 10º.

3.3. Proposed Model Compared with SOTA Object Detection Models

To objectively evaluate the performance of the proposed model; SOTA object detection models are trained on the data set used in this study. According to the test results made after the training processes, the object detection performance comparison of the SOTA object detection models (Ren et al., 2014; He et al., 2017; Zhaowei et al., 2019; Lin et al., 2017; Wei et al., 2016). and the proposed model is given in Table 4. All images in the data set are downscaled to 1024 x 1024 in order not to get an Out of Memory error. The training of all models is completed after 24 epochs. The learning rate is initially chosen as 0.0025, it is reduced by 10% on the 16th and 22nd epochs.

When Table 4 is examined, it is seen that the proposed model shows the best performance by far. The proposed model performs 11% better than the RoI Transformer model it uses as an object detection module. This is because; while the downscale preprocessing process reduces the accuracy value, the proposed model can detect the objects with the help of the Angular-based Merge module without the downscale preprocessing.

As can be seen from the object detection performances; the downscale preprocessing process causes the SOTA models (especially RetinaNet) to perform poorly. However, downscale preprocessing is also a must to get rid of the Out of Memory error, which is explained in detail in Table 2. Although the inference time of the proposed model is slow, it is at a level that can be ignored according to the object detection performance it achieves (It even has a good speed compared to SSD512, RetinaNet, and Mask RCNN models). So, considering the data set used within the scope of the study, it is understood that the proposed model has a reasonable speed. Object detection results on the test images of the proposed model can be seen in Figure 3.

Table 4. Object detection performance comparison of the proposed model and SOTA models.

Model	Inference Time(FPS)	*m*AP
Faster RCNN	4.6	0.539
Mask RCNN	1.5	0.500
Cascade RCNN	3.9	0.623
RetinaNet	1.6	0.103
SSD512	1.3	0.520
RoITransformer	4.2	0.703
Proposed Model	1.7	0.815

(a) (b) (c) (d)

Figure 3. Visualization of detection results. In the images with more than one runway object, each runway's detection is shown in a different color.

4. CONCLUSION

In this study, a simple and effective object detection method is proposed to detect runway objects that have an excessive width in high-resolution remote sensing images. The proposed model aims to detect runway objects in high-resolution images based on the divide and conquer philosophy. To avoid the computational burden and overcome memory problems (especially Out of Memory error), in the proposed method, remote sensing images are first divided into 1024x1024 small images. Then, runway objects are detected as oriented, and obtained detection results are merged taking into account the angular differences. So, the predicted output of the model is obtained. Experiments show that the proposed model achieves 81.5% mAP results. Also, SOTA object detection models are trained on the data set used within the scope of the study, and the object detection performances are compared with the proposed model. According to the comparison results, the proposed model achieves an 11% mAP increase compared to the best-performing SOTA model. In the next study, improvements will be made to enable the proposed model to perform instance segmentation with object detection jointly.

ACKNOWLEDMENT

I would like to thank the Presidency of Defence Industries of The Republic of Turkey for providing the dataset we use in this study.

Conflicts of interest

The authors declare no conflicts of interest.

REFERENCES

Akbar J, Shahzad M, Malik MI, Ul-Hasan A & Shafai F (2019). Runway Detection and Localization in Aerial Images using Deep Learning. Digital Image Computing: Techniques and Applications (DICTA), 1 - 8, Perth,Australia.

Aytekin Ö, Zöngür U & Halici U (2013). Texture-Based Airport Runway Detection. IEEE Geoscience and Remote Sensing Letters, 10-(3), 471-475.

Bengio Y, Goodfellow I & Courville A (2016). Deep Learning. MIT Press. ISBN: 978-0262035613.

Cheng G & Han J (2016). A Survey on Object Detection in Optical Remote Sensing Images. ISPRS Journal of Photogrammetry and Remote Sensing ,117, 11-28.

Ding J, Xue N, Long Y, Xia G & Lu Q (2019). Learning RoI Transformer for Oriented Object Detection in Aerial Images. IEEE Conference Computer Vision and Pattern Recognition (CVPR), 2844 -2853, Seul, Korea.

He K, Zhang X, Ren S & Sun J (2016). Deep Residual Learning for Image Recognition. IEEE Conference Computer Vision and Pattern Recognition (CVPR), 770 -778, Nevada, USA.

He K, Gkioxari G, Dollar P & Girshick G (2017). Mask R-CNN. IEEE International Conference on Computer Vision (ICCV), 324-333, Venice, Italy.

Ju M, Luo J, Zhang P, He M & Luo H (2019). A Simple and Efficient Network for Small Target Detection. IEEE Access, 7, 85771-85781.

Li Z, Liu Z & Shi W (2014). Semiautomatic Airport Runway Extraction Using a Line-Finder-Aided Level Set Evolution. IEEE Journal of Selected Topics in Applied Earth Observations and Remote Sensing, 7(12), 4738-4749.

Lin T Y, Goyal P, Girshick R, He K & Dollar P (2017). Focal loss for dense object detection. IEEE Transactions on Pattern Analysis and Machine Intelligence, 99, 2999-3007.

Liu Z, Yuan L, Weng L & Yang Y A (2017). High Resolution Optical Satellite Image Dataset for Ship Recognition and Some New Baselines. 6th International Conference on Pattern Recognition Applications and Methods, 324 – 333, Porto, Portugal.

Lv W, Dai K, Wu L, Yang X & Xu W (2018). Runway Detection in SAR Images Based on Fusion Sparse Representation and Semantic Spatial Matching. IEEE Access, 6, 27984-27992.

Krizhevsky A, Sutskever I & Hinton G E (2012). ImageNet classification with deep convolutional neural networks. Advances in Neural Information Processing Systems, 25, 1097–1105.

Ren S, He K, Girshick R & Sun J (2015). Faster R-CNN: Towards real-time object detection with region proposal networks. IEEE Transactions on Pattern Analysis and Machine Intelligence, 39-(6), 91–99.

Song Q, Yang F, Yang L, Liu C, Hu M & Xia L (2021). Learning Point-Guided Localization for Detection in Remote Sensing Images. IEEE Journal of Selected Topics in Applied Earth Observations and Remote Sensing, 14, 1084-1094.

Tang G, Xiao Z, Liu Q & Liu H (2015). A Novel Airport Detection Method via Line Segment Classification and Texture Classification. IEEE Geoscience and Remote Sensing Letters, 12 (12), 2408-2412.

Tao C, Tan Y, Cai H & Tian J (2010). "Airport Detection from Large IKONOS Images Using Clustered SIFT Keypoints and Region Information. IEEE Geoscience and Remote Sensing Letters, 8-(1), 128-132.

Tsung-Yi L, Dollar P, He K, Hariharan B & Belongie S (2017). Feature Pyramid Networks. IEEE Conference Computer Vision and Pattern Recognition (CVPR), 936-944, Hi, USA.

Wang Y, Zhang Y, Zhao L, Sun X & Guo Z (2019). SARD: Towards Scale-Aware Rotated Object Detection in Aerial Imagery. IEEE Access, 7, 173855-173865.

Wei L, Anguelov D, Erhan D, Szegedy C, Reed S, Fu S Y & Berg A (2016). SSD: Single Shot MultiBox Detector. The 14th European Conference on Computer Vision (ECCV), 21 -37, Amsterdam, Holland.

Wu W, Xia R, Xiang W, Hui B, Chang Z, Liu Y & Zhang Y (2014). Recognition of Airport Runways in FLIR Images Based on Knowledge. IEEE Geoscience and Remote Sensing Letters, 11, 1534-1538.

Wu Y, Zhang K, Wang J, Wang Y, Wang Q & Li Q (2020). CDD-Net: A Context-Driven Detection Network for Multiclass Object Detection. IEEE Geoscience and Remote Sensing Letters, 3, 1-4.

Xia GS, Bai X, Ding J, Zhu Z, Belongie S, Luo J, Datcu M, Pelillo M & Zhangi L (2018). DOTA: A large-scale dataset for object detection in aerial images. IEEE Conference Computer Vision and Pattern Recognition (CVPR), 3974-3983, Utah, USA.

Yu Y, Yang X, Li J & Gao X (2020). A Cascade Rotated Anchor-Aided Detector for Ship Detection in Remote Sensing Images. IEEE Transactions on Geoscience and Remote Sensing, 2, 1-14.

Zhang Z, Zou C, Han P & Lu X (2020). A Runway Detection Method Based on Classification Using Optimized Polarimetric Features and HOG Features for PolSAR Images. IEEE Access, 8, 49160-49168.

Zhaowei C & Vasconcelos N (2019). Cascade R-CNN: High Quality Object Detection and Instance Segmentation. IEEE Transactions on Pattern Analysis and Machine Intelligence, 43-(5), 1483 – 1498.

Zöngür U, Halici U, Aytekin O & Ulusoy I (2009). Airport runway detection in satellite images by Adaboost learning. SPIE Image and Signal Processing for Remote Sensing XV, 1-12, Berlin, Germany.

International Journal of Engineering and Geosciences
https://dergipark.org.tr/en/pub/ijeg
e-ISSN 2548-0960

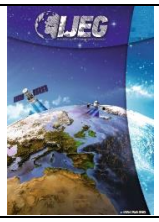

Determining the relationship between the slope and directional distribution of the UAV point cloud and the accuracy of various IDW interpolation

Kemal Ozgur Hastaoglu*[1], Sinan Göğsu [2], Yavuz Gül [3]

[1]*Sivas Cumhuriyet University, Engineering Faculty, Dept. of Geomatics Engineering, Sivas, Turkey*
[2]*Sivas Directorate of Cadastre, General Directorate of Land Registry and Cadastre, Sivas, Turkey*
[3] *Sivas Cumhuriyet University, Engineering Faculty, Dept. of Mining Engineering, Sivas, Turkey*

Keywords
Interpolation
UAV point cloud
Shepard
Slope effect
Anisotropy

ABSTRACT

Inverse Distance Weighted (IDW) based interpolation method is also widely used in earth science studies. In the classical IDW method, the directional distribution of the reference points around the point to be estimated within the critical circle and the slope differences are not taken into consideration. On the other hand, in the IDW-based method developed by Shepard, the ratio of the distances of the reference points within the critical circle to the critical circle radius (r), the anisotropy and the slope differences are taken into consideration. In this study, the results of the classical IDW method and Shepard method were compared to increase the accuracy of interpolation produced from UAV data. A software has been developed to make these comparisons in more detail. The classical IDW and Shepard based interpolation methods used in this software takes into consideration the anisotropy, the slope differences and the ratio of the distances to the critical circle radius. In this study, UAV flights were performed in three different study areas with different topographic features and 3D point cloud data were obtained in order to make detailed analyzes. Using developed software, data from three different study areas have been tested and the results from different Shepard interpolation models have been discussed. The major contribution of this paper is in evaluation of various IDW options when applied to UAV point data. As a result, especially in geodetic studies form UAV data, it was observed that the results improved with 11% to 37% by using the Shepard method with the suitable power parameter value considering the directional distribution of the reference points in the critical circle and the slope differences.

1. INTRODUCTION

IDW interpolation method is one of the most commonly used deterministic models in spatial interpolation models (Lu and Wong 2008). IDW method is widely preferred because it has a simple structure in calculations and programming. Many researchers have done different studies on the effect of the interpolation method on DEM accuracy. In these studies, the IDW-based interpolation method was compared with other interpolation methods, and the weak and successful qualifications of the IDW method were tried to be determined. (Tran and Nguven 2008; Bater and Coops 2009; Guo et al. 2010; Arun 2013; Setianto and Triandini 2013; Ismail et al. 2016; Habib et al. 2018.; Graham et al. 2020).

Today, the IDW interpolation method is used as the standard in many software. In the IDW method used in these software's, the power parameter value (u) is usually taken as 2 (Brimicombe 2009; Stafford 2013; Michael 2020; Envir. Sys. Res. Inst. 2020). However, according to the general characteristics of the field studied and the data distribution, the power parameter value that gives the most appropriate result varies. Therefore, it is necessary to determine the "u" value specific to each study area. Lu and Wong (2008), in the IDW method, they suggested that the value of the weighting parameter be allowed to vary according to the spatial pattern of the sampled points in the

* **Corresponding author**
*(khastaoglu@cumhuriyet.edu.tr) ORCID ID 0000-0002-5077-5889
(sinangogsu@gmail.com) ORCID ID 0000-0003-3853-4473
(ygul@cumhuriyet.edu.tr) ORCID ID 0000-0002-2969-577X

Cite this article
Hastaoglu K O, Gogsu S & Gul Y (2022). Determining the relationship between the slope and directional distribution of the UAV point cloud and the accuracy of various IDW interpolation. International Journal of Engineering and Geosciences, 7(2), 161-173

Research Article / DOI: 10.26833/ijeg.940997
Received: 22/05/2021; Accepted: 09/09/2021

neighborhood. They developed an algorithm to search for ‘‘optimal’’ adaptive distance-decay parameters. They concluded that adaptive IDW performs better than the constant parameter method in most cases and better than ordinary kriging in one of their empirical studies.

The main purpose of this article is to investigate the effect of slope difference and directional distribution between reference points and interpolation points on the accuracy of various IDW interpolation methods. For this purpose, UAV point cloud data were used in the study. Within the scope of this study, it is aimed to develop software that can perform estimates with both the classical IDW method and the Shepard method. For these purposes, a software named IDW_OPTIMAL was developed in this study. Using the IDW_OPTIMAL software for UAV point clouds in three different study sites, the most appropriate u value and the most suitable IDW-based interpolation method were determined and the results were examined. Thanks to the developed software, the results regarding the Shepard method approaches, which take into account the ratio of the distance of the points falling in the critical circle to the critical circle radius, the directional distribution, and the slope differences, were examined in detail. In addition, the directional distribution of reference points and the effects of slope differences on interpolation results were examined in detail. As a result of these evaluations, it was observed that the results were improved between 11% and 37% when the most appropriate u value and the most suitable IDW-based interpolation method were used for the study area.

In many previous studies, the advantages and disadvantages of the classical IDW method compared to other interpolation methods were examined in detail. However, the Shepard method was not discussed in detail in any of these studies. The accuracy assessment and comparative analysis of IDW, Spline and Kriging methods in the spatial interpolation of the earth was investigated by Ikechukwu et al. (2017). It is stated that according to the data set used, the IDW method is more sensitive than the Kriging method, and the Spline method has better results than the other two methods. On the other hand, Agüera et al. (2019) produced DTMs with different grid size from 3D point clouds data using four different interpolation methods. It was seen that the IDW method for each interpolation method and each density is the interpolation method that gives the best accuracy for all densities and GS combinations. Ferreira et al. (2017) analyzed the efficiency of IDW and Universal Kriging by reducing the number of sample points in computational representation of bathymetric surfaces. As a result, they determined the superiority of the inefficiency of Universal Kriging method in creating DMD in bathymetric data.

In addition, some studies have conducted research on the effect of power parameter on accuracy in IDW method. Chen and Liu (2012) determined the most appropriate radius of effect and power parameter values for the IDW method. It has been determined that the radius of effect is between 10-30 km and the power parameter (α) is in the range of 0-5. Zhou et al. (2017), a new IDW method has been proposed by designing a topographic factor in the calculation of the appropriate power parameter and weight, based on the principle of the IDW method. The proposed IDW method compared to the classical IDW method has been shown to improve interpolation accuracy. As a result of this study, with the weight model considering topographic factors, the results were improved by 9% when the power parameter was 2, and a 12% improvement was observed in the results when the power parameter was 3. However, the effect of the radius of the critical circle and the directional distribution of the control points on the accuracy are ignored in this study. In our study, besides topographic effect and power parameter, directional distribution and critical circle radius were taken into consideration and improvements of up to 37% were observed in the results.

In the spatial analysis section of many GIS studies, Shepard (1968) was cited (Paul et al. 2019; Mohamed et al. 2018; Sarkar et al. 2016; Welch et al. 2014; Wang and Huang 2012) In these studies only the classical IDW method was used, and the directional distribution and slope distribution features proposed by Shepard were ignored. The reason for this is that there is only the classic IDW method in the GIS software’s used. In addition, it is mentioned that Shepard method is used when testing the success of interpolation methods in many socio-economic, hydrological, meteorological and environmental pollution GIS studies. (Wu et al. 2019; Meng et al. 2019; Liao et al. 2018; Das et al. 2017) In these studies, the directional distribution and slope distribution features proposed by Shepard were also ignored.

2. INVERSE DISTANCE WEIGHTED INTERPOLATION METHOD (IDW)

In this method, the distances between the interpolation points and the reference points are used in the weight calculation to estimate the unknown points. In the method, it is aimed that the reference points near the point to be interpolated have more weight than the distant reference points.

A different interpolation approach using weighted averages was developed in the study conducted by Shepard in 1968. As a result of this approach, he has developed an IDW based interpolation method that takes account of selection of reference points, directional distributions and slope differences. The interpolation value at any P point in the plane is a weighted average of the values at the Di reference points. The interpolation value at the P point is calculated by the following Eq.1.

$$f_1(P) = \begin{cases} \left[\sum_{i=1}^{N} (d_i)^{-u}.Z_i\right] / \left[\sum_{i=1}^{N} (d_i)^{-u}\right] & d_i \neq 0, (u > 0) \\ Z_i & d_i = 0 \end{cases} \quad (1)$$

In Eq. 1 Z_i is the value at the reference points and di is the distance between the P point and the Di reference points. Depending on the function, point P is approaching the reference point Di and if di=0 it takes the value $f(P)=Z_i$.

In the weighting function in Eq. 1, the calculation can be facilitated by eliminating the remote reference points. A maximum of ten points and minimum of four points is selected to limit the calculation complexity and amount. Also, a first search radius r is created based on the total

density of the data points. If the area of the largest polygon surrounded by the reference points is A, the total number of reference points N is defined as follows, with an average of seven reference points in the circle in the radius r (Shepard 1968).

$$\pi r^2 = 7 * (\frac{A}{N}) \quad (2)$$

After selecting the reference points that fall into the critical circle, the new weighting functions $S_i = S(d_i)$, of the effect of di distances on the interpolation process for each $D_i \in C'$ between the interpolation point P and the reference points can be defined.

$$S(d) = \begin{cases} \frac{1}{d} & 0 \le d \le \frac{r'}{3} \\ \frac{27}{4r'} \cdot (\frac{d}{r'} - 1)^2 & \frac{r'}{3} < d \le r' \\ C_P^{10} & r' < d \end{cases} \quad (3)$$

In Eq.3 function has been defined as permanently distinguishable all over d>0. S(d) = 0 for d> r'. In Shepard (1968) it is stated that a direction factor is required in addition to the distance factor in defining weights to improve the interpolation process. The weighting term that takes into account the direction factor for each reference point near the interpolation point at the P position would be as in Eq. 4.

$$t_i = \left[\sum_{D_j \in C'} S_j [1 - \cos(D_i P D_j)]\right] / \left[\sum_{D_j \in C'} S_j\right] \quad (4)$$

$0 \le t_i < 2$ since $-1 \le \cos(\Theta) \le 1$ for all Θ angles. The cosine function defined in Eq.4 was used as a direction measure due to both convenience and ease of calculation. In interpolation, the effect of the points close to P should be more than the distant points. For this reason, distance factor S_j should be included in the numerator and denominator. A new weight function that takes the direction into account is defined as in Eq.6.

$$w_i = (S_i)^2 . (1 + t_i) \quad (5)$$

In Eq.5, the slope for each D_i in the interpolation function is assumed to be zero. The interpolation function must be rearranged to take into account the slope effect in each D_i. First, for each data point D_i, the constants Ai and Bi representing the desired slope in the x and y directions in D_i are determined. With $C_i'' = C'_{Di} - \{D_i\}$, A_i and B_i constants are calculated as in Shepard, 1968. A parameter v, which is then the combination of the x and y directions, with the total range of Z_i and the distance dimension relative to the desired slopes, is expressed as in Shepard, 1968.

Parameter v limits the maximum effect of slope terms to Z value obtained by interpolation. To add the effect of the slope on the interpolation value at P (x, y), a ΔZ_i increment value for each $D_i \in CP$ is calculated as in Eq.6 as a function of P.

$$\Delta Z_i = [A_i . (x - X_i) + B_i . (y - Y_i)] . \left[\frac{v}{v + d_i}\right] \quad (6)$$

3. MATERIAL AND METHOD

3.1. Study Area

Since the UAV dataset contains cm-level point cloud data, it is possible to sample the UAV data at the desired frequency and density. In our study, it was preferred to use UAV data, especially in terms of needing data with different topographic features and directional distributions and analyzing the results with more data sets. In addition to this, UAV technology has started to be used instead of classical surveying and mapping methods. The time, cost and accuracy advantages of the UAV method have made the use of the method especially common in DEM creation. UAV data were used as test data because the method is new and up-to-date and it is convenient to create a sufficient number of datasets for analyses.

Three different sites with different topographic features were selected as the study area. In order to investigate the effect of directional distribution and topographic effect on the accuracy of the IDW method, these study areas with different topographic characteristics were preferred. The study areas are Hamal, Kızılcakent and Eliktekke (Figure 1). Point clouds obtained by the UAV photogrammetry method related to the study areas were used as a data set. Since the Ground Sample Distance (GSD) value in the point cloud data is less than 7 cm, interpolation cannot be performed using the whole data set, so the data set has been diluted. If the whole data set is used, the interpolation process will lose its meaning as the distance between the interpolation point and reference points will be almost zero. For each study area, first of all, the workspaces with the desired topographic structure were cut and smaller workspaces were created, and then random point clouds were selected for these new study areas with maximum 10 m intervals. Thus, the point cloud data is diluted and the data are made suitable for interpolation.

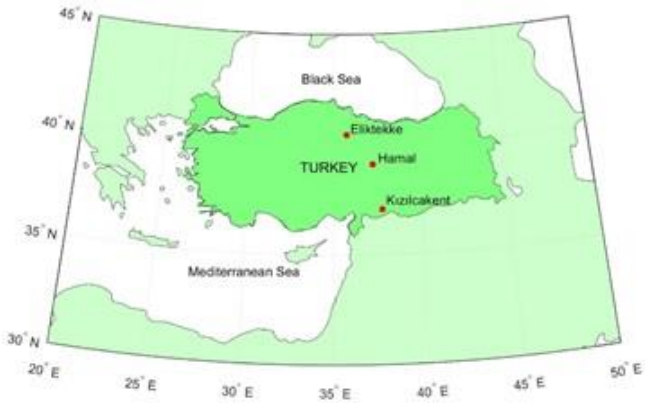

Figure 1. The locations of study areas

Detailed information on the study areas is given in Table 1. The reference points, control points and point cloud on the study areas in Figure 2,3 and 4 are presented.

Table 1. Information of study areas

Study Area	Area (he)	Points		Change of the slope	
		Control (number)	Referance (number)	E-W (%)	N-S (%)
Hamal	168	180	19594	15	5
Kızılcakent	98	250	19036	12	2
Eliktekke	38	73	11231	18	25

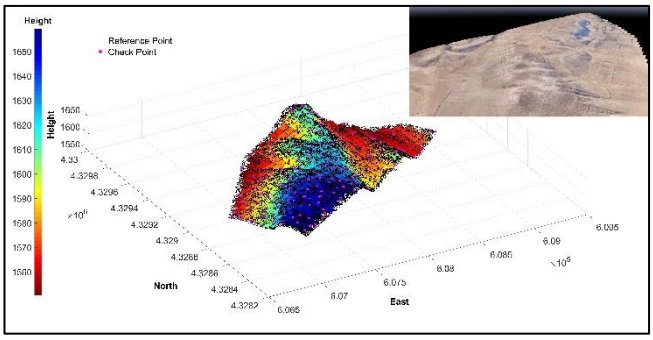

Figure 2. Hamal study area

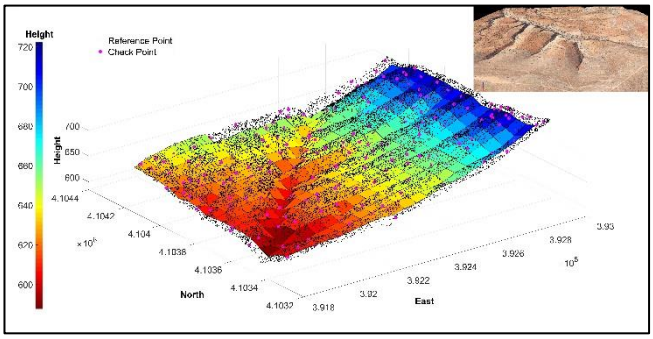

Figure 3. Kızılkent study area

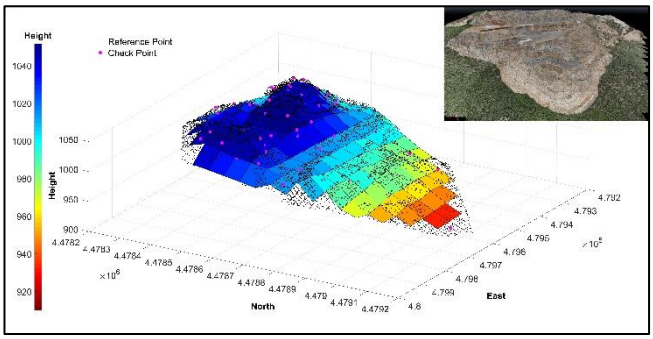

Figure 4. Eliktekke study area

3.2. UAV Photogrammetry Data Acquisition and Processing

In accordance with the purposes mentioned above, flights were carried out at the three different study areas. For the Eliktekke study area, flights were carried out using hexacopter according to the information given in Table 2. On the other hand, flights were carried out using quadcopter according to the information given in Table 2. All technical equipment used for flights belongs to GEOMINE Company. PIX4D software licensed by GEOMINE was used to evaluate aerial photographs. In the study areas, the number of ground control points (GCPs) given in Table 2 were installed and measured by the CORS GNSS method. The knowledge of UAV data acquisition and processing are given in Table 2.

Table 2. The knowledge of UAV data acquisition and processing

Study Area	Eliktekke	Hamal	Kızılcakent
GSD	1.44 cm	5.23 cm	7.26 cm
Area Covered	80 ha	310 ha	250 ha
GCP Number	12	43	50
GCP mean RMSerror	0.7 cm	3.8cm	6.0 cm
Num. of 3D Dens. Points	451924568	107116721	81632904
Cam. Spec. Im. format Focal Length	Sony A7R 7360×4912 35 mm	SonyA6000 4608x3456 16 mm	SonyA6000 4608x3456 16 mm
Flying speed	5.9 m/s	11.0 m/s	11.0 m/s
For. and side overlap (%)	80/60	80/60	80/60
Number of Images	1865	911	842

In order to examine the effect of point cloud accuracy on interpolation methods, Eliktekke was flown to have a lower GSD value compared to the other two fields. Point cloud accuracy obtained with UAV photogrammetry is specified as (1-2) × GSD for horizontal and (1-3) × GSD for vertical in PİX4D program documents (Url-1, 2018). Since GSDs for Eliktekke, Hamal and Kızılcakent study areas are 1.4, 5.2 and 7.3 cm / pixel, respectively, the expected accuracy of point clouds in these study areas are varied between 1.4-2.8, 5.2-10.4 and 7.3-14.6 cm horizontally and 1.4-4.2 5.2-15.6 and 7.3-21.9 cm vertically, respectively.

Some of the point cloud data were selected as control points and these control points were estimated. The estimations were made by using both Standard IDW and Shepard method approaches for different power parameter values. Root mean Squares (RMS) were calculated by taking into account the differences between the estimated values and known values. The approach with which the smallest RMS is obtained has been determined as the most suitable method since the RMS value approaching zero means that the accuracy of the estimation is high. According to the calculated RMS values, the outliers that are not suitable for the standard normal distribution are determined. Since the number of data is greater than 40 (n> 40), the two-sided standard normal distribution value (z = ± 1.96) was used for the 95% confidence level (α = 0.05) in the determination and removal of outliers. When the outliers are examined in detail, it has been observed that these points are usually points that show a sudden change in height (tree, house, hole, etc.). Therefore, these points were excluded from the evaluation. The accuracy of the method is determined using RMS values recalculated using data that are free from outliers.

3.3. IDW _OPTIMAL Software

A Matlab-based program has been developed that can take into account the directional distribution of reference points and slope differences in the Shepard interpolation method. Thanks to this program, calculations are made with different IDW-based options.

In the first stage of the software, the boundaries of the study area (A) are calculated by determining according to the reference point set. Then, the location information of the interpolation points is entered by the user and the interpolation points remaining in the study area are determined. In Shepard method in software, critical circle radius (r) is calculated and reference points around interpolation point are determined.

Interpolation methods in the software are standard IDW (IDW_{std}) and Shepard method. In the second stage, the interpolation method is selected. Shepard method has been accepted as three approaches in itself. These are, respectively, according to the weights calculated without the direction and slope factor (SHP_{std}: Shepard Standard), using only the direction factor (SHP_{DD}: Shepard Directional Distribution) and by considering the direction and slope factor together (SHP_{DD+SD}: Shepard Directional Distribution + Slope Differences) interpolation methods.

3.3.1. Interpolation According to Standard IDW (IDW_{std}) Method

In this method, critical circle in Shepard method is taken as the basis for selection of reference points. The Z value of the interpolation point are estimated by calculating the weights with the weight function in Eq.1 according to the distance between the interpolation point and reference points in the critical circle. The flow diagram of this process is shown in Figure 5. The weight calculation is a function of the inverse of the distance in degrees u, the value of the u parameter is determined by the user.

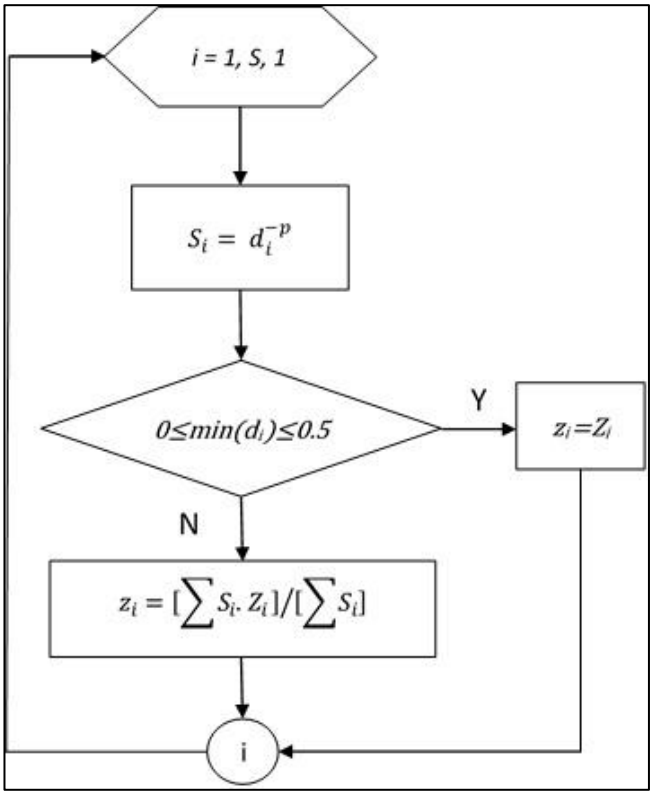

Figure 5. Standard IDW method weight calculation flow diagram

3.3.2. Interpolation with Shepard Method

Shepard interpolation method is examined according to three different approaches. In the first approach (SHP_{std}), weights are calculated according to the function of the only inverse distance by ignoring the direction and slope factor, in the second approach (SHP_{DD}), weighting is done by including the direction factor, In the third approach (SHP_{DD+SD}), interpolation is performed according to the weights calculated by evaluating the direction and slope factor together. Calculations were performed for each of these approaches using the developed software.

3.3.2.1. Weighting according to only inverse distance for the Shepard Method (SHP_{std})

The first approach of the Shepard method (SHP_{std}) is the interpolation process without direction and slope factor. In this approach, weights are calculated by evaluating the ratio (Eq. 2) of the distance between the reference points and interpolation points in the critical circle to the critical circle radius (Figure 6). After the weight calculation, interpolation is performed according to the interpolation function in Eq. 3. The flow diagram of this process is shown in Figure 7.

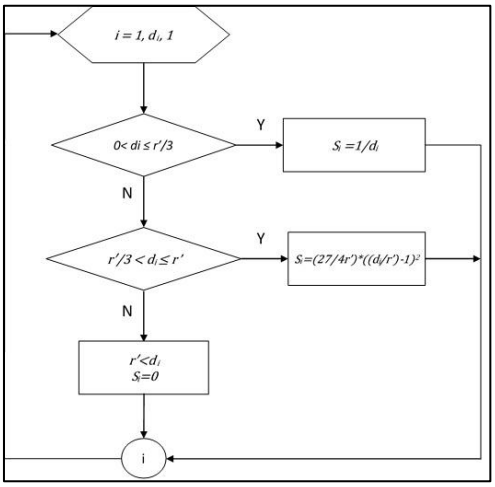

Figure 6. Weight calculation algorithm according to the ratio of the distance to the critical circle radius.

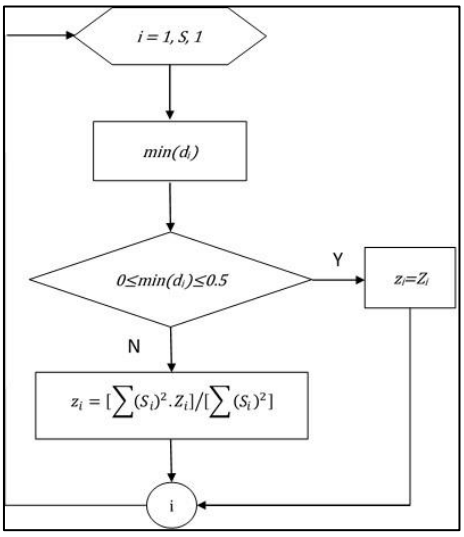

Figure 7. Interpolation points estimation algorithm

3.3.2.2. Weighting according to directional distribution for Shepard Method (SHP_{DD})

The interpolation process in this approach (SHP_{DD}) is based on the recalculation of the S weights, which are calculated by only inverse distance in the first approach, by taking into account the directional distributions of the reference points in the critical circle. The weight calculation algorithm after the addition of the direction factor is shown in Figure 8.

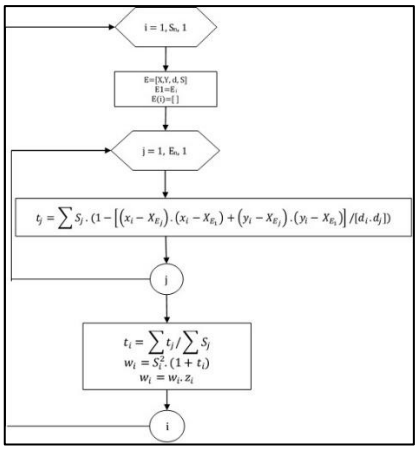

Figure 8. Weight function algorithm obtained by including direction factor.

3.3.2.3. Weighting according to directional distribution and slope difference for Shepard Method (SHP_{DD+SD})

In the third approach of the Shepard method (SHP_{DD+SD}), besides the directional distribution of the reference points, weighting is done by adding the slope differences between the reference points to the weight function. Figure 9 shows the processing algorithm. After the weights are calculated according to the direction and slope factors, interpolation calculation is made according to Eq. 6. The algorithm of this process is given in Figure 10.

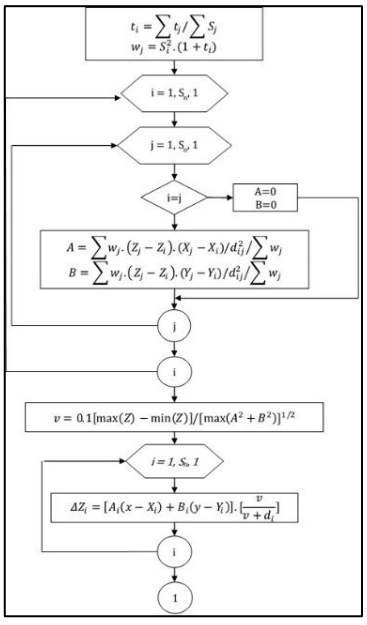

Figure 9. Weight function algorithm according to direction and slope factors.

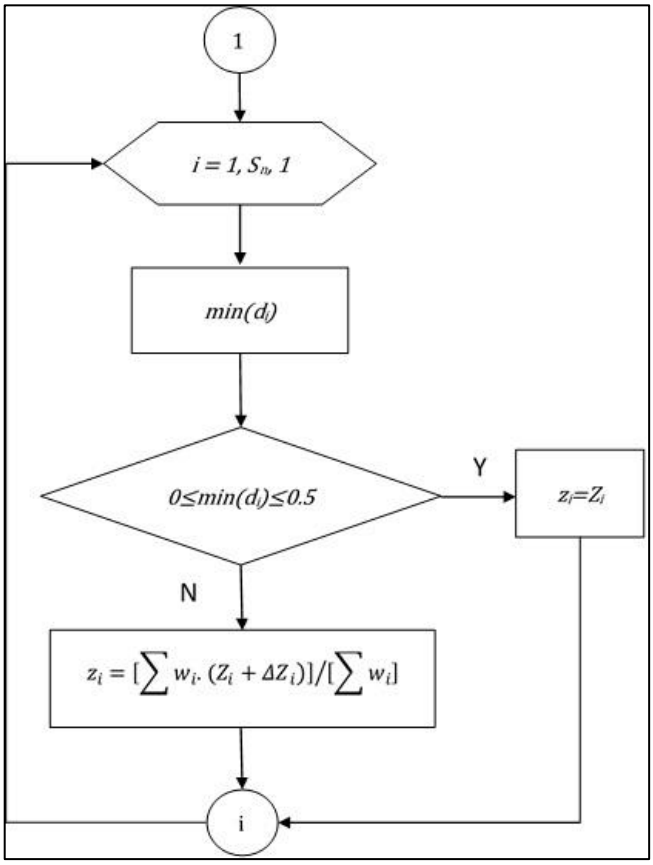

Figure 10. Interpolation process algorithm according to the direction and slope factor.

3.4. Evaluation of the data with the software and determining the most appropriate interpolation approach

Data in the point cloud cluster produced by UAV photogrammetry of three different study sites are used as input data in the software (IDW_OPTIMAL) developed (Figure 11). The points to be interpolated are points selected from the point cloud set in a random distribution and whose height values are known.

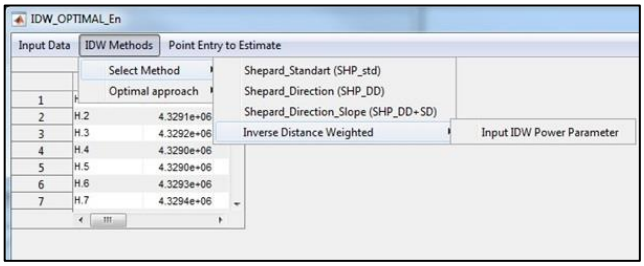

Figure 11. Selection of interpolation method

The data of Hamal, Kızılcakent and Eliktekke study areas were evaluated in the software and the estimation results of IDW_{std}, SHP_{std}, SHP_{DD} and SHP_{DD+SD} approaches were recorded. (Figure 11). RMS values for each method were calculated because the predicted interpolation points are control points.

In Table 3, RMSs calculated after removing outliers are given for the different power parameter (u) values (u=1,2,3,4) in the IDW_{std} approach and for the standart power parameter value (u=2) in the three approaches of the Shepard method.

Table 3. Accuracy of interpolation results according to standard IDW and Shepard approaches (after the outliers are removed)

Method	Root Mean Square (RMS) [m]						
	IDW_{std}				Shepard		
					STD	DD	DD+SD
Study area/Pow. Par. (u)	*u=1**	*u=2**	*u=3**	*u=4**	*u=2*	*u=2*	*u=2*
Ham.	0.36	0.32	0.33	0.35	0.38	0.35	0.32
Kızıl.	0.52	0.52	0.53	0.53	0.61	0.59	0.51
Elik.	0.85	0.81	0.81	0.82	0.90	0.90	0.81

** User-defined power parameter (u=1,2,3,4)*

When Table 3 is examined, it is seen that for the u = 2 value generally used in the application the results obtained with the IDW_{std} approach are close to the results of the Shepard approaches considering the direction and slope factor. Although the RMS values are slightly smaller in the Shepard approaches than the IDW_{std} approach, there is no significant improvement (<5 mm) between the values.

Table 4. Interpolation RMS values, GSD and accuracy of UAV results and change of slope of study areas

Study Area	RMS (m)	Accuracy		Change of the slope	
		GSD (m)	Max. Vertical Pos.(m)	East-West (%)	North-South (%)
Ham.	0.363	0.052	0.156	15	5
Kızıl.	0.519	0.073	0.219	12	2
Elik.	0.849	0.014	0.042	18	25

Table 4 shows RMS values of interpolation results according to standard IDW (u = 1). In addition, GSDs, expected accuracy of maximum vertical position error of UAV results and the directions of change of the slope across the north-south and east-west direction are given for each study area. The Eliktekke study area has the highest RMS value, although it has the lowest expected accuracy of vertical position error. The main reason for this is that the change of the slope across the north-south and east-west direction are very high in the Eliktekke study area. As can be clearly seen here, there is a very large relationship between the slope change and interpolation accuracy. Although the UAV GSD values are 4-5 times higher in the Hamal and Kızılcakent study sites compared to the Eliktekke study area, the interpolation RMS values are much lower. The Hamal and Kızılcakent study areas interpolation RMS values are approximately 2.5 times the expected accuracy of vertical position error values. The slope changes in these two study areas are very similar to each other. The interpolation RMS values are 2.5 times the expected accuracy of vertical position error in the areas where the slope shows little change (between 12-15% for north-south and between 2-5% for east west), while this result is 21 times for the Eliktekke field. While interpolation accuracy is directly related to GSD in areas where the slope shows little variation, this relationship loses its importance in areas with high slope variation (25% for north-south and 18% for east west).

In case the interpolation points are control points, the software determines the most appropriate method according to the smallest value from the RMS obtained according to different power parameter values. For the three study areas, the most appropriate method has been determined for the power parameter values in the range of 1-30 (1,2,3 ... 30). The RMS values obtained after removing outliers are given in Table 5.

Table 5. The most appropriate power parameters and minimum RMS values (after the outliers are removed)

Method	IDW_{std}	Shepard			
		SHP_{std}	SHP_{DD}	SHP_{DD+SD}	The most app*
Study area	RMS (m)	RMS (m)	RMS (m)	RMS (m)	SHP
Ham.	0.32	0.35	0.31	0.28	$_{DD+SD}$
Kızıl.	0.51	0.56	0.52	0.48	$_{DD+SD}$
Elik.	0.81	0.73	0.77	0.72	$_{DD+SD}$

u: The most appropriate power parameters
** It is the approach with the smallest of RMS*

When Table 5 is examined, an improvement is observed in the results when using SHP_{DD+SD} approach, which takes into account the most appropriate power parameter and direction and slope factor in all three study areas. It was observed that the results of SHP_{DD+SD} approach provided 11% improvement in Hamal and Eliktekke study area and 5% in Kızılcakent study area compared to IDW_{std} (u = 2) results.

Table 6. RMS differences of IDW_{std} (u = 1) and SHP_{DD+SD} (u = 1) interpolation methods

Study Area	RMS [m]		RMS Diffences [m]
	IDW_{std} (u=1)	$SHP_{DD+SD\ (u=1)}$	
Hamal	0.363	0.285	0.078
Kızılcakent	0.519	0.484	0.035
Eliktekke	0.846	0.722	0.124

In Table 6, the worst and best results and differences between them are given for the RMS values obtained as a result of interpolation methods. The difference values for the Hamal and Kızılcakent study sites were determined as 7.8 and 3.5 cm, respectively. For these study areas, the expected maximum accuracy of vertical position error is 15.6 and 21.9 cm, respectively. RMS differences are smaller than the expected maximum accuracy of vertical position error values, making the improvement in the average RMS value meaningless in these areas where the slope change is low. However, the mean RMS value of 12.4 cm decreased in the Eliktekke area where the slope change is high. Since the expected maximum accuracy of vertical position error value for this area is 4.2 cm, the improvement in the RMS value of 12.4 cm can be considered as a significant improvement.

In order to more clearly understand the effect of the slope difference and the directional distribution between the interpolation point and reference points on the interpolation results, the points in the area where the directional distribution is disproportionate and the slope difference is higher between the interpolation point and the reference points in the critical circle, a detailed examination was made. For this purpose, firstly, the distribution of reference points falling within the critical circle around the interpolation point was taken into

consideration. For this process, the bearing between the interpolation point and the reference points falling within the critical circle was calculated. Then, according to these bearing angles, it was determined to which region the reference points fell from 4 regions within the geodesic unit circle. Reference point numbers in four different regions were determined and the ratio of the number of reference points per region to the total number of reference points was calculated. Thus, the directional distribution rates of the points for 4 regions were determined. If the directional distribution ratio determined for any region is over 50%, it is thought that there is a disproportionate distribution in the directional distribution between the reference points and the interpolation points. Interpolation points, which have a directional distribution over 50% among all interpolation points, were determined in this way. With the same method, interpolation points with a directional distribution above 60% and 70% were also determined.

After determining the interpolation points whose directional distribution is disproportionate, the slope rates between these interpolation points and reference points were calculated. Interpolation points with a slope value of more than 5%, 10%, 15% and 20%, respectively, were determined and divided into clusters. With these evaluations, the main dataset where the slope difference and directional distribution are not taken into account, three different datasets with only directional distribution above 50%, 60% and 70% regardless of slope difference and finally, with 12 different data sets, with slope differences over 5%, 10%, 15%, 20%, and the directional distribution over 50%, 60% and 70% respectively, a total of 16 data sets were created. Using these datasets, the effect of both the slope difference and the directional distribution for different interpolation methods were examined in detail.

Table 7. RMS values obtained for different slope and directional distribution percentages by using interpolation approaches

Estimation approaches	Power parameters (u)	Slope (%)	**HAMAL** *Directional distribution (%)*				**KIZILCAKENT** *Directional distribution (%)*				**ELİKTEKKE** *Directional distribution (%)*			
			None	*50*	*60*	*70*	*None*	*50*	*60*	*70*	*None*	*50*	*60*	*70*
IDW_{std}	2	*None*	0.321	0.424	0.639	0.530	0.511	0.595	0.517	0.683	0.811	0.853	1.560	1.745
		5	-	0.501	0.654	0.530	-	0.606	0.524	0.707	-	1.251	2.177	2.539
		10	-	0.701	0.755	0.844	-	0.760	0.772	0.819	-	1.478	2.387	2.692
		15	-	0.800	1.061	0.853	-	1.004	1.147	1.329	-	1.645	2.662	3.009
		20	-	1.123	1.267	1.299	-	1.166	1.484	2.172	-	1.706	2.662	3.009
	Optimal	*None*	0.321	0.424	0.444	0.483	0.511	0.595	0.504	0.494	0.808	0.843	1.368	1.643
		5	-	0.501	0.453	0.483	-	0.606	0.511	0.512	-	1.227	2.151	2.443
		10	-	0.639	0.493	0.494	-	0.760	0.672	0.603	-	1.412	2.357	2.589
		15	-	0.783	0.803	0.826	-	1.004	1.137	1.329	-	1.616	2.629	3.133
		20	-	0.922	1.267	1.248	-	1.156	1.484	2.172	-	1.610	2.629	3.133
SHP_{std}	2	*None*	0.380	0.490	0.483	0.537	0.606	0.682	0.590	0.490	0.896	0.991	1.795	1.907
		5	-	0.534	0.494	0.537	-	0.696	0.598	0.508	-	1.204	2.087	2.324
		10	-	0.632	0.705	0.527	-	0.925	0.661	0.840	-	1.332	2.286	2.460
		15	-	0.887	0.822	0.951	-	1.057	0.977	1.419	-	1.718	2.546	2.852
		20	-	0.957	1.484	1.438	-	1.378	1.388	2.243	-	1.474	2.546	2.852
	Optimal	*None*	0.354	0.487	0.447	0.512	0.556	0.627	0.499	0.459	0.731	0.806	1.365	1.279
		5	-	0.530	0.456	0.512	-	0.639	0.505	0.476	-	1.155	1.942	2.237
		10	-	0.632	0.499	0.498	-	0.832	0.661	0.597	-	1.304	2.124	2.366
		15	-	0.849	0.792	0.862	-	1.007	0.977	1.335	-	1.432	2.358	2.738
		20	-	0.957	1.446	1.280	-	1.267	1.354	2.085	-	1.474	2.358	2.738
SHP_{DD}	2	*None*	0.355	0.474	0.470	0.523	0.592	0.665	0.589	0.475	0.901	0.995	1.798	1.909
		5	-	0.516	0.595	0.523	-	0.678	0.597	0.493	-	1.208	2.091	2.327
		10	-	0.648	0.673	0.511	-	0.867	0.648	0.824	-	1.335	2.290	2.463
		15	-	0.861	0.784	0.906	-	1.023	1.074	1.406	-	1.724	2.551	2.857
		20	-	0.916	1.456	1.370	-	1.339	1.345	2.237	-	1.480	2.551	2.857
	Optimal	*None*	0.314	0.450	0.447	0.512	0.517	0.549	0.478	0.417	0.772	0.862	1.365	1.279
		5	-	0.491	0.455	0.512	-	0.581	0.484	0.433	-	1.135	1.926	2.221
		10	-	0.600	0.499	0.498	-	0.781	0.531	0.588	-	1.309	2.106	2.348
		15	-	0.804	0.732	0.799	-	0.951	0.927	1.311	-	1.438	2.340	2.720
		20	-	0.916	1.363	1.184	-	1.196	1.291	2.077	-	1.479	2.340	2.720
SHP_{DD+SD}	2	*None*	0.318	-	-	-	0.514	-	-	-	0.807	-	-	-
		5	-	0.456	0.495	0.446	-	0.600	0.537	0.450	-	1.012	1.927	2.168
		10	-	0.540	0.558	0.584	-	0.775	0.578	0.780	-	1.312	2.108	2.292
		15	-	0.693	0.629	0.721	-	0.934	0.880	1.348	-	1.576	2.347	2.658
		20	-	0.749	1.213	1.034	-	1.164	1.234	2.135	-	1.459	2.347	2.658
	Optimal	*None*	0.285	-	-	-	0.484	-	-	-	0.722	-	-	-
		5	-	0.424	0.372	0.389	-	0.513	0.447	0.416	-	0.999	1.741	2.114
		10	-	0.534	0.558	0.381	-	0.702	0.487	0.499	-	1.139	1.900	2.234
		15	-	0.608	0.629	0.721	-	0.924	0.733	1.288	-	1.218	2.211	2.587
		20	-	0.720	1.173	1.034	-	1.098	1.234	2.048	-	1.275	2.211	2.587

"-"There is no data or approach suitable for this condition.

These 16 data sets were evaluated using, respectively, IDW_{std} (u=2), IDW_{std} (u=optimal), SHP_{std} (u=2), SHP_{std} (u=optimal), SHP_{DD} (u=2), SHP_{DD} (u=optimal), SHP_{DD+SD} (u=2), SHP_{DD+SD} (u=optimal) interpolation approaches with the software developed. RMS values of these evaluation results are given in Table 7 collectively.

When Table 7 is examined, it is seen that the RMS value obtained from the evaluation of all data regardless of the slope and directional distribution data is the smallest values for all methods. Moreover, RMS values increase as slope and directional distribution percentages increase for all methods. As can be seen from here, the increase in slope and directional distribution percentages in all methods increases the RMS value. When directional distribution above 50% with slope differences over 10%, it is observed that the differences in RMS values are greater than the expected maximum accuracy of vertical position error values. This shows that the accuracy of the interpolation method is directly related to the slope and directional distribution of the data set.

To determine the relationship between the accuracy of the IDW based interpolation method and the slope and directional distribution of the data set, the coefficients (p_{nm}) were calculated using the Matlab Curve Tool according to the model given in Eq. 7.

$$RMS = p_{00} + p_{10} * DDR + p_{01} * SR + p_{20} * DDR^2 + p_{11} * DDR * SR + p_{02} * SR^2 + p_{30} * DDR^3 + p_{21} * DDR^2 * SR + p_{12} * DDR * SR^2 \quad (7)$$

It shows n and m: degrees, p_{nm}: coefficients, DDR: directional distribution rate, SR: slope difference and RMS: root mean square in Eq. 8. According to the mathematical model in Eq. 8, p_{nm} coefficients were calculated for each approach. Then, R^2 and RMS values of these modules were calculated to see the consistency of the models created according to Eq. 7 for each approach. Calculated values are given in Table 8.

Table 8. R^2 and RMS values estimated for approaches according to Eq. 7

Estimation approaches	Power parameters (u)	HAMAL		KIZILCAKENT		ELİKTEKKE	
		R^2	RMS (m)	R^2	RMS (m)	R^2	RMS (m)
IDW_{std}	2	0.963	0.081	0.990	0.067	0.994	0.079
	Optimal	0.981	0.059	0.989	0.074	0.987	0.122
SHP_{std}	2	0.967	0.090	0.997	0.037	0.988	0.096
	Optimal	0.961	0.093	0.990	0.067	0.989	0.097
SHP_{DD}	2	0.957	0.098	0.993	0.056	0.988	0.097
	Optimal	0.958	0.088	0.992	0.060	0.989	0.096
SHP_{DD+SD}	2	0.927	0.012	0.998	0.032	0.998	0.037
	Optimal	0.958	0.099	0.992	0.083	0.996	0.063
Mean		0.96	0.08	0.99	0.06	0.990	0.09

When Table 8 is examined, it is seen that the average R^2 values vary between 0.96 - 0.99 and the average RMS values vary between 6 cm and 9 cm. As can be understood from Eq. 7 and Table 8, the accuracy of IDW based interpolation approaches is in a polynomial relation with 3rd degree slope factors and 2nd degree with directional distribution. In Figure 12, polynomial relation and coefficient values calculated for IDW_{std} (u = 2) approach with Matlab Curve Tool are given as examples.

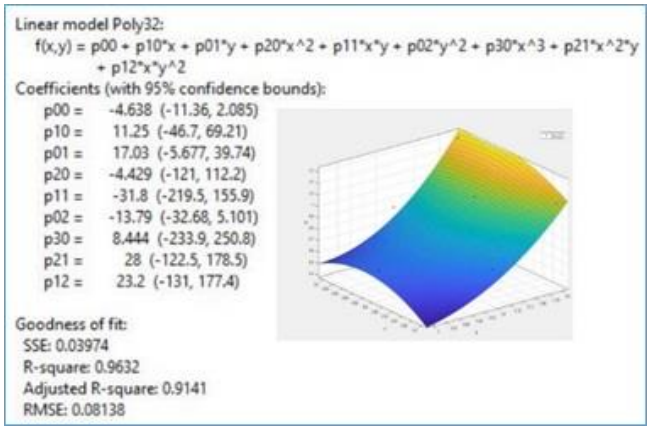

Figure 12. Polynomal relation and coefficient values calculated for the IDW_{std} (u = 2) model with Matlab Curve Tool

At this stage, the following questions arise. Does using the approaches developed by Shepard instead of IDW_{std} (u = 2) method contribute positively to the estimation accuracy? If so, what is this rate? To answer these questions, IDW_{std} (u = 2) estimation results for the same datasets in Table 3 were compared with the estimation results of other Shepard approaches. For this, the improvement rates of the approaches were calculated by using Eq.8. The results are given in Table 6.

$$RIR = \frac{(RMS_{IDW(u=2)} - RMS_{approach})}{RMS_{IDW(u=2)}} \times 100 \quad (8)$$

In Eq. 8, RIR: Result improvement rate, $RMS_{approach}$: root mean square of approaches, $RMS_{IDW(u=2)}$: root mean square of IDW_{std} (u=2) approach.

Table 9 gives the calculated RIR values for the slope differences and directional distribution of three different study area. As can be seen from here, the rate of improvement of the estimation results of the approaches varies between 3% and 22%. The SHP_{DD+SD} (u=optimal) approach gives the highest improvement rates of the estimation results 3-dimensional (Slope Difference - Directional Distribution - Result Improvement Rate) graphs of mean RIR values were drawn to better analyze and visually express improvement rates. In the drawing of the graphics,

firstly a grid network was created then the grid corner values were estimated by linear interpolation method. Graphics created with the help of these values are given in Figure 13.

When Figure 13 is evaluated, it is seen that if the directional distribution is above about 55% for all approaches, an increase in RIR values is observed, on the other hand, if the slope difference exceeds approximately 15%, the increase trend in RIR values turns towards a decrease. However, it was seen that the highest RIR values were obtained from the SHP_{DD+SD} (optimal) approach (Table 9, Figure 13). The mean result improvement rate of SHP_{DD+SD} (optimal) approach is 22%. Sorting of approaches results according to the result improvement rates are SHP_{DD+SD} (optimal), SHP_{DD+SD} (u=2), SHP_{DD} (optimal), SHP_{std} (optimal), IDW_{std} (optimal), SHP_{DD} (u=2), SHP_{std} (u=2).

Table 9. RIR values of approaches

			RIR (%)											
			HAMAL			**KIZILCAKENT**			**ELİKTEKKE**			**MEAN**			
Est. appr.	Pow. par. (u)	Slope (%)	*Directional dist. (%)*			*Directional dist. (%)*			*Directional dist. (%)*			*Directional dist. (%)**			*All***
			50	*60*	*70*	*50*	*60*	*70*	*50*	*60*	*70*	*50*	*60*	*70*	
IDW_{std}	Opt.	*None*	0	31	9	0	3	28	1	12	6	**0**	**15**	**14**	
		5	0	31	9	0	2	28	2	1	4	**1**	**11**	**13**	
		10	9	35	41	0	13	26	4	1	4	**4**	**16**	**24**	**7**
		15	2	24	3	0	1	0	2	1	-4	**1**	**9**	**0**	
		20	18	0	4	1	0	0	6	1	-4	**8**	**0**	**0**	
SHP_{std}	2	*None*	-16	24	-1	-15	-14	28	-16	-15	-9	**-15**	**-2**	**6**	
		5	-7	24	-1	-15	-14	28	4	4	8	**-6**	**5**	**12**	
		10	10	7	38	-22	14	-3	10	4	9	**-1**	**8**	**15**	**3**
		15	-11	23	-11	-5	15	-7	-4	4	5	**-7**	**14**	**-4**	
		20	15	-17	-11	-18	6	-3	14	4	5	**3**	**-2**	**-3**	
	Opt.	*None*	-15	30	3	-5	3	33	6	13	27	**-5**	**15**	**21**	
		5	-6	30	3	-5	4	33	8	11	12	**-1**	**15**	**16**	
		10	10	34	41	-9	14	27	12	11	12	**4**	**20**	**27**	**10**
		15	-6	25	-1	0	15	0	13	11	9	**2**	**17**	**2**	
		20	15	-14	1	-9	9	4	14	11	9	**7**	**2**	**5**	
SHP_{DD}	2	*None*	-12	26	1	-12	-14	30	-17	-15	-9	**-13**	**-1**	**7**	
		5	-3	9	1	-12	-14	30	3	4	8	**-4**	**0**	**13**	
		10	8	11	39	-14	16	-1	10	4	9	**1**	**10**	**16**	**4**
		15	-8	26	-6	-2	6	-6	-5	4	5	**-5**	**12**	**-2**	
		20	18	-15	-5	-15	9	-3	13	4	5	**6**	**0**	**-1**	
	Opt.	*None*	-6	30	3	8	8	39	-1	13	27	**0**	**17**	**23**	
		5	2	30	3	4	8	39	9	12	13	**5**	**17**	**18**	
		10	14	34	41	-3	31	28	11	12	13	**8**	**26**	**27**	**13**
		15	-1	31	6	5	19	1	13	12	10	**6**	**21**	**6**	
		20	18	-8	9	-3	13	4	13	12	10	**10**	**6**	**8**	
SHP_{DD+SD}	2	*None*	-	-	-	-	-	-	-	-	-	-	-	-	
		5	9	24	16	1	-2	36	19	11	15	**10**	**11**	**22**	
		10	23	26	31	-2	25	5	11	12	15	**11**	**21**	**17**	**14**
		15	13	41	15	7	23	-1	4	12	12	**8**	**25**	**9**	
		20	33	4	20	0	17	2	14	12	12	**16**	**11**	**11**	
	Opt.	*None*	-	-	-	-	-	-	-	-	-	-	-	-	
		5	15	43	27	15	15	41	20	20	17	**17**	**26**	**28**	
		10	24	26	55	8	37	39	23	20	17	**18**	**28**	**37**	**22**
		15	24	41	15	8	36	3	26	17	14	**19**	**31**	**11**	
		20	36	7	20	6	17	6	25	17	14	**22**	**14**	**13**	

** Mean of result improvement rates for all three study areas.*

*** Mean of result improvement rates for each interpolation approaches.*

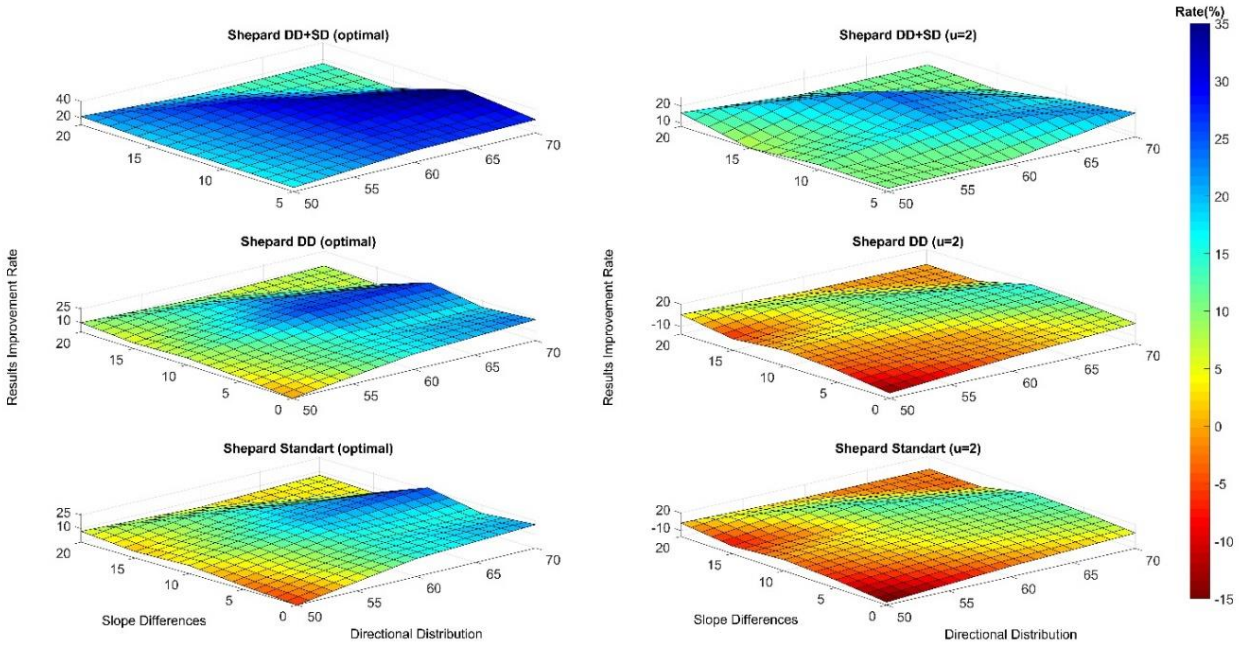

Figure 13. Three dimensional (Slope Difference, Directional Distribution, Result Improvement Rate) graphs for mean RIR values

4. RESULTS

The following results were obtained for interpolation approaches in this study conducted in three different study areas. In the IDW_{std} method, it has been seen that using different power parameters for each study site increases the estimation accuracy. The interpolation accuracy of the SHP_{std} approach, where the direction and slope factors are not taken into account, is lower than the IDW_{std} approach. The accuracy of the interpolation results obtained from the SHP_{DD} approach, taking into account the directional distribution, is slightly improved compared to the SHP_{std} approach, but a noticeable improvement cannot be achieved compared to the IDW_{std} method. In the SHP_{DD+SD} (u=2) approach estimation results there was no significant improvement (<5 mm) compared to the results of the IDW_{std} approach. The interpolation accuracy is improved when using "u = 1" instead of "u =2" used in the literature for Shepard method in our study sites. In the Shepard method, which uses the slope change between the reference points and the directional distribution of the reference points in the weight calculation, if the interpolation is performed by determining the most appropriate power parameter (SHP_{DD+SD} (u: optimal) approach), the results show an improvement between 5% and 11% according to the IDW_{std} (u=2) method. When all approaches are taken together, it is observed that in areas where slope differences between reference points increase, result improvement rates for SHP_{DD+SD} (u: optimal) approach improve proportionally with slope difference. For the accuracy of all IDW-based interpolation approaches used in this study was found a polynomial relationship with 2nd degree with directional distribution and 3rd degree with slope factors. For all the approaches used in the study, an increase in RIR values is observed if the directional distribution is above 55%, besides this if the slope difference rises above about 15%, the increase trend in RIR values turned towards a decrease. The best RIR value was obtained as 22% with SHP_{DD+SD} (u: optimal) approach.

5. CONCLUSION AND DISCUSSION

Today, IDW method is used by many software. These software's use the standard IDW method, which takes the power parameter "2" for ease of calculation. Shepard approaches are not used by existing software. Using the software developed in this study, it was researched whether Shepard approaches provide an advantage over standard IDW method. The developed software can determine the most suitable inverse distance weight interpolation approach for each study area. The developed software is a first in terms of determining the most suitable inverse distance weight interpolation approach as well as calculating IDW approaches (IDW_{std} and Shepard) according to different power parameters. Using this software, interpolations can be performed according to various IDW for the study areas. Thanks to this software, when the number of points falling within the critical circle falls below 4 in the Shepard approaches, the software automatically determines at least 4 reference points closest to the interpolation point from the reference point set and performs the interpolation process. In addition, while the power parameter is used as "2" standard in the Shepard approaches in the literature, calculations can be made by determining the most suitable power parameter for the study region in the developed software.

In order to test the success of the above-mentioned inverse distance weighted interpolation methods for UAV point clouds, tests were carried out in three different fields in this study. In the developed software, point cloud data produced by UAV photogrammetry belonging to three different study areas were used. By comparing the known height values with the estimated

height values of the interpolation points, the reliability of the software algorithm developed with the accuracy of the interpolation methods was tested. These tests have shown that using a suitable power parameter in the study area instead of using a fixed power parameter in IDW approaches will increase the DEM estimation accuracy. However, in cases where the directional distribution is over 55% and the slope difference does not exceed 15%, the results improved between 11% and 37% using the SHP_{DD+SD} (optimal) approach compared to the IDW_{std} (u = 2) method.

The results pointed out above show that using models that take into account field slope and directional distributions of reference points in IDW based interpolations will increase accuracy.

ACKNOWLEDMENT

We would like to thank GEOMINE R & D Company for providing software and hardware support for this study. In this study, MATLAB software licensed by Sivas Cumhuriyet University was used.

Author contributions

Kemal Özgür Hastaoğlu: Conceptualization, Methodology, Software development. Statistical analysis. **Sinan Göğsu:** Data curation, Software development, Statistical analysis Writing-Original draft preparation. **Yavuz Gül:** Data curation, Visualization, Statistical analysis, Writing-Reviewing and Editing.

Conflicts of interest

The authors declare no conflicts of interest.

REFERENCES

Agüera-Vega F, Agüera-Puntas M, Mancini F, Martínez-Carricondo P & Carvajal-Ramírez F (2019). Effects of Structure from Motion Data density, interpolation method and grid size on micro topography Digital Terrain Model accuracy. Preprints doi: 10.20944/preprints 201908.0283.v1.

Arun P V (2013). A comparative analysis of different DEM interpolation methods. The Egyptian Journal of Remote Sensing and Space Science, 16(2), 133-139.

Bater C W & Coops N C (2009). Evaluating error associated with lidar-derived DEM interpolation. Computers & Geosciences, 35(2), 289-300.

Brimicombe A (2009). GIS, environmental modeling and engineering. CRC Press

Chen F W & Liu C W (2012). Estimation of the spatial rainfall distribution using inverse distance weighting (IDW) in the middle of Taiwan. Paddy and Water Environment, 10(3), 209-222.

Das M, Hazra A, Sarkar A, Bhattacharya S & Banik P (2017). Comparison of spatial interpolation methods for estimation of weekly rainfall in West Bengal, India. Mausam, 68(1), 41-50.

Envir. Sys. Res. Inst.: How IDW Works (2020). https://desktop.arcgis.com/en/arcmap/10.3/tools/3d-analyst-toolbox/how-idw-orks.htm . Accessed 04 February 2020

Ferreira I O, Rodrigues D D, Santos G R D, & Rosa L M F (2017). In bathymetric surfaces: IDW or Kriging? Boletim de Ciências Geodésicas, 23(3), 493-508.

Guo Q, Li W, Yu H & Alvarez O (2010). Effects of topographic variability and lidar sampling density on several DEM interpolation methods. Photogrammetric Engineering & Remote Sensing, 76(6), 701-712.

Graham A N, Coops N C, Tompalski P, Plowright A & Wilcox M (2020). Effect of ground surface interpolation methods on the accuracy of forest attribute modelling using unmanned aerial systems-based digital aerial photogrammetry. International Journal of Remote Sensing, 41(9), 3287-3306.

Habib A, Khoshelham K, Akdim N, Labbassi K & Menenti M (2018). Impact of spatial resolution, interpolation and filtering algorithms on DEM accuracy for geomorphometric research: a case study from Sahel-Doukkala, Morocco. Modeling Earth Systems and Environment, 4(4), 1537-1554.

Ikechukwu M N, Ebinne E, Idorenyin U & Raphael N I (2017). Accuracy assessment and comparative analysis of IDW, spline and kriging in spatial interpolation of landform (Topography): An experimental study. Journal of Geographic Information System, 9(03), 354.

Ismail Z, Abdul Khanan M F, Omar F Z, Abdul Rahman M Z & Mohd Salleh M R (2016). EVALUATING ERROR OF LIDAR DERIVED DEM INTERPOLATION FOR VEGETATION AREA. International Archives of the Photogrammetry, Remote Sensing & Spatial Information Sciences, 42.

Liao Y, Li D & Zhang N, 2018." Comparison of interpolation models for estimating heavy metals in soils under various spatial characteristics and sampling methods". Transactions in GIS, 22(2), 409-434.

Lu G Y & Wong D W (2008). An adaptive inverse-distance weighting spatial interpolation technique. Computers & geosciences, 34(9), 1044-1055.

Meng Y, Cave M & Zhang C (2019). Comparison of methods for addressing the point-to-area data transformation to make data suitable for environmental, health and socio-economic studies. Science of The Total Environment, 689, 797-807.

Michael S (2020). GRASS Development Team: GRASS GIS 7.6.2 dev Reference Manual. https://grass.osgeo.org/grass76/manuals/v.surf.idw.html. Accessed 04 February 2020

Mohamed K S, Sajikumar K K, Ragesh N, Ambrose T V, Jayasankar J, Said Koya K P & Sasikumar G (2018). Relating abundance of purpleback flying squid Sthenoteuthis oualaniensis (Cephalopoda: Ommastrephidae) to environmental parameters using GIS and GAM in south-eastern Arabian Sea. Journal of Natural History, 52(29-30), 1869-1882.

Paul R, Brindha K, Gowrisankar G, Tan M L & Singh M K (2019). Identification of hydrogeochemical processes controlling groundwater quality in Tripura, Northeast India using evaluation indices, GIS, and multivariate statistical methods. Environmental Earth Sciences, 78(15), 1-16.

Sarkar S, Parihar S M & Dutta A (2016). Fuzzy risk assessment modelling of East Kolkata Wetland Area: A remote sensing and GIS based approach. Environmental modelling & software, 75, 105-118.

Setianto A S & Triandini T T (2013). Comparison of kriging and inverse distance weighted (IDW) interpolation methods in lineament extraction and analysis. Journal of Southeast Asian Applied Geology, 5(1), 21-29.

Shepard D (1968). A two-dimensional interpolation function for irregularly-spaced data. In Proceedings of the 1968 23rd ACM national conference (pp. 517-524).

Stafford JV (2013) Precision agriculture'13. Wageningen Academic Publishers

Tran Q B & Nguyen T T (2008). Assessment of the influence of interpolation techniques on the accuracy of digital elevation model. VNU Journal of Science. Earth Sciences 24, 176-183.

Wang G & Huang L (2012). 3D geological modeling for mineral resource assessment of the Tongshan Cu deposit, Heilongjiang Province, China. Geoscience Frontiers, 3(4), 483-491.

Welch M C, Kwan P W & Sajeev A S M (2014). Applying GIS and high-performance agent-based simulation for managing an Old-World Screwworm fly invasion of Australia. Acta tropica, 138, 82-93.

Wu C Y, Mossa J, Mao L & Almulla M (2019). Comparison of different spatial interpolation methods for historical hydrographic data of the lowermost Mississippi River. Annals of GIS, 25(2), 133-151.

Zhou M, Guan H, Li C, Teng G & Ma L (2017). An improved IDW method for linear array 3D imaging sensor. In 2017 IEEE International Geoscience and Remote Sensing Symposium (IGARSS) (pp. 3397-3400). IEEE.

Url-1 <https://support.PIX4d.com/hc/en-us/articles/202558889-Accuracy-of-PIX4Doutputs >, date of access: 2020

International Journal of Engineering and Geosciences
https://dergipark.org.tr/en/pub/ijeg
e-ISSN 2548-0960

Multithreaded wedge detection method on triangular 3D CAD objects using mesh traversal method

Özkan Kırık*[1], Caner Özdemir[1]

[1]*Mersin University, Engineering Faculty, Department of Electrical-Electronics Engineering, Mersin, Turkey*

Keywords
Wedge Detection
Triangular Mesh
CAD
Mesh Traversal

ABSTRACT

In this study, a multithreaded method for triangular mesh three-dimensional computer aided design objects is proposed to detect and extract wedges. Wedge detection is time consuming process for such objects that have large number of facets. To take the advantage of parallel computing opportunities, the algorithm is refactored in this study. Scope of variables, memory management and stack use are optimized for efficient use of computational resources. The proposed method is focused to calculation efficiency and performance on multicore / multithreaded processors and it is evaluated with benchmark, complex and realistic objects.

1. INTRODUCTION

Computer aided design (CAD) objects are widely used in nearly all engineering fields. Triangular mesh modelling is used mostly due to its simplicity and efficiency (Kim et al. 2009). Triangular meshes consist of Cartesian coordinates of points called vertices and collection of triangle corner vertices called facets. Wavefront obj file format is preferred for storing triangular mesh data (Possemiers and Lee 2015). File format of the wavefront obj is shown in Figure.1. For vertex definition, the line should start with a letter "v" and three numbers separated by spaces are x, y, and z Cartesian coordinates respectively should be followed. Afterwards, three-dimensional (3D) facet definition lines are listed with a letter "f" and followed by 3 vertex indexes delimited with a space character. It should be further noticed that the order of vertex indexes is important for calculating surface normal direction. The wavefront obj definition shown in Fig.1, constructs a 2D plate that its center is at origin and has a dimension of 15 x 15. The unit is not stored in wavefront obj file.

Wedge outline of a triangular mesh is a very important feature that used by many calculation techniques such as ray traversal diffraction and physical theory of diffraction methods (Kirik and Ozdemir 2019; Griesser and Balanis 1987; Pyotr 2014). Calculation of wedges of CAD object is a time and processor consuming process for objects that have large number of facets (Kuo et al. 2009; Sun et al. 2002; Wang et al. 2012; Zhang et al. 2003).

```
# Vertex Definitions
v 0.000000 7.500000 -7.500000
v 0.000000 -7.500000 -7.500000
v 0.000000 -7.500000 7.500000
v 0.000000 7.500000 7.500000

# Facet Definitions
f 2 1 4
f 3 4 2
```

Figure 1. Wavefront obj file format

Parallel computation is an important opportunity that provides efficient use of computational resources. Modern central processing units (CPU) have many cores within single package that provides many computational resources even for personal use.

The purpose of this study is to detect wedges of triangular mesh CAD models using parallel computation techniques. Other techniques are using sequential scan principles which is a single threaded operation for detecting wedges. For this paper, 4 benchmark and 2 complex objects' wedge detection is performed using the purposed method.

* **Corresponding Author**

*(ozkan@mersin.edu.tr) ORCID ID 0000-0002-6996-6239
(cozdemir@mersin.edu.tr) ORCID ID 0000-0003-2615-4203

Cite this article

Kirik O & Ozdemir C (2022). Multithreaded wedge detection method on triangular 3D CAD objects using mesh traversal method. International Journal of Engineering and Geosciences, 7(2), 174-178

Research Article / DOI: 10.26833/ijeg.947235 **Received: 03/06/2021; Accepted: 25/06/2021**

2. METHOD

Since the conventional solutions are single threaded, multithreaded mesh traversal is needed and implemented throughout this study.

2.1. Single threaded traversal of triangular mesh

Fully closed 3D CAD models defines a volume. But open-3D CAD models defines a surface instead of volume. Therefore, object wedge detection process was studied within the next two subsections: wedge detection for volumes and wedge detection for surfaces.

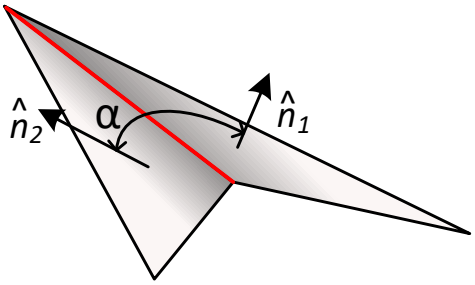

Figure 2. Neighboring triangular facets normal vectors and definition of wedge angle

The α angle shown in Fig. 2 between normal vectors of two neighboring facets which are sharing same edge is called the wedge angle. The α angle defines an important information about sharpness of edge. When the α value is 0 °, the facets are located on the same plane.

2.1.1. Wedge detection approach for volumes

The implementation of deciding whether two triangular facet contains a wedge or nor is given below:

i. Read three vertex indexes of the triangular facet from the CAD file,
ii. Find intersections of these two selected facets' members.
iii. If the intersections result;
   a. contain three elements then the facets are basically the same. The second facet should be removed for simplicity.
   b. contain two elements then the facets are neighbors.
   c. else continue to the next iteration till the end of file.

Found neighborhoods between facets should be checked if the angle between the facet normal vectors is larger than a user-defined threshold value. This threshold value can be changed from application to application. For electromagnetic solvers that uses edges/wedges for diffraction calculations; for instance, the wedge angle usually taken at least 30° since diffraction coefficients do not contribute significant energy to the total scattered field if the wedge angle is smaller than this value (Kirik and Ozdemir 2019; Griesser and Balanis 1987). If the angle is greater than this user-defined value, the intersection is decided to be a wedge so that an edge line should be calculated that is to be used in the selected application.

2.1.2. Wedge detection approach for surfaces

In addition of 3D volumetric wedge detection problem, there is also a need to find the edges for two-dimensional (2D) surfaces. This is because of the fact that some CAD file definitions have outside of surfaces that do not have any neighboring facets such as wing and air-flaps that are constituted of 2D plates. For example, an 2D plate triangular mesh like shown in Fig. 2, the most outsite rectangle edges represent surface wedges which don't have any neighbor facets.

Both of the volume and surface wedge detection approach used together in numerical examples section.

2.2. Multicore / Multithreaded Traversal

Instead of sequentially scanning of collection of facets, the methods described at section 2.1.1 and 2.1.2 are implemented as scalable to multicore and multithreaded computing architectures.

Scalable architecture, depends on worker threads that created at the startup step. The number of worker threads are decided according to the number of available hardware resources. The started worker threads, polls tasks from job queue. Spinlock mechanism is also used to prevent race conditions (Crummey and Scott 1991).

3. NUMERICAL EXAMPLES

The above method was implemented in Microsoft .NET framework with C# language. Both sequential mesh traversal and multithreaded mesh traversal was implemented.

Numerical experiments are accomplished against four benchmark and two complex 3D triangular meshes listed in Table 1. Each facet represents a triangle that consists of 3 vertices. The minimum wedge angle is selected as 30° in all experiments.

Table 1. Numerical experiments for wedge detection

Type	CAD	Vertices	Facet Count	Wedges Found
Benchmark	2D Plate	4	2	4
Benchmark	Dihedral	6	4	7
Benchmark	Cube	24	12	12
Benchmark	Cone-sphere	802	1600	0
Complex	Backhoe Loader	4618	9387	5850
Complex	T72M1 Tank	69042	137384	32659

3.1. Benchmark Object #1: 2D Plate

To examine the purposed method for a surface and validate the detected wedges, a 2D plate object chosen as the first example.

The 2D plate object's dimensions are 15cm x 15cm. Center of the 2D plate shown in Fig. 2 is aligned to be centered at the origin of (0,0,0). As listed in Table.1, this benchmark object consists of 4 vertices and 2 facets.

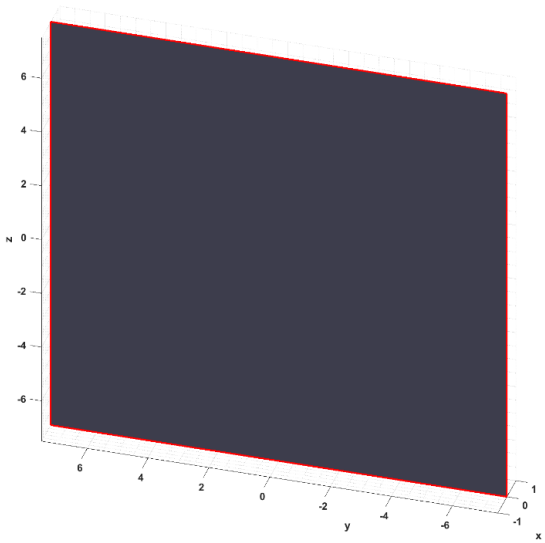

Figure 3. Wedge Detection Result for 2D Plate Object

Result of the method is shown in Fig. 3 with four red lines. Only outside of the rectangle is red colored as expected. The diagonal line that corresponding the neighboring line between the triangular facet is not red colored because the angle between their surface normals is equal to 0° which is not greater than the threshold value of 30°. Execution times are measured as 0.053 ms for the sequential mesh traversal calculation and 0.292 ms for the multithreaded mesh traversal calculation.

3.2. Benchmark Object #2: Dihedral Corner Reflector

As another benchmark object a Dihedral corner reflector model is chosen for the different assessment. This object is built to be a Wavefront obj file with six vertices and four facets in total.

As shown in Fig. 4, the corner edge is highlighted with red color in addition to perimeter of the rectangles as expected. Execution times are measured as 0.075 ms for the sequential mesh traversal and 0.292 ms for the multithreaded mesh traversal as listed in Table 2.

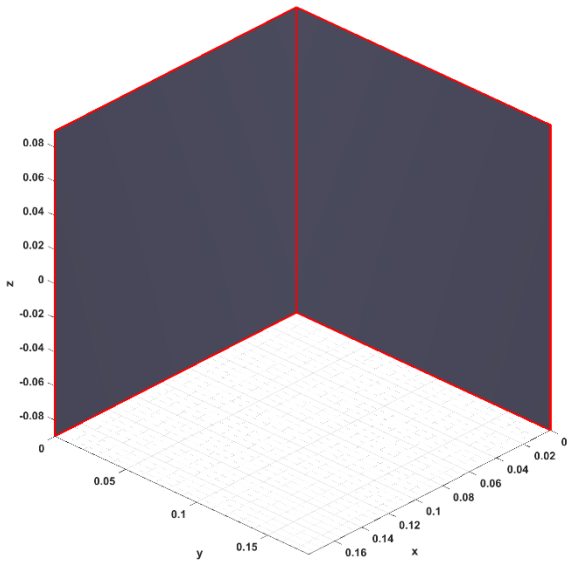

Figure 4. Wedge Detection Result for Dihedral Corner Reflector Object

3.3. Benchmark Object #3: Cube

Another benchmark target is selected to be a cube that has the dimension of 16 cm x 16 cm x 16 cm as shown in Fig. 5. It is aligned to be centered at the origin of the coordinate system. This target is used to validate the volume wedge detection of a closed 3D triangular mesh. This particular triangular mesh contains twenty-four vertices and twelve facets.

After applying the proposed approach given above, the total number of detected wedges is found to be twelve as shown in Table.1 which is the correct result. Execution times of the algorithms are measured as 0.083 ms for the sequential mesh traversal process and 0.295 ms for the multithreaded mesh traversal process as listed in Table 1.

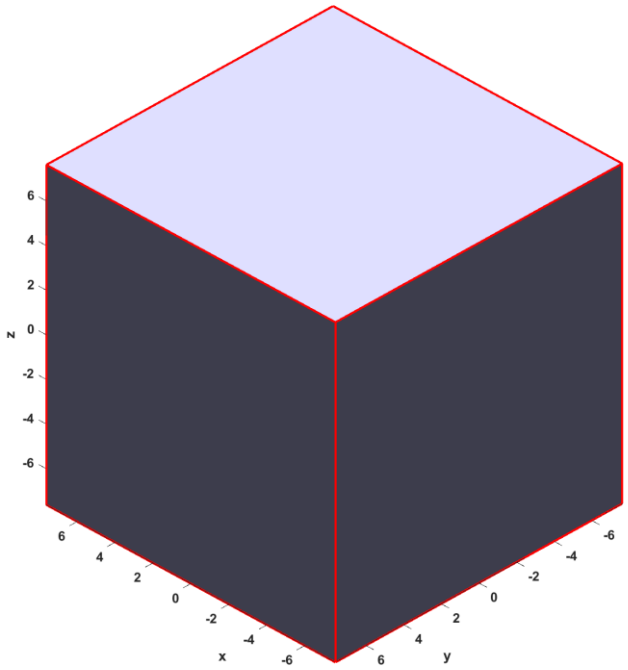

Figure 5. Wedge Detection Result for Cube Object

3.4. Benchmark Object #4: Cone-sphere

Cone-sphere benchmark target has no neighbor facets which exceeds the angle threshold. So this experiment is also important to validate the correctness of the proposed wedge detection method. The cone-sphere structure shown in Fig. 6 with the half-sphere part with a radius of 74 mm and the cone part with the height of 605 mm (Griesser et al. 1989).

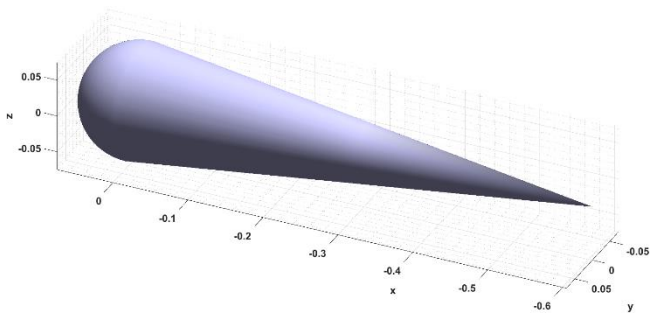

Figure 6. Cone-sphere Object Wedge Detection Result

After applying the proposed method, there is no detection of wedges listed at the end as expected. Therefore, we see no red lines or curves in Fig. 6. Run times for this particular object are measured as 329 ms for the sequential mesh traversal calculation and 115 ms for the multithreaded mesh traversal calculation.

3.5. Complex Object #1: Backhoe Loader

To implement the proposed method on a more realistic complex-shaped object, a Backhoe loader model is chosen whose CAD file can be viewed in Fig. 7. This wavefront obj CAD model has a detailed design that is constituted via 4618 vertices and 9387 facets. The dimensions of the target are 6.33 m (length), 1.99 m (width) and 2.33 m (height) (Demirci et al. 2020).

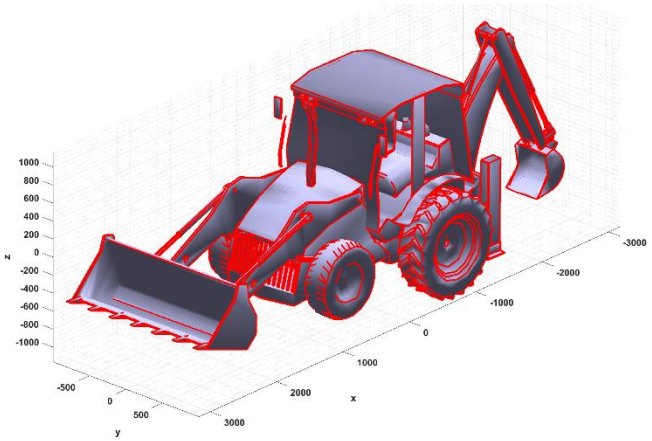

Figure 7. Wedge Detection Result of Backhoe Loader Object

After applying the proposed wedge detection algorithm to this complex object, a total of 5850 different wedges are detected. As can be fairly seen from Fig. 7, all the joint and sharp lines are found and highlighted with good fidelity. Execution times are measured as 4.007 s for the sequential mesh traversal process and 1.33 s for the multithreaded mesh traversal process.

3.6. Complex Object #2: T72M1 Tank

For the last example, a much more complex object that is a tank model is chosen to comprehend the effectiveness of the proposed method. The CAD model of T72M1 tank is depicted in Fig. 8. This triangular mesh model is highly detailed and complex such that a total of 137384 facets are used to form the structure (Demirci et al. 2020). The size of this tank model is 10.4 m in length, 3.74 m in width and 2.76 m in height. It is no doubt that this model is much more complex when compared to previous backhoe loader object.

After applying the proposed wedge detection method, the wedges are extracted perfectly as there are pointed out red lines in Fig. 8. The total execution times are measured as 1439 s for the sequential mesh traversal calculation and 501 s for the multithreaded mesh traversal calculation.

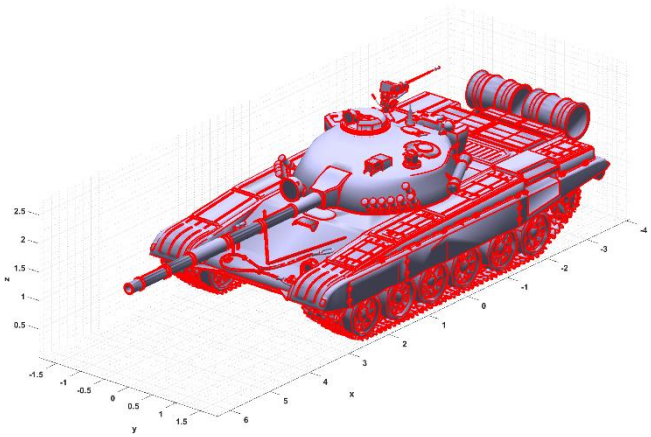

Figure 8. T72M1 Tank Object Wedge Detection Result

Table 2. Execution Times of the Conducted Experiments

Experiment	Facet Count	Seq. Trav. Time	Multi Thr. Trav. Time	Speed-up Ratio
2D Plate	2	53 ns	292 ns	0,18x
Dihedral	4	75 ns	292 ns	0,25x
Cube	12	83 ns	295 ns	0,28x
Cone-sphere	1600	329 ms	115 ms	2,86x
Backhoe Loader	9387	4 s	1.33 s	3,01x
T72M1 Tank	137384	1439 s	501 s	2,87x

4. CONCLUSION

In this study, we have presented an assessment of multithreaded wedge detection method that can be applied universally to any triangularly meshed CAD object from benchmark CAD models to complex-shaped models. The first four experiments, applied to benchmark objects, have been utilized to validate the base functionality of both surface and volume wedge detection approached. Then, much more complex objects were chosen to assess the availability and the effectiveness of the proposed method.

Execution times of all experiments are listed in Table 2. In fact, the mesh traversal process has the order of N^2 complexity. So the execution time increases quadratic manner by total number of facets, N. In the multithreaded mesh traversal method, the main goal is to decrease the execution time of the process by the use of parallel computing opportunity. On the other hand, the main drawback of this method is the initialization cost that independent from the number of facets. The initialization cost of multithreaded applications has the order of N complexity. It is also important to mention that it also depends on number threads to start as expected.

The multithreaded execution times of the 2D plate, the dihedral corner reflector and the cube objects are almost the same although total number of facets are different. This is because the thread initialization cost is the same for all these three experiments. Sequentially mesh traversal is much faster than multithreaded mesh traversal when the facet count of object is relatively very small. As a solution, usage of multithreaded traversal should be decided according to facet count of object. A good speed-up values have been achieved using this method for large and complex-shaped triangular meshed models as obvious from Table 2.

ACKNOWLEDMENT

This work was supported in part by the Mersin University Scientific Research Unit under Grant 2015-TP3-1160.

Author contributions

Barnali Das: Conceptualization, Methodology, Analysis, Mapping, Compilation, Writing-Original draft and its preparation. **Anargha Dhorde:** Visualization, Checking draft and Editing.

Conflicts of interest

The work is original and authors declare no conflicts of interest.

REFERENCES

Crummey J M, Scott M L (1991). Algorithms for scalable synchronization on shared-memory multiprocessors. ACM Transactions on Computer Systems, 9(1), 21–65.

Demirci S, Kirik O, Ozdemir C (2020). Interpretation and Analysis of Target Scattering from Fully-Polarized ISAR Images Using Pauli Decomposition Scheme for Target Recognition. IEEE Access, 8, 155926-155938.

Griesser T, Balanis C A (1987). Backscatter analysis of dihedral corner reflectors using physical optics and the physical theory of diffraction. IEEE Transactions on Antennas and Propagation, 35(10), 1137-1147.

Griesser T, Balanis C A, Liu K (1989). RCS analysis and reduction for lossy dihedral corner reflectors. Proceedings of the IEEE, 77(5), 806-814.

Kim H S, Choi H K, Lee H K (2009). Feature detection of triangular meshes based on tensor voting theory. Computer-Aided Design, 41(1), 47-58.

Kirik O, Ozdemir C (2019). An Accurate and Effective Implementation of Physical Theory of Diffraction to The Shooting and Bouncing Ray Method via Predics Tool. Sigma Journal of Engineering and Natural Sciences, 4, 1153-1166.

Kuo Ct, Cheng Sc, Wu Dc, Chang Cc (2009). A Blind Robust Watermarking Scheme for 3D Triangular Mesh Models Using 3D Edge Vertex Detection. Asian Journal of Health and Information Sciences, 4(1), 36-63.

Possemiers A L, Lee I (2015). Fast OBJ file importing and parsing in CUDA. Computational Visual Media, 1, 229-238.

Pyotr Ya. Ufimtsev (2014) Fundamentals of the Physical Theory of Diffraction, Second Edition. John Wiley & Sons. ISBN: 9781118753668

Sun Y, Page D L, Paik J K, Koschan A, Abidi M A (2002). Triangle mesh-based edge detection and its application to surface segmentation and adaptive surface smoothing. International Conference on Image Processing, 825-828 vol.3, Newyork, USA.

Wang Xc, Cao Jj, Liu Xp. (2012). Feature detection of triangular meshes via neighbor supporting. Journal of Zhejiang University Science C, 13, 440–451.

Zhang X, Zhou M, Geng G (2003). A Method of Detecting the Edge of Triangular Mesh Surface. China Knowledge Network (CNKI) China Academic Journal.

International Journal of Engineering and Geosciences
https://dergipark.org.tr/en/pub/ijeg
e-ISSN 2548-0960

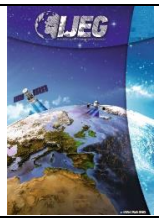

Evaluating bank erosion and identifying possible anthropogenic causative factors of Kirtankhola River in Barishal, Bangladesh: an integrated GIS and Remote Sensing approaches

Shaikh Ashikur Rahman [*1], **Md. Muzahidul Islam**[1], **Md. Abdullah Salman**[1], **Muhammad Risalat Rafiq**[1]

[1]*University of Barishal, Department of Geology and Mining, Barishal, Bangladesh*

Keywords
Remote sensing
Riverbank erosion
Anthropogenic factors
Meandering
GIS

ABSTRACT

In Bangladesh, riverbank erosion has turned into one of the most frequently occurring natural disasters, and it affects the socio-economic and livelihood status as well as the environment of the adjoining areas. Kirtankhola River in Barishal, is this kind of river. This study assesses the amount of erosion-accretion, examines river profile, detecting key anthropogenic factors behind it, and signifying channel shifting of the river within 10 years (from 2009 to 2019). The study used Landsat Satellite imageries, geospatial techniques, and a semi-structured questionnaire survey throughout the study area. The study showed that erosion dominants at the left bank of river (17.1 ha/year), whereas the accretion rate is higher at the right (19.72 ha/year). Besides, cross-section at selected points of the river providing an evident indication of the river widening thus river course shifting. According to 61% of the participants in the questionnaire, high waves generated through water vehicles are the main culprit for this extensive erosion. The number of launches has increased significantly within the studied time-period, and most of the launches run over 30 km/h velocity, where it should be less than 20km/h. The study explored a mechanism of how centrifugal force produced by water vehicles increases the intensity of riverbank erosion in the meandering area.

1. INTRODUCTION

River is one of the most common geomorphological features in Bangladesh. Here, almost seven percent of the total land is covered by rivers (Hasan et al. 2018). The livelihood of the local people of the country vastly depends on these rivers (Khan et al. 2014). Therefore, the rivers are a blessing for the people of Bangladesh; however, this blessing often turns into a curse when it comes to bank erosion. In Bangladesh no other natural disaster is as devastating as riverbank erosion (Khan et al. 2014). Around one million inhabitants are losing their home per year and even they have to leave their village due to large-scale bank erosion (Mahmud et al. 2020). This frequently happening bank erosion takes tolls less in lives but more responsible for the immense quantity of land consumption, demography dislocation, and landlessness (Rabbi et al. 2013). Though the shifting of river courses is a natural phenomenon, it becomes a disaster when considered from the perspective of human settlements. Even though bank erosion is mostly controlled by morphological structure, vegetation cover, bending of the channel, and discharge water (Mazumdar and Talukdar 2018). Kirtankhola River is a distributary of the Mighty Meghna. Sustainability and development of the Barishal Sadar is often threatened by intensive bank erosion. This phenomenon has been acute in recent years. Since 2009, it has already consumed about 320 hectares of land in the study area and a huge amount of land is at high risk. The Barishal City is located on the bank of the Kritankhola River, which flows through the Active Ganges Delta where the uppermost section consists of recently deposited Holocene sediments (Umitsu 1993). Because of unconsolidated recent deltaic sediments, the banks of the Kirtankhola River are highly vulnerable to

* **Corresponding Author**

*(sk.ashikur@gmail.com) ORCID ID 0000-0002-3003-2738
(muzahid031@gmail.com) ORCID ID 0000-0003-0260-3449
(masalman@bu.ac.bd) ORCID ID 0000-0001-8637-5388
(mrrafiq@bu.ac.bd) ORCID ID 0000-0001-8837-8312

Cite this article

Rahman S A, Islam Md M, Salman Md A & Rafiq M R (2022). Evaluating bank erosion and identifying possible anthropogenic causative factors of Kirtankhola River in Barishal, Bangladesh: an integrated GIS and Remote Sensing approaches. International Journal of Engineering and Geosciences, 7(2), 179-190

Research Article / DOI: 10.26833/ijeg.947493

Received: 03/06/2021; Accepted: 03/08/2021

bank consumption (Hasan et al. 2018). High instream siltation is also accelerating the bank erosion activity (Hohensinner et al. 2018). Anthropogenic factors sometimes have more influence in particular areas (Nahar 2015).

From the perspective of Barishal, Kirtankhola plays a crucial role in the transportation system connecting Barishal to different parts of Bangladesh through waterways. The second-largest inland river port is on the bank of it. Every day, numerous cargoes, launches, and speed boats run through the river. Those vehicles produce large hydraulic waves continuously. Nanson et al. (1994); Oswalt and Strauser (1983) postulated that boat-induced waves play an important role to erode river bank. Except on very large-scale rivers, boat-generated waves have notably greater influence than wind waves (Nanson et al. 1994). The meandering shape of the river in the selected study area is responsible for the excessive centrifugal force of boat-generated hydraulic waves which then hammer on the cut bank of the river. Regular hitting by waves upon the unprotected banks is facilitating bank erosion. Moreover, cutting down trees for making settlements and sand extraction for the landfill as well as soil excavation for brickfields are also increasing the intensity of bank consumption. Local communities are usually dependent on this river for their livelihood. Rigorous bank erosion in Kirtankhola disappearing roads, schools, houses, croplands, and rural markets. On the other hand, accreted land is not being well distributed among depreciated people. Along with this, poor navigability of the river is also disrupting the busiest river traffic system.

Previous studies had been conducted mostly on bank migration and subsequent socio-economic impacts due to riverbank erosion of major rivers in Bangladesh (Mahmud et al. 2020; Billah 2018; Hasan et al. 2018; Hassan and Akhtaruzzaman 2010; Islam and Rashid 1970; Nahar 2015). A few studies had been carried out on the Kirtankhola River, however, most of these concentrated on the flow pattern and velocity distribution according to the depth as well as geotechnical analysis (Hasan et al. 2018; Ahmed and Afrin 2016). Nevertheless, none of these studies incorporated anthropogenic factors particularly strong centrifugal forces induced by robust hydraulic waves propagated by a wide range of vessels which are accelerating severe bank erosion in the Kirtankhola River.

All over the world, different methods are used for assessing riverbank erosion (Mazumdar and Talukdar 2018), quantifying erosion (Sarkar et al. 2012), and identifying causative factors of erosion (Thakur et al. 2012). However, all those techniques are costly, time-consuming, and sometimes difficult to do properly rather than using new GIS and RS methods (Mahmud et al. 2020 and Salman et al. 2018). Most of the GIS and RS methods are easy to perform and cost-efficient and receiving great interest in recent times (Joshi et al. 2002). An NDWI method has been performed to depict river channel shifting within the selected time period. Surfer software has been used to identify the changes of channel shape. An unstructured questionnaire survey was conducted in the villages along both sides of Kirtankhola and identified three unions, Charmonai, Charbaria and Charkawa respectively upstream to downstream, where bank erosion is prominent. Secondary data acquired from satellite images, government websites, journals, news articles, and books. The primary objectives of this study are (1) calculating the total erosion and accretion as well as rates over the study period (2) identifying the potential anthropogenic key factors (3) delineating the most vulnerable points in terms of bank consumption (4) illustrating the elevation profiles as well as overall cross-section changes of the river and (5) demonstrating the channel movement in the study area.

2. STUDY AREA

The Kirtankhola is a meandering river; the local socio-economy, as well as the transportation system, predominantly depend on it. So the river is a lifeline of Barishal district. The river originates from Arial Khan River near Shayestabad and ends in Gajalia near Gabkhan channel. The total length of the river is about 160 km (DoE 2016). The maximum width between the banks of the river is 800 m (approx.) near Char Upen whereas 300 m is the minimum width near Barishal launch terminal as well as depth variation of Kirtankhola approximately 26 m to 9 m in the thalweg (Ahmed and Afrin 2016). This study was carried out at three unions of Barishal Sadar Upazila; Charkawa, Charbaria, and Charmonai (Fig. 1). The study area falls between 22°41’ and 22°45’ north latitudes and between 90°22’ and 90°27’ east longitudes (Fig. 1). The study area shows plane topography where the bank soil of the Kirtankhola River is mostly medium to fine-grained sand along with coarse to fine-grained sand and a small amount of silt and clay (Hasan et al. 2018). The Kirtankhola riverbank contains loosely compacted sandy soils with high moisture content and less cohesiveness (Hasan et al. 2018). This area is also highly influenced by the daily semi-diurnal tide. During the dry season, the tidal variation was about 1.5 m whereas 0.5 m in the wet season, 2 m/s was the maximum velocity of the river as well (Ahmed and Afrin 2016). The variation of discharge during the high-water flow was about 4000 m^3/s and during low water flow it was 3000 m^3/s (Ahmed and Afrin 2016).

3. MATERIALS AND METHODS

3.1. Data Used

Comprehensive literature reviews were carried out at every stage of this study. Secondary data was collected from different scientific journals, articles, websites, newspapers, textbooks, satellite images, etc. The images of Landsat 4-5 TM C1 Level-1 of 2009 and Landsat 8 OLI/TIRS C1 Level-1 of 2019 were taken from USGS Earth Explorer (Table 1). Time series data of 10 years of the study area were collected from Google Earth Pro. Elevation profiles and two cross-sections were illustrated by Surfer 13 software. Arc GIS 10.4 Software was used for identifying amount of bank consumption as well as river shifting.

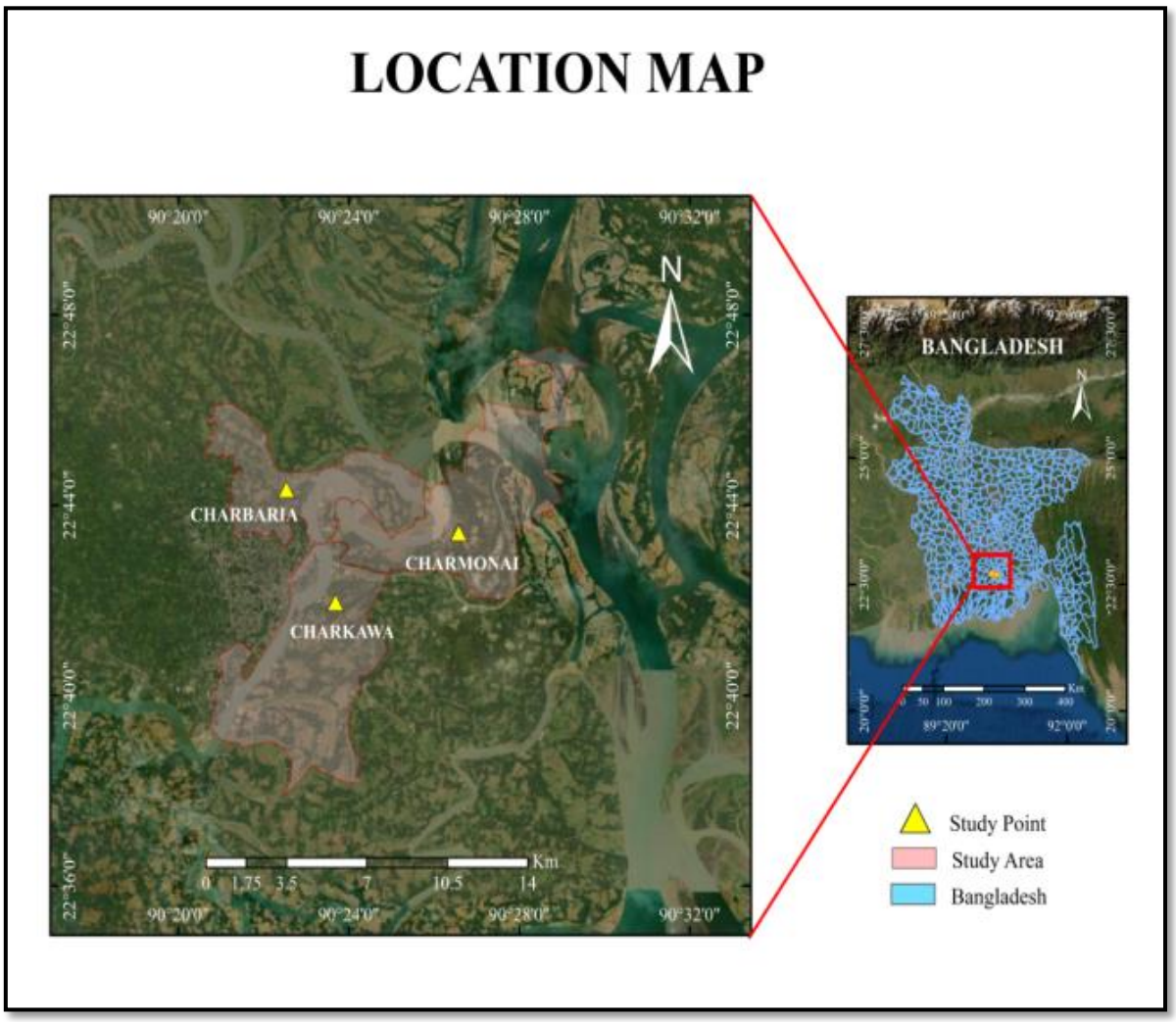

Figure 1. The study was carried out at three unions of Barishal Sadar Upazila; Charbaria, Charmonai, and Charkawa

Table 1. Landsat satellite images used for this study purposes

Satellite/ Sensor	Spatial Resolution(m)/Row/Path	Date of Acquisition	Spectral Bands (μm)	Data Source
Landsat-8 (OLI/TIRS)	30/45/136	23/11/2019	B3 (Green): 0.53-0.59 B5 (NIR): 0.85-0.88	https://earthexplorer.usgs.gov/
Landsat-5 (TM)	30/45/136	26/10/2009	B2 (Green): 0.52-0.60 B3 (NIR): 0.77-0.90	

3.2. Satellite Images and GPS Data Analysis

Current data about the number of active launch routes, the number of running steamers, and waterbus in Barishal were collected from different news reports and "www.barisal.govt.bd" website. Google Earth Pro software was also used to compare the number of steamers and boats in Barishal Launch terminal jetty between 2009 and 2019. A GERMIN eTrex-20 GPS device was used to obtain the average velocity data of running launches, waterbuses, and speed boats, etc., and made a data table contained the maximum and average velocity, total travel time, traveling distance, the name of the routes as well as investigated passenger ships (Table 2). Total of 15 launches and speed boats were investigated to collect data.

3.3. Field Survey

The study area was selected based on news reports, scientific articles as well as in situ observation of the affected area. Most significantly, the questionnaire was made in artless and explicit way so that the participants and volunteers could easily understand. A semi-structured questionnaire survey was based on finding the real scenarios of the natural and anthropogenic causes of bank erosion as well as the status of local people migration. Total fifty respondents were collected from local people who are more or less affected by riverbank erosion. All participants independently expressed their point of view about the potential man-made and natural factors which are responsible for the disastrous bank erosion at their unions. Samples were collected randomly aiming so that outcomes become more vigorous. Finally, the most vulnerable points in the study area were picked up according to this field survey.

Table 2. Name of the route and investigated steamers/launches running along Kirtankhola River in 2019, distance from Barishal, travel time, and maximum and average velocity of those launches and speed boats.

SL	Name of Route	Name of Launch	Total Distance (Km)	Travel Time (Hour)	Maximum Velocity of Launch/Boat	Average Velocity of Launch
1	Dhaka-Barishal	M.V Suravi-9	161	6 hours 45 minutes	32.17 Km/h	23.85 Km/h
2	Dhaka-Barishal	M.V Sundarban-10	161	6 hours 52 minutes	32.65 Km/h	23.40 Km/h
3	Dhaka-Barishal	M.V Parabat-11	161	7 hours 15 minutes	29.08 Km/h	22.21 Km/h
4	Dhaka-Barishal	M.V Kirtankhola-2	161	7 hours	29.90 Km/h	23 Km/h
5	Dhaka-Barishal	M.V Kirtankhola-10	161	6 hours 35 minutes	33.27 Km/h	24.47 Km/h
6	Dhaka-Barishal	Adventure-9	161	6 hours 28 minutes	37.12 Km/h	24.88 Km/h
7	Dhaka-Barishal	M.V Green Line-2	161	5 hours 21 minutes	41.51 Km/h	30.08 Km/h
8	Dhaka-Barishal	M.V Green Line-3	161	5 hours 15 minutes	43.30 Km/h	30.67 Km/h
9	Dhaka-Barishal	M.V Manami	161	6 hours 46 minutes	34.80 Km/h	23.78 Km/h
10	Dhaka-Barishal	M.V Kuakata-2	161	6 hours 40 minutes	35.10 Km/h	24.17 Km/h
11	Barishal-Ilisha	M.V Supersonic-5	46.78	4 hours 12 minutes	16.33 km/h	11.61 Km/h
12	Barishal-Hizla	M.V Inzam	37.35	3 hours 8 minutes	15.92 Km/h	11.93 Km/h
13	Barishal-Bhola (Veduria ghat)	M.V Awlad Express	23.60	2 hours 35 minutes	14.25 Km/h	9.53 Km/h
14	Barishal-Bhola (Veduria ghat)	Local Speed Boat	23.60	40 minutes	44.21 km/h	35.76 Km/h
15	Barishal-Bhola (Veduria ghat)	Local Speed Boat	23.60	45 minutes	39.65 Km/h	31.47 Km/h

3.4. Evaluation of Erosion and Accretion

The measurement of lost land and newly formed land from 2009 to 2019 was done separately for the two different banks (Table 3). River bank lines of two selected year were drawn and then the movement was detected in kml file format. Where the recent bank line entered through the past line that means erosion and where it comes away means accretion. Erosion and accretion amount was determined precisely. With the help of conversion tools of GIS, kml file was converted into a layer and a map was produced. Finally, an erosion-accretion diagram was delineated (Fig. 2).

3.5. Channel Migration, River Flow Pattern and Cross-section

River channel migration was identified by analyzing satellite images. The study used Landsat satellite images 4-5 TM C1 Level-1 and Landsat 8 OLI/TIRS C1 Level-1. Arc GIS 10.4 was used to make an unsupervised classification of the target area which depicted the river flow pattern. Surfer 13 software was used to draw river cross-sections through an illustration of the elevation profiles at selected points. This drawing process involves several steps. Firstly, geographic coordinate data of each point was collected by Google Earth Pro software in kml file format. Total six set of data was gathered from the study area. Every point has two data set, one is from 2009 and another contains data from the year of 2019. Secondly, the altitude values of these sites were updated by using GPS Visualizer and converted into GPX format. Further, these GPX files were processed and converted into CSV format by TCX and Microsoft Excel Office 2016 software. Finally, these data were plotted into Surfer 13 software to delineate contour maps as well as elevation profiles of each site (Fig. 3).

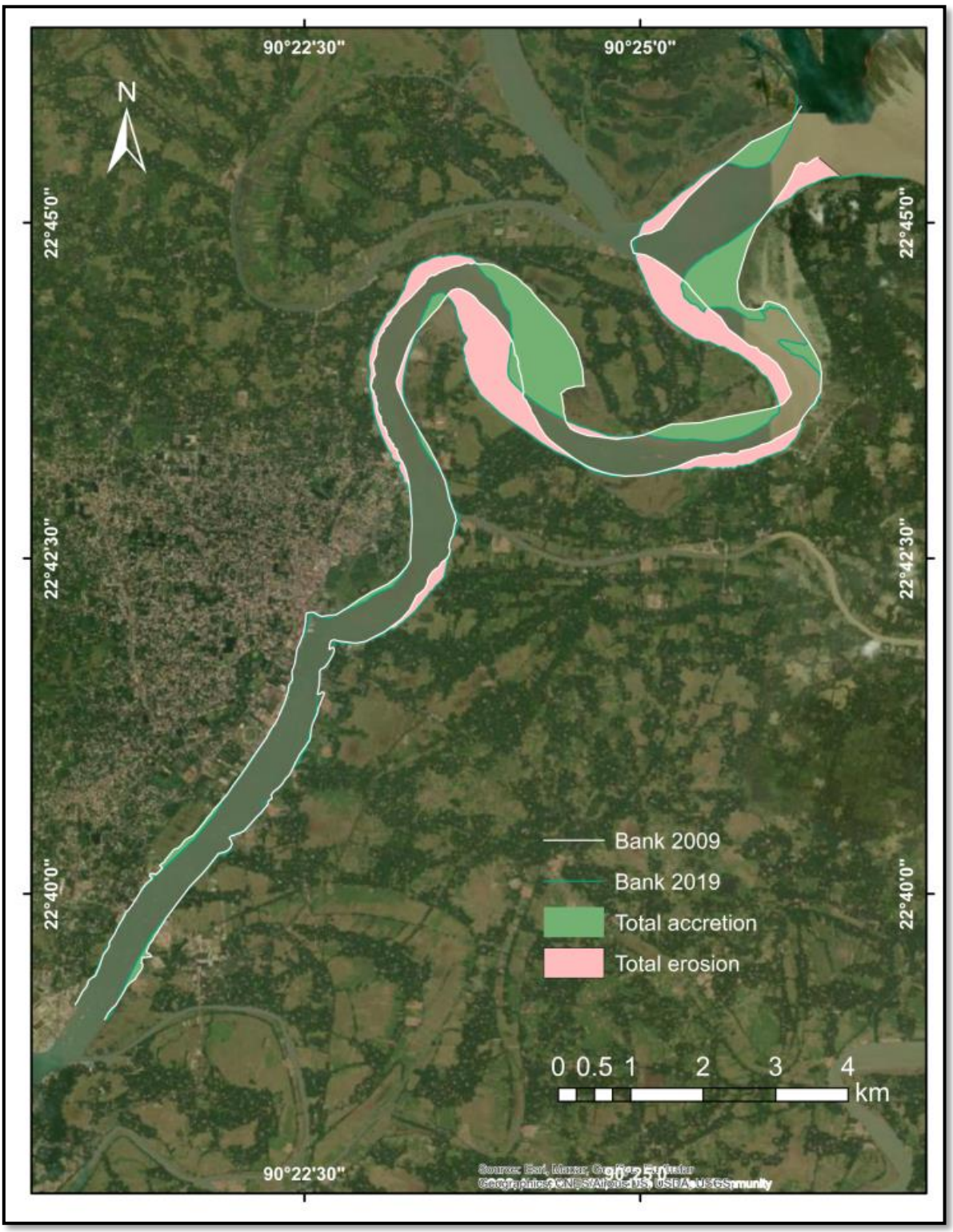

Figure 2. Map illustrates the amount of bank erosion and accretion of Kirtankhola River in the study area from 2009 to 2019

Table 3. Net erosion and accretion statistics of the Kirtankhola River, Barishal

Time Duration (year)	Location (Kirtankhola River)	Erosion (ha)	Erosion Rate (ha/year)	Accretion (ha)	Accretion Rate (ha/year)
2009-2019	Right bank	147.73	14.774	197.22	19.72
	Left bank	171.05	17.1	89.8	8.98
	Total reach	318.78	31.878	287.02	28.7

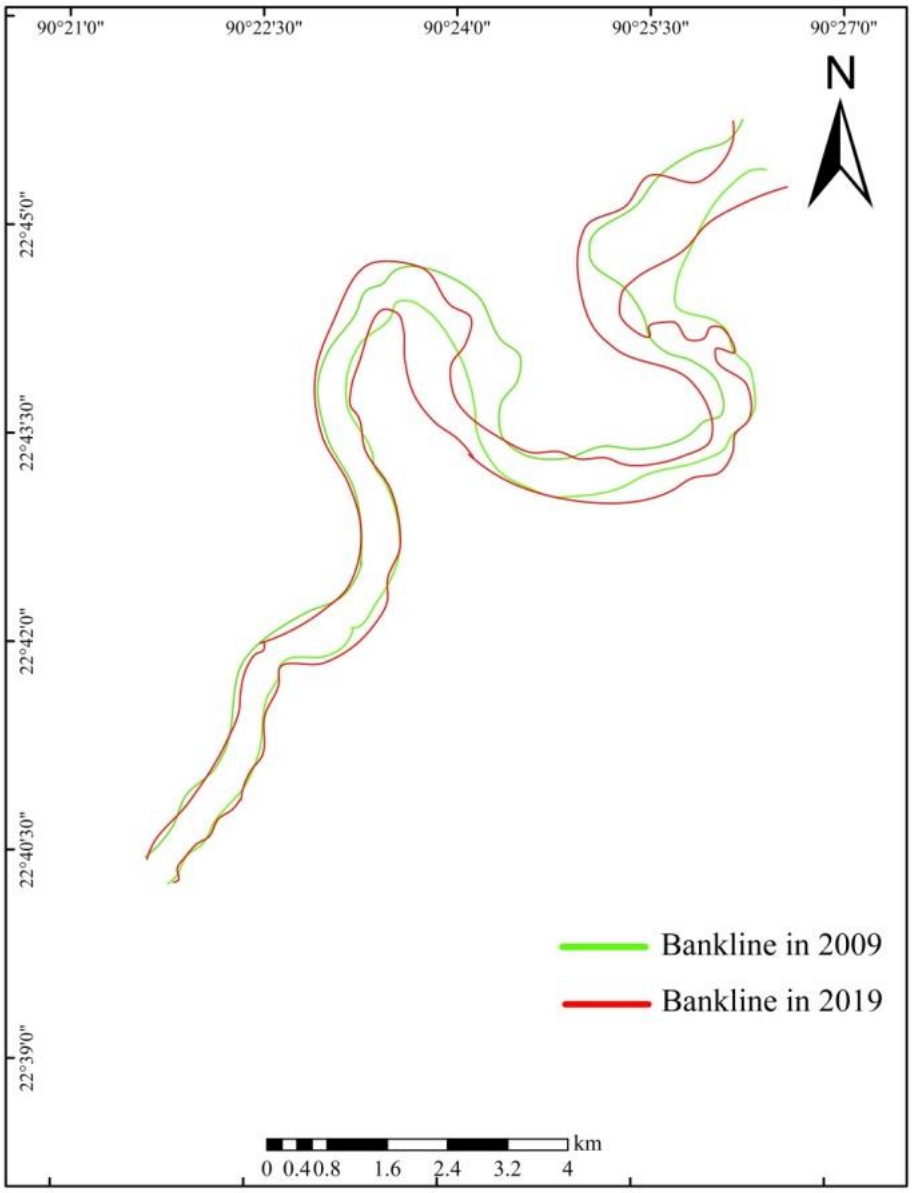

Figure 3. Diagram represents channel shifting over the study period, the red line representing the bank line in 2019 and green line is the bank line in 2009.

3.6. Normalize Difference Water Index (NDWI)

The satellite images of 26 October 2009 and 23 November 2019 were processed to visualize the riverbank erosion. Normalize Difference Water Index (NDWI) map was created to make a comparison of riverbank line of two different images. However, in this study, NDWI is used to differentiate the water body, vegetation, and open land in the study area.
This following formula has been used to make the NDWI map:

$$NDWI = \frac{GREEN-NIR}{GREEN+NIR}$$

NDWI values in between -1 to 1 indicate water body because of higher reflectance of NIR band than G band whereas, negative NDWI values indicate vegetation.

4. RESULTS AND DISCUSSION

4.1 Morphological Changes of Kirtankhola River

The amount of erosion and accretion in the study area from 2009 to 2019 was 318.78 hectare and 287.02 hectares respectively (Table 2). The river was eroding at a rate of 31.676 (ha/year) and accreting at 28.70 (ha/year). However, erosion was severe at the left bank but accretion was far more at the right. At the right bank, erosion was 147.73 hectare, whereas accretion was 197.22 hectare so the net gain of land was 49.49 hectare. In contrast, at the left bank, erosion was 171.05 hectare and accretion was 89.8 hectare so the net land loss was 81.25 hectare. Finally, the study showed that the overall erosion and the rate of erosion was more dominant than accretion and the rate of accretion and in terms of vulnerability, the left bank is more in danger (Fig. 2).

Riverbank migration map (Fig. 3) illustrates the bank line movement from 2009 to 2019. This lateral movement is pronounced in the study area shown in Fig. 3. The river had been widening at the meandering zone adjoining to Chaekawa, Charbaria, and Charmonai unions due to tremendous bank consumption. This map also depicts how much of both banks of Kirtankhola are shifting throughout 10 years (Fig. 3). The shape of the Kirtankhola was being changed due to extensive erosion along with sediment deposition in the study area.

It is obvious from the comparison maps given in Fig. 4. Riverbank erosion was pronounced at investigated sites. A huge amount of land had already disappeared by the river and specifically the area adjacent to meander strongly affected by bank erosion (Fig. 4). Not only landform but also the difference of vegetation amount had been identified clearly from the comparison maps. At Charkawa point, erosion was prominent at the left bank, whereas accretion was occurred mainly at right bank (Fig. 4a,b). At the left, it can be seen that river has migrated to the land and a significant change of vegetation also visible. Finally, the river in 2019 at Charkawa was wider than in 2009 (Fig. 4;a,b).

Similarly, at Charbaria point a clear view of large-scale erosion and accretion was shown (Fig. 4;c,d). The left bank which is the point bar had squeezed and turned into one-third of 2009. In contrast, the right bank had cut across the land area about 200 m. Significantly, a new land area is also visible at the right bank (Fig. 4;c,d).

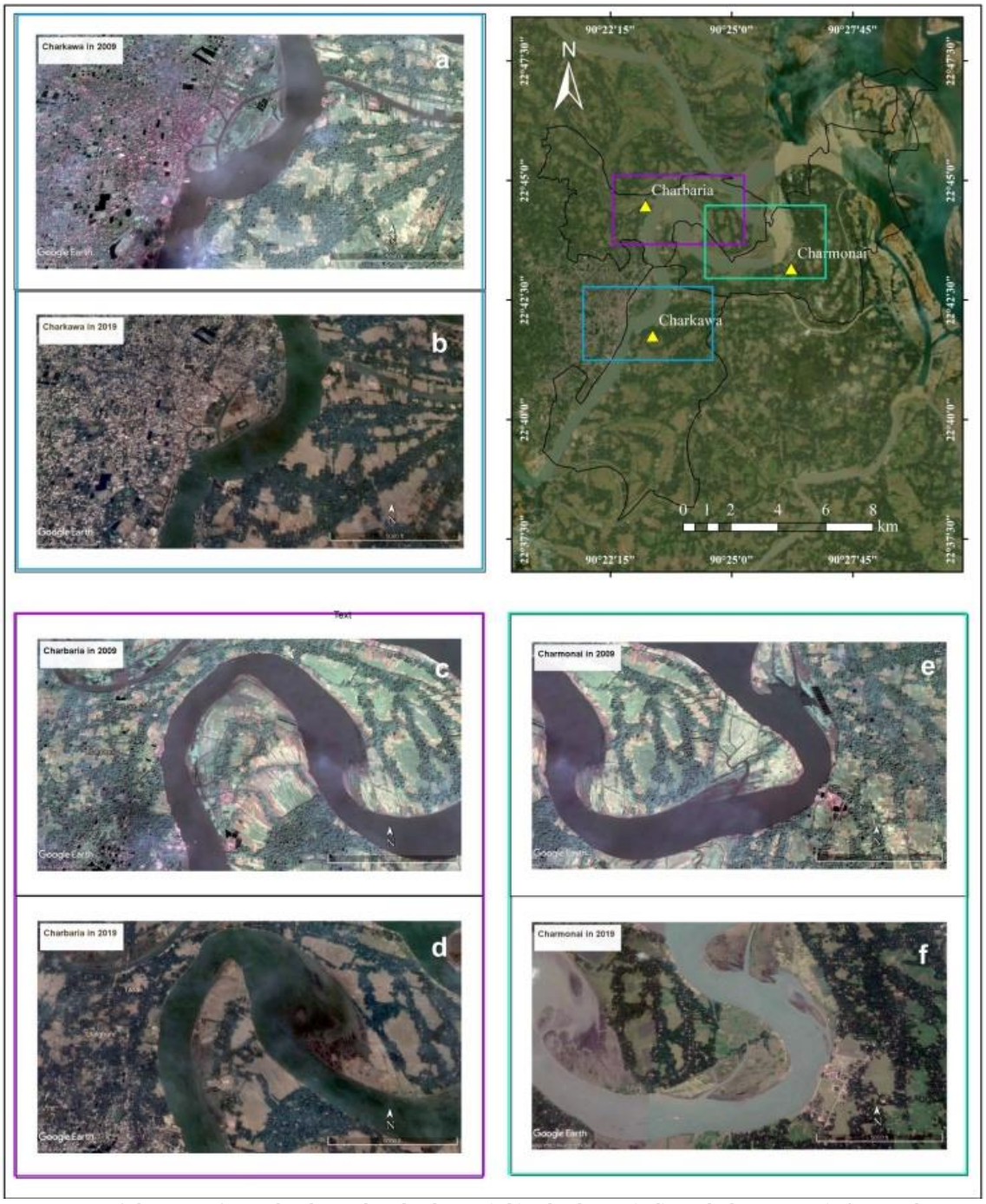

Figure 4. Comparison of changes of river banks at the Charkawa (a,b), Charbaria (c,d), and Charmonai (e,f) point between 2009 and 2019

At Charmonai point, the most change visible at the right bank of the river where mostly accretion was occurred (Fig. 4; e, f). The amount of erosion is respectively less. However, the left bank is considerably constant. Neither noticeable erosion nor accretion was visible at the left side.

The normalize difference water index (NDWI) maps were depicted the distinction of Kirtankhola river water body migration, the amount of vegetation and open land areas between 2009 and 2019 (Fig. 5). From the maps, it is obvious that the water body area of the Kirtankhola River has been increasing due to severe bank erosion at Charbaria, Charmonai, but comparatively less increased at the Charkawa. On the other hand, open land has been increasing due to deforestation as well as sediment accumulation at point bars and some particular places along the river bank notably at Charmonai and Charbaria but at Charkawa union newly formed areas are relatively lower than the first two.

Elevation profile maps show the cross-sectional difference of the Kirtankhola River at Charkawa section (Fig. 6a, b). Here, the cut bank of the river cross-section at the right-hand side in elevation profile map is showing the bank slope is being steeper with time. Cut bank slope at the left side of Kirtankhola was comparatively gentle in 2009 than in 2019. In 2019, the river bed has become relatively wider than in 2009. Consequently, riverbank erosion is gradually changing the shape of the bank lines as well as the river bed of the Kirtankhola at Charkawa like the rest of the sections.

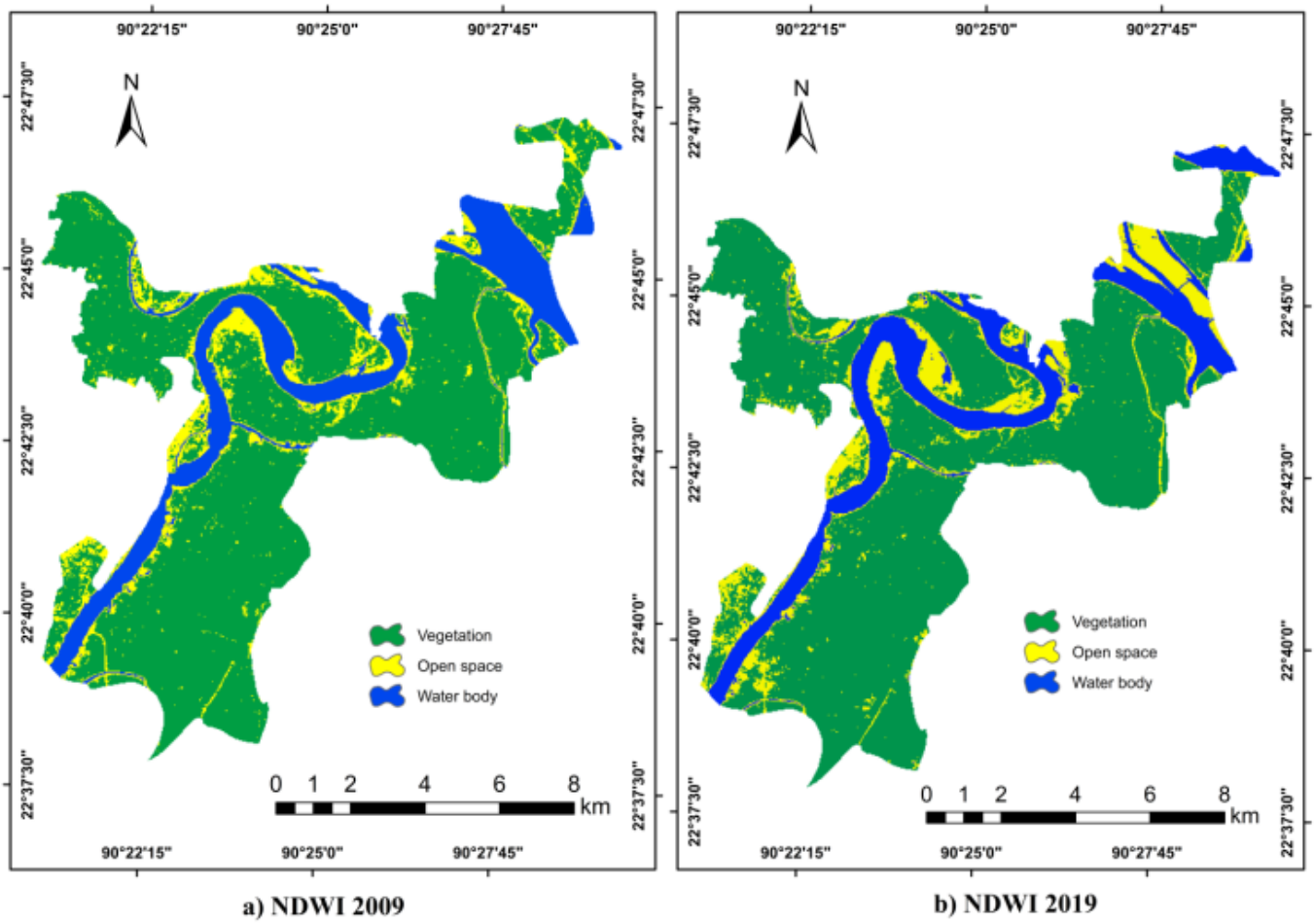

Figure 5. Normalize Difference Water Index (NDWI) Maps (a) NDWI in 2009 (b) NDWI in 2019. Map shows the difference of landforms,vegetation, and open land area at Charbaria, Charkawa and Charmonai respectively

Likewise, the elevation profile maps demonstrate the transformation of the cross-section at the Charbaria section (Fig. 6;c,d). Here in the contour maps, the blue occupied area indicates the water body. The red circled area in the contour map indicating the river cross-section. Significant change is identifiable from the elevation profile maps where in 2009 the cross-section was almost V-shaped and the cut bank at the right side had relatively less flat river bed, but in 2019 the river cross-section at a similar point is wider and flattered. The U-shaped channel indicates that, the river has become wider at this point due to bank erosion.

The change of cross-section of Kirtankhola River at Charmonai section is clearly identifiable in (Fig. 6; e, f). The river bed has become U-shaped in 2019 and the cut bank slope of the river at the left side has become steeper than 2009. In 2009 at the same point river cross-section was V-shaped. Elevation map at Charmonai also indicates the right bank or point bar has become more steady-state due to sediment deposition (Fig. 6; e, f). So, the change of shape of the cross-section and bank slope indicates the horrific riverbank erosion at the Charmonai section.

4.2 Questionnaire Survey

The questionnaire survey shows that about 61% of local affected people opined that boat generated waves are the anthropogenic key factor that triggered bank erosion in the study area, about 15% of them commented deforestation is the key factor. Besides, around 13% and 11% of people believed that excessive sand extractions, as well as river mismanagement, are the man-made key factor that facilitated bank erosion.

Meanwhile, the bar diagram is demonstrating the number of displacements of the respondents in their life so far due to acute bank erosion (Fig. 7). Forty respondents out of 50 had experienced migration more than once and two of them had to shift 7 times. The 6, 5 and 4 respondents retreated 4, 5, and 6 times respectively owing to bank erosion (Fig. 8).

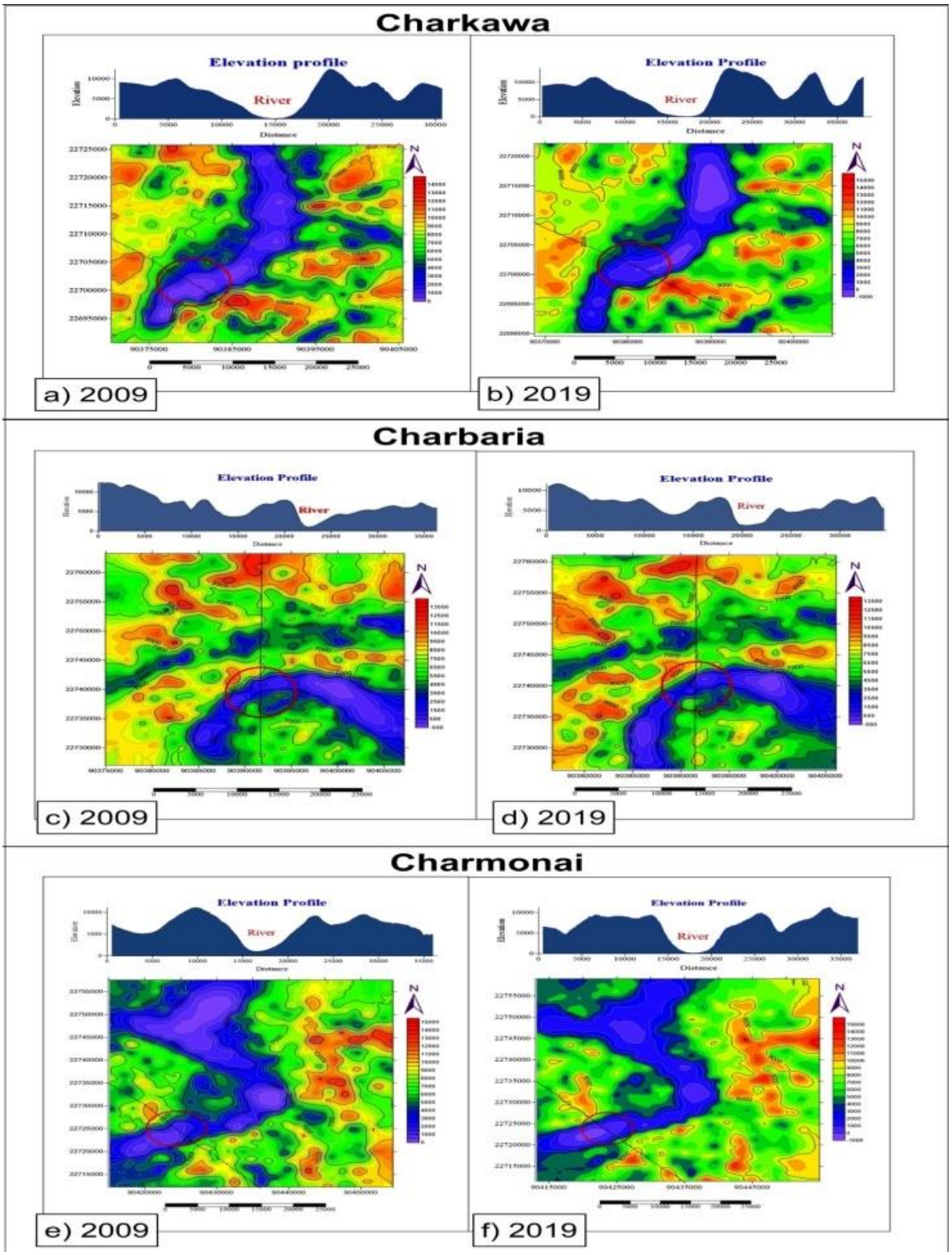

Figure 6. Comparative Elevation Profile at Charkawa (a) cross-section in 2009 (b) cross-section in 2019. Comparative Elevation Profile at Charbaria (c) cross-section in 2009 (d) cross-section in 2019. Comparative Elevation Profile at Charmonai (e) cross-section in 2009 (f) cross-section in 2019 of Kirtankhola river.

4.3 Factor Accelerating Bank Consumption

Kirtankhola is a meandering river and there are three meanders in our study area. Every union contains one of them. The cut banks at Charkawa,Charbaria, and Charmonai sections are often displaced due to boat-induced strong water waves. Powerful centrifugal forces are formed when a launch or water bus cross the meander (Fig. 9). As meander is a semicircular path along with the velocity of the running boat, the circle radius deduces the formula of centrifugal force formulated by Newton.

The formula of centrifugal force is:

$$F = m\omega^2 r$$

The centrifugal force is denoted by F, m is the mass of the rotating object, ω is the angular velocity of the moving object and r is the distance from the center of the circle.

Hence, the centrifugal force is proportional to the mass of the object, square of angular velocity, and radius or distance from the origin. Centrifugal force is zero at the origin where r = 0. At meander or the edge of the circle, the r-value could be reached up to the maximum. When a launch or speed boat passing through a semicircular meander with high velocity, it forms a mighty centrifugal force that results from powerful hydraulic waves that hit repeatedly and forcefully on the banks of the river and facilitate bank erosion.

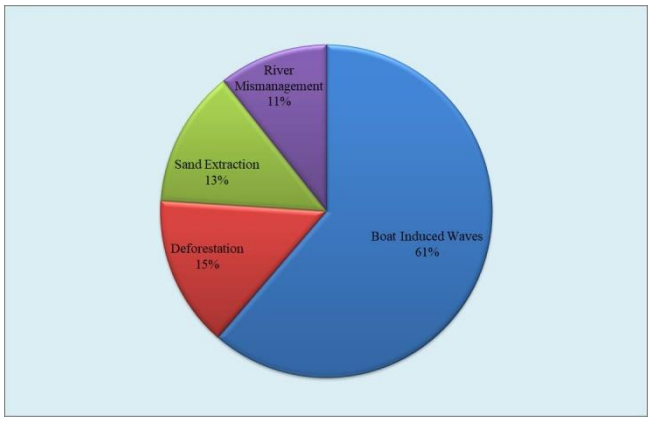

Figure 7. Feasible anthropogenic key factors based on questionnaire survey data.
[Participants were asked the question: "What are the natural and anthropogenic causes of the riverbank erosion?"]

Satellite images show the remarkable change at Barishal Launch Terminal and nearby Barishal Speed boat terminal (Fig. 10). The number of large and small size motorized steamer, as well as speed boat, has been increased dramatically with time (Islam and Degiuli, 2015). In the google image of 2009 a small number of launches were standing at the terminal jetty, among those three large-size launches are noticeable, whereas in 2019 satellite image shows the number of both large and small size launches has been climbing up and at least seven large scale launches are standing at the jetty. A similar scene is salient in the satellite image of 2019 where the number of speed boats has been increased at the speed boat terminal.

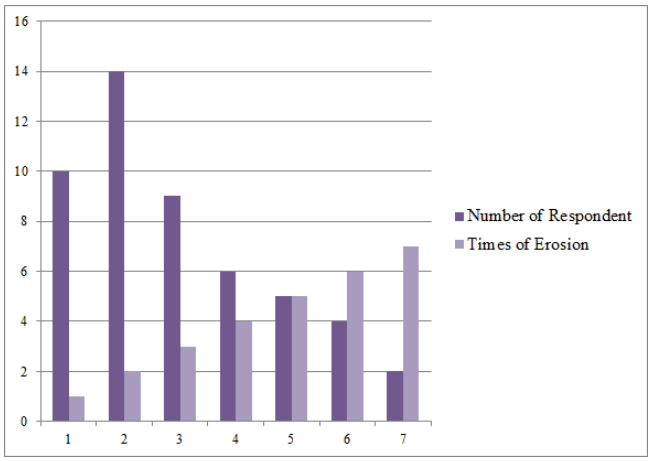

Figure 8. Times of land loss due to bank erosion experienced by the respondents in their entire life.
[Participants were asked the question: "How many times you have faced riverbank erosion in your entire life?"]

At present Kirtankhola has become busy river traffic. Everyday 22 large sized launches having capacity of carrying 1200-1500 passenger and more than 50-speed boats are actively running through Kirtankhola River (www.barisal.govt.bd). According to rules for safe and fast boating in Netherland, the speed of inland river vessels/launches should be below 20 km/h. But in the Dhaka-Barishal route, most of the launches and water buses along with local speed boats have a velocity over 30 km/h resulting in strong hydraulic waves. Due to poor navigability in the Kirtankhola river these swift-moving launches, water bus and speed boats often move along relatively deeper cut bank side and result from powerful waves repeatedly hit on unconsolidated cut banks and making the river banks more vulnerable to deteriorate.

5. CONCLUSION

The riverbank community of Kirtankhola River, Barishal is one of the disastrous localities due to various natural calamities of which riverbank erosion is an important one that is affecting and displacing millions of bank people. In addition, the situation could be even deteriorated by direct and indirect human influences and recently it's also imposing danger on the existence of many infrastructures near to the bank. In this study found a high rate of land loss on both side of the riverbank. The total erosion in the study area within ten years was 318.78 ha whereas the accreted new land amount was 287.02 ha. Most of the victims pointed out that strong currents produced by high-speed vehicles are accelerating this erosion. About 80% of the questionnaire participants have been affected more than one time. In addition, the newly formed lands in not being well distributed among the victims. As a result, many of them have to move to another place for their livelihood.

The study used GIS and RS techniques and there may present some uncertainties. But these methods are really very useful to do this kind of works. The results that are obtained through research may help the authorities to take decisions related to bank protection in Barishal and to develop the socio-economic and

livelihood status in the studied area. Still some detailed sedimentological and geotechnical analysis is needed to evaluate the vulnerability of Kirtankhola River.

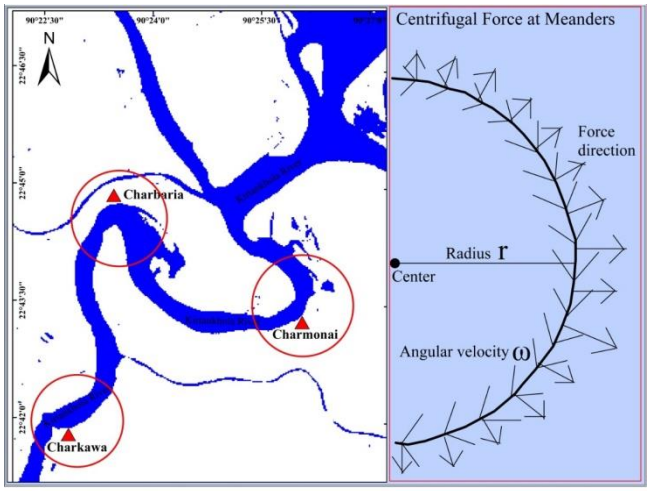

Figure 9. Mechanism of generating Centrifugal force by water vessels at meanders.

Figure 10. Satellite images of Barishal launch and speed boat terminal (a) image taken in 2009 (b) image taken in 2019. The ted circled area in satellite images indicates the comparative launch and speed boat number in 2009 and in 2019.

ACKNOWLEDMENT

The corresponding author greatly thankful to Department of Geology and Mining, University of Barishal, USGS authorities and Government of Bangladesh for technical support, availability of data through the entire study. The author specially thanks to MAS and MRR for reviewing the manuscripts, their valuable remarks and preparing for final draft.

Author contributions

Shaikh Ashikur Rahman: Conceptualization, Methodology, Software Interpretation, Writing-Original draft preparation. **Md. Muzahidul Islam**: Conceptualization, Methodology, Software Interpretation, Writing-Original draft preparation. **Md. Abdullah Salman:** Visualization, Investigation, Writing-Reviewing and Editing. **Muhammad Risalat Rafiq**: Visualization, Investigation, Writing-Reviewing and Editing.

Conflicts of interest

The authors declare no conflicts of interest.

REFERENCES

Ahmed K R & Afrin S (2016). Physical Modelling for the Improvement of Barisal Harbor Area. *Tech. J. River Res. Inst. 13(1): 11-25, 2016 (October), ISSN: 1606-9277*, *13*(1), 11–25.

BDoE (Department of Environment) (2016). River Water Quality Report 2015. Ministry of Environment and Forest, Government of People's Republic of Bangladesh. *Natural Resource Managment Section, Department of Environment.*, 50.

Billah M M (2018). Mapping and monitoring erosion-accretion in an alluvial river using satellite imagery - The river bank changes of the Padma River in Bangladesh. *Quaestiones Geographicae*, *37*(3), 87–95. doi.10.2478/quageo-2018-0027

Hasan M, Quamruzzaman C, Rahim A, Hasan I, Methela N J & Imran S A (2018). Determination of River Bank Erosion Probability: Vulnerability and Risk in Southern Shoreline of Bangladesh. *International Journal of Energy and Sustainable Development*, *3*(3), 44–51.

Hassan S & Akhtaruzzaman F M (2010). Environmental Change Detection of the Padma River in the North-Western part of Bangladesh using Multi-date Landsat Data. *Proc. of International Conference on Environmental Aspects of Bangladesh (ICEAB10)*, (October), 193–195.

Hohensinner S, Hauer C & Muhar S (2018). River Morphology, Channelization, and Habitat Restoration. *Riverine Ecosystem Management*, 41–65. https://doi.org/10.1007/978-3-319-73250-3_3

Islam M F & Rashid A B (1970). Riverbank erosion displacees in Bangladesh: need for institutional response and policy intervention. *Bangladesh Journal of Bioethics*, *2*(2), 4–19. https://doi.org/10.3329/bioethics.v2i2.9540

Islam M R & Degiuli N (2015). *INVESTIGATION OF THE CAUSES OF MARITIME ACCIDENTS IN THE INLAND WATERWAYS OF BANGLADESH*. *66*(1).

Joshi C, Leeuw J De & Duren I C Van (2002). Remote Sensing and Gis Applications. *GeoInformation Science*, *2*(Graph 1), 669–677.

http://citeseerx.ist.psu.edu/viewdoc/download?doi=10.1.1.138.2861&rep=rep1&type=pdf

Khan I, Ahammad M & Sarker S (2014). A study on River Bank Erosion of Jamuna River using GIS and Remote Sensing Technology. International Journal of Engineering Development and Research, 2(4), 2321–9939.

Mahmud I, Mia A J, Islam A, Peas M H & Farazi A H (2020). *Assessing bank dynamics of the Lower Meghna River in Bangladesh: an integrated GIS-DSAS approach*.

Mazumdar, N., & Talukdar, B. (2018). *Assessment Of River Bank Erosion Potential in Brahmaputra River in Lower Assam Region Using Modified Rosgen 's Bank Erosion Hazard Index Method. 08*(8), 21–27.

Nahar, N. (2015). Causes of River Bank Erosion, Its Effects on Life and Livelihood and Nature of Aids: A Case Study on Habashpur Union. 12, 85–98.

Nanson G C, Von Krusenstierna A, Bryant E A & Renilson M R (1994). Experimental measurements of river-bank erosion caused by boat-generated waves on the gordon river, Tasmania. *Regulated Rivers: Research & Management*, *9*(1), 1–14. https://doi.org/10.1002/rrr.3450090102

Noel R. Oswalt, Claude N. Strauser (1983) Prototype Experience and Model Studies of Navigation Effects on Inland Waterways. American Society of Civil Engineers

Rabbi H, Saifullah A S M, Sheikh S, Sarker M H & Bhowmick A C (2013). *Study on River bank Erosion and its Impact*. *2*(2), 36–43.

Salman M A, Hasan S M R, Ahmed S, Tahsin M & Khan N (2018). Shoreline Change Rate along the Southern Coast of Bangladesh due to Climate Change using Remote Sensing & ArcGIS Technology. IJETAE. Volume 8, Issue 3, March 2018.

Sarkar A, Garg R D & Sharma N (2012). RS-GIS Based Assessment of River Dynamics of Brahmaputra River in India. *Journal of Water Resource and Protection*, *04* (02),63–72. https://doi.org/10.4236/jwarp.2012.42008

Thakur P K, Laha C & Aggarwal S P (2012). River bank erosion hazard study of river Ganga, upstream of Farakka barrage using remote sensing and GIS. *Natural Hazards*, *61*(3), 967–987. https://doi.org/10.1007/s11069-011-9944-z

Umitsu M (1993). Late quaternary sedimentary environments and landforms in the Ganges Delta. *Sedimentary Geology*, *83*(3–4), 177–186. https://doi.org/10.1016/0037-0738(93)90011-S

Waterways I, Regulation P, Navigation R, Regulations P, n.d. *Rules for safe and fast boating*.

International Journal of Engineering and Geosciences
https://dergipark.org.tr/en/pub/ijeg
e-ISSN 2548-0960

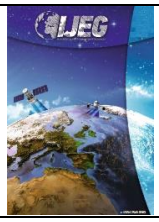

Change detection and future change prediction in Habra I and II block using remote sensing and GIS – A case study

Swapan Paul[*1]

[1]*West Bengal State University, Department of Geography, Kolkata, India*

Keywords
Change detection
Urban Expansion
Hotspot/Coldspot
Change prediction
Cellular automata

ABSTRACT

Mapping, analysis, and monitoring of landuse and landcover in micro region is necessary for sustainable land development, planning and management. The present study is, therefore, aimed to identify the spatio-temporal change of LULC in two central administrative C.D. blocks of North 24 Parganas in West Bengal, India during period 1987-2020. To figure out the essence of the transition, the supervised classification along with post-classification change detection using the 'From'-'To' approach was employed. Furthermore, hotspot analysis has been utilized to identify all of the areas that are the most variable in terms of change potentiality. Besides, cellular automata were also introduced to find out the character of urban growth and future trend of LULC change. The results show that between 1987 and 2020, agricultural area and vegetation with settlement decreased by -11.60 % and -4.34 %, respectively, while dense settlement increased by +15.69 % due to significant population growth and overcrowding from neighboring countries. The prediction model also supports this argument. So, the very high and uncontrolled growth of urban settlement in the study area, may become a big challenge for the district authority to control the unplanned urban expansion.

1. INTRODUCTION

Human research on the global environment as well as on Landuse-Landcover (LULC) change detection began decades ago (Lambin et al., 2003). Although landuse and landcover are two different terms and distinct in nature (Barnsley et al., 2001), they are often used almost interchangeably (Comber et al., 2008; Kuldeep & Kamlesh, 2011; Liping et al., 2018; Rawat & Kumar, 2015). Landcover refers to a region's natural coverage in terms of forest, hilly areas, rivers, oceans, barren land, etc., where there is no role of humans to play in their development. Landuse, on the other hand, refers to human interference with the natural state of the surface of the earth, i.e., how humans utilize the land of nature (Prasad & Ramesh, 2018). The skinnier of LULC of a specific area determines the physical and socio-economic factors of the respective area and their exploitation in respect of space and time (Rawat & Kumar, 2015). In recent years, anthropogenic activities have been the leading factor in defining the pattern of land use (Rai, 2017). Nonetheless, this is nothing new. Some of the economically important man-made alterations, including cultivation in different forms by changing the forest cover, reservoir development by reducing the ecological balance of any hilly area, settlement construction by altering the forest as well as barren cover, livestock grazing and so on, has modified the earth surface from the early age of civilization (Turner et al., 1994). The Centre for Geographic Information and Analysis (CGIA) of USA has classified the entire LULC into 7 major classes, 16 subclass, 28 mini classes, and 10 micro classes in Landcover categories and 7 major classes, 25 subclass, 65 mini classes and 179 micro classes in landuse categories. The gradual rise in population concentration and subsequent urban expansion, industrial growth, and development in mining industry since 18th century have greatly influence the landuse and landcover (Riebsame et al., 1994; Sharma et al., 2007) and at the same time, have affect the temperature budget of the urban areas (Ha et al., 2018; Voogt & Oke, 2003). So, the magnitude, scale and rate of human interference of earth's natural characteristics are unprecedented (Lambin et al., 2001; Turner et al., 1994).

Change detection is a method to identify the modification of the attributes of an object or phenomena of a particular area during a certain time (Amaral et al., 2013;

* **Corresponding Author**
*(spaul5481@gmail.com) ORCID ID 0000 – 0002 – 9373 – 6310

Cite this article
Paul S (2022). Change detection and future change prediction in Habra I and II block using remote sensing and GIS – A case study. International Journal of Engineering and Geosciences, 7(2), 191-207

Research Article / DOI: 10.26833/ijeg.975222
Received: 27/07/2021; Accepted: 16/09/2021

Singh, 1989). Change detection analysis can be formulated either by primary field survey and mapping at consecutive times or by comparing temporal datasets, normally two satellite image or aerial photograph at different times (Wang & Xu, 2010). However, primary field survey-oriented studies are itself not very sufficient and accurate to quantify and analyze the spatio-temporal variation of LULC at a macro level study (Wood & Skole, 1998). Furthermore, it is not possible to accurately predict the future pattern of change through field observation alone. On the other hand, if the accuracy of the map obtained from remote sensing data is not assessed, it is also worthless (Congalton, 2001). So, the map obtained through remote sensing data and the verification of that map by field-based ground truthing -these two makes a systematic method for any change detection analysis (Cai et al., 2018). Thus, change detection analysis is important and essential for acquiring a very good understanding of the bi-directional interaction as well as relationship between natural occurrences and landscape dynamism. This understanding is essential for the proper resource management and as such various organizations like state, regional, local government, and private corporations use this information for a variety of purposes (Chowdhury et al., 2018; Ha et al., 2018; Hussain et al., 2013; Lu et al., 2004; Petit et al., 2001).

In modern day, the collaboration of remote sensing and geographical Information System (GIS) has an improved and detailed way that makes an easy and intelligible method to map LULC of any location (Selcuk et al., 2003). Currently, the most widely used change detections from the Geographical point of view are change in forest cover and health, spatio-temporal transformation of different coastlines, change along the longitudinal and cross-sectional profile of a river, urban expansion, seasonal productivity of agricultural land, etc. Among them change detection on the urban encroachment into other LULC is predominant. A number of research work have been published around the world from mid 1980s regrading urban encroachment into surrounding organic areas and consequent reduction of agricultural land, filling of wetlands, etc. (Chaurasia et al., 1996; Dewan & Yamaguchi, 2009; Fortin, 2003; Kushwaha, 1990; Stauffer & McKinney, 1978).

In present day numerous techniques and algorithms have been established to detect the change among different phenomenon, which in turn have increased the use of remotely sensed data in academic level to predict the future of LULC (Butt et al., 2015). Civco et al. (2002) had examined some popular change detection methods viz. a) traditional post-classification b) cross-tabulation c) cross-correlation analysis d) neural networks e) knowledge-based expert systems and f) image segmentation and object-oriented classification keeping in consideration of seven LULC classes. Their result revealed that the detection of change in each method have some similarities, though a huge difference was also there. They conclude that there is no such single method which can be used without justification. Although they have some confidence on some improved methodology like image-segmentation and rule-based classification. Besides, a compact discussion on various updated image classification technique and associated change detection methods has been summarized in Bhatta (2018), Canty (2014), Jensen (2015). Furthermore, a number of updated change detection method has also been used using binary based change recognition including different image differencing and ratioing like different indices (like NDVI, EVI, MSAVI, NDMI), Principal Component Analysis (PCA) and differencing, Change Vector Analysis (CVA), etc. (Coppin & Bauer, 1996; Gong et al., 1992; Im et al., 2007; Kefalas et al., 2018; Singh, 1989). So, it is clear that there are two broad type of change detection technique– 1) category one, which detect the change and reveal a detailed trajectory and 2) category two, binary based change detection which uses Change or No Change technique. Though, the former focuses on a 'From'- 'To' approach which makes a more detailed change interface, while from the later one, anyone can not perceive that what kind of landuse has changed from what kind of landcover and vice versa (Lu et al., 2004; Lu et al., 2005).

North 24 Parganas is a one of the most populated administrative districts in southern West Bengal, of eastern India, was actually the northern part of undivided 24 Parganas district (divided in 1983, 1 March) of several legendary kingdom as well as British ruled West Bengal. The major part of this district lies within the limit of Moribund part of Gangetic delta, are flat and little elevated above the sea level, configured its physical characteristics are common to any deltaic land. Besides, the position of three major rivers namely Bidyadhari, Ichhamati and Yamuna have made the district favorable for agriculture through enormous deposition of silt up to mid-20th century (Bagchi, 1944; Majumdar, 1942; Mukherjee, 1938; O'Malley, 1917) and the position of Hugli river to the far west increases the potentiality for industry– are the major factor of population growth as well as LULC change in this region. However, the former three rivers have become dilapidated either due to excessive siltation or due to conversion of the river course into aquaculture fisheries through damming the flow of the river. Habra I and II blocks are in nearly the central part of the district having a population density of 1918/km^2 and 1566/km^2 (Handbook, 2011).

A number of Change detection work have been finished on different parts of North 24 Parganas District. Bhattacharjee & Hazra (2014) have highlighted the regional growth of urban body of Barasat town (district head quarter of North 24 Parganas) as well as its impact on environment in terms of Urban Heat Island (UHI) with the help of Landsat ETM+ image. Basu & Saha (2017) also have tried to outlined the rate of urbanization in Barasat town. Dhar et al. (2019), on the other hand, has done another work of almost the same kind on newly developed Rajarhat block. A different kind of work, relevant with the southern part of North 24 Parganas by Mondal & Bandyopadhyay (2014), examined the change in aquaculture of Sandeshkhali I and II block during 1990 to 2013. Hazra & Saradar (2014) have tried to observe the change of LULC along the Bidyadhari basin within the time period 2001-2008 using Landsat TM and ETM image. At a course scale, Bera & Das Chatterjee (2019) have tried to examined the LULC change of overall North 24 Parganas district during the time period 1990-2017 using Maximum Likelihood classification technique. Other works related with LULC

of the district can be found in Mondal et al. (2017), Rahaman (2018), Saritha & Kumar (2019).

Thus, numerous studies have been conducted in different parts of the district in the recent past, but no detailed and localized study have been done on Habra I and II block in spite of being located in the central most part of the district. Consequently, by using the modern remote sensing data the author started working with the following objectives in mind– 1) to explore the change in LULC of Habra I and II block in a quantitative way, and 2) to find out the future trend of LULC change of the area.

2. MATERIAL AND METHODS

2.1. Study Area

Habra I and II C.D block are two administrative division in Barasat Sadar subdivision of North 24 Parganas district in the Indian state of West Bengal, located between Gaighata CD block and Haringhata CD block in the north, Swarupnagar and Baduria CD block in the east, Deganga and Barasat I CD block in the south, and Amdanga CD block in the west. The area extends between 22°46′18″ to 22°55′24″ N and 88°30′30″ to 88°47′30″ E, covered by Survey of India (SOI) topographical sheets no. 79B/9 and 79B/13 (Fig. 1). The Habra-I and Habra-II block occupies a total number of 58 mouzas and 78 mouzas respectively (revenue villages) under Barasat subdivision. The total area of Habra-I is nearly 117.36 km^2 while the total area of Habra-II is nearly 112.67 km^2. Since the natural and cultural landscape of the two blocks are almost same, and because of their united location even a few years ago, the LULC changes in these blocks have been measured together.

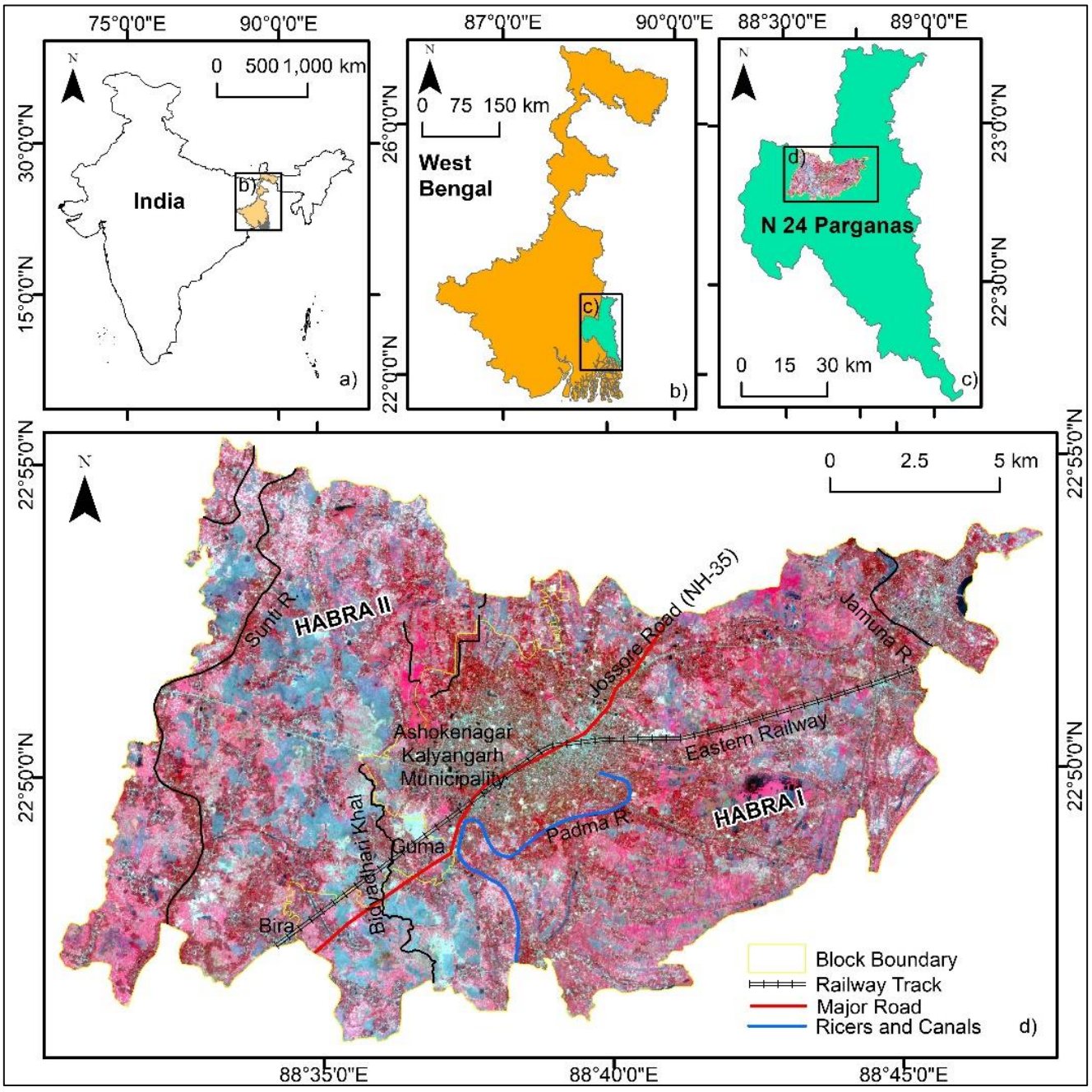

Figure 1. Location map of the study area. in (d) standard FCC has been generated using the red, green, blue and NIR of Landsat image.

2.2. Data collection

The data that are used in this research can be categorized into two independent datasets–a) spaceborne images and b) subsidiary data. It is worth to mentioned that the spaceborne image refers to different multispectral satellite images of different satellite of Landtsat series, whereas subsidiary data refers to topographical sheets, ground truth data, documentary photographs, etc. Satellite data for three different years (1987, 2001, and 2020) comprising of Landsat Thematic Mapper (TM) image, Landsat Enhanced Thematic Mapper (ETM) image, and Landsat Operational Land Imager (OLI) image, were collected from the United States Geological Survey (USGS) Earth Explorer portal (https://earthexplorer.usgs.gov/), to interpret and detect LULC of Habra I and II block. A detailed description of each image is shown in Table 1. Nearly cloud free imagery had been chosen as a major criterion during image selection, because the presence of cloud in the image could pervert the accuracy of image classification work.

Accordingly, we could not take all the imageries for the same month. Although for the convenience of work, the satellite images that have less than 10 percent of cloud had also been accepted. In Indian sub-continent, being a monsoonal affected region, experiences winter season from November to February and the sky remains nearly clear. Thus, imageries from this winter season were the main sources of data for this study assuming that the acquisition period of imageries would have minimal seasonal variation. Besides, ground truth data in the form of reference point, were collected by Garmin hand Global Positioning System (GPS) during the period January, 2020 to February, 2020, used for generating signature file for supervised image classification and subsequent accuracy assessment. A topographical sheet (at a scale of 1:50000) of Survey of India (SOI), surveyed in 1969, were also collected from self-organizing website of SOI to support the work.

Table 1. Description of all the satellite images used in the study.

Satellite	Sensor	Path/Row	Date of Acquisition	Band used	Spatial Resolution	Source
Landsat-5	TM	138/44	24-12-1987	Visible (B1, B2, B3) NIR (B4)	30 30	USGS
Landsat-7	ETM	138/44	26-02-2001 12-01-2011	Visible (B1, B2, B3) NIR (B4)	30 30	
Landsat-8	OLI and TIRS	138/44	17-01-2020	Visible (B2, B3, B4) NIR (B5)	30 30	

Table 2. Description of all the landuse and landcover classes and range of reflectence in terms of DN in that class.

Sl No.	Class Name	Description	Range of DN Value				
			Year	Band			
				Blue	Green	Red	Near Infra-red
1	Agricultural Land	Crop fields, nurseries, floricultural areas and current fallow lands	1987	80-134	65-127	57-142	45-122
			2001	91-136	75-131	61-147	45-122
			2020	90-135	69-127	61-149	45-126
2	Vegetation with Settlement	plantation, mixture of vegetation and settlement	1987	87-116	69-100	58-113	38-107
			2001	89-110	70-99	56-101	50-104
			2020	89-112	70-102	59-102	66-106
3	Dense Settlement	Urban and rural crowded buildings, road network, industrial zone	1987	99-116	78-99	74-107	56-77
			2001	95-118	75-99	72-109	56-82
			2020	90-121	71-108	61-119	47-107
4	Waterbody	River, canals, lakes, ponds	1987	88-109	66-96	55-110	33-120
			2001	87-108	65-94	55-92	32-88
			2020	92-109	68-99	58-98	33-109

2.3. Pre-processing and Image classification

The downloaded images were imported in ArcGIS 10.6 and composite band tool from data management toolbox was used to stack the useful bands of the image to convert the individual bands into a single file and generate the FCC for the study area. The actual Area of Interest (AOI) of stacked images were then extracted by a georeferenced vector polygon layer of Habra I and II block boundary through the process of clipping. After that the extracted images were exported to Erdas Imagine 2016 for the atmospheric correction (Haze and Noise reduction) and then the corrected images were again imported in ArcGIS 10.6 environment to complete the rest of the work. It is worth to mention that since each AOI was completely free from cloud as well as of nadir view, no cloud removal process and orthorectification was required. Thus, initially all the satellite images were studied through visual interpretation and delineated four classes depending on the characteristics of an image like shape,

size, tone, texture, association and site. For each predetermined LULC class, polygons were drawn to extract the training samples around the representative sites with the support of the ground truth verification data, high resolution satellite image of Google Earth Pro and topographical sheet of the study area. An acceptable spectral signature must be obtained from that site that ensuring there is 'minimal confusion' among the LULC to be classified. An average of more than 25000 pixels were recorded to create the signature file for each image classification. Therefore, supervised image classification was conducted based on the maximum likelihood algorithm. There were four classes were categorized viz. agricultural land, vegetation with settlement, dense settlement, and waterbody (Table 2). The prime problem during training sample collection was to differentiate between actual vegetation and settlements that are surrounded by vegetation. For this reason, these two classes were shown together as vegetation with settlement.

2.4. Post-Classification processing and change detection

A post classification smoothing and refinement in forms of majority filter and boundary cleaning were applied to enhance the accuracy of classification and to reduce the misclassified solitude parts. Thereafter, a post-classification change detection was employed to understand the modification of LULC taking the benefit of "From, -To" approach. To do this, the selected classified images (1987, 2001, and 2020) were converted from raster to polygon layer and then intersected on the basis of a common id of each LULC class. Thus, a change detection was then done by adding a new field in attributes and then keeping the information of each polygon characterized by both of its previous and present LULC class side by side. Finally, four change detection maps–1) change in agricultural area 2) change in vegetation 3) change in settlement area and 4) change in waterbody were generated using Eq. (1).

$$\begin{array}{r|ccc} & Time\ t+1 & & \\ \hline & C_{t11} & C_{t12} & C_{13} \\ Time\ t & C_{t21} & C_{t22} & C_{t23} \\ & C_{t31} & C_{t32} & C_{33} \end{array} \quad (1)$$

Which means

$$\begin{array}{r|ccc|c} & Time\ t+1 & & & (Gross\ Loss) \\ \hline Time\ t & NC_1 & \frac{C_{t12}}{\sum_{i=1}^{3}\sum_{j=1}^{3}C_{tij}} & \frac{C_{t13}}{\sum_{i=1}^{3}\sum_{j=1}^{3}C_{tij}} & \frac{C_{t12}+C_{t13}}{\sum_{i=1}^{3}\sum_{j=1}^{3}C_{tij}} \\ & \frac{C_{t21}}{\sum_{i=1}^{3}\sum_{j=1}^{3}C_{tij}} & NC_2 & \frac{C_{t23}}{\sum_{i=1}^{3}\sum_{j=1}^{3}C_{tij}} & \frac{C_{t21}+C_{t23}}{\sum_{i=1}^{3}\sum_{j=1}^{3}C_{tij}} \\ & \frac{C_{t31}}{\sum_{i=1}^{3}\sum_{j=1}^{3}C_{tij}} & \frac{C_{t32}}{\sum_{i=1}^{3}\sum_{j=1}^{3}C_{tij}} & NC_3 & \frac{C_{t31}+C_{t32}}{\sum_{i=1}^{3}\sum_{j=1}^{3}C_{tij}} \\ \hline Gross\ Gain\ in\ each & \frac{C_{t21}+C_{t31}}{\sum_{i=1}^{3}\sum_{j=1}^{3}C_{tij}} & \frac{C_{t12}+C_{t32}}{\sum_{i=1}^{3}\sum_{j=1}^{3}C_{tij}} & \frac{C_{t13}+C_{t23}}{\sum_{i=1}^{3}\sum_{j=1}^{3}C_{tij}} & \sum_{i=1}^{3}\left[\left(\sum_{i=1}^{3}C_{tij}\right)-C_{tij}\right] \end{array}$$

Here, in raw transition matrix for three categories, the transitions from category *i* at time *t* to category *j* at time *t+1* is represented by c_{ij}. The right-most column of the Flow matrix gives the gross losses of each category, while the bottom row gives the gross gains. NC_1, NC_2, and NC_3 are the cells that were not changed during time interval *t* and *t+1*.

2.5. Accuracy assessment of classified image

Accuracy assessment refers to the number of pixels in a classified image that is consistent with the reality, explicitly, how many have been accurately classified using the algorithm. It is very significant for understanding the exactness of the results and use in enforcing various policies (Lu et al., 2004). In this study, accuracy assessment of the classified image was carried out using a total number of 160 ground truth data (40 in each class), obtained from the actual field by the means of random sampling. A confusion matrix was used here (classification result is given in rows while reference is shown in column) because of its popularity and simplicity in the ground of remote sensing. The confusion matrix appears to deliver an excellent summary of the two types of thematic error that can occur, namely, underestimation or omission and overestimation or commission (Foody, 2002). Depending on the information obtained from the contingency table, a number of analytical measures viz. overall accuracy, producer's accuracy, and user's accuracy have been used to calculate the classification accuracy from different perspectives (Richards, 1996; Stehman, 1997). The commission error of any generic class *X1* occurs when the classifier assigns some pixels as *X1* which do not fit to that class according to the reference data, i.e., number of pixels erroneously assigned, found in off-diagonal elements in each row. Omission on the other hand, is the percentage of pixels situated in a class *X1* in the verification or reference data, but have not been assigned in classified image, i.e., the off-diagonal elements in each column are those samples being omitted by the classifier (Bhatta, 2018; Boschetti et al., 2004). Besides, Kappa statistics of the classified image was also performed along with the overall accuracy to enhance the degree of acceptance of the result. The formula of kappa statistics K is as follows

$$k = \frac{N\sum_{i=1}^{r} x\,ii - \sum_{i=1}^{r} x_i + * x_i + i}{N^2 - \sum_{i=1}^{r} x_i + * x_i + i} \quad (2)$$

The perfect agreement of *K* is represented when the kappa value is +1, while a value of 0 represents no agreement (Ha et al., 2018).

2.6. Measurement of rate and speed of landuse dynamics

The rate of land use transition represents the magnitude of the change in land use in the study area over a given time span. This measurement of the dynamicity of LULC either can be measured by single dynamic degree (SDD), or by a comprehensive dynamic degree (CDD) (Jing & Yue, 2016; Xiao et al., 2012; Yi et al., 2013). The single dynamic degree describes the rate of change in spatial/regional land use, while the comprehensive dynamic degree is determined on the basis of the sum of the single land use dynamics, which quantifies the rate of transformation of the total land use categories and their relationship during the study period (Bera & Das Chatterjee, 2019; Wang et al., 2001). In this study, the author has followed both of these approaches. The formula for calculating SDD and CDD are described in Eq. (3) and (4).

$$S_1 = \frac{LA_{(i,t1)} - LB_1}{LA_{(i,t1)}} \times \frac{1}{t_2 - t_1} \times 100\% \quad (3)$$

$$S_2 = \frac{\sum_{i=1}^{n}\{LA_{(i,t1)} - LB_1\}}{\sum_{i=1}^{n} LA_{(i,t1)}} \times \frac{1}{t_2 - t_1} \times 100\% \quad (4)$$

Where, S_1 and S_2 are single landuse dynamic degree and comprehensive landuse dynamic degree respectively, $LA_{(i,t1)}$ is the area of a certain type of land use in previous time, LB_1 is the area of a certain type of land use at a later time, t_2 and t_1 are the time of study period, n is the number of landuse landcover classes.

In addition to this, the land use dynamic degree (the rate of change) given by Liu & He (2002), was also employed to compare the differences between SDD and CDD, following Eq. (5, 6, and 7).

$$X_1 = \frac{LA_{(i,t1)} - NC_1}{LA_{(i,t1)}} \times \frac{1}{t2 - t1} \times 100\% \quad (5)$$

$$X_2 = \frac{LA_{(i,t2)} - NC_1}{LA_{(i,t1)}} \times \frac{1}{t2 - t1} \times 100\% \quad (6)$$

$$SCDI = X_1 + X_2 \quad (7)$$

Where, X_1 and X_2 are the transfer out rate and transfer in rate respectively, *SCDI* is the spatial-based land use dynamic degree, $LA_{(i,t2)}$ is the area of a certain type of land use at a later time, NC_1 is the area that is not changed during the study period.

2.7. Spatial Change Hotspot Analysis

In the current review, hotspots were identified as areas with a high density of land cover transition in space. This scientific analysis compares the distribution of attributes to a hypothetical random distribution and helps to define spatial characteristics of the information (Mitchell & Minami, 1999). Thus, in order to explain the statistical measurement of land-use dynamics around the Habra I and II block, the G_i* statistics has been used in this article. Integrated Hotspot Analysis tool in ArcGIS determines statistically significant high-value (hotspot) and low-value spatial clusters (coldspots). To complete the work, 750 sample points were randomly generated by creating a random point tool and then attributed using the dynamic degree of LULC change (% value) in ArcGIS 10.6 software for the entire study area. Hotspot analysis involves each raster pixel in the sense of the adjacent features in the estimation and produces a new vector with z-score, p-value and confidence level. Areas with a high z-score and a low p-value (represent clusters that are, on average, greater than the mean) demonstrate statistically significant hotspots, and areas with a low negative z-score and a small p-value (represent clusters that are less than the mean) reveal statistically significant cold spots (Getis & Ord, 1996). The formula for calculating the G_i* are as follows

$$G_i^* = \frac{\sum_{j=1}^{n} w_i x_j - \bar{x}\sum_{j=1}^{n} w_{ij}}{s\sqrt{\left[n\sum_{j=1}^{n} w_{ij}^2 - \left(\sum_{j=1}^{n} w_{ij}\right)^2\right]}} \quad (8)$$

$$\bar{x} = \frac{n\sum_{j=1}^{n} xj}{n} \quad (9)$$

$$S = \sqrt{\frac{\sum_{j=1}^{n} x_j^2}{n} - (\bar{x})^2} \quad (10)$$

Where, G_i* is a *Z* score, *xj* is the attribute value for feature *j*, w_{ij} is the spatial weight between feature *i* and *j*, *n* is equal to the total number of LULC classes. Here, if the distance from a neighbor *j* to the feature *i* is within the distance, *wij* = 1, otherwise *wij* = 0.

Hot and cold spots were classified into seven categories based on their G_i Bin values: very hot spot (99% significant), hot spot (95% significant), warm spot (90% significant), not statistically significant, cool spot (90% significant), cold spot (95% significant), and very cold spot (99% significant). Finally, IDW interpolation method was employed based on the Z score to show the distribution of hot and cold spot throughout the study area for the period 1987-2001, 2001-2020, and 1987-2020.

2.8. Cellular Automata Model for future prediction of built-up extension

In the present analysis, the potential estimation of built-up growth was predicted in open source QGIS 2.16.3 software using the MOLUSCE (Modules for Land Use Change Evaluation) tool that uses the Cellular Automata Model formula. In QGIS, the Cellular Automata (CA) function is Markovian in nature since it relies on the present state of land use but not on the former one (Yatoo et al., 2020). It first modelled the change potential matrix using the Multi-Layer Perceptron-Artificial Neural Network (MLP-ANN) and then forecast possible LULC changes using the CA model. In the CA-ANN collaboration module, the initial pre-processing of the given data into a

series of independent variables of the land use classes is performed by dummy coding of different categories into variables such as 0 and 1 (Jogun et al., 2019). It also conducts the normalization of factor variables using the linear normalization formula as shown in Eq. (11).

$$x_n = \frac{X - m_x}{\sigma_x} \tag{11}$$

Where, X is a variable, X_n is normalized variable, m_x is mean of X and σ_x is standard deviation of X.

The prediction was based on two types of variables viz. the dependent variables such as past pattern of LULC changes estimated from 2001 to 2011 Landsat images, and the independent variables such as distance to roads, distance from the CBD, slope, and population density of the area. The distance from road and distance from CBD was generated using the Euclidian distance function in ArcMap software, slope was calculated from the Alos Pulser DEM (12.5m), and the population density map was created using the census data of 1991 and 2011. All the variables were used as input to generate transition potential matrix. To define maximum iteration and neighborhood pixel for the model, the maximum iteration was 1000 and neighborhood pixel was 9 cells i.e., 3 × 3 cells.

$$A_{i,j}^{t} = \begin{bmatrix} a_{i-1,j-1}^{(t)} & a_{i-1,j}^{(t)} & a_{i-1,j+1}^{(t)} \\ a_{i,j-1}^{(t)} & a_{i,j}^{(t)} & a_{i,j+1}^{(t)} \\ a_{i+1,j-1}^{(t)} & a_{i+1,j}^{(t)} & a_{i+1,j+1}^{(t)} \end{bmatrix} \tag{12}$$

Matching the geometry of layers is crucial to ensure that any random pixel $a_{i,j}$ represents the same piece of land in all the raster layers. Finally, the simulated built-up development for 2030 and 2050 was generated. The validation of the CA-ANN model is important; therefore, the CA-ANN model was validated by comparing simulated LULC for 2020 with classified LULC of 2020 using MOLUSCE QGIS validation module.

The overall methodology of the current study is diagrammatically described in Fig. 2.

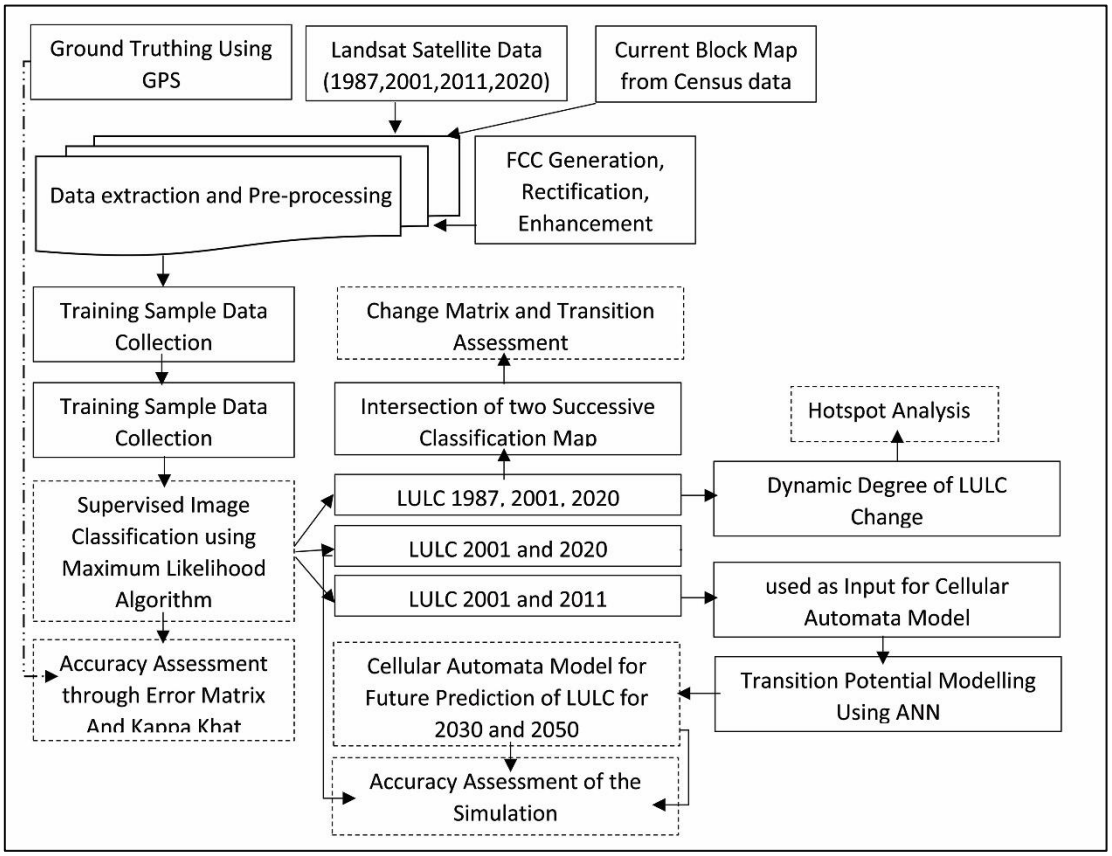

Figure 2. Schematic representation of the methods that were followed in the present study.

3. RESULT

3.1. LULC Status

The result, obtained from multi-temporal satellite images through supervised LULC classification, covering four major classes viz. agricultural land, vegetation with settlement, dense settlement, and waterbody of the year 1987, 2001, and 2020 are shown in Fig. 3. In addition, the spatial distribution of each LULC class along with the percentage of the total area occupied by each class is summarized in Table 3. Result demonstrates that in 1987, 59.75% (168.78 km^2) of the total land was under agricultural land, 0.78% (2.21 km^2) under dense settlement, 38.76% (109.48 km^2) of land under vegetation with settlement class, and less than 1% (1.98 km$_2$) was covered by waterbody. On the other hand, in 2001, 55.23% area of Habra I and II block (155.96 km^2) was covered by agricultural land, 12.91% (36.46 km^2) under dense settlement against 0.78% in 1987 reveals a sharp increase in

dense settlement within 14 years. There is a sharp decrease in vegetation with settlement area, which is evident from 30.52% (86.18 km²) in 2001 instead of 38.76% in 1987. In this time waterbody covered 1.33% (3.76 km²) of the total LULC area which portrays a slight increase from the aforementioned period. Results from the classified image of 2020 demonstrates that, nearly 48% (136.02 km²) of total area was covered by agricultural land, which illustrates a further decrease compared to the 2001. The other classified classes viz dense settlement, vegetation with settlement, and waterbody, covered 16.48% (46.55 km²), 34.42 % (97.24 km²), and 0.93% (2.65 km²) of total land respectively.

3.2. Net and Overall Change

The change in different landuse and landcover classes are depicts in Fig. 4. Besides, two change matrices for consecutive decades have also been used to determine the net amount of land encroachment from one LULC class to another during last 33 years. During the period 1987-2001, the net changes (Table 4) are as follow–

a) 10.80% of agricultural land has been converted into vegetation with settlement, 5.70% into dense settlement, and 0.83% area from agricultural land was changed to waterbody. That is, about 82% of land under agriculture were almost unchanged during this period

b) Nearly 32.27% of vegetation with settlement area was turn into agricultural land, 18.23% into dense settlement, and about 1% land has been converted into waterbody.

c) Almost 9% of waterbody has been converted into agricultural landuse, 11.56% towards dense settlement, and about 18% of waterbody was changed to vegetation with settlement class.

On the other hand, the transformation of different landcover and landuse classes from 2001-2020 (Table 5) is much like this–

a) About 7% of agricultural land has been converted into dense settlement, 17.77% of land into settlement with vegetation and 0.30% of land has been turned into waterbody.

b) During this two decades, about 68.89% of vegetation with settlement was remain unchanged, but nearly 19% and 12% land has been transformed into dense settlement and agricultural landuse, respectively. Besides, 0.48% area has also been changed to waterbody.

c) 41.77% area of waterbody has been converted into agricultural land, 14.88% area into dense settlement, and about 7.78% area was changed to vegetation with settlement zone.

Thus, after considering each class separately from 1987 to 2020, the overall changes states that a total of 32.76 km² of agricultural land has been reduced from its actual area, and with it the area of vegetation with settlement has also been reduced from 109.48 km² in1987 to 97.24 km² in 2020 with a net reduction of 12.24 km². On the contrary, with the decline in these two landuse classes, the area of dense settlement has increased at a proportional rate. Result shows that it has increased from 2.21 km² in 1987 to 46.55 km² in 2020 with a net increase of 44.34 km². Although a net change in waterbody also reveals that there is a net positive change occurred in last 33 years (+0.67 km²).

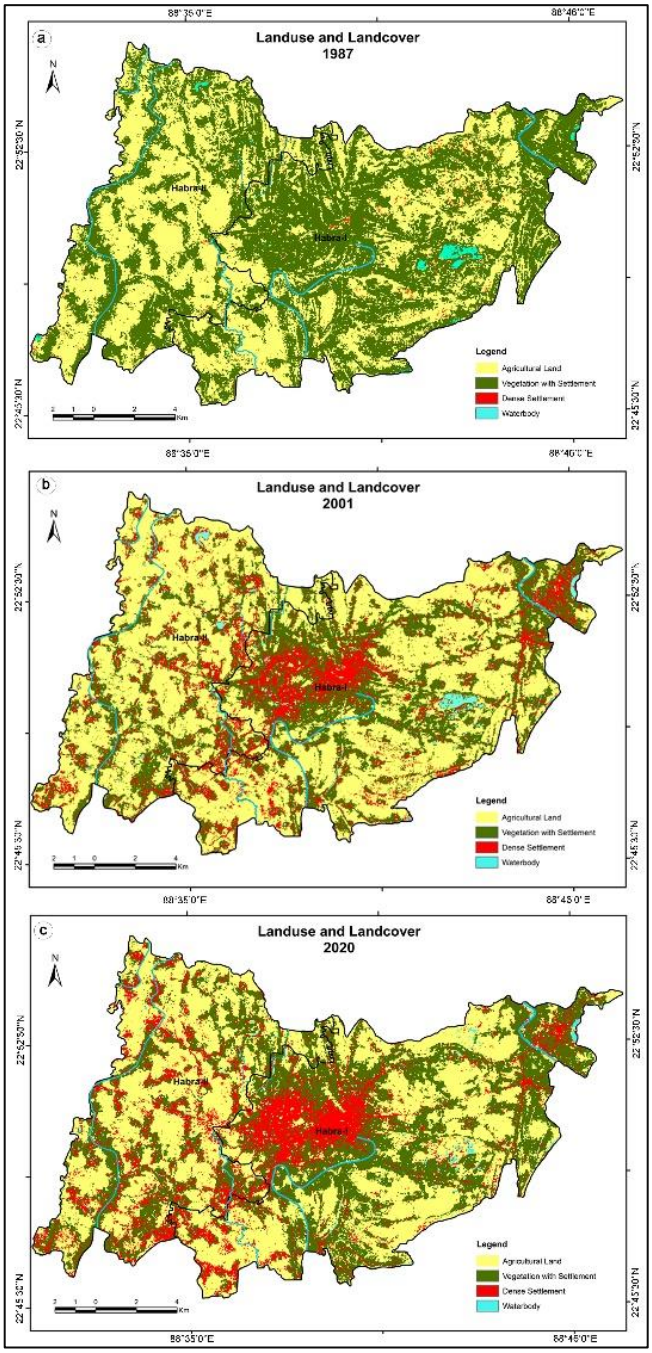

Figure 3. Landuse and Landcover scenario during years 1987, 2001, and 2020 in Habra I and II block (Based on Landsat TM, ETM, and OLI imagery).

3.3. Accuracy Assessment of classified images

Overall accuracy, producers' accuracies, users' accuracies, and Kappa coefficient were calculated from the confusion matrix to understand the accuracy of the 2020 image, which is tabulated in Table 6. Accuracy assessment for classified image of 2020 shows that the overall accuracy is equivalent to about 95%. Producers' accuracies and users' accuracies are also high. As such Producers' accuracies of individual classes are ranging from 92.5% to 97.5%, while users' accuracies fluctuating between 92.5% and 100%. The kappa coefficient of the classified image 2020 is about 0.93.

3.4. Change Hotspot analysis

Spatial autocorrelation is required to know the spatial structure of the LULC data as shown in Fig. 5. The spatial autocorrelation in terms of Moran's I was conducted over three different periods viz. 1987-2001, 2001-2020, and 1987-2020, indicates that the spatial pattern of LULC dynamics is different from case to case. Result demonstrated that the Moran's I value for three different periods is statistically significant. In comparison, the derived Z score from the spatial autocorrelation indicates that its values are 6.82, 9.83, and 11.80 for 1987-2001, 2001-2020 and 1987-2020 respectively, suggesting that the distribution is strongly clustered and that there is less than 1% probability that this clustered trend may be the result of random chance. The hotspot and Coldspot estimates of the Habra I and II blocks, which were computed on three consecutive periods, are presented in Fig. 6 after incorporating Getis-Ord Gi* statistics. Result demonstrates that nearly 13.75% and 16.12% area has been categorized as evolving hotspots at more than 90% confidence level during period 1987-2001 and 2001-2020, respectively,

Table 3. Spatial distribution of each landuse and landcover class and overall change of that class during 1987-2020

	1987		2001		2020		Overall Change (1987-2020)	
LULC class	Area(km²)	%	Area(km²)	%	Area(km²)	%	Area(km²)	%
Waterbody	1.98	0.70	3.76	1.33	2.65	0.93	0.67	0.23
Agricultural Land	168.78	59.75	155.96	55.23	136.02	48.15	-32.76	-11.60
Vegetation with Settlement	109.48	38.76	86.18	30.52	97.24	34.42	-12.24	-4.34
Dense Settlement	2.21	0.78	36.46	12.91	46.55	16.48	44.34	15.69

Table 4. Landuse and landcover change matrix during 1987-2001

	1987 (in percentage)			
2001(in percentage)	Agricultural Land	Dense Settlement	Vegetation with Settlement	Waterbody
Agricultural Land	82.66	0.00	32.27	8.99
Dense Settlement	5.70	100.00	18.24	11.56
Vegetation with Settlement	10.80	0.00	48.53	18.26
Waterbody	0.83	0.00	0.97	61.19
Grand Total	100.00	100.00	100.00	100.00

Table 5. Landuse and landcover change matrix during 2001-2020

	2001 (in percentage)			
2020 (in percentage)	Agricultural Land	Dense Settlement	Vegetation with Settlement	Waterbody
Agricultural Land	74.98	0.00	12.01	41.77
Dense Settlement	6.96	100.00	18.62	14.88
Vegetation with Settlement	17.77	0.00	68.89	7.78
Waterbody	0.30	0.00	0.48	35.58
Grand Total	100.00	100.00	100.00	100.00

Table 6. Error matrix for accuracy assessment of classified image 2020 with user's accuracy, Producer's accuracy, and kappa coefficient

	Reference data						
Classified image	Agricultural Land	Vegetation with Settlement	Dense Settlement	Waterbody	Classified Total	Commission Error	User's Accuracy
Agricultural Land	37	2	1	0	40	7.5%	92.5
Vegetation with Settlement	1	38	1	1	41	7.32%	92.68
Dense Settlement	2	0	38	0	40	5%	95
Waterbody	0	0	0	39	39	0%	100
Reference Total	40	40	40	40	160		
Omission Error	7.5%	5%	5%	2.5%			
Producer's Accuracy	92.5%	95%	95%	97.5%			
Kappa coefficient	0.93						

While in the case of total transition (1987-2020), the proportion of hotspots in the area dropped to 11.06 per cent. Also, most of the hotspots are concentrated in the urban center, along the main road, and near the industrial area. The spatial distribution, on the other hand, shows that during 1987-2001 hotspot regions are clustered in north eastern (Gabardanga municipal area), middle (Habra and Ashokenagar-Kalyangarh municipal area), and in the south-western corner of the block. While, during 2001-2020, former hotspots remained un-

changed and some new hotspots were introduced adjacent to the Guma, Bira and Joypul CT centers. Notice that according to the LULC attributes, dense settlements have the maximum hotspots, while water bodies have the largest concentration of cold spots. Agricultural land plays the second most important role in the production of cold spots next to the water bodies. The Gi_Z score derived from the hotspot analysis reveals that the distribution of hotspots was more clustered (value ranging from 6.29 to -1.73) during period 1987-2001 than the period 2001-2020 (value ranging from 5.63 to -3.19).

3.5. Cellular Automata for future trend of LULC change

The cellular automata simulation method based on the specific landuse change parameters (Fig. 7) was used to detect the changes in the future landuse and landcover in Habra I and II block. In that case, the LULC of 2001 and 2011 has been taken as input to simulate the predicted 2030 and 2050 (Fig. 8). The simulation result indicates that the area under dense settlement will increase from 46.55 km^2 in 2020 to about 71.23km^2 in 2030, and 87.90 km^2 in 2050 and most of it will be occupied by residential, industrial, and commercial areas. Side by side, the cumulative area under vegetation with settlement and agricultural land will start decreasing proportionally. According to the simulation result, the vegetation with settlement area will decrease to 85.79km^2 in 2030 and further decrease to 79.23km^2 in 2050. Similarly, the agricultural land area in 2030 and 2050 will stand at 124.09km^2 and 114.78km^2, respectively which was 136.02km^2 in 2020.

3.6. Transition potential modelling using artificial neural network

Transition Potential Modelling by means of Artificial Neural Network is mandatory before simulating the cellular automata. To do this, 1px neighborhood, 0.10 learning rate, a maximum iteration of 1000, and 0.050 momentum was given as inputs to train the CA-ANN model for best result. Result shows that validation Kappa value after ANN was 0.75510, which is preferably good for simulation (Fig. 9).

3.7. Prediction Accuracy

The findings of the CA-ANN system must be checked after simulation using the validation tool of MOLUSCE plugin. In that case, reference map of 2020 and simulation map of 2020 was used as input layer to validate the result. Validation result shows that the overall accuracy is about 83.47% whereas the kappa value is 0.7823.

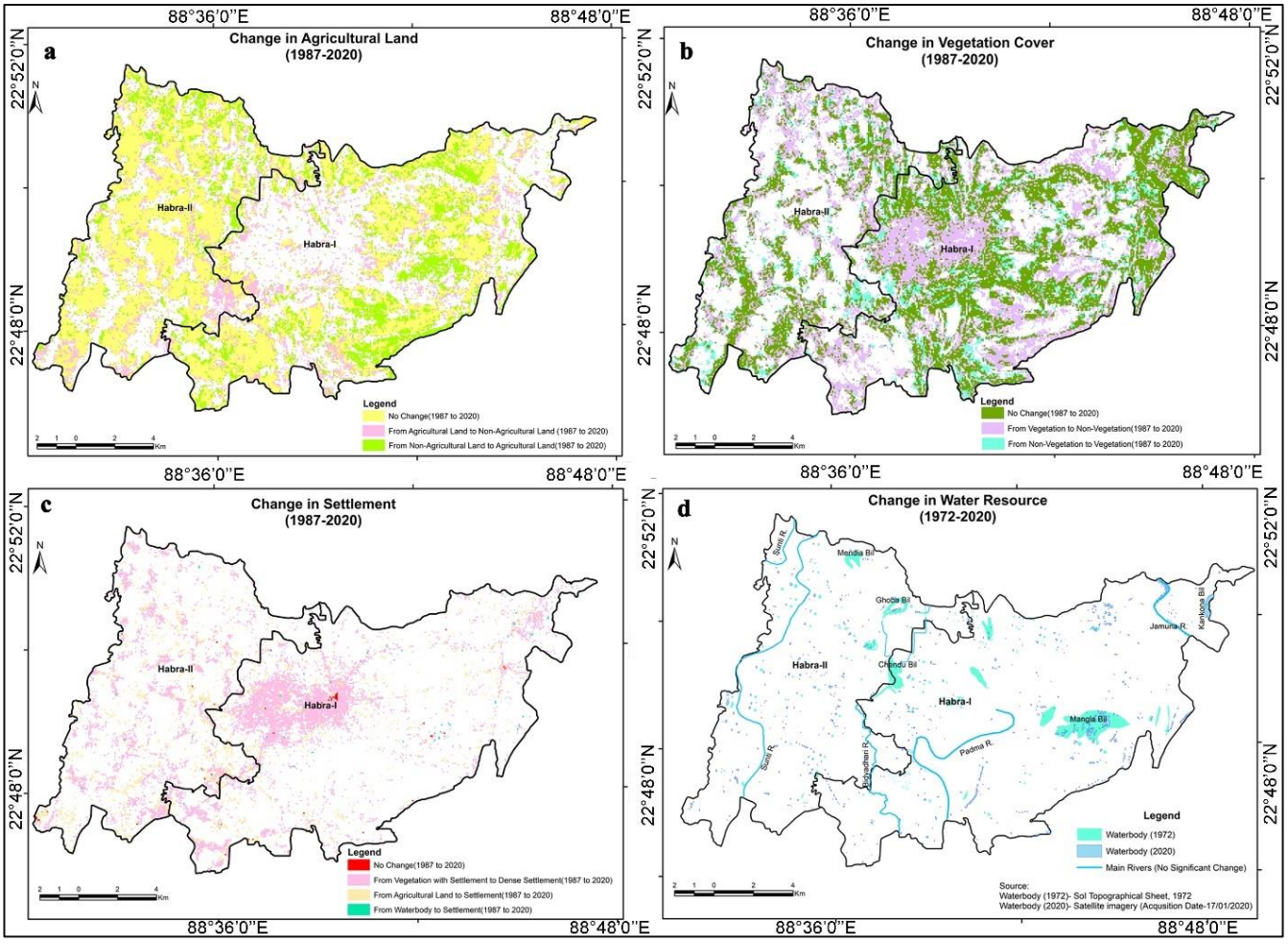

Figure 4. Changing status in Landuse and landcover during 1987-2020. Change in a) agricultural land b) Vegetation cover c) settlement and d) Water resource.

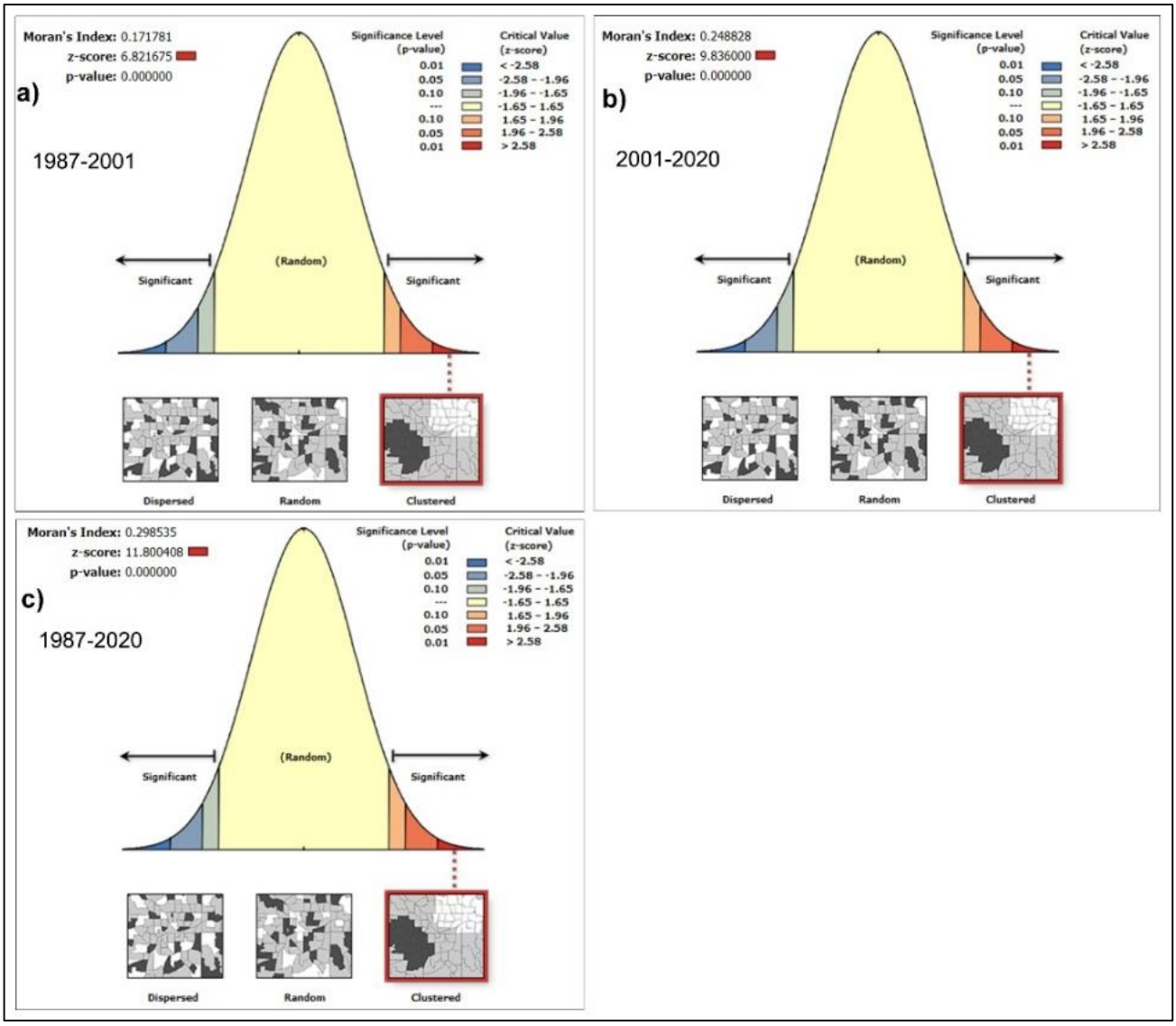

Figure 5. Moran's I significant value, Z score, and p value to determine the spatial autocorrelation dur-ing period a)1987-2001 b)2001-2020, and c)1987-2020.

4. DISCUSSION

The present research focuses primarily on the spatial-temporal dynamics of land use and land cover transition in the Habra I and II blocks of the North 24 Parganas district and its changing scenario. Now it is clear that the type of LULC did not change parallelly during period 1987-2020, rather at a very fast rate in the first half and then stabilized somewhat. Crowds of refugees from the erstwhile East Pakistan during 1967-1971 due to Indo-Pakistan war, and after 1985 illegal infiltration from today's Bangladesh (Datta, 2004; Kumar, 2009), can be blamed for the havoc conversion from agricultural and vegetative land to dense settlement. Although, most of the population of these district are concentrated around the Habra, and Ashokenagar-Kalyangarh municipal area (Rahaman, 2018) due to the whole sale business center in Habra which is renowned for selling jute, rice, building materials, cloths, electronic goods, etc., made the area as the second largest wholesale market in West Bengal next to Barabazar in Kolkata (Roy, 2011). Besides, due to the location of the Sealdah-Bangaon branch of the Eastern Railway of India and national highway NH-35 (the Jessore Road), and several other state highways, every portion of these blocks are well connected with the respective municipal town. Therefore, a number of census town has increased in each corner of these municipality by reducing the number of true villages due to household growth, residential progress, commercial influences (viz. industries, tertiary activities), job availability, an increase in the connectivity network, higher educational facility, etc. So, a positive correlation of urban growth can be found between geometric center of the town and distance from major roads and railway station (Majumdar & Sivaramakrishnan, 2015). Thus, started from the urban center, the trend of urbanization proceeds towards the peripheral zone.

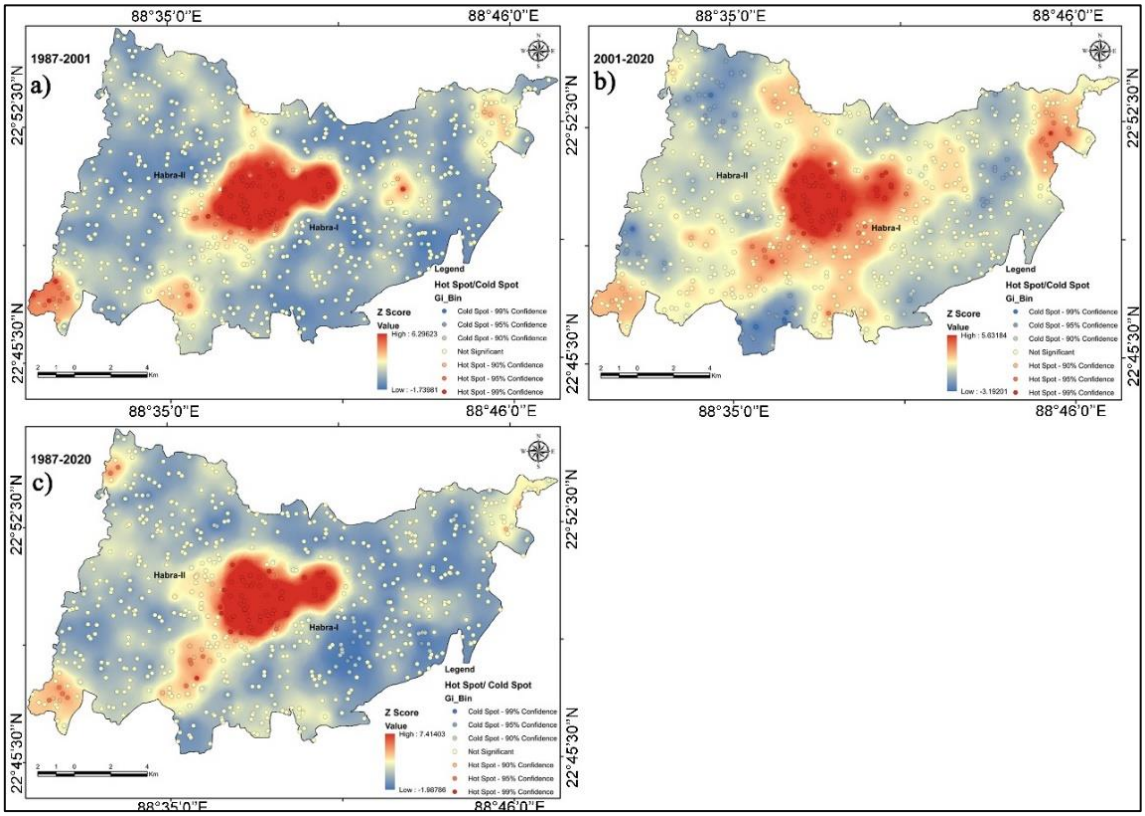

Figure 6. Hot and coldspots, along with the GiZscore variability during a) 1987-2001 b) 2001-2020, and c) 1987-2020.

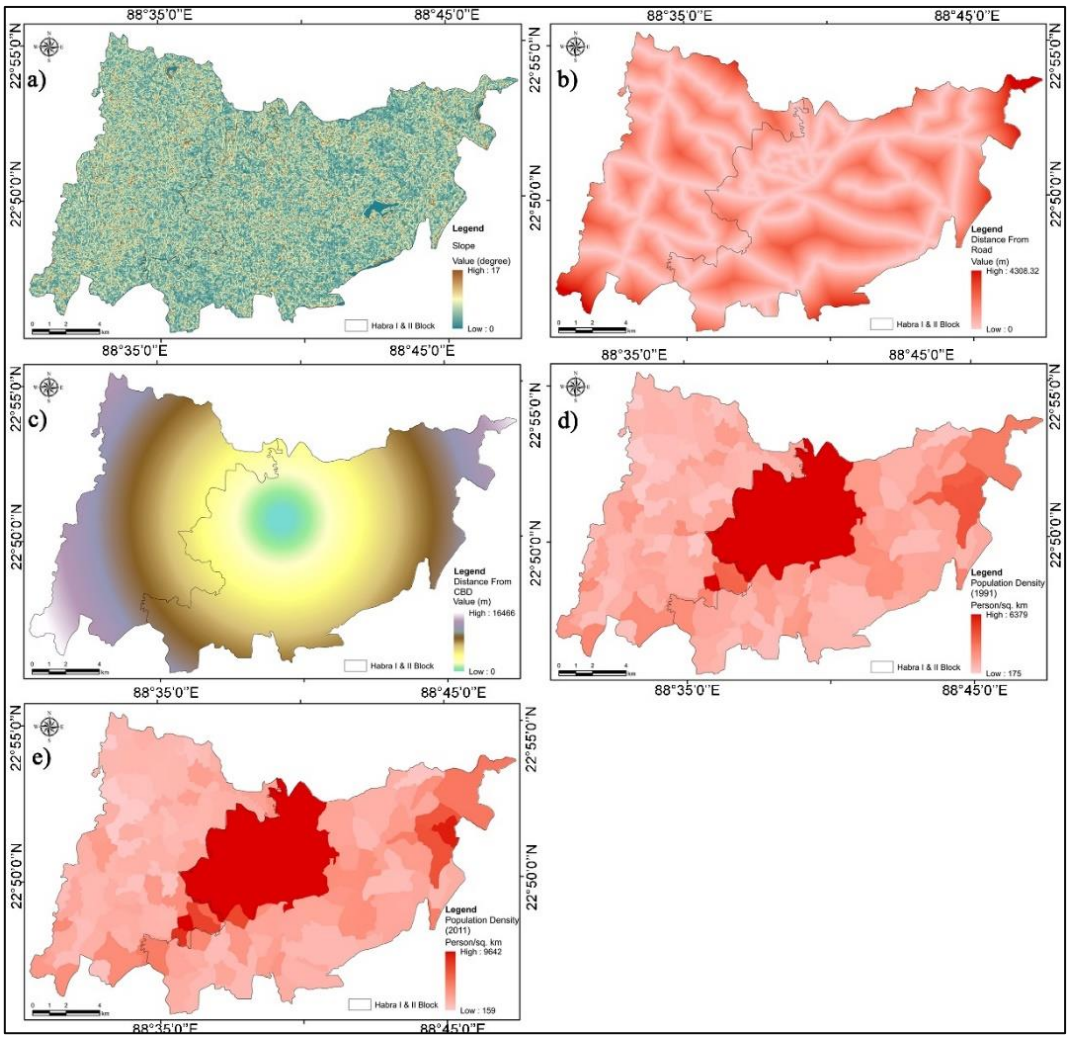

Figure 7. Input factors for the simulation of Cellular Automata Model. Here, a) Slope map b) Distance from the road c) Distance from the CBD d) Population density of 1991, and e) Population density of 2011

The reason for the steady decline in agricultural land since 1987 can be attributed to the construction of human settlement on the agricultural land. At the same time, the amount of vegetation has also decreased as densely settlements areas have gradually taken over the zones that were characterized by isolated settlements surrounded by trees. Dhali et al. (2019) has evaluated the rate and growth of urban expansion for some selected blocks of the north 24 parganas through Shannon's Entropy Index model and their result demonstrated that the index value increased from 0.21 to 0.78 in Habra-I and increased from 0.23 to 0.67 in Habra-II during period 1989-2016, indicates a high urban growth in last 27 years. Besides, Bera & Das Chatterjee (2019) also have supported the fastest urbanization of Habra I and II block within North 24 Parganas district and according to them, maximum transformations have taken place from agricultural and vegetation land. On the contrary, the reason for the slight increase in the waterbody area in 2001 as compared to 1987 can be attributed to the flood caused by excessive rainfall in 1999 which had turned the relatively low-lying areas into swamp. Mangla bil, Ghoba bil, Mendia bil, etc. are the perfect example of this occurrence. Besides, by digging ponds on the agricultural land, a lot of new water bodies were created to use the soil as brick material in brick kilns (Bera & Das Chatterjee, 2019). However, after 2001, the area of waterbody was further reduced either by siltation in the ponds due to disposal of domestic, agricultural and industrial waste (Prabakaran et al., 2013) or by construction of settlements by filling the low-lying areas due to the unusual increase of land price.

It is, therefore, detected that there was an expansion in dense settlement, which could be ascribed to the existing birth and growth rate of the area, infiltration from neighboring countries, development of industrial area etc. Moreover, since the establishment of a commercial drilling station for new oil and gas wells in Ashokenagar-Kalyangarh area by Oil and Natural Gas Corporation (ONGC) after 2020, it is expected that more people will gather in this area (ONGC, 2020) in the near future.

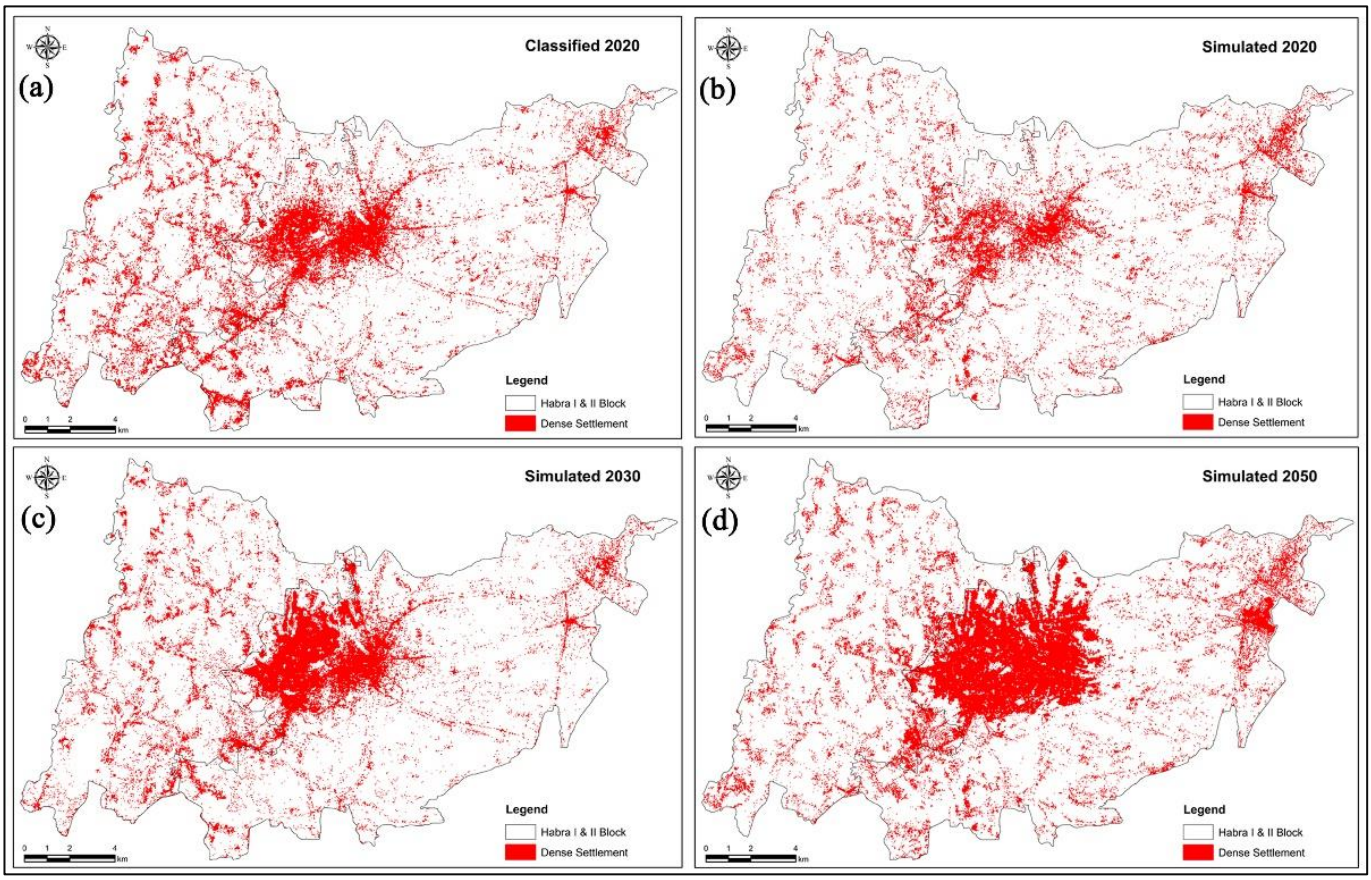

Figure 8. Simulation result from the Cellular Automata showing a) Classified 2020 b) Simulated 2020 c) Simulated 2030, and d) Simulated 2050.

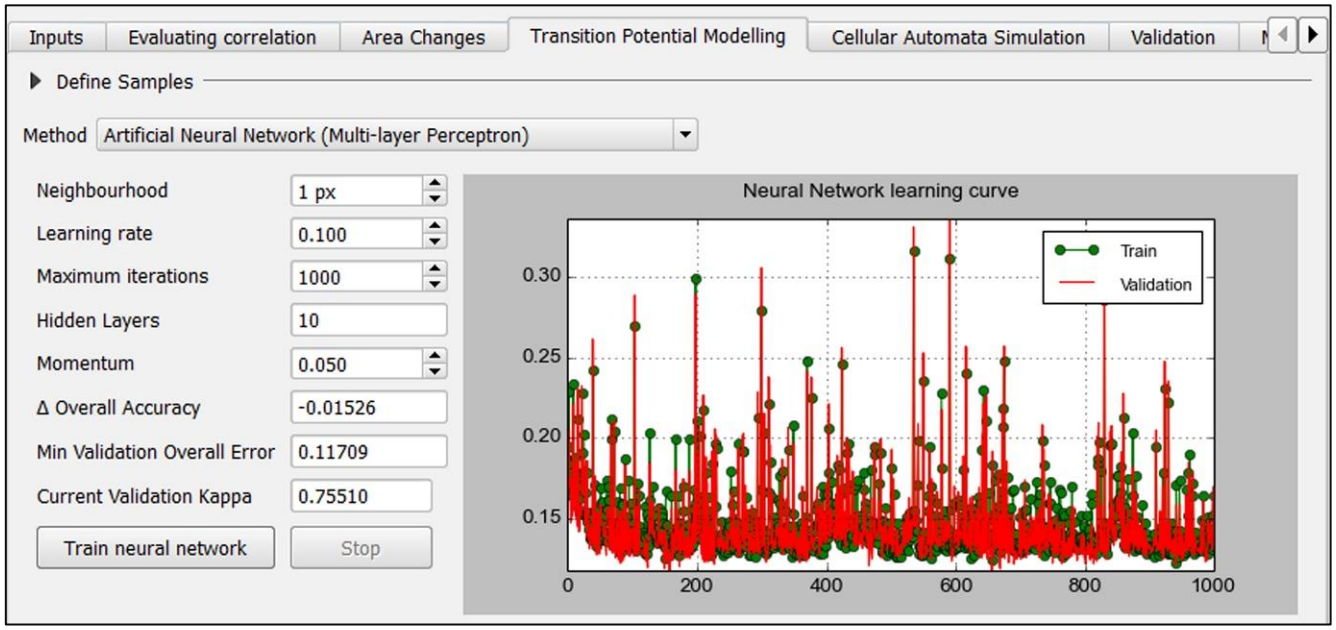

Figure 9. Validation result of the Transition Potential Modelling using ANN.

5. CONCLUSION

The present study conducted in one of the populated and developed blocks of North 24 parganas district in West Bengal using a combination of satellite data and GIS to achieve the specific research objectives, advocates the potentiality of remote sensing data over large areas and demonstrates the spatial changes with regard to landuse and landcover information in timely and accurate way for efficient land management and policy decisions. Since, in present day, dense settlement is the principal dynamic part of LULC, but just three decades ago, there was a harmonious balance between agricultural land and vegetation. So, in terms of change matrix, expansion of dense settlement is highest due to the development of small and medium enterprises, proximity to wholesale market, job opportunities, rural-urban migration, and demand for density factor, denotes a clear view of rapid urbanization. Waterbodies, on a contrary, have the lowest rate of spatial change. In other words, a negative correlation exists between urban expansion and all other landuse-landcover classes. Thus, based on the results, it is concluded that the LULC in the study area have transformed from its original condition significantly in past 33 years.

Therefore, although an effective outline of the change in landuse and landcover of Habra I and II block has been summarized through an integration of spaceborne data and subsidiary data, some limitations and uncertainties are also present in this work. Due to the moderate resolution (30m) of the Landsat images, it was not possible to perform very fine classification, leaving out very minor objects like small ponds, scatter settlements, etc. In addition, the cover of aquatic vegetation on the streamless rivers, very shallow water, etc., has somewhat reduced the accuracy of the work. Besides, after the termination of the monsoon season, due the lack of rainfall for a prolonged period, the behavior of the agricultural land has become more like an impervious body, which has caused some complications between the agricultural land and the urban area. So, the very high and uncontrolled growth of urban settlement in the study area, may become a big challenge for the district authority to control the unplanned urban expansion. Although, it is very difficult to alter the current system in the already constructed urban body, but some measures like green belt around the urban center, green building, etc. can be adopted to hinder the future effects.

ACKNOWLEDGEMENT

I am thankful to United States Geological Survey for providing me the Landsat images for free of cost. I would also like to acknowledge all my friends who had helped me in various ways during the fieldwork.

Conflicts of interest

The authors declare no conflicts of interest.

REFERENCES

Amaral G, Bushee J, Cordani U G, KAWASHITA K, Reynolds J H, ALMEIDA F F M D E, … Junho M. do C B (2013). Change detection of urban body. Journal of Petrology, 369(1), 1689–1699. https://doi.org/10.1017/CBO9781107415324.004

Bagchi K (1944). The Ganges delta. Calcutta: University of Calcutta.

Barnsley M J, Mollar-Jensen L & Barr S L (2001). Inferring Urban Land Use by Spatial and Structural Pattern Recognition. In J. P. Donnay, M. J. Barnsley, & P. A. Longley (Eds.), Remote Sensing and Urban Analysis (pp. 102–130). London: Taylor & Francis.

Basu T & Saha S K (2017). The Analysis of Land Use Land Cover Changes Using Geoinformatics and Its Relation to Changing Population Scenariosin Barasat Municipality in North Twenty-Four Parganas, West Bengal. International Journal of Humanities and Social Science Invention, 6(8), 1–13.

Bera S & Das Chatterjee N (2019). Mapping and monitoring of land use dynamics with their change hotspot in

North 24-Parganas district, India: a geospatial- and statistical-based approach. Modeling Earth Systems and Environment, 5(4), 1529–1551. https://doi.org/10.1007/s40808-019-00601-2

Bhatta B (2018). Remote sensing and GIS (2nd ed.). Oxford University Press.

Bhattacharjee D & Hazra S (2014). Distribution of Land Surface Temperature Over Built-up Area by Web-GIS Techniques. Indian Journal of Spatial Science, 5(2), 70–76.

Boschetti L, Flasse S P & Brivio P A (2004). Analysis of the conflict between omission and commission in low spatial resolution dichotomic thematic products: The Pareto Boundary. Remote Sensing of Environment, 91(1), 280–292. https://doi.org/10.1016/j.rse.2004.02.015

Butt A, Shabbir R, Ahmad S S & Aziz N (2015). Land use change mapping and analysis using Remote Sensing and GIS: A case study of Simly watershed, Islamabad, Pakistan. The Egyptian Journal of Remote Sensing and Space, 18(2), 251–259. https://doi.org/10.1016/j.ejrs.2015.07.003

Cai L, Shi W, Miao Z & Hao M (2018). Accuracy assessment measures for object extraction from remote sensing images. Remote Sensing, 10(2), 303. https://doi.org/10.3390/rs10020303

Canty M J (2014). Image analysis, classification and change detection in remote sensing With Algorithms for ENVI/IDL and Python (3rd ed.). Boca Raton: CRC Press, Taylor & Francis Group.

Chaurasia R, Loshali D C, Dhaliwal S S, Sharma P K, Kudrat M & Tiwari A K (1996). Land use change analysis for agricultural management—A case study of Tehsil Talwandi Sabo, Punjab. *Journal of the Indian society of remote sensing*, *24*(2), 115-123.https://doi.org/doi.org/10.1007/BF03016124

Chowdhury M, Emran M & Abdullah-al-mamun M M (2018). Land use/land cover change assessment of Halda watershed using remote sensing and GIS. The Egyptian Journal of Remote Sensing and Space Sciences, 23(1), 63–75. https://doi.org/10.1016/j.ejrs.2018.11.003

Civco D L, Hurd J D, Wilson E H, Song M & Zhang Z (2002). A comparison of land use and land cover change detection methods. ASPRS-ACSM Annual Conference and FIG XXII Congress.

Comber A J, Wadsworth R A & Fisher P F (2008). Using semantics to clarify the conceptual confusion between land cover and land use: the example of 'forest.' Journal of Land Use Science, 3(2–3), 185–198. https://doi.org/10.1080/17474230802434187

Congalton R G (2001). Accuracy assessment and validation of remotely sensed and other spatial information. International Journal of Wildland Fire, 10(3–4), 321–328. https://doi.org/10.1071/wf01031

Coppin P R & Bauer M E (1996). Digital Change Detection in Forest Ecosystems with Remote Sensing Imagery. Remote Sensing Reviews, 13(3–4), 207–234. https://doi.org/https://doi.org/10.1080/02757259609532305

Datta P (2004). Push-pull factors of documented migration from Bangladesh to west Bengal: a perception study.

Dewan A M & Yamaguchi Y (2009). Using remote sensing and GIS to detect and monitor land use and land cover change in Dhaka Metropolitan of Bangladesh during 1960 – 2005. Environmental Monitoring and Assessment, 150(1–4), 237–249. https://doi.org/10.1007/s10661-008-0226-5

Dhali M K, Chakraborty M & Sahana M (2019). Assessing spatio-temporal growth of urban sub-centre using Shannon's entropy model and principal component analysis: A case from North 24 Parganas, lower Ganga River Basin, India. Egyptian Journal of Remote Sensing and Space Science, 22(1), 25–35. https://doi.org/10.1016/j.ejrs.2018.02.002

Dhar R B, Chakraborty S, Chattopadhyay R & Sikdar P K (2019). Impact of Land-Use / Land-Cover Change on Land Surface Temperature Using Satellite Data: A Case Study of Rajarhat Block, North 24-Parganas District, West Bengal. Journal of the Indian Society of Remote Sensing, 47(2), 331–348. https://doi.org/10.1007/s12524-019-00939-1

Foody G M (2002). Status of land cover classification accuracy assessment. Remote Sensing of Environment, 80(1), 185–201. https://doi.org/https://doi.org/10.1016/S0034-4257(01)00295-4

Fortin M (2003). On the role of spatial stochastic models in understanding landscape indices in ecology. Oikos, 102(1), 203–212. https://doi.org/https://doi.org/10.1034/j.1600-0706.2003.12447.x

Getis A & Ord J K (1996). Spatial analysis and modeling in a GIS environment. In R. B. McMaster & E. L. Usery (Eds.), A research agenda for geographic information science (pp. 157–160). CRC Press,Taylor & Francis Group.

Gong P, Ledrew E F & Miller J R (1992). Registration-noise reduction in difference images for change detection. International Journal of Remote Sensing, 13(4), 773–779. https://doi.org/10.1080/01431169208904151

Ha T V, Tuohy M, Irwin M & Tuan P V (2018). Monitoring and mapping rural urbanization and land use changes using Landsat data in the northeast subtropical region of Vietnam. The Egyptian Journal of Remote Sensing and Space Sciences, 23(1), 11–19. https://doi.org/10.1016/j.ejrs.2018.07.001

Handbook D C (2011). West Bengal.

Hazra S & Saradar J (2014). Monitoring of landuse and landcover – a case study of Bidyadhari basin, North 24 Parganas, West Bengal. Geographical Review of India.

Hussain M, Chen D, Cheng A, Wei H & Stanley D (2013). Change detection from remotely sensed images: Frompixel-based to object-based approaches. ISPRS Journal of Photogrammetry and Remote Sensing, 80(1), 91–106. https://doi.org/10.1016/j.isprsjprs.2013.03.006

Im J, Rhee J, Jensen J R & Hodgson M E (2007). An automated binary change detection model using a calibration approach. Remote Sensing of Environment, 106(1), 89–105. https://doi.org/10.1016/j.rse.2006.07.019

Jensen J R (2015). Introductory digital image processing a Remote Sensing Perspective (4th ed.).

Jing Y & Yue Z (2016). Change and prediction of the land use /cover in Ebinur Lake Wetland Nature Reserve based on CA-Markov model. Chinese Journal of Applied Ecology, 27(11), 3649–3658. https://doi.org/1001-9332.201611.027

Jogun T, Lukić A & Gašparović M (2019). Simulation model of land cover changes in a post-socialist peripheral rural area: Požega-slavonia county, croatia. Hrvatski Geografski Glasnik, 81(1), 31–59. https://doi.org/10.21861/HGG.2019.81.01.02

Kefalas G, Xofis P, Lorilla R S & Martinis A (2018). The use of vegetation indices and change detection techniques as a tool for monitoring ecosystem and biodiversity integrity. International Journal of Sustainable Agricultural Management and Informatics, 4(1), 47–67. https://doi.org/10.1504/IJSAMI.2018.10013626

Kuldeep T & Kamlesh K (2011). Land Use / Land cover change detection in Doon valley (Dehradun Tehsil), Uttarakhand: using GIS & Remote Sensing Technique. International Journal of Geomatics and Geosciences, 2(1), 34–41.

Kumar C (2009). Migration and refugee issue between India and Bangladesh. Scholar's Voice: A New Way of Thinking, 1(1), 62–84.

Kushwaha S P S (1990). Forest-type mapping and change detection from satellite imagery. Journal of Photogrammetry and Remote Sensing, 45(3), 175–181. https://doi.org/https://doi.org/10.1016/0924-2716(90)90057-I

Lambin E F, Geist H J & Lepers E (2003). Dynamics of land-use and land-cover change in tropical regions. Annual Review of Environment and Resources, 28(1), 205–241. https://doi.org/10.1146/annurev.energy.28.050302.105459

Lambin E F, Turner B L, Geist H J, Agbola S B, Angelsen A, Folke C, … Veldkamp T A (2001). The causes of land-use and land-cover change: moving beyond the myths. Global Environmental Change, 11(4), 261–269. https://doi.org/https://doi.org/10.1016/S0959-3780(01)00007-3

Liping C, Yujun S & Saeed S (2018). Monitoring and predicting land use and land cover changes using remote sensing and GIS techniques:A case study of a hilly area, Jiangle, China. PLoS ONE, 13(7), 1–23. https://doi.org/https://doi.org/10.1371/journal.pone.0200493

Liu S & He S J (2002). A spatial analysis model for measuring the rate of land use change. Journal of Natural Resources, 17(5), 533–540.

Lu D, Li G, Valladares G S & Batistella M (2004). Mapping soil erosion risk in Rondônia, Brazilian Amazonia: Using RUSLE, remote sensing and GIS. Land Degradation and Development, 15(5), 499–512. https://doi.org/10.1002/ldr.634

Lu D, Mauselt P, Batistells M & Moran E (2005). Land-cover binary change detection methods for use in the moist tropical region of the Amazon: a comparative study. International Journal of Remote Sensing, 26(1), 101–114. https://doi.org/https://doi.org/10.1080/01431160410001720748

Majumdar (1942). Rivers of the Bengal delta. University of Calcutta.

Majumdar S & Sivaramakrishnan L (2015). Patterns of land use in and around Kolkata city: A spatio-temporal analysis. Indian Cartographer, 35, 218–223.

Mitchell A & Minami M (1999). The ESRI guide to GIS analysis: geographic patterns & relationships (1st ed.). ESRI, Inc.

Mondal B, Dolui G, Pramanik M, Maity S & Sarathi S S (2017). Urban expansion and wetland shrinkage estimation using a GIS-based model in the East Kolkata Wetland, India. Ecological Indicators, 83(November 2016), 62–73. https://doi.org/10.1016/j.ecolind.2017.07.037

Mondal I & Bandyopadhyay J (2014). Studies on the nature of studies on the nature of change in aquaculture through application of remote sensing & GIS techniques: a case study on Sandeshkhali- i & ii blocks, North 24 Parganas, West Bengal, India. Indian Cartographer, 34(1).

Mukherjee R (1938). The changing face of Bengal-A study in riverine economy. Calcutta: University of Calcutta.

O'Malley L S S (1917). Bengal Bihar Orissa and Sikkim (t. H. Holland, ed.). Cambridge university press.

ONGC (2020). ONGC starts oil and gas production from West Bengal after 60 years endeavor. Financial Express, p. 2.

Petit C, Scudder T & Lambin E (2001). Quantifying processes of land-cover change by remote sensing: resettlement and rapid land-cover changes in south-eastern Zambia. International Journal of Remote Sensing, 22(17), 3435–3456. https://doi.org/10.1080/01431160010006881

Prabakaran K, Pal R & Chitra J (2013). Hydrobiological characteristics of Freshwater Habitats of South Dum Dum Municipality, North 24 Parganas District, West Bengal, India. Journal of Academia and Industrial Research (JAIR), 2(3), 3–6.

Prasad G & Ramesh M V (2018). Spatio-Temporal Analysis of Land Use/Land Cover Changes in an Ecologically Fragile Area—Alappuzha District, Southern Kerala, India. Natural Resources Research, 28(2), 31–42. https://doi.org/10.1007/s11053-018-9419-y

Rahaman M (2018). Urban Population Growth in the Municipalities of North 24 Parganas: A Spatio-Temporal Analysis. World Wide Journal of Mul t Idiscipl Inary Research and Development, 4(3), 68–73.

Rai R (2017). A Synthesis of Studies on Land Use and Land Cover Dynamics during 1930 – 2015 in Bangladesh. Sustainability 2017, 9, 1–20. https://doi.org/10.3390/su9101866

Rawat J S & Kumar M (2015). Monitoring land use / cover change using remote sensing and GIS techniques: A case study of Hawalbagh block, district Almora , Uttarakhand , India. The Egyptian Journal of Remote Sensing and Space Sciences, 18(1), 77–84. https://doi.org/10.1016/j.ejrs.2015.02.002

Richards J A (1996). Classifier performance and map accuracy. 57(3), 161–166. https://doi.org/https://doi.org/10.1016/0034-4257(96)00038-7

Riebsame W E, Meyer W B & Turner B L (1994). MODELING LAND USE AND COVER AS PART OF GLOBAL ENVIRONMENTAL CHANGE. Climatic Change, 28(10), 45–64. https://doi.org/doi.org/10.1007/BF01094100

Roy T (2011). Nature and dynamism of rural urban continuum of North 24 Parganas with special reference to Barasat town. University of Calcutta.

Saritha S & Kumar G S (2019). Change detection in urban landscapes: a tensor factorization approach. Patial Information Research, 27(5), 587–600. https://doi.org/doi.org/10.1007/s41324-019-00255-3

Selcuk R, Recep N, Bayram U & Ali Y (2003). Monitoring Land –Use Changes by GIS and Remote Sensing Techniques: Case Study of Trabzon. 2nd FIG Regional Conference, (December 2-5), 1–11.

Sharma R, Xu J & Sharma G (2007). Traditional agroforestry in the eastern Himalayan region: Land management system supporting ecosystem services. Tropical Ecology, 48(2), 189–200.

Singh A (1989). Digital change detection techniques using remotely-sensed data. International Journal of Remote Sensing, 10(6), 989–1003. https://doi.org/10.1080/01431168908903939

Stauffer M L & McKinney R L (1978). Landsat image differencing as an automated land cover change detection technique (interim report).

Stehman S V (1997). Selecting and Interpreting Measures of Thematic Classification Accuracy. Remote Sensing of Environment, 62(1), 77–89. https://doi.org/10.1016/S0034-4257(97)00083-7

Turner A B L, Meyer W B & Skole D L (1994). Global Land-Use/Land-Cover Change: Towards an Integrated Study. Ambio: Integrating Earth System Science, 23(1), 91–95. https://doi.org/https://doi.org/10.2307/4314168

Voogt J A & Oke T R (2003). Thermal remote sensing of urban climates. Remote Sensing of Environment, 86(3), 370–384. https://doi.org/10.1016/S0034-4257(03)00079-8

Wang F & Xu Y (2010). Comparison of remote sensing change detection techniques for assessing hurricane damage to forests. Environmental Monitoring and Assessment, 162(1–4), 311–326. https://doi.org/10.1007/s10661-009-0798-8

Wang J, Fu B, Qiu Y & Chen L (2001). Soil nutrients in relation to land use and landscape position in the semi-arid small catchment on the loess plateau in China. Journal of Arid Environments, 48(4), 537–550. https://doi.org/10.1006/jare.2000.0763

Wood C H & Skole D (1998). Linking Satellite, Census, and Survey Data to Study Deforestation in the Brazilian Amazon. In D. Liverman, E. F. Moran, & R. R. Rindfuss (Eds.), People and Pixels, Linking Remote Sensing and Social Science (pp. 70–93). Washington, D.C.: National Academy Press.

Xiao M, Wu J, Chen Q, Jin M & Zhang Y (2012). Dynamic change of landuse in Changhua downstream watershed based on CA-Marcov model. Transactions of the Chinese Society of Agricultural Engineering, 28(10), 231–238.

Yatoo S A, Sahu P, Kalubarme M H & Kansara B B (2020). Monitoring land use changes and its future prospects using cellular automata simulation and artificial neural network for Ahmedabad city, India. GeoJournal, 5. https://doi.org/10.1007/s10708-020-10274-5

Yi L, Zhang Z, Wang X, Liu B, Zuo L, Zhao X & Wang J (2013). Spatial-temporal change of major reserve resources of cultivated land in China in recent 30 years. Transactions of the Chinese Society of Agricultural Engineering, 29(6), 1–12.